

Investigating the roles of cohesin acetylation and the configuration of the coiled coil domain modelled by *Saccharomyces cerevisiae*.

A thesis submitted for the degree of:

Doctor of Philosophy

Thane Than, MBio.

University of Sheffield

Department of Molecular Biology and Biotechnology

October 2016 – October 2020

Contents

Title page	I
Contents.....	II
Acknowledgements	VI
Abbreviations	VII
Nomenclature	X
Index of figures and tables	XI
1.0 Abstract	1
2.0 Introduction and literature review	3
2.1 The cell cycle	3
2.2 Sister chromatid cohesion proteins: The SMC family, history and application ..	7
2.2.1 Prokaryotic <i>SMC</i> complexes.....	11
2.3 The ring model of <i>SMC</i> complexes	12
2.4 Current understanding of cohesin structure and function.....	15
2.5 Loading of cohesin onto the chromatid	28
2.6 Maintaining sister chromatid cohesion & disjunction.....	38
2.7 Acetylation of <i>SMC</i> proteins.....	46
2.8 <i>Saccharomyces cerevisiae</i>	55
2.9 Aims of this study.....	57
3.0 Materials and methods	59

3.1 Materials	59
3.1.1 Media.....	59
3.1.2 Stock solutions.....	61
3.2 Methods	61
3.2.1 Yeast culture.....	61
3.2.2 <i>E. coli</i> culture	63
3.2.3 Molecular biology and biochemistry	63
4.0 Results	82
4.1 Chapter 1	82
4.1.1 Introduction	82
4.1.2 Chapter 1 part 1: <i>smc3K112Q, K113Q, R1008I</i> suppressor screen	85
4.1.3 Chapter 1 part 2: Testing the effects of mutations in the vicinity of <i>smc3QQ</i>	95
4.1.4 Chapter 1 part 3: Testing the effects of mutations in the cohesin loader <i>Scs2</i>	97
4.1.5 Chapter 1: Summary.....	100
4.2 Chapter 2	101
4.2.1 Introduction	101
4.2.2 Chapter 2 part 1: Investigating interactions near <i>smc3R1008I</i>	104
4.2.3 Chapter 2 part 2: Testing the effect of <i>smc3QQ</i> suppressors on coiled coil configuration	128
4.2.4 Chapter 2 part 3: Producing a novel structural model of cohesin.....	132

4.2.5 Chapter 2 part 4: The effect of QQ on the E and J configurations	159
4.2.6 Chapter 2: Summary.....	167
4.3 Chapter 3	168
4.3.1 Introduction	168
4.3.2 Chapter 3 part 1: Finding Smc3 / Smc1 interaction sites in Scc2	169
4.3.3 Chapter 3 part 2: Testing the effect of <i>smc3QQ</i> and suppressor mutants on cohesin interactions with Scc2.....	180
4.3.4 Chapter 3 part 3: Investigating ATP hydrolysis activity of cohesin	182
4.3.5 Chapter 3: Summary.....	186
5.0 Discussion	187
5.1 General discussion	187
5.2 Future topics of research	197
5.2.1 Resolving Scc2 and Pds5 interaction with cohesin.....	197
5.2.2 Pre-loading complex	198
5.2.3 Future topics of research summary	200
6.0 References.....	201
7.0 Appendix	221
7.1 Primer list.....	221
7.2 Plasmid list.....	226
7.3 Yeast strain list.....	231
7.4 Additional figures	253
7.4.1 Chapter 1 part 1	253

7.4.3 Chapter 2 part 4.....	255
7.5 Publications.....	256

Acknowledgements

I began this endeavour to hew a stone from the realm of natural science, and lay it with all others in the building of human knowledge. I give my thanks first to Dr Bin Hu, whom without, this opportunity would not have found me. And after, to all those who have provided assistance; great or small. I am especially grateful to my mother and brother, whom at the very end provided the last helping hands.

This journey taught me many lessons, both professional and personal. Of these, I dare stress a couple. Dr Jeffery So, who taught me that life is filled with hidden beauty which often transcends my understanding, but nevertheless worthy of never-ending pursuit to adorn the inward man. Dr Hasan Fayiz Hasan Al-Naser, for teaching me that all divisions between men are by choice, and that there are no distinctions among us beyond reconciliation.

These are two lessons above all else that I have learned during this endeavour; of which, I will remember until the end of my days. My stone is complete and may it be laid in the temple of mankind's knowledge forever. Lastly, for all those who follow after:

“As we have fared, may others fare.”

Abbreviations

5-FOA	5-Fluoroorotic Acid
aaRS	Aminoacyl tRNA synthetase
ABC	ATP binding cassette
Amp	Ampicillin
APS	Ammonium persulfate
BLAST	Basic local alignment search tool
BMOE	Bismaleimidoethane
BPA	Benzoyl-L-phenylalanine
BSA	Bovine serum albumin
Cdk1	Cyclin dependent kinase 1
ChIP	Chromatin immunoprecipitation
CRISPR	Clustered regularly interspaced palindromic repeats
DDK	Dbf4-dependent kinase
DSB	Double-strand break
DTT	1,4-Dithiothreitol
EDTA	Ethylenediaminetetraacetic acid
ELISA	Enzyme-linked immunosorbent assay

EM	Electron microscopy
FACS	Fluorescence activated cell sorting
FISH	Fluorescence in-situ hybridisation
FRET	Förster resonance energy transfer
GD	Globular domain
GFP	Green fluorescent protein
gRNA	Guide ribonucleic acid
HAWK	Heat repeat proteins associated with kleisins
HEAT	Huntingtin, elongation factor 3 (EF3), protein phosphatase 2A (PP2A), and the yeast kinase TOR1
Hi-C	High-throughput chromosome conformation capture
KITE	Kleisin interacting tandem winged-helix elements of SMC complexes
MAD	Mitotic arrest deficient
NP-40	Tergitol-type NP-40, nonyl phenoxyethoxyethanol
PBS	Phosphate buffered saline
PMSF	Phenylmethylsulfonyl fluoride
RSC	Re-modelling the structure of chromatin
SAC	Spindle assembly checkpoint
SDS	Sodium dodecyl sulfate

SMC	Structural maintenance of chromosomes
TCA	Trichloroacetic acid
TEMED	N,N,N',N'-Tetramethylethylenediamine
Tet-O	Tetracycline operon
Tet-R	Tetracycline repressor
TPR	Tetratricopeptide repeat
TS	Temperature sensitive

Nomenclature

Wildtype genes are presented in italicised upper case letters, e.g. *SMC3*.

Mutant genes are presented in italicised lower case letters, e.g. *smc3*.

Proteins are presented with no text modification; first letter in upper case, e.g. Smc3.

Latin names of organisms are presented in italicised letters, e.g. *S. cerevisiae*.

Generic names are presented with no additional text modification, e.g. *Saccharomyces*.

Index of figures and tables

Figures

Figure 1: Diagram showing the phases of the cell cycle in eukaryotes.....	3
Figure 2: A simplified description of mitosis consisting of five main phases: prophase, prometaphase, metaphase, anaphase, and telophase.	5
Figure 3: Illustration of the strong ring and weak ring models.	13
Figure 4: Diagram to illustrate the importance of Scc3 in maintaining sister chromatid cohesion.	16
Figure 5: Electron micrographs of cohesin.	17
Figure 6: A cartoon representation of the cohesin tetramer with highlighted resolved regions.	18
Figure 7: Cartoon diagrams of four different types of SMC complexes and their core subunits as visual aid to table 1.	20
Figure 8: Simplified diagram to show how the elbow region of cohesin allows crosslinking between the distant hinge and subunits near to the head domains.	22
Figure 9: A diagram showing possible DNA entrapment configurations of cohesin and which combinations of these states captured DNA during crosslinking experiments.	24
Figure 10: Diagram showing the structure of Scc2 and Scc4 along identified domains and electron microscopy images from <i>S. cerevisiae</i>	31
Figure 11: A diagram showing mechanism of cohesin recruitment to chromatin in yeast. ...	33

Figure 12: A diagram of a potential mechanism for DNA loop extrusion as described by Diebold-Durand and co-workers.....	35
Figure 13: Cartoon diagrams of <i>in vitro</i> Rad61-Pds5 complex dependent releasing activity using purified <i>S. cerevisiae</i> proteins as described by Murayama and co-workers.	40
Figure 14: Diagrams to show the Rad61 independent releasing mechanism of cohesin which is blocked by Scc2 in G1 phase as described by Srinivasan and co-workers.	44
Figure 15: Diagram showing the chemical changes during the acetylation and deacetylation of lysine.	47
Figure 16: Map of Smc3 domains.....	50
Figure 17: A cartoon showing the relative position of smc3K112Q, K113Q.....	52
Figure 18: Agarose gel image of Pst1 restriction enzyme digested plasmids and plasmid map.	87
Figure 19: Survival ratings given to mutant Smc3 carriers in comparison to wild type Smc3 and the rating criteria.....	88
Figure 20: Diagram showing the relative locations of the <i>smc3QQ</i> suppressor mutations...	90
Figure 21: Cartoons of Smc3 head domain structure along with essential motifs and locations of QQ suppressor mutants.	91
Figure 22: Smc3 head domain structure cartoon showing the location of acetylation sites (K112, K113) and residues that have been mutated.....	95
Figure 23: Tetrad dissection results showing that <i>scc2EKL</i> is able to rescue <i>smc3QQ</i> , <i>R1008I</i> to normal viability but not <i>smc3QQ</i>	98
Figure 24: Diagram showing the mechanism behind the BPA crosslinking system.....	103
Figure 25: Streak to single colonies of various strains containing plasmids testing for functionality on two +5-FOA, +BPA, -leucine, -tryptophan plates.	105

Figure 26: Western blot showing a BPA crosslinking control experiment.	107
Figure 27: Anti-HA western blot of the cohesin coiled coil BPA crosslink screen.	110
Figure 28: Three western blots showing the proteins crosslinked to smc3E202BPA.	112
Figure 29: Three western blots showing the crosslink profile of smc3Q195BPA.	114
Figure 30: A cartoon diagram of partial cohesin structure as resolved by Gligoris and co-workers with marked crosslink and acetylation sites smc3K112 and K113.	116
Figure 31: Alternate view (180 degree rotation about the Y axis) of a cartoon diagram depicting partial cohesin structure as resolved by Gligoris and co-workers with marked crosslink and acetylation sites smc3K112 and K113 (Gligoris et al., 2014).	117
Figure 32: A diagram showing how the TEV protease cleavage system allows the detection of a crosslink site by analysing the pattern produced by the western blot.	120
Figure 33: A diagram highlighting the key features of the CRISPR-Cas9 plasmid used for transforming yeast.	123
Figure 34: Western blots of TEV cleaved BPA crosslinked proteins with BPA substitutions in the coiled coil region of Smc3.	125
Figure 35: Western blot and graph showing the effect of two coiled coil mutations, <i>smc3R1008I</i> and <i>E199A</i> on smc3E202BPA crosslinking efficiency.	129
Figure 36: Western blot and graph showing the effect of two coiled coil mutations, <i>smc3R1008I</i> and <i>E199A</i> on smc3Q195BPA crosslinking efficiency.	130
Figure 37: A diagram showing how BMOE crosslinks cysteine residues within 8.0 Ångströms <i>in vivo</i>	133
Figure 38: Western blots showing Smc1 cysteine residues which crosslink with smc3E202C near to both the N and C terminals.	136

Figure 39: Western blots showing Smc1 cysteine residues which crosslink with smc3Q195C near to both the N and C terminals.....	137
Figure 40: Western blots showing Smc1 cysteine residues which crosslink with smc3E213C near to both the N and C terminals.....	139
Figure 41: Cartoon diagram showing the structural model of cohesin using the data collected from the coiled coil BMOE crosslink data.....	140
Figure 42: Cartoon diagram comparing the head engaged model as resolved by Gligoris and co-workers with the predicted structural model produced in this study.	141
Figure 43: A cartoon showing the structural model of cohesin J state with predicted potential BMOE crosslink sites.	142
Figure 44: Four western blots showing crosslink products between smc3E188C and smc3K184C with various cysteine substituted residues in Smc1.....	143
Figure 45: Cartoon showing the locations of all the cysteine-substituted residues tested with the BMOE crosslinking system thus far.....	145
Figure 46: Cartoon showing cysteine substituted residues in the Smc3 and Smc1 head domain. Smc3 is coloured red while Smc1 is coloured green.....	147
Figure 47: Western blots showing the crosslinking of various cysteine substituted residues in the Smc1 and Smc3 head domain.....	148
Figure 48: A cartoon showing the refined J state model, highlighting cysteine substituted residues in the Smc1 and Smc3 coiled coil domain.	150
Figure 49: Western blot showing crosslink between smc3K184C and various cysteine substituted residues in Smc1.....	151
Figure 50: A cartoon showing a pair of cysteine residues predicted to crosslink in the resolved structure of Smc1 and Smc3 fragments.....	153

Figure 51: Western blot showing crosslink products made between cysteine pairs in Smc1 and Smc3.	154
Figure 52: Western blots showing the crosslinks formed between the coiled coil of Smc1-Smc3 and the head domains.....	157
Figure 53: Western blots showing resolution of crosslink products produced by the E and J state cysteine pairs with and without smc3K112Q, K113Q.	159
Figure 54: Western blot showing the effect of the QQ mutation on the formation of E and J state crosslink products at various stages of the cell cycle.....	163
Figure 55: Graph showing the effect of <i>smc3QQ</i> on the E and J state crosslink product formation of cohesin during various phases of the cell cycle.	165
Figure 56: Western blots showing crosslink products of BPA substituted residues near the hinge region of Smc1.....	170
Figure 57: Western blots showing crosslink products of smc1K620BPA in strains containing various tagged proteins.	171
Figure 58: Western blot showing crosslink products of various Smc3 residues that are known to crosslink Scc2 or are possible candidates.....	172
Figure 59: Western blots showing the proteins crosslinked by smc3Q67BPA.....	173
Figure 60: Western blots showing TEV cleavage products of Scc2 crosslinked by smc1K620BPA.	175
Figure 61: Western blots showing TEV cleavage products of Scc2 crosslinked by smc1K620BPA within a smaller range.	177
Figure 62: Western blots showing TEV cleavage products of Scc2 crosslinked by smc3Q67BPA.	178

Figure 63: Map of the BPA crosslinking sites between Smc1, Smc3 and Scc2 found by TEV cleavage..... 179

Figure 64: Western blot and a graph showing the effect of various mutations on the crosslinking efficiency of smc3Q67BPA with Scc2. 180

Figure 65: Diagram of the proposed loading mechanism and effect of QQ. 195

Figure 66: FACS histograms showing DNA content in cultures used during the cell cycle arrest experiments. 255

Tables

Table 1: Comparison of various <i>SMC</i> complexes (Palecek and Gruber, 2015).	19
Table 2: Amino acid supplement mixture.	60
Table 3: All possible haploid genotypes with “mutation” representing a candidate <i>smc3QQ</i> suppressor mutation.	85
Table 4: Viability of mutations in the KKD strand opposing helix.	96
Table 5: Factors affecting <i>in vitro</i> ATP hydrolysis activity in tabular form.	184
Table 6: Primer list. All primers listed are sourced from this study.	221
Table 7: Plasmid list.....	227
Table 8: Yeast strain list. Background: W303, <i>S. cerevisiae</i>	231
Table 9: Results of QQ suppressor screen.	253

1.0 Abstract

Cohesin is a protein complex involved in creating sister chromatid cohesion during mitosis and performs this role by forming topological entrapment around both chromatids. Cohesin consists of four subunits: Smc1, Smc3, Scc1 (Mcd1 in yeast), and Scc3. Cohesin is loaded onto DNA by the action of a loading complex composed of Scc2 and Scc4. Cohesin is released from the DNA by the releasing complex composed of Wapl (Rad61 in yeast) and Pds5. Both loading and releasing processes are ATP-dependent and rely on machinery present in Smc1 and Smc3. Acetylation of the cohesin subunit, Smc3, at position K112, K113 is required for successful cohesion as this abolishes the cohesin releasing activity of Wapl and likely the loading action of Scc2-Scc4. Why acetylation may abolish releasing and loading activity is not understood. However, changes to ATP binding and hydrolysis activity may be involved. Data in this study suggest that acetylation may reduce potential Scc2 dependent ATP hydrolysis activity, as acetylated cohesin mimicking forms of cohesin (smc3K112Q, K113Q) have been shown to have significantly lower activity than wild type cohesin. Further data suggests that smc3K112Q, K113Q may inhibit loading and releasing activity by promoting a different configuration between Smc3 and Smc1, forming either a rod or a ring structure. The two configurations investigated in this study, E state (Smc1-Smc3 head domains engaged) and J state (Smc1-Smc3 head domains juxtaposed) may be controlled by cohesin loading and releasing complexes via certain interaction sites located near Smc3K112, K113 and R1008. Mutations near these sites are shown to either contribute to rescuing Scc2 interaction, which is largely abolished by smc3K112Q, K113Q or interact with Scc2 itself. The interaction between

the coiled coils of Smc3 and Smc1 was shown to be incompatible with certain head domain configurations via crosslinking assays, thus verifying their mutual exclusivity. The difference between these configurations determines whether ATP hydrolysis activity is possible or not, thereby controlling loading and releasing activity.

2.0 Introduction and literature review

2.1 The cell cycle

All eukaryotic cells follow the cell cycle and reproduce via mitotic cell division in a sequence shown in figure 1. Prior to mitosis, a period known as S phase takes place where DNA replication occurs. The duplication of the genome allows a copy to be distributed to each daughter cell during mitosis.

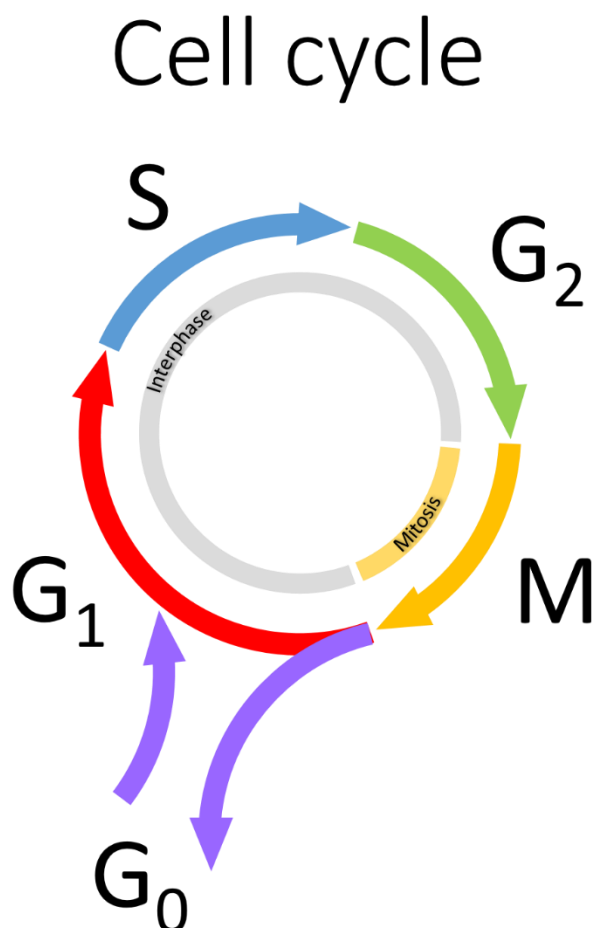


Figure 1: Diagram showing the phases of the cell cycle in eukaryotes.

Interphase consists of G_1 , S, and G_2 phase. Cell division occurs only during M phase. G_0 phase is a state of quiescence where cells exit the cell cycle and stop replicating. There is low expression of cell cycle regulating proteins and other proteins involved in DNA replication during this phase. This state is reversible unlike senescence which is a permanent transition to G_0 (Foster et al., 2010). G_1 phase is a stage where growth occurs in preparation for S phase. This growth involves expression of proteins necessary for metabolic processes, cell cycle regulating proteins and assembly of organelles which further aid DNA replication (Foster et al., 2010). S phase is characterised by the beginning of DNA replication. During this phase, inactive replication machinery assembled in G_1 phase is activated and DNA is replicated. DNA damage accumulated before this stage is repaired during replication (Takeda and Dutta, 2005). G_2 phase comprises of a period of rapid growth in the form of expressing proteins in preparation of M phase which are required for physical separation of the cell (Kousholt et al., 2012). M phase stands for mitosis and is the stage where the chromosomes of the cell are segregated equally in two separate nuclei. This stage can be divided into five further stages. Diagram adapted from Vermeulen and co-workers (Vermeulen et al., 2003).

Mitosis itself contains five visibly distinct stages and can be identified by the activity of the chromosomes within the cell.

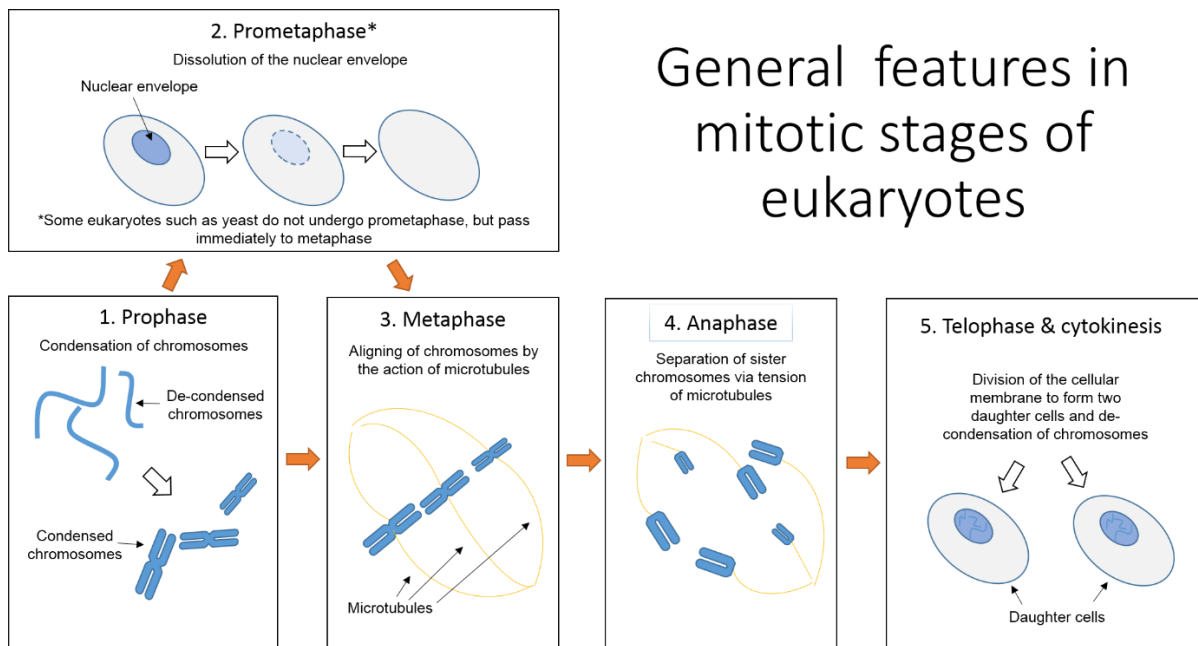


Figure 2: A simplified description of mitosis consisting of five main phases: prophase, prometaphase, metaphase, anaphase, and telophase.

As mitosis is an incredibly diverse process across eukaryotes, the diagram shows only the behaviour of the chromosomes and not the rest of the cell. The diagram is therefore not representative of mitosis in any particular organism but rather a visual aid to assist the description of common processes between eukaryotes.

During prophase, identical copies of each chromosome known as sister chromatids are condensed into a compact form and associate with spindle fibres via the kinetochore. At metaphase, the action of the spindle fibres orient the chromosomes along the metaphase plate. By anaphase, the sister chromatids are pulled away from each other towards the poles of the cells. Finally, at telophase, each complete set of sister chromatids de-condense and mitosis is completed. Although this process may

differ slightly between eukaryotic organisms, the principle of faithful chromosome segregation during the cell cycle remains the same.

For the cell cycle to be completed successfully, the sister chromatids must remain associated with each other throughout S phase until anaphase. Failure to do so may lead to an improper segregation of sister chromatids, known as nondisjunction and cause aneuploidy, or even anucleate cells (cells without a nucleus). This is because faithful segregation of chromosomes depends on pulling forces generated by the mitotic spindle. These forces pull the sister chromatids in opposite directions and balance them on the metaphase plate. Such bi-orientation is only possible if the sister chromatids are held together in some way, allowing the generation of spindle forces. The phenomenon of the sister chromatids remaining within very close proximity of each other between S phase and anaphase is known as sister chromatid cohesion (Nasmyth and Haering, 2009).

2.2 Sister chromatid cohesion proteins: The SMC family, history and application

DNA replication is known to cause concatenated DNA loops. Sister chromatid cohesion was originally thought to be produced only by DNA catenation resulting from DNA replication. DNA type II topoisomerase was thought to resolve this concatenation during anaphase by creating a double-strand break in the DNA before passing the loop through, thus untangling the strands. Holm and co-workers showed this with temperature sensitive alleles of DNA type II topoisomerase that caused cell death at mitosis in *S. cerevisiae* above the permissive temperature (Holm et al., 1985). DNA gyrase (DNA type II topoisomerase subclass) was also found to be critical in bacterial chromosome partitioning (Luttinger et al., 1991), accompanied with an accumulation of DNA catenanes when it is mutated (Adams et al., 1992). However, the idea of DNA catenation based sister chromatid cohesion was later disproven by Koshland and co-workers, which showed that mini-chromosomes are not topologically intertwined in arrested *S. cerevisiae* cells before anaphase (Koshland and Hartwell, 1987). This was achieved by extracting mini-chromosomes from cells arrested in various stages of the cell cycle and visualising the DNA using Southern blot. Most of the mini-chromosomes were not dimerised which was to be expected if the principle mechanism of sister chromatid cohesion was DNA catenation (Koshland and Hartwell, 1987). This finding made it likely that sister chromatid cohesion was more dependent on protein interaction. Genes involved in sister chromatid cohesion were identified by multiple genetics screens which involved mutating these genes and observing the rate of mini-chromosome loss. The loss of a mini-chromosome could easily be identified in two ways. The first method is by fluorescently staining chromosomes and observing the segregation under low-light conditions to prevent arrest (Kouprina et al., 1988;

Larionov et al., 1985; Maine et al., 1984). The second method was by introducing an artificial mini-chromosome with the gene of an enzyme involved in adenine synthesis, *ADE2* (Shero et al., 1991). Strains with $\Delta ade2$ but without the mini-chromosome, form colonies red in colour, thus colouration is the assay for loss of the mini-chromosome. Later, a particular protein was found in yeast, named Smc1 (Structural Maintenance of Chromosomes 1). Smc1 was found to be essential in cell division at all temperatures and mutations in the gene caused non-disjunction of chromosomes (Strunnikov et al., 1993). SMC proteins were also discovered to be highly conserved amongst many eukaryotic organisms (Strunnikov et al., 1993). Soon after, other proteins with similar structures involved in the condensation of chromosomes were found using immunocytochemistry in *Xenopus* and chicken cells (Hirano and Mitchison, 1994; Saitoh et al., 1994). Strunnikov and co-workers showed that Smc1 and the chromosome condensing Smc2 perform different essential roles despite protein sequence similarity as deletion of either is lethal in *S. cerevisiae*. These similarities were found from genetic, biochemical and evolutionary data. For example, the presence of all the same putative domains as Smc1, the ability to bind ATP and comparisons to homologues in other related organisms. Phylogenetic analysis of sister chromatid cohesion associated proteins from various organisms revealed that all of the proteins are in fact likely to be genetically related (Strunnikov et al., 1995). Furthermore, immunocytochemistry experiments visibly showed that Smc2 and not Smc1 is responsible for chromosome condensation as mutations in the *SMC2* gene lead to inability to condense chromosomes before mitosis (Strunnikov et al., 1995). SMC proteins were also found to have utility beyond cohesion and condensation. Smc4, much like Smc2 is also critically involved in chromosome condensation. A homologue of Smc4 called Dpy-27 in *C. elegans* was shown to down-regulate genes

in the X chromosome as part of dosage compensation which required translocation of *DPY* proteins to the nucleus (Chuang et al., 1994). By mutating the dosage compensation controller, *XOL-1*, this prevented localisation, as seen by immunohistochemistry. This was the first evidence of a selective mechanism which controlled gene expression by way of SMC proteins (Chuang et al., 1994).

In addition to cohesion and condensation SMC proteins, a further distinct complex type consisting of Smc5-Smc6 was discovered with implications in DNA damage repair. Mutations in the *S. pombe* gene *RAD18* was found to cause ionising radiation hypersensitivity and deletion is lethal. Repair of DNA lesions between pyrimidines caused by UV light and cyclobutane is impaired by *RAD18* mutations. These DNA lesions were detected by enzyme linked immunosorbent assay (ELISA). The structure of Rad18 and the *S. cerevisiae* homologue, Rhc18, both share the basic characteristics of SMC proteins consisting of ATP binding domains separated by a long coiled coil and hinge, sharing considerable similarity in amino acid sequences, especially at the ATP binding domains (Lehmann et al., 1995). At this point, SMC type proteins were known to be involved in critical cellular processes such as: DNA repair, gene expression, sister chromatid cohesin, and chromosome condensation. More similarities of these complexes were later found which eventually lead towards a unified model of SMC complex function which would attempt to answer how a single protein platform can perform roles in a variety of DNA involved processes (Michaelis et al., 1997). In 1997, a protein associated with SMC proteins in yeast was discovered (Michaelis et al., 1997). The protein Scc1 (Mcd1 in *S. cerevisiae*), was shown by fluorescent *in-situ* hybridisation (FISH) to produce sister chromatid cohesion and dissociate after proteolysis during anaphase, via analysis of mutants and chromosome

spreading. Interaction with chromosomes and Smc1 was also detected using chromosome spreading with immunofluorescence. The term “cohesin” was then coined; describing a complex responsible for sister chromatid cohesion involving Smc1, Smc3, and Scc1 (Michaelis et al., 1997). Cohesin was then found to be responsible for generating dynamic tension between the spindle pole bodies connected to kinetochores by microtubules. FISH showed that sister chromatid cohesion is lost and not regained after the cleavage of Scc1 (Tanaka et al., 2000). The highly evolutionarily conserved proteins that interacted with all three SMC protein complexes were later identified by basic local alignment search tools (BLAST) as a superfamily, named the kleisins (Schleiffer et al., 2003). Kleisins contain conserved globular N and C termini that associate with SMC proteins, joined together with a variable length linker region (Schleiffer et al., 2003). Experimentally, this was already confirmed in cohesin and condensin by co-immunoprecipitation (Guacci et al., 1997; Hirano et al., 1997; Michaelis et al., 1997; Onn et al., 2007). Finally, a kleisin, Nse4, was confirmed to associate with Smc5-Smc6 complexes by co-immunoprecipitation and yeast two hybrid analysis in *S. cerevisiae* (Hu et al., 2005; Palecek et al., 2006).

2.2.1 Prokaryotic SMC complexes

Bacteria also possess SMC-related complexes. In 1989, *E.coli* with mutations in an undescribed gene coding for a large 177 kDa protein were discovered to regularly produce anucleate cells (Hiraga et al., 1989). The gene was named *MUKB* and further investigation of its protein product, MukB, led to the conclusion that mutations of this protein were linked to chromosome partitioning (Hiraga et al., 1989). This process is not the same as eukaryotic disjunction as bacteria do not have spindle apparatus, but is related in the way that it does topologically hold sister chromatids together. It was also found that MukB was required for normal cell division at higher temperatures (Niki et al., 1991). Electron microscopy later revealed that as predicted by the amino acid sequence of MukB, the structure consisted of globular ATP binding domains separated by a long coil region containing a hinge in the middle, much like SMC proteins (Niki et al., 1992). Chromatography of purified MukB and gel retardation assays in the same study showed DNA binding capabilities (Niki et al., 1992). Finally, the cohesin-like complex was found in bacteria which began by the discovery that the phenomenon of sister chromatid cohesion did not exclusively depend on the SMC-like MukB in *E.coli* (Yamanaka et al., 1996). MukB was found to be expressed alongside two other proteins important for faithful chromosome segregation, MukE and MukF. Null mutants of these two proteins exhibit the same anucleate production characteristics of MukB null mutants (Yamanaka et al., 1996). This complex is similar to cohesin but not the same, as the SMC-dimer protein is heterodimeric while the MukBEF is homodimeric. For reference, figure 7 and table 1 highlight the various differences between SMC complexes found in both eukaryotic and prokaryotic organisms.

2.3 The ring model of SMC complexes

The jump to the contemporary model of cohesin came in 2002, when the ring model consisting of the rod shaped Smc1-Smc3 dimer and kleisin Scc1 was proposed (Haering et al., 2002). A simple illustration found below in figure 3 shows the first models of operation. Scc1 was shown to interact with the head domains of Smc1 and Smc3, forming a tripartite ring-like structure. This was demonstrated by removing the head domains of Smc1 and Smc3 which abolished Scc1 co-immunoprecipitation. The head domains alone of either SMC protein also may bind to Scc1 (Haering et al., 2002). The new ring model entailing the topological entrapment of DNA by cohesin became a distinct possibility; and has only been further strengthened with experiments concatenating closed DNA loops using cohesin. The first evidence of the ring model came by Gruber and co-workers where the introduction of artificial cleavage sites in the Smc3 coiled coil also induced loss of sister chromatid cohesion (Gruber et al., 2003). Further support of concatenation of chromosomal DNA by cohesin came by the capture of mini-chromosomes in *S. cerevisiae* using immunoprecipitation. The ability of cohesin to capture mini-chromosomes was lost when either were cleaved (Ivanov and Nasmyth, 2005). The strongest evidence of topological entrapment involved trapping mini-chromosomes together in yeast with single cohesin complexes which had Smc1, Smc3 and Scc1 interfaces covalently crosslinked using bismaleimidoethane (BMOE) and by splicing Scc1 and Smc3 together, forming a fusion protein. BMOE is a chemical which attacks sulfhydryl bonds and covalently join two of these groups together. Cysteine contains these groups and strategically introduced amino acid substitutions can yield highly efficient crosslinks (further explained in 4.2.4.1). This result involved treatment of the cohesin-DNA concatenates

at high temperatures and in the presence of SDS treatment, suggesting that the interaction is likely topological (Haering et al., 2008). This was later repeated without the use of fusion proteins and identification of captured products was verified (Srinivasan et al., 2018). Despite the evidence for topological entrapment, there are numerous methods of which cohesin may produce sister chromatid cohesion. The possibilities however may be categorised into two types; the strong and weak ring models.

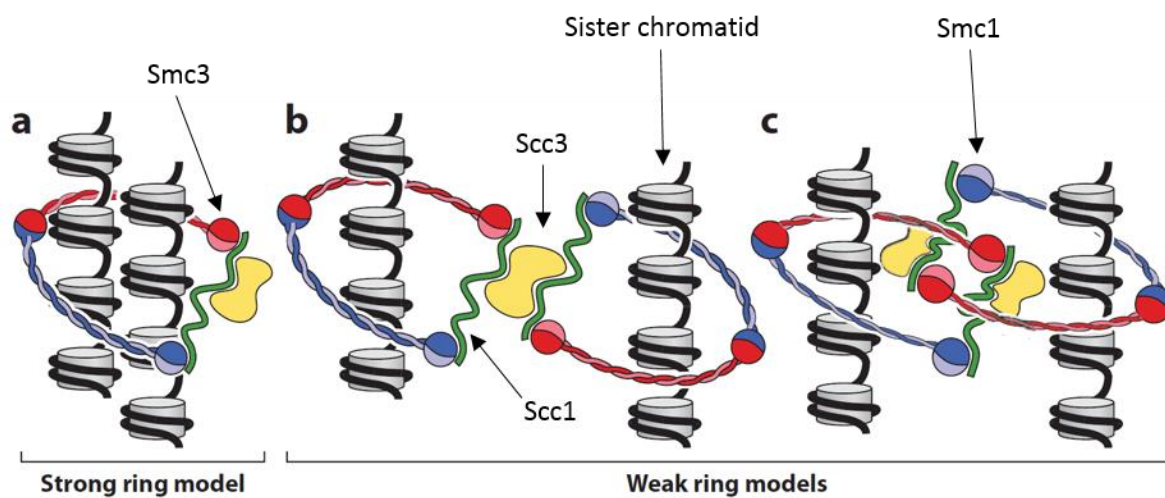


Figure 3: Illustration of the strong ring and weak ring models.

(a) The strong ring model: A single cohesin complex embraces both sister chromatids after DNA replication. (b) Weak ring model: Each sister chromatid is embraced by a single cohesin complex and are held together by a non-topological interaction. (c) A variation of the weak ring model: Similar to (b) however, the cohesin complexes embracing each sister chromatid are also topologically linked with each other. Also known as the “handcuff” model. Diagram from Nasmyth and co-workers (Nasmyth and Haering, 2009).

Evidence for the strong ring model is more established as this arrangement has been detected as mentioned previously (Haering et al., 2008). Concatenated or oligomeric cohesin complexes may exist *in vivo* but have proven difficult to detect and for that reason are probably not the principle mechanism of which sister chromatid cohesion is generated. Förster resonance energy transfer (FRET) failed to detect hinge to hinge or head to head interactions between different complexes of cohesin, indicating that any interaction between cohesin complexes is probably not of this nature (Mc Intyre et al., 2007). Interaction between Smc1 and Smc3 have been detected in mammalian cells by co-immunoprecipitation. However, this has only been achieved with the use of high-expression plasmids and not at physiological levels which casts doubts to whether this actually occurs normally *in vivo* (Zhang et al., 2008). Other overexpression experiments in insect cells using the baculovirus system have found that certain interactions such as Scc1 connecting two Smc1-Smc3 heterodimers, simply does not occur at normal levels (Zhang et al., 2013). In any case, these concatenated or oligomeric cohesin complexes should have been detected in the supporting mini-chromosome experiments (Gruber et al., 2003; Haering et al., 2008).

2.4 Current understanding of cohesin structure and function

Cohesin is now known as a protein complex, consisting of at least four subunits and critically involved in normal chromosome partitioning during cell division in eukaryotes. These subunits are highly conserved across eukaryotic species with all known eukaryotes possessing homologues of the four core subunits of cohesin: Smc1, Smc3, Scc1 and Scc3. In yeast, the core subunits are of the same name with exception to Scc1 and Scc3; which are known as Mcd1 and Irr1 respectively (Nasmyth, 2001; Uhlmann, 2016). Scc3, is an essential subunit of cohesin discovered in yeast and can be co-immunoprecipitated with the rest of the complex (Kurlandzka et al., 1995; Tóth et al., 1999). This protein associates with cohesin via Scc1 and is necessary for recruitment to DNA and maintaining entrapment (Hu et al., 2011). Mutating the critical Scc1 sites for Scc3 binding prevents visualisation of GFP tagged cohesin from accumulating on the pericentromere (Hu et al., 2011). As Scc1 tagged with GFP produces barrel formations on the pericentromere, indicating loaded cohesin, deleting a short part of Scc1 (residues 319-327) responsible for Scc3 interaction causes the GFP to be distributed dispersedly within the nucleus which represents loss of successful chromatin association (Hu et al., 2011). Temperature sensitive and auxin induced degradation variants of Scc3 also cause loss of sister chromatid cohesion as seen by fluorescent live cell imaging (Roig et al., 2014). Figure 4 illustrates the effect of Scc3 interaction loss on sister chromatid cohesion. The structure of Scc3 has been determined using X-ray crystallography but not its interaction orientation with Scc1 (Roig et al., 2014).

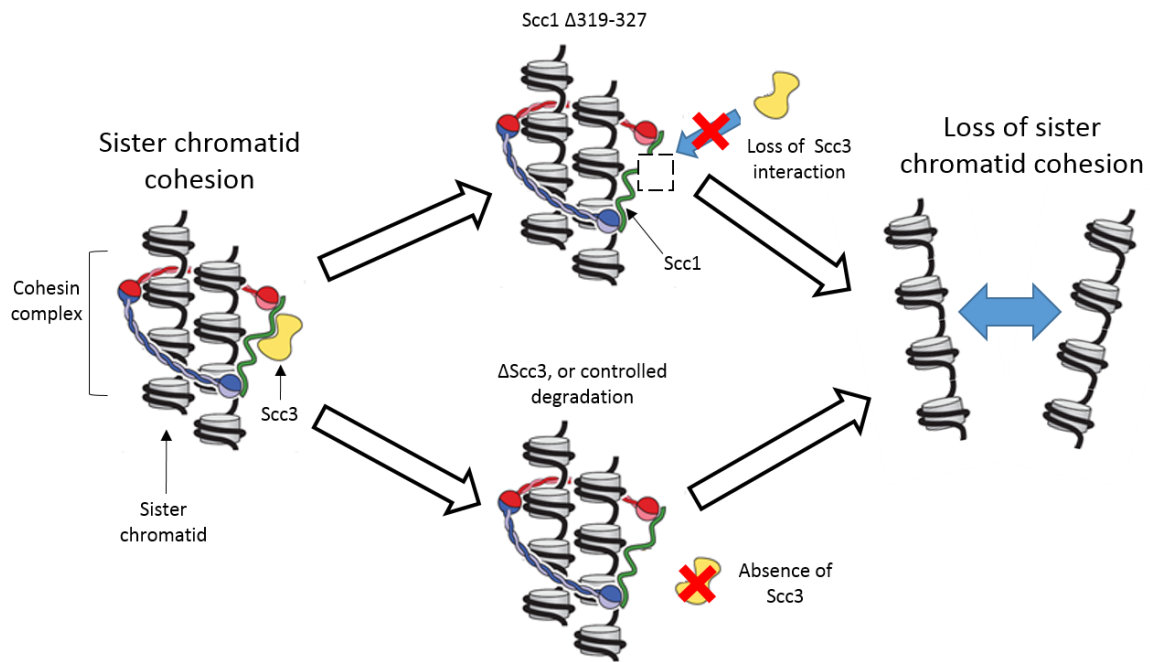


Figure 4: Diagram to illustrate the importance of Scc3 in maintaining sister chromatid cohesion.

Deletion of Scc3 or the Scc3 interaction site in Scc1 will cause loss of cohesion. Diagram adapted from Nasmyth and co-workers (Nasmyth and Haering, 2009).

All of the four subunits are essential and known to form a complex. Epitope tagging of these proteins allows simultaneous capture by immunoprecipitation of Scc1 and identification by western blot (Tóth et al., 1999). There are other notable proteins for producing sister chromatid cohesion associated with cohesin such as: Scc2, Eco1, Pds5, and Wapl but these are not immediate members of the complex. This is because once cohesin has entrapped sister chromatids, it is stable and only by the action of other proteins is it removed, or modified (Beckouët et al., 2016).

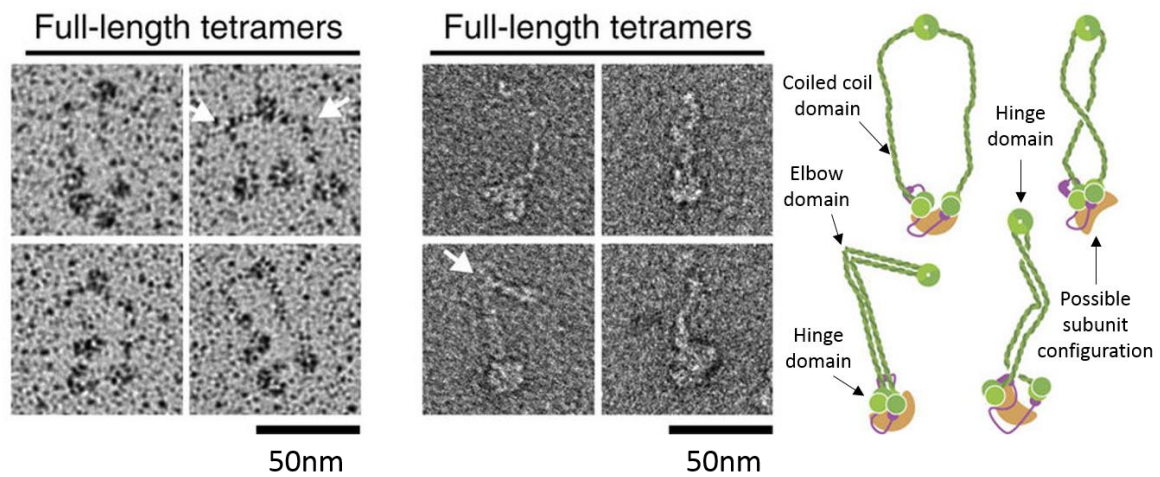


Figure 5: Electron micrographs of cohesin.

Left: Metal shadowed electron micrographs of fully assembled modified human cohesin with all four core subunits. *Centre:* Further micrographs, but with uranyl formate staining. *Right:* Cartoon representations of the cohesin complexes seen at centre. Scale bar: 50nm. Diagram from Hons and co-workers (Hons et al., 2016).

Figure 5 shows what form the cohesin complex takes and the flexibility of the coiled coil domains. Cohesin most definitely may form a ring like structure but due to the flexibility of the coiled coil domains attempts at using electron microscopy (EM) or X-ray crystallography to resolve the structure in entirety have failed. In theory, combining EM with crosslinking of amino acids between subunits of cohesin could stabilise the configuration sufficiently for structural resolution. This has been attempted by truncating the coiled coil domains to achieve enough stability for EM to resolve the orientation of Pds5 crosslinked to the head domains of Smc1-Smc3 using disuccinimidyl suberate. This allowed resolution of 35 Ångströms, which was enough to see that Pds5 bridges across the interfaces between Scc3, Scc1 and Smc3 near

the Smc head domains (Hons *et al.*, 2016). This structural position may later explain the mechanical function of Pds5. Figure 6 shows the parts of cohesin that have been successfully determined by X-ray crystallography.

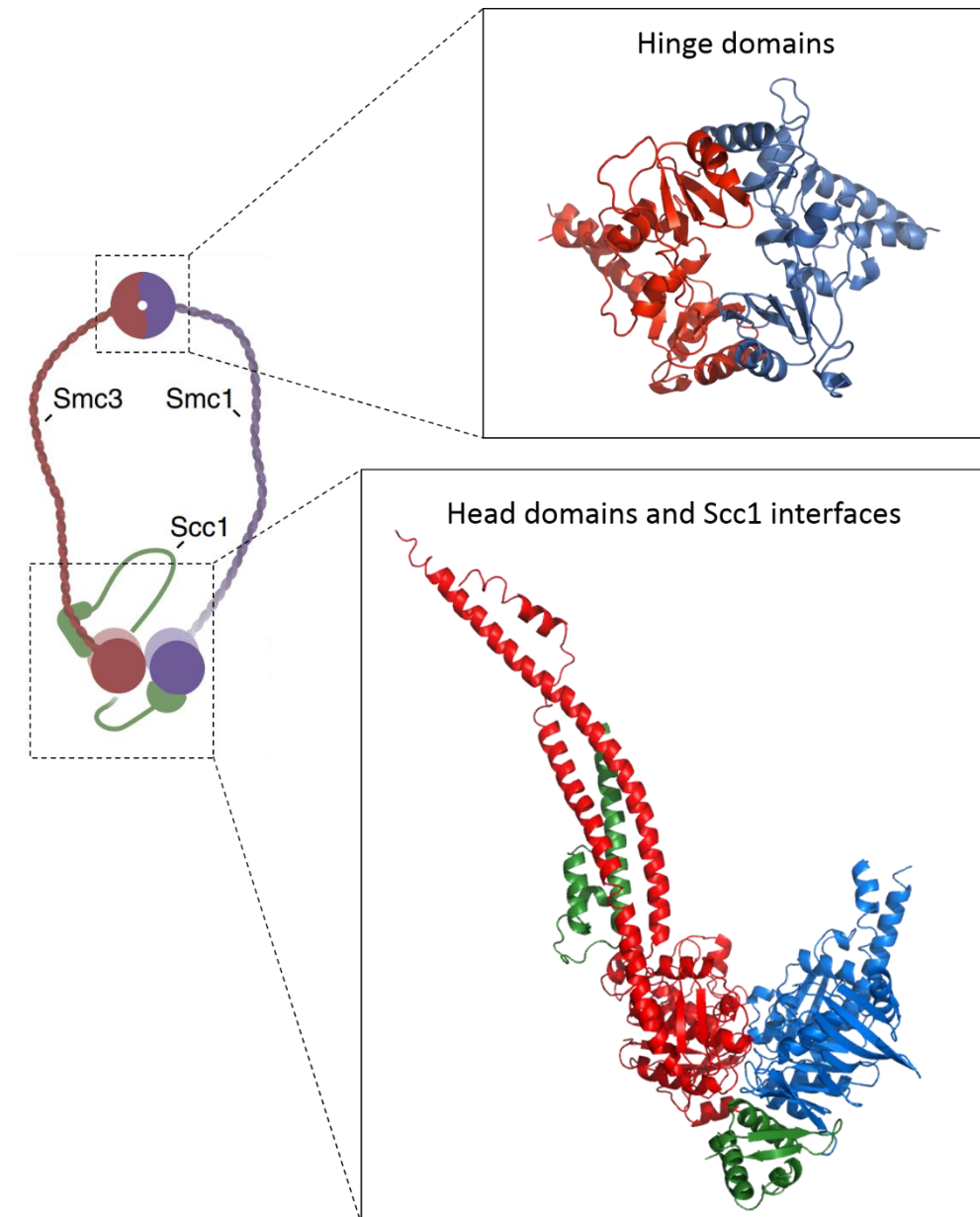


Figure 6: A cartoon representation of the cohesin tetramer with highlighted resolved regions.

Left: A model of cohesin approximately to proportion of the subunits. *Top right:* Resolved X-ray crystallography structure of the hinge dimerization region. *Bottom right:* Resolved X-ray crystallography structure of the Smc1-Smc3 head domains in the ATP binding configuration

with limited coiled coil regions and Scc1 binding sites. Diagram adapted from Hons and co-workers (Hons et al., 2016).

Other SMC complexes share similar characteristics as cohesin and possess related subunits. Below is table 1 and figure 7 comparing various elements of four different complexes.

Table 1: Comparison of various *SMC* complexes (Palecek and Gruber, 2015).

Name of complex	Cohesin	Condensin	Smc5-Smc6	MukBEF
SMC protein constituent	Smc1-Smc3	Smc2-Smc4	Smc5-Smc6	MukB-MukB
Kleisin constituent	Mcd1	Cap-H	Nse4	MukF
HAWK / KITE constituent	Scc3 (HAWK)	Cap-D2, Cap-G (HAWK)	Nse1, Nse3 (KITE)	MukE (KITE)
Origin	<i>S. cerevisiae</i>	<i>D. melanogaster</i>	<i>S. cerevisiae</i>	<i>E. coli</i>
Primary role	Sister chromatid cohesion	Chromosome condensation	DNA damage repair	Sister chromatid cohesion

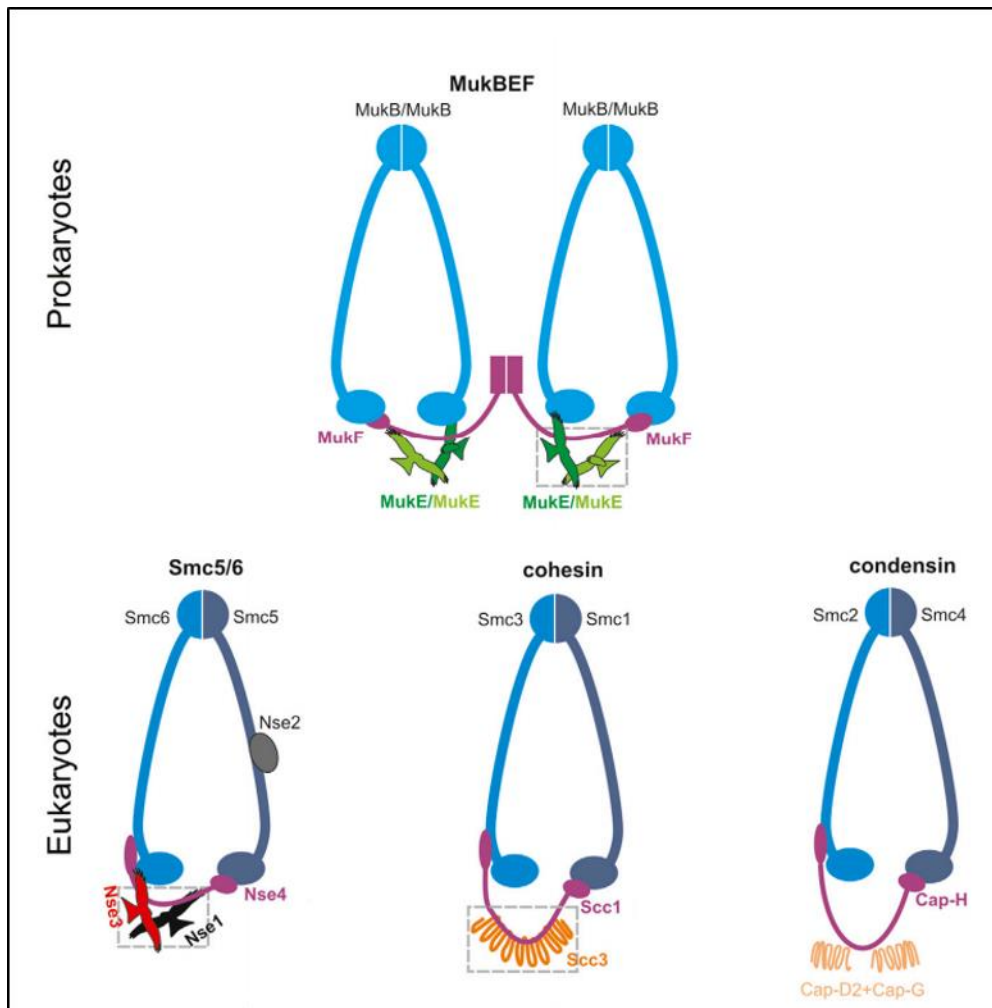


Figure 7: Cartoon diagrams of four different types of SMC complexes and their core subunits as visual aid to table 1.

Diagram adapted from Palecek and co-workers (Palecek and Gruber, 2015).

Although current understanding of the structure of cohesin is incomplete, a number of key features have been established. For example, it is known exactly where Scc1 binds to Smc3 and Smc1, where Scc3 binds to Scc1, and that Scc1 possesses two cleavage sites (Hons *et al.*, 2016). The ATP binding head domain of Smc3 have been resolved using X-ray crystallography, but without its hinge and much of the coiled coil

domains. This was achieved by expressing only the head domain and a part of the coiled coil along with a short N terminal fragment of Scc1 which self-assembled in *E.coli* suitable for crystallisation (Gligoris et al., 2014). The head domain of Smc1 has also been resolved using X-ray crystallography, including association with Scc1 which is included in figure 6. Unlike Gligoris and co-workers, this was performed by expression in insect cells using the baculovirus expression system (Haering et al., 2004). UV crosslinking demonstrated that the N terminal of Scc1 binds to Smc3 at the coiled coil region very close to the head domain (Gligoris et al., 2014). The coiled coil regions and Scc1 have not been resolved in entirety due to the difficulty of crystallisation and the low electron density of these parts. Full-length prokaryotic SMC protein has been resolved but only in parts before joining the sections together *in silico* (Diebold-Durand et al., 2017). This approach, although a first step towards understanding the possible configurations of cohesin, tells little about the dynamics of cohesin during the performance of critical functions. Another important feature of SMC proteins are a supposed “elbow” region where the coiled coil regions allow bending of the complex to obtuse angles (see figure 5 for EM evidence and figure 8 for a model of elbow function). This region was found by crosslinking folded SMC complexes in *E. coli* and *S. cerevisiae* as found by EM and using mass-spectrometry to find the crosslink sites (Bürmann et al., 2019). This is supported by crosslinking Pds5 to both the hinge and head domains in yeast which indicated that the two regions may be bridged by folding and in addition, conservation analysis shows that a predicted break in alpha helix structure is conserved in all types of SMC protein in yeast and MukB (Bürmann et al., 2019).

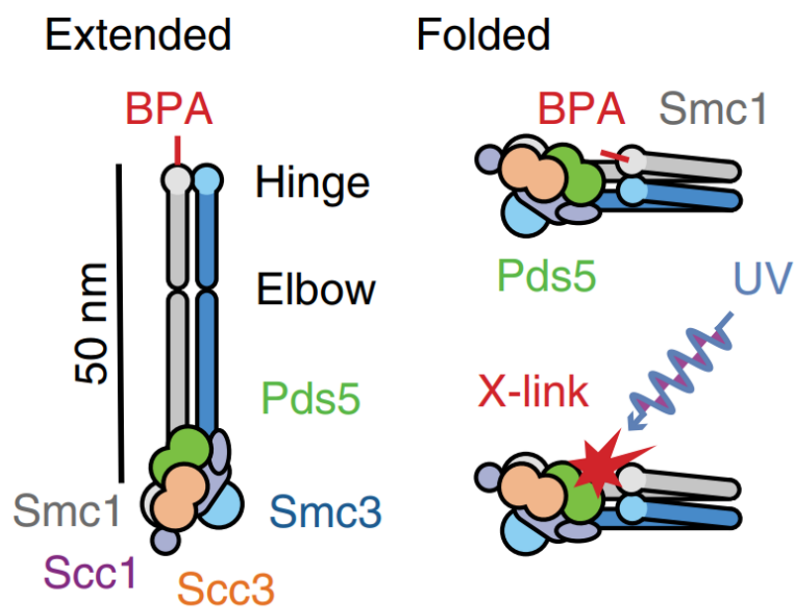
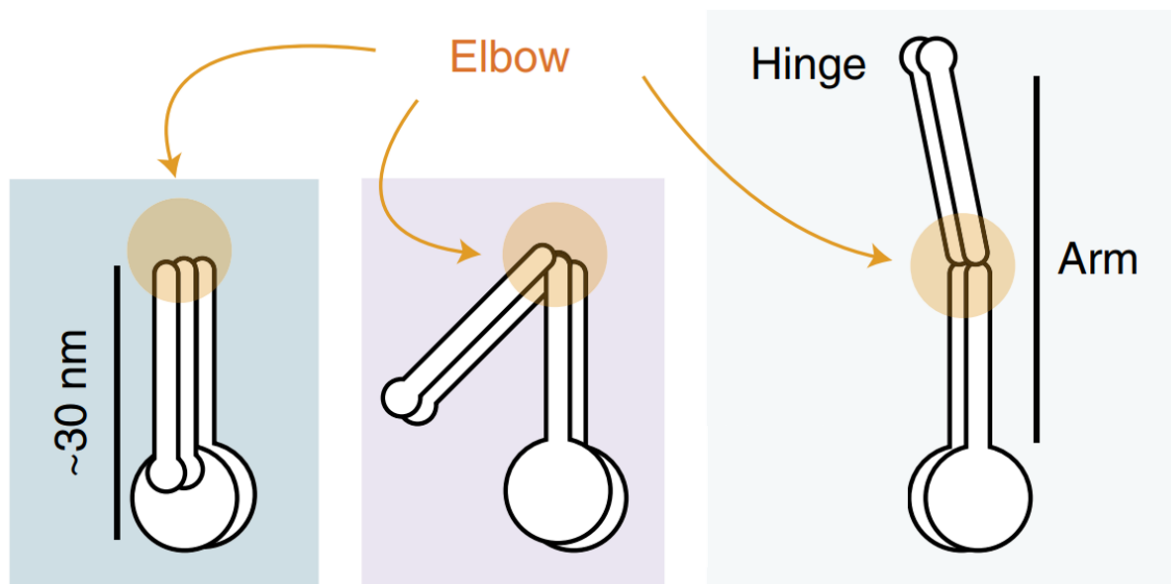


Figure 8: Simplified diagram to show how the elbow region of cohesin allows crosslinking between the distant hinge and subunits near to the head domains.

(Top): A simple 3-part cartoon showing that a hyper flexible elbow region is necessary to bridge the gap between the hinge and the bulbous head domains of cohesin. (Bottom): A more elaborate 2-part cartoon showing the relative positions of cohesin subunits to allow the

possibility of crosslinking between the hinge domain and Pds5. Diagram adapted from Bürmann and co-workers (Bürmann et al., 2019).

Diebold-Durand and co-workers along with Bürmann and co-workers together suggest that cohesin is a ring but does not entrap DNA in the lumen of Smc1-Smc3, but rather form a rod shape which does not appear to have space to house sister chromatids. To explain where the housing could be, further entrapment of DNA mini-chromosomes using cohesin and BMOE cysteine crosslinking revealed that DNA is captured in a particular compartment of the cohesin ring. This area is encircled by the head domains of the two SMC proteins and the kleisin (Chapard et al., 2019). This result has also been demonstrated in condensin using similar methods (Vazquez Nunez et al., 2019). However, capture of DNA in the lumen of cohesin is possible when ATP hydrolysis activity of the head domains is abrogated by mutation, suggesting that passage across the lumen is a transient but essential step involved in entrapment (Vazquez Nunez et al., 2019). Figure 9 shows various configurations which cohesin has been tested to entrap DNA.

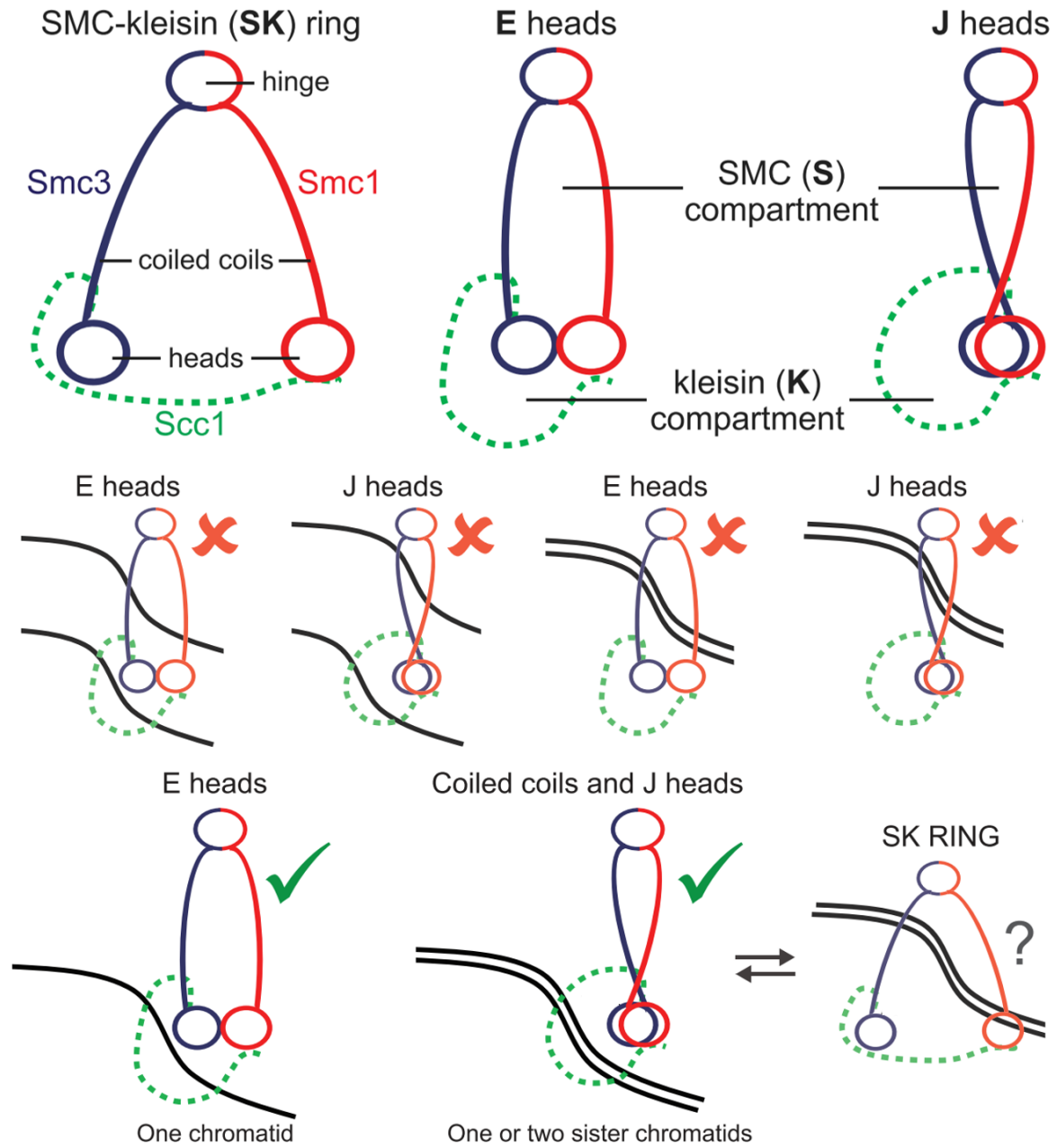


Figure 9: A diagram showing possible DNA entrapment configurations of cohesin and which combinations of these states captured DNA during crosslinking experiments.

From the diagram, only the kleisin (K) compartment captured DNA in any combination and was able to capture one or two sister chromatids. The S compartment, also known as the lumen, may only capture DNA in the SK ring form however it is unknown whether there is a transitional stage between coiled coils and J state capture. The E state heads configuration is

a configuration of cohesin where the Smc1-Smc3 head domains are engaged in the ATP binding state which can be seen in figure 6. The J state is different configuration of which structure was investigated later on in this study and has also been confirmed experimentally in the literature. Diagram adapted from Chapard and co-workers. (Chapard et al., 2019)

As for the function of cohesin, it has been implicated in a number of overlapping roles. For example, the yeast Scc1 kleisin subunit, Mcd1, has been shown to be essential for sister chromatid cohesion and condensation by FISH (Guacci et al., 1997). The role of cohesin in regulating genes may be in bringing enhancer and promoter DNA close together for activation by a transcription factor. Cohesin is heavily involved in forming loops in the DNA. The loss of cohesin eliminates all DNA loops but with little widespread effect on gene expression which is reflected in high-throughput chromosome conformation capture (Hi-C) mapping of topological association (Rao et al., 2017). Hi-C is a technique where the chromatin is crosslinked using formaldehyde which captures any loops of DNA where two distantly separated sequences are folded together. The DNA is then extracted and treated with restriction nucleases which digests the DNA into small fragments. The ends of these small fragments are ligated together and the crosslinking is reversed, leaving a recombinant strand of DNA. This strand is sequenced to reveal the locations of these DNA loops when compared to the fully sequenced genome of the organism. This technique allows the detection of cohesin-mediated topologically associated domains.

Condensin possesses the ability to entrap and traverse DNA in an ATP-dependent manner. This was demonstrated by observing fluorophore tagged condensin move

along DNA *in vivo* and *in vitro* using total internal reflection and epi-fluorescence microscopy (Ganji et al., 2018; Terakawa et al., 2017). It is hypothesised that cohesin produces loops in DNA by capturing nearby loops of DNA from a chromosome in the same way. Models of the exact biochemical mechanism have been designed (Diebold-Durand *et al.*, 2017).

Cohesin is involved in cellular-controlled DNA damage repair as part of meiosis and other forms of damage such as base pair mismatch due to methylation found during mitosis (Ladstätter and Tachibana-Konwalski, 2016; Eijpe et al., 2003). In eukaryotes, the Scc1 kleisin is replaced in the complex with Rec8 for meiotic applications and can be visualised during meiosis using immunofluorescence (Eijpe et al., 2003). During meiosis, cohesin holds together the synaptonemal complex; the structure which allows chromosomal crossover. Deletion of *REC8* or inactivation of Smc3 causes defects in synapsis (Klein et al., 1999).

During the mitotic cycle, cohesin is required for double-strand break (DSB) repair induced by replication or gamma radiation in the sister chromatid exchange pathway. Inactivation of temperature sensitive cohesin subunits in yeast prevents DSB resolution (Cortés-Ledesma and Aguilera, 2006; Sjögren and Nasmyth, 2001).

As eukaryotic organisms tend to have much larger and more complex genomes, it is thought that cohesin/cohesin-like complexes are conserved more strongly across eukaryotes than prokaryotes as a necessity (Uhlmann, 2016). All of these functions

associated with cohesin rely on the ability to selectively control association and entrapment of DNA. Therefore, there must be methods of directing cohesin loading onto chromatin and mechanisms of control to activate these functions selectively.

2.5 Loading of cohesin onto the chromatid

The exact mechanism of action behind loading cohesin onto chromatin to create sister chromatid cohesion that SMC proteins are directly linked to is still unknown; however the sequencing of SMC genes identified a number of key features that have shed light on the inner workings of the proteins (Strunnikov et al., 1993). SMC proteins contain elements that are structurally related to ABC transporters often found in the cellular membrane. Most notably, these are the Walker motifs and ABC signature motifs which necessarily require to be localised in order to perform ATP hydrolysis that is essential for transporter function (Ter Beek et al., 2014). The current model of cohesin loading involves ATP binding to the Walker A and B motifs of Smc3 and the ABC signature motif of Smc1. These features are contained in the head domains of Smc1 and Smc3 and the ATP binding conformation brings both heads together as shown by EM (Gligoris et al., 2014; Hons et al., 2016). ATP binding is also critical for assembling the cohesin ring by facilitating binding of Scc1 to Smc1. Mutations in the Smc1 ATP binding domain, abrogate binding and prevent co-immunoprecipitation of Smc1 and Scc1. These mutations also prevent association of cohesin with chromatin as normally found by chromosome spreading (Arumugam et al., 2003).

Two proteins, known as Scc2 and Scc4 then interact with cohesin forming the pre-loading complex. Scc2 is hook-shaped protein composed of a series of protein motifs known as huntingtin, elongation factor 3 (EF3), protein phosphatase 2A (PP2A), and the yeast kinase TOR1 (HEAT) repeats much like Scc3 and Pds5. These HEAT composed proteins known as HAWKs (heat repeat proteins associated with kleisins)

are all involved in regulating cohesin function (Petela et al., 2018). HAWKs are related to another type of proteins called KITEs (kleisin interacting tandem winged-helix elements of SMC complexes) which interact with condensin and cohesin but not Smc5-Smc6. Condensin interacts with two HAWK proteins compared to a single HAWK with cohesin, thus creating a definable difference between the two. SMC protein with KITE or HAWK interactions have already been defined through co-immunoprecipitation and X-ray crystallography (Palecek and Gruber, 2015). HAWKs and KITEs have been shown to be related through phylogenetic analysis, indicating that these complexes likely diverged to fill different roles (Wells et al., 2017). In a process dependent on ATP hydrolysis, cohesin is loaded onto the chromatid. Mutant forms of Scc2 and Scc4 that Ciosk and co-workers refer to as scc2-4 and scc4-4 allow cohesin to form normally but interaction with DNA is abolished (Ciosk et al., 2000). Scc2 may interact with cohesin, but in HeLa (human cancer cell line) cells, the complex is unable to associate with chromatin without Scc4 as seen by immunofluorescence (Watrín et al., 2006). Mutation of a specific highly-conserved part in the middle of Scc4 causes increased plasmid mis-segregation and increased metaphase spindle length; both of which are associated with weakened sister chromatid cohesion. Deletion of the *CHL4* gene, coding for a centromeric protein in *S. cerevisiae* also causes the same phenotype. Chromatin immunoprecipitation (ChIP) sequencing shows that Scc4 mutation significantly reduces cohesin loading at the centromere, implying that Scc4 recruits cohesin to the centromere via Chl4. The structure of Scc2 and Scc4 along with their interaction orientation have also been partially resolved using X-ray crystallography, supporting that Scc2-Scc4 is a complex required for loading. The structure of Scc4 has been fully determined including interaction with a fragment of the Scc2 N terminal (Hinshaw et al., 2015) Full length Scc2 structural determination

has been attempted, however some small highly flexible domains remain unresolved but can be estimated from homological similarities with the human protein symplekin (Chao et al., 2017a). Symplekin is a human nuclear protein which promotes gene expression and assists in regulation of polyadenylation which is the addition of multiple adenosine monophosphates to the end of messenger RNA. Scc2 forms a hook shape structure with distinct states depending on a highly flexible region connecting the N terminal of Scc2 with Scc4 as seen by electron microscopy (Chao et al., 2017a). Figure 10 shows the structure of Scc2 found by X-ray crystallography and electron microscopy.

This large range of motion is hypothesised to be involved in the dynamic loading processes of cohesin by the Scc2-Scc4 complex (Chao et al., 2015). The loading process itself however may be performed by Scc2 alone *in vitro*. Cohesin can be observed having captured circular DNA which is visible from immunoprecipitation and comparison of electrophoretic shift with cohesin and circular DNA alone. Scc4 is dispensable in this case (Murayama and Uhlmann, 2014). An orthologue of human Scc4 exists in *S. cerevisiae* and may serve a similar function (Nasmyth and Haering, 2009).

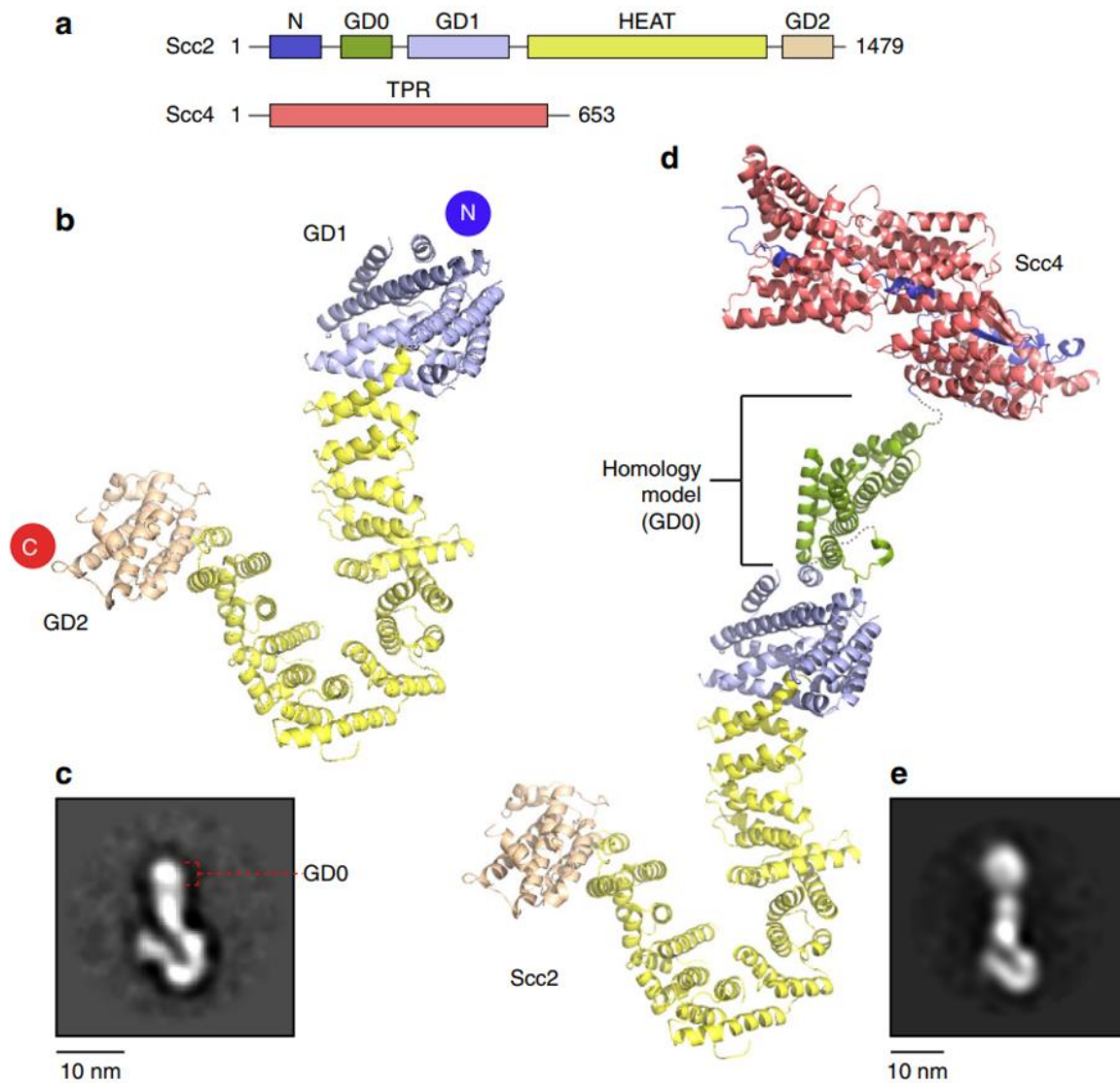


Figure 10: Diagram showing the structure of Scc2 and Scc4 along identified domains and electron microscopy images from *S. cerevisiae*.

(a): Schematic of Scc2 and Scc4 domain structure. Scc2 consists of two adjacent globular domains (GD) a HEAT domain and a final third GD. GD0 represents the undetermined region which was aligned with the homology model symplekin. Scc4 consists wholly of tetratricopeptide repeats (TPR). (b): Cartoon diagram of the determined structure of Scc2 as determined by X-ray crystallography. (c): Electron microscopy image of Scc2. (d): Cartoon diagram of the determined structure of Scc2 with the predicted homology model and Scc4

orientation. (e): Electron microscopy image of the Scc2-Scc4 complex. Image from Chao and co-workers (Chao et al., 2017a).

Cohesin is loaded onto the chromatin in G1 before S phase with the action of Scc2 and Scc4, as single mini-chromosomes are concatenated by cohesin and detected by Southern blotting (Srinivasan et al., 2018). It is unknown whether additional proteins are also included in the pre-loading complex, however from the *in vitro* experiments of Murayama and co-workers, it is possible that no more additions are necessary as cohesin and Scc2-Scc4 are sufficient (Murayama and Uhlmann, 2014). There is significant evidence that cohesin is largely loaded around the centromere by proteins involved in constituting the heterochromatin (Fernius and Marston, 2009). Mutations in subunits of the kinetochore protein complex Ctf-19, caused increased chromosome loss, reduced Scc1 association with the pericentromere and increased sister chromatid separation (Fernius and Marston, 2009) This is supported by experiments which introduced an additional ectopic heterochromatic region or centromere sequence in a chromosome, causing cohesin to accumulate, suggesting that cohesin is loaded at these locations due to centromere associated proteins such as the Ctf-19 complex (Hu et al., 2011; Oliveira et al., 2014). The Ctf-19 complex is an essential component of the kinetochore in the centromere. Furthermore, phosphorylation of Ctf-19 has been demonstrated to be critical for the localisation of Scc2 to the centromeres (see figure 11). Mutating the phosphorylation sites of Ctf-19 abolishes recruitment of Scc2, visible by GFP tagged fluorescent microscopy. Phosphorylated Ctf-19 also binds Scc4 and can be co-immunoprecipitated *in vitro*. This interaction has also been resolved with X-ray crystallography (Hinshaw et al., 2017).

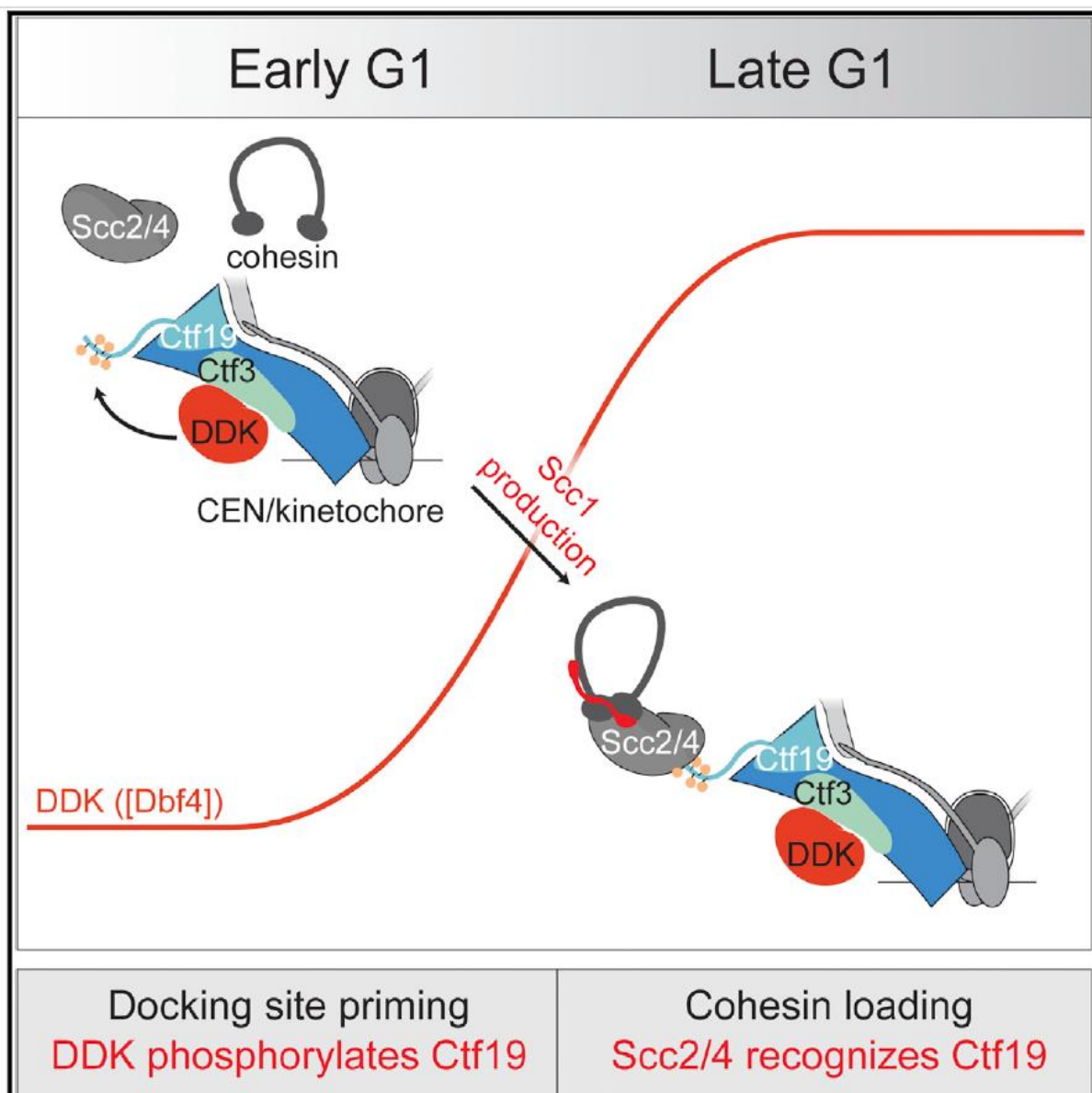


Figure 11: A diagram showing mechanism of cohesin recruitment to chromatin in yeast.

The diagram shows how loading is controlled in the cell cycle by the phosphorylation of Ctf-19 by Dbf4-dependent kinase (DDK). This interaction is made possible by Ctf3 which is a trimeric complex responsible for the recruitment of DDK. Cohesin, along with its loader Scc2-Scc4 is then free to localise to the kinetochores where it encounters chromatin and is loaded. Diagram from Hinshaw and co-workers (Hinshaw et al., 2017).

Loading of cohesin may also occur at highly transcribed gene locations. CHIP sequencing data shows that Scc2 is localised with various polymerases with high correlation (Hu et al., 2011). The exact method of loading may involve the re-modelling the structure of chromatin (RSC) complex which is involved in the removal of nucleosomes to remodel the chromatin, allowing access to DNA for processes such as transcription. Nucleosomes interfere with cohesin loading *in vitro* as cohesin complexes capture more naked DNA than chromatin. Auxin-induced degradation of the essential RSC ATPase subunit, Sth1, in *S. cerevisiae* causes lethality and reduces Scc2 localisation to chromatin as seen by CHIP sequencing (Muñoz et al., 2019). The essential cohesin recruitment protein, Scc4, is also dispensable when a RSC complex-Scc2 fusion product is introduced, suggesting that Scc4 may recruit cohesin to RSC (Muñoz et al., 2019). Once cohesin is loaded however, it seems that cohesin may translocate in an ATP-dependent manner. CHIP sequencing data shows that cohesin may concentrate at the centromere but be dispersed further away. This dispersion is abolished with the introduction of an ATP hydrolysis mutant form of Smc3 (Hu et al., 2011). The mechanism of translocation is unknown but it has been suggested that it may be similar to the DNA loop extrusion mechanism proposed by Diebold-Durand and co-workers which is outlined in figure 12 (Diebold-Durand et al., 2017).

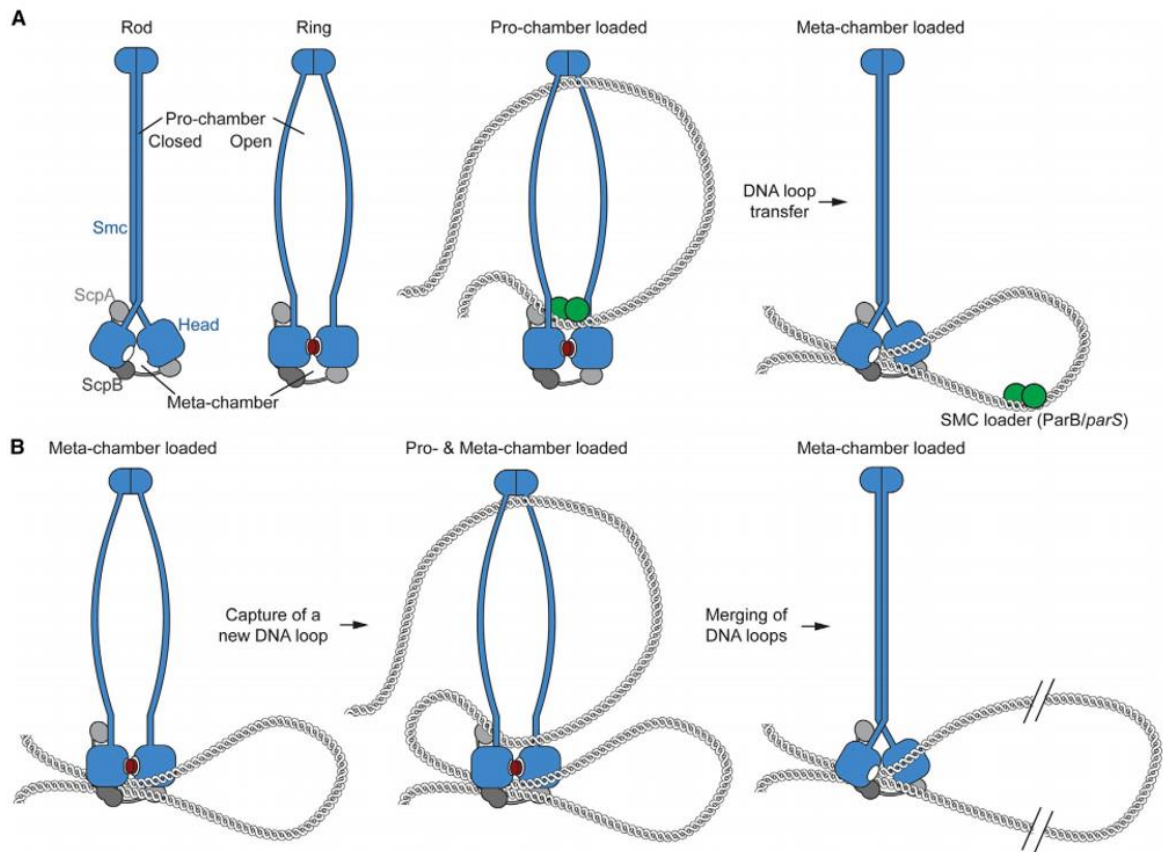


Figure 12: A diagram of a potential mechanism for DNA loop extrusion as described by Diebold-Durand and co-workers.

(A): Cartoon representation of how the SMC complex in *B. subtilis* may entrap DNA in the meta-chamber by first transferring DNA strands from the pro-chamber in an ATP-dependent manner. (B): Cartoon representation of how the SMC complex may expand a captured loop already entrapped in the meta-chamber by capturing a further loop before allowing them to merge in the meta-chamber. Image from Diebold-Durand and co-workers (Diebold-Durand et al., 2017).

During the loading process, there is strong evidence that the hinge between Smc1 and Smc3 is the entrance gate. By incorporating the proteins FKBP12 and Frb into the

hinge domains of Smc1-Smc3 an artificial bridge may be constructed when rapamycin is introduced (Gruber et al., 2006). This bridge prevents the establishment of sister chromatid cohesion as Scc1 distribution is reduced in CHIP sequencing results. In contrast, the FKBP12 and Frb rapamycin-dependent bridge can be introduced between the SMC subunits and kleisin interfaces and these do not hinder cohesin loading (Gruber *et al.*, 2006). *In vitro* loading experiments show that entry may occur through the Smc3-Scc1 interface but this may not be the primary mechanism of loading as this does not explain the lethality of bridging the hinge domains (Murayama and Uhlmann, 2015). Conversely, an explanation for the loading defect could be that the FKBP12 and Frb rapamycin-dependent bridge may interfere with loading processes of Scc2-Scc4 and not the topological closing of the hinge domain interface. Rad61, a cohesin associated protein implicated in removing cohesin from DNA, may have some loading activity, or at least some contribution to cohesin establishment on chromatids (Murayama and Uhlmann, 2015). Mutation or deletion of Rad61 reduces cohesin association with chromatin as seen by measuring chromosome separation or CHIP sequencing (Rowland et al., 2009; Sutani et al., 2009).

It is clear that cohesin exists as a ring, being a tetramer of the four core subunits. However, the orientation of the subunits within the complex and further associated proteins is still unknown. For example, the preloading complex involving cohesin and Scc2-Scc4. As it is known that ATP hydrolysis activity and Scc2-Scc4 are required for loading with the hinge domain being the entry gate, the energy supplied from ATP must somehow be transmitted to the hinge for opening. This notion was first suggested by Gruber and co-workers (Gruber et al., 2006) before interactions between Scc2 and the fragments of the hinge domain were detected by co-immunoprecipitation

(Murayama and Uhlmann, 2015). Finally, Pds5 was found to strongly crosslink with the Smc1 hinge domain and as interaction with Scc1 near the Smc head domains had already been established (K. L. Chan et al., 2013), it was shown that Pds5 could bridge this gap (Bürmann et al., 2019). Data in this study also show that Scc2 may do the same.

Once cohesin is loaded on the chromatin, sister chromatid cohesion must be sustained before anaphase where faithful disjunction of chromosomes occurs. This is achieved by a number of processes which start before replication (Uhlmann, 2016).

2.6 Maintaining sister chromatid cohesion & disjunction

Sister chromatid cohesion may be established through the stable association of cohesin around both chromatids. This stability is dependent on Scc3 and Pds5. Deletion of Scc3 is lethal and mutations cause loss of sister chromatid cohesion demonstrated by observations made from increased separation between tagged centromere protein via fluorescent microscopy (Tóth et al., 1999). Scc3 binds to parts of Scc1, as fragments of Scc3 and Scc1 may co-immunoprecipitate. The structure of Scc3 has also been found by determining the structure of fragments via X-ray crystallography before combining the structural data into a single map. Like Scc2, Scc3 also takes the shape of a hook (Roig et al., 2014).

Pds5 is also an essential gene and temperature sensitive alleles of Pds5 cause loss of sister chromatid cohesion but do not prevent establishment. This can be seen by either using FISH to detect centromere separation or fluorescent microscopy (Hartman et al., 2000; Panizza et al., 2000). The structure of Pds5, being yet another hook shaped protein, has been resolved using X-ray crystallography and found to change shape when bound to a Scc1 fragment (Lee et al., 2016). Cohesin can bind Scc2 or Pds5, but not both simultaneously as Pds5 co-immunoprecipitated with cohesin is depleted when Scc2 is introduced. In addition, ATP hydrolysis activity of cohesin induced by Scc2 is dramatically reduced with added Pds5 but not when the binding site of Pds5 in Scc1 is mutated. Scc2 may be responsible for cohesin translocation as it is localised with cohesin on the arms of chromosomes seen by ChIP sequencing.

Thus Scc2 and Pds5 may compete for the same binding sites in cohesin and control ATP hydrolysis dependent translocation across the chromatin (Petela et al., 2018).

Cohesin may be removed from the DNA via the action of a protein complex consisting of two separate proteins known in yeast as Rad61 (Wapl in humans) and Pds5. Rad61 and Pds5 form a stable complex *in vitro* and can be co-immunoprecipitated. Circular DNA with cohesin loaded onto it by Scc2-Scc4 cannot be unloaded by Rad61 without Pds5; however together they are very efficient at unloading (Murayama and Uhlmann, 2015). Figure 13 illustrates the function of Rad61 and Pds5 *in vitro*.

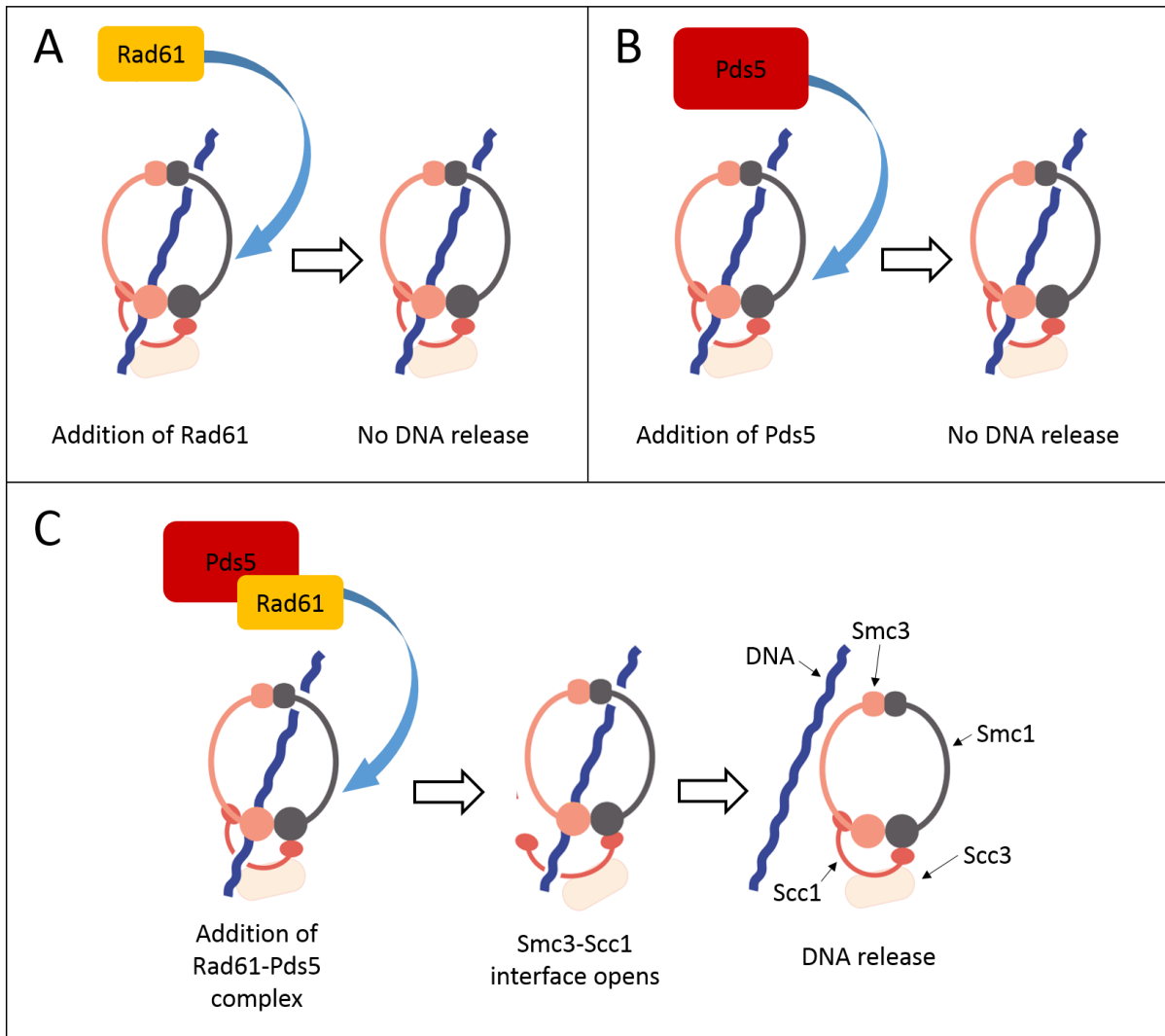


Figure 13: Cartoon diagrams of *in vitro* Rad61-Pds5 complex dependent releasing activity using purified *S. cerevisiae* proteins as described by Murayama and co-workers.

(A): Tetramer cohesin was pre-loaded *in vitro* on to circular DNA by the addition of the Scc2-Scc4 complex with ATP. The cohesin entrapped DNA was then purified and Rad61 was introduced with ATP. This combination did not yield the release of DNA from cohesin. (B): The result is the same as (A) when Rad61 is substituted for Pds5. (C): When Rad61 and Pds5 are introduced in an equimolar amount, a complex between them is formed, allowing for the release of DNA from the kleisin compartment via the opening of the Smc3-Scc1 interface. This

process is ATP-dependent. Adapted from Murayama and co-workers (Murayama and Uhlmann, 2015).

It is suggested that Rad61-Pds5 releases cohesin from the chromosome by opening the Smc3-Scc1 N-terminal interface in an ATP-dependent manner, as experiments have shown that the creation of a Smc3-Scc1 fusion protein fails to turnover on chromosomes (Beckouët et al., 2016). *In vitro* experiments also supports this by showing that Rad61-Pds5 can release fragments of Scc1 from Smc3 but not from Smc1, indicating this interface is opened by Rad61-Pds5 (Murayama and Uhlmann, 2015). As Rad61 is expressed throughout the cell cycle, it will constantly remove cohesin loaded onto the chromatids. This is shown by the loss of sister chromatid cohesion when artificially controlled Rad61 expression is induced at G2 phase, triggering cell cycle arrest in Eco1 deletion yeast backgrounds (Eco1 is a protein critical for maintaining stable entrapment of DNA by cohesin). The sister chromatid cohesion is lost and can be seen by fluorescent microscopy. Expression of fusion protein between Smc3 and Scc1 prevents the releasing activity of Rad61 (Chan et al., 2012). This further shown by *GAL* expressed Rad61 artificially causing disjunction after metaphase in Rad61 and Eco1 deleted yeast strains (Lopez-Serra et al., 2013). *GAL* is an operon which controls the expression of proteins responsible for galactose metabolism when galactose is detected by proteins expressed from this operon. This system can be exploited to express any protein when galactose is introduced into growth media of an organism containing this modification (Weickert and Adhya, 1993).

As cohesin is loaded in G1 phase during DNA replication of yeast cells, it may therefore be subject to removal by Rad61-Pds5. The evidence of loaded cohesin in G1 phase is the presence of cohesin dependent DNA loops found by chromosome conformation capture (Hadjur et al., 2009; Nativio et al., 2009). The loading and unloading processes in G1 phase appears to be unnecessary, however these cycles provide dynamic association. The role of dynamic association may be to remove tangles created by cohesin loops which may be captured by cohesin as part of thermal production. Thermal production is a process where random configurations of a system are created as a result of thermal energy; in this instance, a biological system where loops of DNA in close proximity happen to be captured by cohesin. Tension is hypothesised to cause translocation stalling which could be relieved by Rad61-Pds5 (Marko et al., 2019). Another releasing mechanism in supplement to the Rad61-Pds5 process may exist, because ChIP sequencing shows that Scc2 counteracts a Rad61-Pds5 mechanism as the deletion of Rad61 and the temperature inactivation of Scc2 causes substantial loss of cohesion. This mode of release is somehow prevented upon entry into G2 phase but related to cyclin dependent kinase 1 (Cdk1). Cdk1 is a protein which activates many critical proteins for the progression of the cell cycle by phosphorylating them. It has also been shown that Scc4 and Pds5 are not required for this Rad61-Pds5 independent process, however ATP hydrolysis activity is necessary (Srinivasan et al., 2019). The Rad61-Pds5 independent releasing activity is illustrated in figure 14. Further investigation is required to characterise the mechanism as this may lead to the discovery of more cohesin functions or interactions.

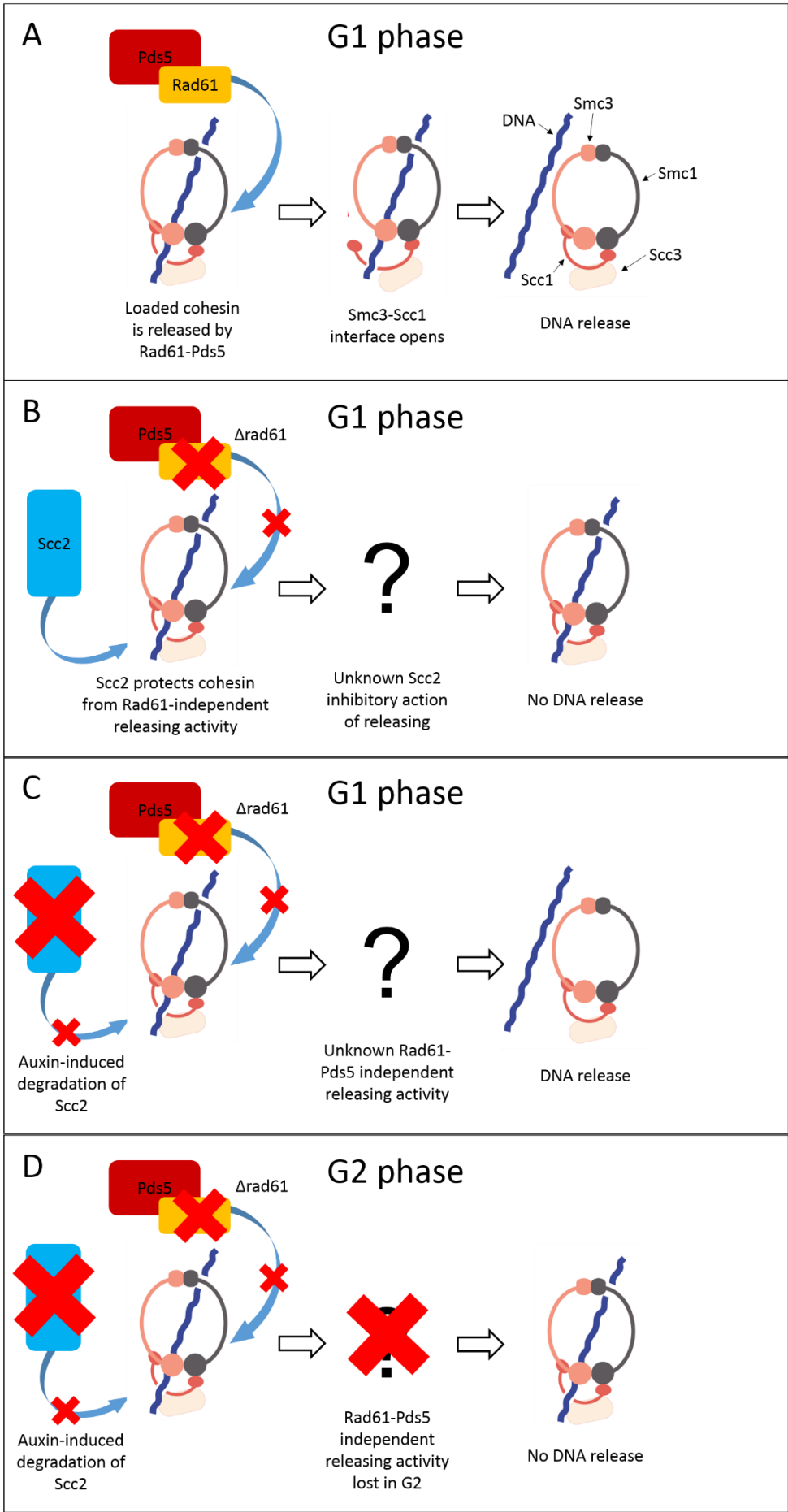


Figure 14: Diagrams to show the Rad61 independent releasing mechanism of cohesin which is blocked by Scc2 in G1 phase as described by Srinivasan and co-workers.

(A): The Rad61-Pds5 complex in yeast releases loaded cohesin by opening the Smc3-Scc1 interface. (B): By deleting Rad61, it is expected that releasing activity is also abrogated, however this is only true when Scc2 is present to counteract another Rad61-independent releasing mechanism. (C): By auxin-induced degradation of Scc2, and deletion of Rad61, the effect of the Rad61-independent releasing mechanism can be observed. (D): In G2 phase, the Rad61-independent releasing mechanism is somehow deactivated.

Cohesin is maintained on the chromatids until anaphase where Scc1 is cleaved in two places by separase, a cysteine protease (Esp1 in *S. cerevisiae*). Demonstrated both *in vivo* and *in vitro*, separase activity is considered the primary initiator of anaphase. Separase cut sites are recognised by adjacent arginine residues and if the two separase cut sites at Scc1 position 180 and 268 are removed, then disjunction is prevented (Uhlmann et al., 1999, 2000). Expression of the Scc1 C terminal fragment also causes the ring to open, by binding to Smc1 and displacing Smc3 (Weitzer et al., 2003) The releasing activity caused by the Scc1 C terminal fragment explains why expression of this cleavage product is lethal, causing premature loss of sister chromatid cohesion (Rao et al., 2001). The action of Rad61-Pds5 releases cohesin from chromatin constantly. In order to prevent this occurring at the critical moment after DNA replication, a process called acetylation is performed at specific residues on Smc3 (Ben-Shahar et al., 2008; Rowland et al., 2009). This prevents the releasing activity of Rad61-Pds5 and allows preservation of sister chromatid cohesion until

anaphase where separase cleaves Scc1 and disjunction occurs. The precise mechanism of acetylation in preventing releasing activity is not understood.

2.7 Acetylation of SMC proteins

Acetylation is the addition of an acetyl group to another molecule. Acetylation of Smc3 occurs at a pair of adjacent lysine residues at position 112 and 113. The acetyl residue is added to the amino group of lysine by the acetyltransferase, Eco1. Eco1 is an essential protein which is necessary to produce stable entrapment of chromatin by cohesin. Deleting Eco1 much like other subunits of cohesin, causes observable loss of sister chromatid cohesion by fluorescent microscopy (Tóth et al., 1999). Acetylation of Smc3 is critical for cohesin to remain loaded onto the chromatid after S phase and occurs at the time of replication as Eco1 is associated with the replication fork. This was first discovered by stalling replication forks around known origins of replication in early S phase using hydroxyurea, which prevents DNA replication. ChIP sequencing was then used to find Eco1 which was localised to the same regions (Lengronne et al., 2006). The mutation *smc3K113N* was found to suppress Δ *eco1*, and mass spectrometry showed that this lysine residue is in fact acetylated by Eco1 (Ben-Shahar et al., 2008) along with Smc3K112 (Ünal et al., 2008). This reversible reaction is illustrated by figure 15.

Acetylation of lysine

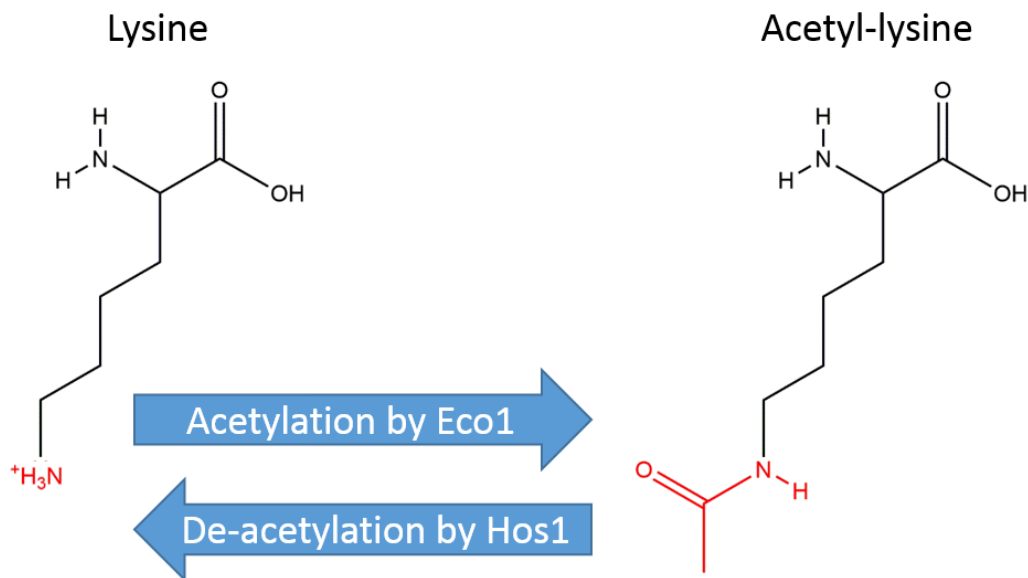


Figure 15: Diagram showing the chemical changes during the acetylation and deacetylation of lysine.

Eco1 acetylates the amine group of lysine by transferring an acetyl group from acetyl-coenzyme A to form acetyl-lysine. Hos1 removes this group by reversing this reaction (Borges et al., 2010; Chao et al., 2017b).

As mentioned previously, the primary purpose of acetylation is to negate the releasing effect of Rad61-Pds5, therefore the deletion of both Eco1 and Rad61 is not lethal in yeast which has been verified by viability of spores after tetrad dissection. The deletions do however, cause a significant loading defect (Chan et al., 2012). As acetylation blocks releasing activity of Rad61-Pds5, $\Delta eco1$ can be rescued by fusion of the Smc3-Scc1 interface (Chan et al., 2012). In support, $\Delta wapl$ and Rad61

mutations reduces Scc1 N terminal fragment degradation as seen by western blot. Releasing activity dissociates this fragment from Smc3 after cleavage; this can be seen with live cell imaging (Beckouët et al., 2016).

There are two ATPase sites in cohesin, one located in each of the Smc1 or Smc3 head domains. Mutations affecting ATP hydrolysis in each ATPase reveals that a Smc1 ATPase mutant is able to bypass $\Delta eco1$ but not a similar mutant in Smc3. This indicates that the mutant Smc1 ATPase is deficient in releasing activity. Loading however, involves use of both ATPase sites. The Smc1 and Smc3 ATPase mutations both cause significant reductions in cohesin association with chromatin observable by ChIP sequencing (Elbatsh et al., 2016). Acetylation of Smc3K112, K113 prevents releasing but this site is near to the Smc3 ATPase which is not required for this process, therefore acetylation of these residues may not prevent loading by reducing ATP hydrolysis activity alone. A supplementary or alternative mechanism of releasing activity abrogation is likely.

The acetyl residues on Smc3K112, K113 are removed by the class 1 histone deacetylase (HDAC) family member known as Hos1, found by detecting acetylated Smc3 in G1 of the following cell cycle by western blot of a $\Delta hos1$ strain (Borges et al., 2010). Smc3 deacetylation is an important step in releasing cohesin from chromatin during anaphase as cleavage of Scc1 will release cohesin but only after a significant delay without Hos1 (Li et al., 2017). Chan and co-workers found a range of specific Scc1 residues which when deleted or mutated, causes the loss of Pds5 interaction. Cleavage by separase may remove the Scc1 residues necessary from Pds5

interaction, as a range of residues deleted or modified between the two cleavage sites is lethal presumably for this reason. Pds5 protects deacetylation by Hos1. Auxin induced degradation of Pds5 during S phase causes near complete loss of acetylated cohesin detectable by western blot (Chan et al., 2013). Inactivation of temperature sensitive Pds5 during mitosis leads to rapid deacetylation of Smc3 also detectable by western blot, but not in Δ hos1 cells (Chan et al., 2013). Scc1 cleavage is necessary for deacetylation of Smc3 as expression of cleavage defective mutant Scc1 leads to prevention of disjunction and loss of detectable acetylated Smc3 by western blot (Beckouët et al., 2010).

Without Pds5 protection, Hos1 may deacetylate cohesin and allow removal of the Scc1 N terminal fragment from the Smc3 head domain. This fragment has been shown to be released from Smc3 after anaphase by lack of BMOE crosslinking at the interface (Beckouët et al., 2016). In Δ rad61 cells, this fragment is retained and crosslinking occurs after anaphase. Live cell imaging also shows separation of GFP-tagged N terminal Scc1, and the stably associated cohesin subunit, Scc3. This ATP-dependent process is thought to drive the release of cohesin much more efficiently (Beckouët et al., 2016). Li and co-workers supports this by showing that the Smc3-Scc1 fusion protein has slower segregation time in Δ hos1 cells (Li et al., 2017). This suggests that the releasing activity of Rad61-Pds5 and/or ATPase activity assists in dissociation along with the release of the Scc1 N terminal fragment.

Acetylation of other Smc residues important for cohesin function also occurs. The coiled coil regions of Smc1 and Smc3 contain acetylated lysine residues that are

identifiable by mass-spectrometry (Choudhary et al., 2009; Ünal et al., 2008). Mutation of these residues creates a defect in Scc1 recruitment to the Smc3 heterodimer and association with chromatin. Loss of Scc1 association is found through inability to co-immunoprecipitate, and chromosomal spreading fails to detect mutant cohesin (Kulemzina et al., 2016). Atomic force microscopy reveals that the overall length, width and shape of the Smc1-Smc3 heterodimer is reduced by replacing lysines found in the coiled coil break regions of Smc3 (see figure 16) and the coiled coil region of Smc1, indicating dependent supercoiling of Smc1-Smc3 (Kulemzina et al., 2016). This may be linked to the Rad61-Pds5 independent releasing activity described by Srinivasan *et al.*, 2019 (Srinivasan et al., 2019).

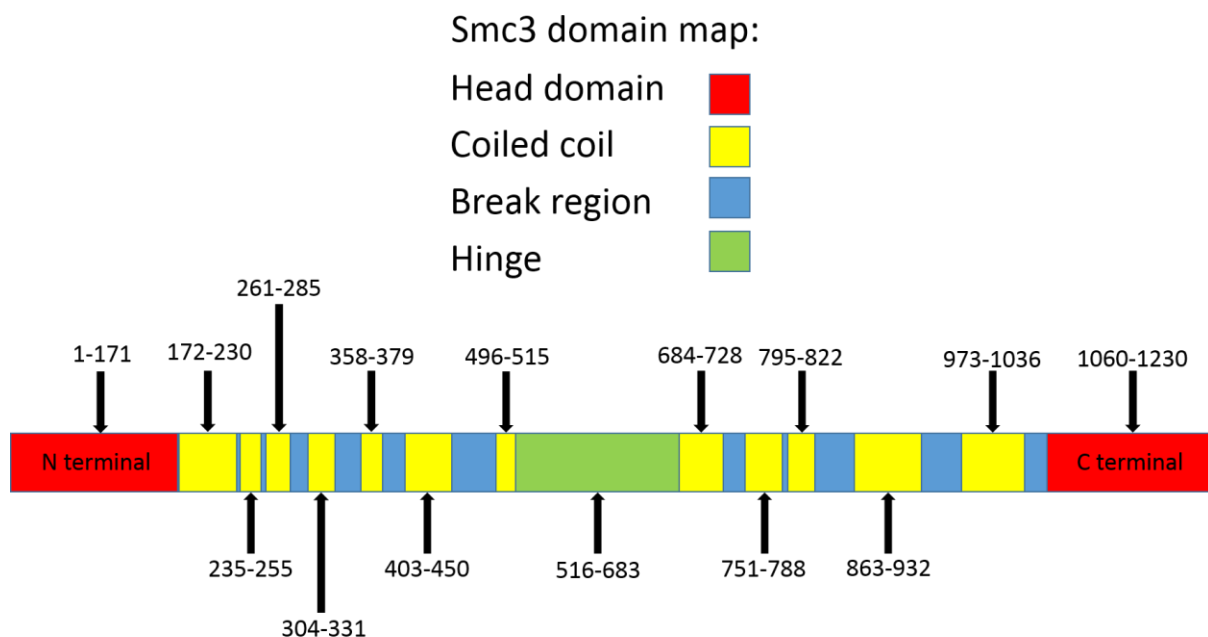


Figure 16: Map of Smc3 domains.

The coiled coil regions are formed by two alpha helices supercoiling around each other which can be seen in figure 6. The break regions are where the secondary structure of the protein

changes and there are interruptions in the alpha helices. More information about how this diagram was made can be found in 4.1.2.

An acetylation cycle of cohesin is critical for normal cellular function. At anaphase, sister chromatid cohesion is lost and cohesin dissociates. It is at this point of dissociation where cohesin is de-acetylated by Hos1 and recycled in the next mitotic event. If *HOS1* is deleted, *S. cerevisiae* is viable but suffers significant defects to sister chromatid cohesion due to a depleted supply of non-acetylated cohesin from the previous cell cycle, thus acetylation is shown to cause a cohesion defect (Borges et al., 2010). Hence, acetylation may affect the loading processes of cohesin. As acetylation is a post translational modification, acetylated Smc3 is difficult to study. As a result, mimicking forms are used to model acetylated cohesin. One such mimicking form is smc3K112Q, K113Q (smc3QQ or QQ) (Beckouët et al., 2016). This mutated form of Smc3 has two glutamine residues substituted for the critical lysine pair required for acetylation, with the consequence being that the positive charges provided by lysine are lost and replaced with glutamine which is neutrally charged. This also mimics the loss of positive charge after lysine acetylation. Figure 17 shows the location of these two residues.

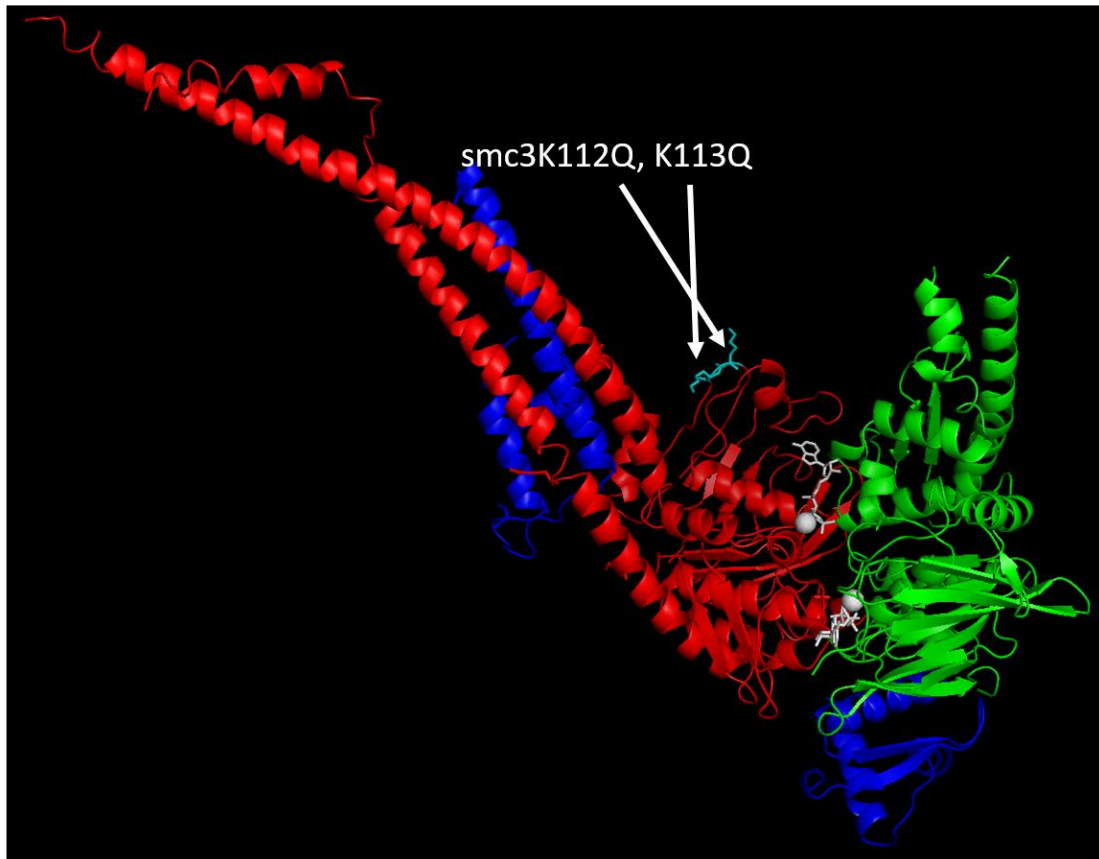


Figure 17: A cartoon showing the relative position of smc3K112Q, K113Q.

The residues are highlighted in cyan and indicated by white arrow, lying on the outer edge of the head region. Smc3 (red), Smc1 (blue), Scc1 (blue). Diagram produced from crystal structure provided from Gligoris and co-workers using Pymol (Delano Scientific) (Gligoris et al., 2014).

It is not known whether acetylation mimics behave exactly like acetylation or only exhibit certain characteristics. Another mimic smc3K112N, K113N is also lethal and like QQ, has neutral charge and cannot be rescued by $\Delta rad61$, indicating that this mutation lacks loading activity (Borges et al., 2010). In addition, the glutamine mutant smc3K112Q, K113Q prevents loading and association with the centromere as shown

by ChIP sequencing (Hu et al., 2015). The mutant *smc3K112R, K113R* is also lethal (Beckouët et al., 2016; Ben-Shahar et al., 2008) but can be rescued by $\Delta rad61$. This indicates that *smc3K112R, K113R* is capable of loading and releasing but is lethal due to the activity of Rad61-Pds5. These results suggest that the positive charge is necessary for loading and releasing activity. Curiously, mixing the two mutations and producing *smc3K112N, K113R* and *smc3K112R, K113N* produces two viable mutants, both of which suffer significant growth defects. Both mutants are also able to survive $\Delta eco1$ showing that they are able to resist Rad61-Pds5 releasing activity (Borges et al., 2010). This may be due to the fact that Eco1 is not necessary when ATP hydrolysis is impaired. Certain mutations in the Smc3 and Smc1 ATPase sites which all prevent Rad61-Pds5 releasing activity, also prevent crosslinking at specific positions of the Smc1-Smc3 head domain interface (Çamdere et al., 2015; Elbatsh et al., 2016; Huber et al., 2016). All of these mutations may survive $\Delta eco1$. The QQ mutation did not affect the head domain interface crosslinks, and may prevent Rad61-Pds5 mediated release by another method. ATP hydrolysis allows translocation of cohesin along the chromatin (Hu et al., 2011), whereas acetylation promotes translocation *in vitro*. Acetylated cohesin was purified from baculo-virus infected insect cells and then loaded onto DNA by Scc2-Scc4 before motion viewing using total internal reflection fluorescent microscopy. This suggests that acetylated cohesin does possess at least some ATP hydrolysis activity (Kanke et al., 2016).

How acetylation blocks both loading and releasing activity is not understood as there are many variables to both processes. The three main candidates for mechanism of action are: impairment of ATP hydrolysis activity, changes to the configuration of cohesin, or changes to the binding site of proteins involved with loading and releasing

processes. In order to produce the data to test these hypotheses, the model organism *Saccharomyces cerevisiae* was selected.

2.8 *Saccharomyces cerevisiae*

Saccharomyces cerevisiae is a eukaryotic organism classified as a species of yeast. This organism is unicellular and may reproduce via asexual budding in both a haploid and diploid form. It is widely utilised in industry to produce foodstuffs such as bread, beer and wine. For these applications, *S. cerevisiae* is also known as baker's or brewer's yeast (Vargas-Trinidad et al., 2020).

The *S. cerevisiae* variant, W303, was selected as the model organism for this project for the following reasons:

1. W303 is a eukaryote. Only eukaryotic organisms possess cohesin. The site of acetylation is conserved between eukaryotes and that may make study in W303 applicable in these also.
2. W303 being yeast, is easily cultured in a variety of liquid and solid media at permissible temperatures and reproduces quickly for rapid experimentation.
3. W303 may exist in both a haploid and diploid form. This property allows flexibility in the experimental approach of this project. Modifying genes via transformation is easier in haploids as there is only one copy of a gene per genome and combining genotypes is a simple matter of mating to produce

diploids which may also be used to retain a functional copy of a select gene.

4. W303 has been modified for superior transformation efficiency, allowing the genome/transcriptome of the organism to be edited via plasmids more easily. As the intention of the project is to study particular proteins, extensive modification will be involved; hence the most desirable trait of this variant. W303 is a derivative of S288C, sporting the distinct advantage of enhanced transformation efficiency along with the culture qualities of S288C which include non-invasive growth in agar and no clumping in liquid media.
5. W303 is fully sequenced, allowing for much more convenient genetic modification and experimental design. For example, modifying the genome via homologous recombination may require the transformed DNA integration cassette to be flanked with homologous regions. This would not be possible without a sequenced genome.

These qualities constitute the appropriateness of the organism, along with the strong tradition of discoveries made using *S. cerevisiae* (Ralser et al., 2012; Uhlmann, 2016).

2.9 Aims of this study

Cohesin research is the study of an essential part of eukaryotic life. As cohesin is so widely implicated in many cellular processes, elucidation of all functions will help complete understanding of gene expression, chromatin organisation, DNA repair, and sister chromatid cohesion. Practical applications include understanding the physiological reasons behind different phenotypes caused by cohesinopathies, (diseases involving defects in cohesin) and other diseases that involve damage to the genome such as cancer (Losada, 2014). Cohesinopathies include developmental disorders such as Cornelia de Lange and Roberts syndrome, which have symptoms ranging from mild to lethal (Bose and Gerton, 2010). By understanding the nature of cohesin, data can be gathered which can help identify problematic mutations to the involved genes. This improves diagnosis of medical conditions in the future as genome sequencing may become standard practice. Carcinogenesis is often caused by translocation of genes of which cohesin plays a role in stabilising double stranded breaks. General improvement of pathway knowledge can perhaps help identify potential drug targets for cancer or improve our ability to manipulate the genome without causing widespread damage like current CRISPR/Cas9 practices (Horsfield et al., 2012; Sansbury et al., 2019). As cohesin incorporates SMC proteins, understanding cohesin will also benefit all other SMC complexes such as condensin and Smc5-Smc6, as these are evolutionarily conserved and share similar modes of action (Uhlmann, 2016). The aims of this study were to investigate the role of acetylation in the function of cohesin and how acetylation may affect the configuration of, or interaction between, cohesin and other proteins that could help to understand the loading mechanism.

The approach of this study is as follows:

1. Study acetylation using the mimicking form smc3K1121Q, K113Q by genetic screens searching for mutations that can rescue the known growth defect. The mutant smc3K112Q,K113Q was selected to continue work by Hu and co-workers (Hu et al., 2015).
2. Map locations of QQ suppressor mutants and interaction of proteins around these, along with the site of acetylation for changes in structure of cohesin or interactions with other associated proteins.
3. Use the acetylation mimic established in (1) to produce an assay studying the effect on the structure or interactions of cohesin found in (2).

3.0 Materials and methods

3.1 Materials

3.1.1 Media

All media was prepared using Milli-Q® prepared H₂O and autoclaved at 120°C for 15 minutes after preparation prior to use.

4% agar: This was produced by dissolving 10g/L of agar (Formedium) in 250mL of dH₂O. This was mixed with 250mL 2x stock solutions of other media to produce 500mL with a final agar concentration of 2%, sufficient for producing a variety of agar plates.

Yeast Extract Peptone Adenine Dextrose (YPAD) media: *S. cerevisiae* yeast strains were cultured on YPAD agar plates or in YPAD liquid media. Liquid media was made up using: yeast extract 10g/L (Formedium), Bacto™ peptone 20g/L (BD), D-glucose 20g/L (Fisher Scientific), Adenine hydrochloride hydrate 40mg/L (Sigma Aldrich). Bacto™ agar 20g/L (BD) was added to liquid YPAD to make YPAD media agar plates.

Minimal media (MM): Liquid media was prepared using yeast nitrogen base without amino acids (YNB) 6.8 g/L (Formedium) and D-glucose 20 g/L (Fisher Scientific). This 2x stock solution was dissolved in an equal volume of 4% agar solution (Formedium) to produce minimal media agar plates.

Dropout media: Various drop out media were prepared for *S. cerevisiae* strains carrying plasmids in which marker genes allowed them to grow on the types of media.

Minimal media 1x stock solution was used to produce all dropout media by mixing it with 0.87g/L of drop out master mix. Appropriate master mixes were produced with the following amino acid proportions, save for the omitted amino acid(s) to produce the desired drop out:

Table 2: Amino acid supplement mixture.

Amino Acid (Sigma-Aldrich)	Mass in master mix (mg)
Adenine	800
Argenine	800
Aspartic Acid	4000
Histidine	800
Leucine	2400
Lysine	1200
Methionine	800
Phenylalanine	2000
Threonine	8000
Tryptophan	800
Tyrosine	1200
Uracil	800

Dropout plates were made by adding 0.87 g/L of the appropriate amino acid dropout master mix to 2x minimal media before dissolving in 4% agar.

SpoVB agar: This solid sporulation media was produced with: sodium acetate 8.29 g/L (Sigma-Aldrich), 1.9 g/L potassium chloride (Sigma-Aldrich), 350 mg/L magnesium sulphate (Sigma-Aldrich), 1.2 g/L sodium chloride (Sigma-Aldrich) and 2% w/v agar.

2x Tryptone Yeast Extract (2xTY) media: This was prepared using tryptone 16 g/L (Formedium), yeast extract 10 g/L (Formedium) and sodium chloride 5 g/L (Fisher Scientific). An equal volume of this stock solution was added together with 4% agar to produce 2xTY agar plates with the addition of ampicillin at approximately 55°C as required.

Lysogeny broth (LB media): This was prepared using Tryptone 10g/L (Formedium), yeast extract 5g/L (Formedium) and sodium chloride 10g/L (Fisher Scientific).

YEPR media was prepared using 20g/L raffinose, 20g/L yeast extract, 50mg/L adenine hydrochloride, 20g/L peptone, all dissolved in MQ water and autoclaved.

3.1.2 Stock solutions

50x TAE (Agarose gel electrophoresis running buffer for DNA): 2M Tris-acetate pH 8.5, 50mM EDTA pH 8.0.

10x running buffer (SDS-PAGE): 3% Trisma base (Sigma Aldrich), 14.4% glycine, and 1% SDS.

10x PBS(T): 1.37M NaCl (Fisher Scientific), 27mM KCl (BDH), 81mM Na₂HPO₄ (Fisher Scientific), 18 mM KH₂PO₄ (Merck) (0.1% (v/v) Tween-20 (Sigma Aldrich))

3.2 Methods

3.2.1 Yeast culture

Only one yeast background was used in all experiments; W303. Incubations at temperatures of 4°C, 30°C, and 37°C were all performed using temperature controlled rooms.

3.2.1.1 Mating, tetrad dissection, and genotype verification

All mating of haploid yeast to form diploid strains was performed on YPAD agar media plates. An *a* and α haploid strain were selected and thoroughly mixed together using a 10 μ L sterile, disposable inoculating loop on a plate and incubated at 25°C for 4-6 hours. Zygotes were selected from this population using a dissection microscope (MSM 400, Singer Instruments) and incubated for approximately 48 hours. An appropriate amount of cells were patched onto SPOVB agar plates for sporulation and incubated at 30°C for approximately 24 hours. An optical microscope was used to check for sporulation efficiency. An appropriate amount of cells was diluted in 10 μ L of 1.2M sorbitol solution with 1 μ L of 10mg/mL Zymolase enzyme solution (Sigma Aldrich) and incubated at 30°C for 15 minutes in order to digest the ascus. An appropriate volume of this digestion was streaked onto a YPAD agar plate. Tetrads were selected from the plates using a dissection microscope and incubated at 25°C for approximately 48 hours. Replica plating on appropriate dropout media marker plates was performed using a plate replicator and sterile velvet. To test mating types, yeast strains 216 and 217 were spread onto MM plates and also used in the replica plating. The replica plates were incubated at 25°C for approximately 48 hours. The colony growth on the marker plates was recorded to verify the genotype of the newly created diploid strain and the strain may be used in further experiments. This replica plating method testing for genetic markers and mating types will be henceforth referred to as “genotyping”.

3.2.1.2 Yeast strain storage and recovery

Yeast strains were stored by patching them on appropriate agar media and incubating at 30°C for approximately 16-20 hours before transferring the cells to a 1.8mL cryotube containing 1mL of 15% glycerol solution and storing at -80°C. Yeast strains were recovered by patching to appropriate agar plates and incubated at 30°C for approximately 24 hours.

3.2.2 *E. coli* culture

E. coli was cultured in LB media. Transformed *E. coli* was incubated in 2xTY media containing 100mg/L ampicillin. Incubation of *E. coli* was performed at 37°C with intense shaking.

3.2.3 Molecular biology and biochemistry

3.2.3.1 Polymerase chain reaction (PCR) protocols

The PCR kit used in all protocols was PCR BIO Taq DNA Polymerase containing enzyme and included 10x reaction buffer. All PCR protocols were derived from a 50µL reaction template. A typical 50µL reaction contained: 10µL of PCR BIO 10x reaction buffer, 2µL of 10µM forward primer, 2µL of 10µM reverse primer, 1µL of 5u/µL

PCRBIO Taq DNA Polymerase, template DNA of an appropriate concentration, and MQ H₂O (Milli-Q®) to a total reaction volume of 50µL. The thermocycling protocol template used in all experiments included: an initial denaturation step at 95°C for 1 minute, then 25 cycles of denaturation (95°C, 15 seconds), annealing (55°C, 15 seconds) and extension steps (72°C, 30 seconds per kilobase of amplicon), final extension (72°C, 5 minutes) and an indefinite hold at 10°C.

3.2.3.2 PCR product purification

The GeneJET PCR purification kit (Thermo Fisher) was used to purify PCR products by mixing them with a 1:1 ratio of binding buffer before being vortexed to ensure thorough mixing (Vortex Genie 2, Scientific Industries). The solution was then transferred into a GeneJET column and centrifuged at 20,238 x g for 1 minute (Centrifuge 5424, Eppendorf). The flow-through was discarded and 700µL of wash buffer was pipetted into the column. The column was centrifuged at 20,238 x g for 1 minute and the flow-through was discarded. The column was centrifuged again at 20,238 x g for 1 minute to remove all of the wash buffer before transferring the column into a microfuge tube. 50µL of MQ water was pipetted into the column and left to rest at room temperature for 1 minute. The column was centrifuged at 20,238 x g for 1 minute and the microfuge tube containing the purified DNA was retained while the column was discarded.

3.2.3.3 Agarose gel DNA electrophoresis

To check the results of a PCR reaction, some of the product was run on a 0.8% agarose gel. An appropriate sized gel was prepared using 0.8g of agarose per 100mL of 1x TAE buffer and completely dissolving the agarose using a microwave. This solution was left to cool until it could be handled comfortably before adding 5µL of 10mg/mL ethidium bromide (Sigma-Aldrich) per 100mL of solution. The solution was thoroughly mixed and poured into an appropriate gel cast with well comb and left to set for at least 20 minutes. The gel was then transferred into an appropriately sized electrophoresis tank (BioRad) and with fully submerged in 1x TAE. The DNA samples were mixed with 6x loading dye (Thermo Fisher) to an appropriate volume and a 1 kilo-base DNA ladder (GeneRuler, NEB) along with the samples were loaded into the wells of the gel and ran at an appropriate voltage and amperage according to the size of the tank, for 18-30 minutes. The gel image was then captured using a UV light camera to analyse the fragment size.

3.2.3.4 DNA gel extraction

The QIAquick Gel Extraction Kit (Qiagen) was used for all DNA gel extractions. After agarose gel electrophoresis described in 3.2.3.3, appropriate gel bands were removed and transferred to a microfuge tube using a glass cover slip and a UV trans-illuminator (UV transilluminator, UVP Inc.). The gel was weighed using a top pan balance (BP 310 P, Sartorius) and 300µL of solubilisation buffer per 100mg of gel was added before incubating at 50°C for 10 minutes in a thermomixer (Eppendorf). 100µL of propan-2-

ol (Sigma-Aldrich) was added per 100mg of gel and vortexed. The solution was transferred to a QIAquick Gel Extraction column and centrifuged at 20,238 x g for 1 minute. The flow-through was discarded and 700µL of QIAquick wash buffer was pipetted into the column. The column was centrifuged at 20,238 x g for 1 minute and the flow-through was discarded. The column was centrifuged again at 20,238 x g for 1 minute to remove all of the wash buffer before transferring the column into a microfuge tube. An appropriate volume of MQ water was pipetted into the column and left to rest at room temperature for 1 minute. The column was centrifuged at 20,238 x g for 1 minute and the microfuge tube containing the extracted DNA was retained while the column was discarded.

3.2.3.5 Plasmid cloning

Plasmids were constructed using the parental vectors Yiplac211, Ycplac111, and Ycplac33. Commercial restriction enzymes (Thermo Fisher) were used at a concentration of 10 units per 1µg of DNA with 10% 10x FastDigest buffer (Thermo Fisher) and incubated at 37°C for 30 minutes to digest DNA at specific sites for insertion of genes. Vectors in preparation for ligation with an insert were treated with 1 unit of rSAP (Shrimp Alkaline Phosphatase, NEB) enzyme and incubated at 37°C for 20 minutes. The vector and insert samples were run according to 3.2.3.3 and the vector and insert bands were co-purified according to 3.2.3.4 using 6µL of MQ water to elute in the final step. 5µL of ligation solution 1 (Takara) was pipetted into the vector-insert solution, mixed thoroughly and incubated at 16°C for 30 minutes. Competent *E.coli* (XL1-Blue) was then transformed by adding 100µL of cells prepared according

to 3.2.2 to the ligation mixture, mixed thoroughly and incubated on ice for 40 minutes. The cells were then heat shocked at 42°C for 90 seconds and cooled on ice for 2 minutes. 1mL of LB media was added to the tubes and mixed gently. The tubes were incubated at 37°C in a shaker (Vibrax VXR S1, IKA) for 1 hour. The tubes were then centrifuged at 20,238 x g for 1 minute and the supernatant was discarded, leaving the cell pellet. The pellet was resuspended in 100µL of MQ water and spread onto a 2xTY ampicillin agar plate. The plate was incubated at 37°C for 16-20 hours; sufficient time for clones transformed with the plasmid to emerge, but not satellite clones.

3.2.3.6 Alternative plasmid construction methods

Site directed mutagenesis was used to create mutations in plasmids and was performed using appropriately designed primers and the PCR protocol described in 3.2.3.1 using 5µL of 5ng/µL template plasmid DNA. Triplicate 50µL reactions were performed per mutation attempt. After the PCR reaction was completed, the triplicate reaction products were combined and 135µL of this solution was transferred to a microfuge tube. 15µL of 3M sodium acetate dihydrate solution was added along with 450µL of ice cold 100% ethanol to aid precipitation. The tube was mixed and left to precipitate at -20°C for at least 12 hours. The tube was centrifuged at 20,238 x g for 10 minutes at 4°C (Centrifuge 5415R, Eppendorf). The supernatant was removed using a water pump, taking care not to disturb the pellet. 100µL of 70% ethanol was added to the tube, vortexed and centrifuged at 20,238 x g for 5 minutes at 4°C (wash step). The supernatant was removed and the wash step was repeated. The supernatant was removed and the pellet was dried using a vacuum centrifuge at 45°C

for 5 minutes. 10µL of MQ water was added and the tube was incubated in a thermomixer at 65°C for 30 minutes. The tube was incubated on ice for 5 minutes before adding 1µL (10 units) of Dpn1 restriction enzyme (Thermo Fisher) along with 10% 10x SmartCut buffer (Thermo Fisher). The tube was mixed thoroughly and incubated at 37°C for 30 minutes. The mixture was then used to transform competent *E.coli* as described in 3.2.3.5.

3.2.3.7 Plasmid amplification

The purification of plasmids was performed using the Thermo Fisher GeneJET Plasmid Miniprep Kit. Transformed *E.coli* clones mentioned in 3.2.3.5 and 3.2.3.7 were used to inoculate approximately 10mL of liquid 2xTY ampicillin media in 25mL universal tubes and incubated at 37°C with rolling for 16-20 hours. The tubes were centrifuged at 3,803 x g and the supernatant was removed. The *E.coli* pellets were resuspended using 250µl of Resuspension Solution (Thermo Fisher), transfer into 1.5mL microfuge tube and vortexed. 250µL of Lysis Solution (Thermo Fisher) was added and the tube was inverted to mix gently. 350µL of Neutralization Solution was added next and gently mixed by tube inversion. The tubes were then centrifuged at 20,238 x g for 10 minutes and the supernatant was poured into GeneJET spin columns. The columns were centrifuged at 20,238 x g for 1 minute and the flow-through was discarded. 750µl of Wash Buffer (Thermo Fisher) was added to the columns, centrifuged at 20,238 x g for 1 minute, and the flow-through was discarded. The columns were centrifuged at 20,238 x g for 1 minute and the flow-through was discarded for a sEcond time to ensure total removal. The columns were transferred

into 1.5mL microfuge tubes and 70 μ L of MQ H₂O was pipetted to the center of the column membrane and left to rest at room temperature for 1 minute. The columns were centrifuged at 20,238 x g for 1 minute and the eluted plasmid DNA was collected.

In order to check that the obtained plasmid is of the expected size, appropriate restriction enzymes were used to digest the plasmid and run on a gel according to 3.2.3.5 and 3.2.3.4.

3.2.3.8 Sequencing

Sequencing of plasmids was performed by using Mix2Seq kits from Eurofins Genomics. 1.5 μ g of plasmid DNA was diluted in 15 μ L of MQ water and 2 μ L of 10 μ M appropriate primer at least 100 base pairs upstream of the desired sequencing region was added to the supplied tubes.

3.2.3.9 High efficiency transformation of yeast

Yeast cells were inoculated in a 25mL universal tube containing liquid YPAD media and incubated overnight at 30°C with rolling (200 rpm).

Upon reaching an optical density of between 0.2 and 0.5, the cells were harvested by centrifugation at 2,301 x g for 2 minutes. The supernatant was discarded and the cell pellet was resuspended in 1mL of 100mM lithium acetate (Sigma-Aldrich). The cells

were harvested again by centrifugation at 2,301 x g for 2 minutes. The resuspension and harvesting was repeated for a second time. The pellet was resuspended using between 200-50 μ L of 100mM lithium acetate (approximately 3x the pellet volume). Aliquots of 50 μ L were prepared in microfuge tubes and incubated at 30° C for 30 minutes. Single stranded DNA (10mg/mL salmon sperm, (Thermo Fisher) was incubated at 95°C for 5 minutes and chilled on ice for 2 minutes prior to use. The single stranded salmon sperm DNA was sonicated at 10 μ m amplitude for 10 seconds a single time after initial preparation. 240 μ L of 50% (w/v) polyethylene glycol (PEG, Sigma Aldrich) was added to the aliquot followed by 36 μ L of 1.0M lithium acetate and 25 μ L of single stranded DNA prepared earlier. For transformation of yeast using a plasmid 1 μ g of DNA in 5 μ L of MQ water was added. For genomic integration 250ng of DNA fragment in 5 μ L of MQ water was used. For integrative vectors, 250ng of plasmid in 5 μ L of MQ water was used, digested using a single cut site restriction enzyme. 45 μ L of MQ water was added to the aliquot in addition to the 5 μ L of selected DNA solution. The mixture was gently mixed using a pipette and incubated for 30 minutes at 30°C and heat shocked at 42°C for 20 minutes. The cells were then harvested by centrifugation at 3,381 x g for 3 minutes. The supernatant was removed and the cells were gently resuspended in 1mL of liquid YPAD media. The tube was then placed in a microfuge tube rack with lid and incubated for 90 minutes at 30°C with gently shaking. The cells were harvested by centrifugation at 20,238 x g for 30 seconds. The supernatant was removed and the cells were resuspended in 1mL of MQ water. The cells were harvested again by centrifugation at 20,238 x g for 30 seconds. The supernatant was removed and the cells were resuspended in 100 μ L of MQ water. The cells were then spread onto appropriate agar plates according to the

selection markers of the desired strain and incubated at 30°C for 48-72 hours to allow for clones to appear but not long enough for satellite clones.

3.2.3.10 Quick yeast DNA extraction

A small amount of yeast cells were grown on agar media and a 1µL inoculation loop was used to suspend cells in 100µL of 200mM lithium acetate / 1% SDS solution in a 1.5mL microfuge tube. The tube was vortexed and incubated at 70°C for 5 minutes. 300µL of 100% ethanol was added and vortexed. The tube was centrifuged at 20,238 x g for 5 minutes. The supernatant was removed and 500µL of 70% ethanol was added. The tube was vortexed and centrifuged at 20,238 x g for 5 minutes. The supernatant was removed and the tubes were left open to dry in a fume hood for 30 minutes. 100µL of MQ water was added and the tube was incubated with shaking at 37°C. The tube was centrifuged at 20,238 x g for 1 minute and the supernatant containing the DNA was collected.

3.2.3.11 BPA crosslinking using UV light

Cells of the yeast strain carrying the BPA substituted proteins were grown in 100mL of appropriate media with 1mM BPA at 25°C until the OD reached 0.6 per mL (total ~60 OD/100mL). The cells were transferred into a 50mL falcon tube and centrifuged at 2,301g for 2 minutes to pellet the cells. The supernatant was removed and the pellet was resuspended in 1mL of ice cold PBS before transferring the suspension to and

transfer into a 1.5mL microfuge tube. From this point, the cells were kept on ice throughout the rest of the BPA crosslinking procedure. The tube was centrifuged at 20,238 x g for 30 seconds and the supernatant was discarded. The cells were resuspended in 1mL of ice cold PBS and transferred into an 8-well plate. The plate was placed on a bed of ice and put into a UV crosslinker (Spectrolinker XL-1500W crosslinker, Spectronics Corporation) equipped with a 360nm wavelength emitting bulb. The cells were subjected to UV light at 360nm for 1 minute with a 5 minute rest interval. This was repeated 3 times. The cells were transferred into a 2mL tube and centrifuged at 20,238 x g for 30 seconds. The supernatant was removed.

3.2.3.12 TCA protein extraction

4 OD per 1mL of cells were cultured and harvested by centrifugation at 2,301 x g for 2 minutes. The supernatant was removed and the cell pellet was resuspended with 1mL of ice cold MQ water and transferred to a 1.5mL microfuge tube. The tube was centrifuged at 20,238 x g for 30 seconds and the supernatant was removed. The cells were resuspended using 1mL of ice cold water. 150 μ L of extraction buffer was added to the cell suspension and incubated on ice for 15 minutes. The extraction buffer contained: 1.7M sodium hydroxide, 7.5% 2-Mercaptoethanol, and 7.5% water. 150 μ L of 55% TCA was added, mixed by tube inversion, and incubated on ice for 10 minutes. The tube was centrifuged at 20,238 x g for 10 minutes and the supernatant was removed. The pellet was resuspended in 150 μ L of 2x protein loading buffer. The 2x protein loading buffer contained: 0.25M Tris-HCl pH 6.8, 4% SDS, 20% glycerol, 10% 2-Mercaptoethanol, 0.25% Bromophenol blue, 4.75% MQ water. 50 μ L of 1M Tris pH

8.8 was added and then vortexed to mix. The protein-lysate solution was then sonicated at an amplitude of 7 μ m for 10 seconds. The protein-lysate was then incubated at 95°C for 5 minutes and then centrifuged at 20,238 x g for 10 minutes.

3.2.3.13 Native protein extraction

Cells were cultured in liquid growth media and the OD was measured using a Helios Delta spectrophotometer (Thermo Electron). The number 30 was divided by this OD reading to produce a numerical quantity of cells used in native protein extraction experiments known as “30 OD”. 30 OD of cells were suspended in 500 μ L of ice cold 1x PBS solution and centrifuged in a 2mL tube at 20,238 x g for 30 seconds. A lysis buffer was prepared containing: 0.05M Tris pH 7.5, 0.15M NaCl, 5mM EDTA pH 8.0, 0.5% NP-40 (Sigma Aldrich), 1mM DTT (Sigma Aldrich), 1mM PMSF (Sigma Aldrich), and one cOmplete™ Protease Inhibitor Cocktail tablet (Roche); all dissolved in water. The cells were resuspended in 1mL of lysis buffer and centrifuged at 20,238 x g for 30 seconds. The supernatant was removed and the cells were resuspended in 300 μ L of lysis buffer (1mL per 10 OD of cells). An excess of 0.5mm glass beads (Sigma Aldrich) were added until the cell suspension was completely covered and then placed in a (Minibeadbeater, Biospec Products) which was run for three 1 minute intervals with a 5 minute incubation period on ice between each interval. The bottom of the 2mL tube was punctured using a hypodermic needle heated using a Bunsen burner. The 2mL tube was then placed in a 5mL Eppendorf tube with the lid removed and was centrifuged at 3,803 x g for 2 minutes at 4°C. The supernatant was collected in the 5mL Eppendorf tube and transferred into a 1.5mL microfuge tube before being

centrifuged at 20,238 x g for 20 minute at 4°C. The supernatant was removed and transferred into a 1.5mL microfuge tube. A Bradford assay was performed using Bio-Rad protein assay solution (Bio-Rad) to determine an appropriate protein concentration as described in 3.2.3.23.

3.2.3.14 Immunoprecipitation

An antibody specific for the tag used on the protein of interest was diluted 1:3000 using 5% milk solution in PBS-T (Thermo Fisher) and 2mL was added to the protein-lysate. The tube was put on a roller at 4°C for 2 hours. 30µL of Dynabeads (Thermo Fisher) carrying an appropriate anti-antibody were washed using 1mL of lysis buffer and a magnetic tube rack by rotating the tubes. The lysis buffer was removed and the Dynabeads were washed using 1mL of lysis buffer two further times. The Dynabeads were added to the protein lysate, mixed gently using a pipette and incubated with rolling at 4°C for approximately 16 hours. The tube was centrifuged at 60 x g for 30 seconds and then placed into a magnetic tube rack. The Dynabeads were washed three times using a magnetic tube rack and 1mL of lysis buffer per wash with a 5 minute incubation with rolling at 4°C between each wash. The lysis buffer was removed and 50µL of x2 protein loading buffer was added as prepared in 3.2.3.12. The protein-lysate was then incubated at 95°C for 5 minutes.

3.2.3.15 SDS PAGE

SDS PAGE acrylamide resolving gels were prepared at an appropriate acrylamide concentration according to resolution needs. All gels contained: 0.375M Tris pH 8.8, 0.1% SDS, 0.1% APS, 0.1% TEMED, and variable amount of 30% acrylamide/water to produce a final concentration of acrylamide between 7.5 and 15%. A 4% stacking gel was cast directly on top of the resolving gel constituting of: 73% water, 4% acrylamide, 0.125M Tris pH 6.8, 0.1% SDS, 0.1% APS, and 0.1% TEMED. Miniprotean Tetra Cell (Biorad) were used to run SDS PAGE gels with broad range protein ladders (NEB). x10 running buffer was diluted to x1 before filling the gel tanks.

For all crosslinking experiments, the gels used were pre-cast Tris-Acetate 3-8% gradient gels (Invitrogen) and were run for 4 hours at constant voltage of 150v.

3.2.3.16 Western blot

Protein from an SDS PAGE resolving gel was transferred to a Hybond C nitrocellulose membrane (Amersham) using the wet transfer method. The membrane and gel was sandwiched between three pieces of Whatman 3MM paper and transferred at 150 mA for 2 hours or at constant 16 V for approximately 16 hours at 4°C. Ponceau solution (Sigma Aldrich) was added to check the efficacy of the transfer. The membrane was then washed with water and cut to size before blocking with 5% milk solution in PBS-T for 30 minutes. The membrane was added to a 50mL falcon tube containing the primary antibody incubated at room temperature for 1 hour with rolling. The membrane was washed with PBS-T three times consisting of 5 minutes incubation at room

temperature with gentle shaking per wash. The membrane was then added to the secondary antibody and incubated at room temperature for 1 hour with rolling. The membrane was washed again three times with PBS-T and drained. The Millipore Immobilon western solution system was applied to the membrane and was visualised using GeneTool capture (Syngene) on the G:BOX (Syngene) imaging system with automatic exposure conditions. The same gel running and capture conditions were used for all crosslink experiments in this study.

3.2.3.17 BMOE crosslinking

A stock solution of 125mM BMOE was prepared in DMSO and dissolved at 37°C with shaking. 20 OD of cells were harvested using centrifugation at 2,301 x g for 2 minutes and washed with 500µL of PBS twice before being re-suspended in 500µL of PBS. 25µL of 125mM BMOE solution was added to the suspension and vortexed thoroughly before being left to incubate at room temperature for 6 minutes. 3µL of 1M DTT was then added to stop the crosslinking reaction. The cells were then washed with 1mL of 5mM DTT in PBS twice and transferred to a 2mL tube ready for native extraction as per 3.2.3.13.

3.2.3.18 TEV protease cleavage

TEV cleavage was performed after the wash step during the immunoprecipitation as described in 3.1.5.14. The Dynabeads were then washed once with 500µL of digestion

buffer containing 25mM Tris pH 8.0, 150mM NaCl, and 2mM 2-Mercaptoethanol. The beads were then incubated for 16 hours at 20°C with shaking in 30µL of digestion buffer supplemented with 10µg of TEV protease (Sigma).

3.2.3.19 CRISPR-Cas9 gene editing system

The CRISPR-Cas9 gene editing system used in all experiments was the method described by Daniels *et al.*, 2018. 500ng of the vector 750 or 263 was co-transformed with a digested integrative plasmid as described in 3.1.5.5 and 3.1.5.9 after deactivating the enzymes used to digest the integrative plasmid by incubating the solution at 80°C for 5 minutes. The protocol for transforming yeast in 3.1.5.9 was used as normal afterwards.

3.2.3.20 Alpha factor cell cycle arrest

S.cerevisiae cells were arrested in G1 phase using the yeast mating pheromone; alpha factor. Strains with the modified leu2 locus: “leu2::Gal1p-Sic1(9m)/His3p-Gal1/His3p-Gal2/Gal1p-Gal4::Leu2” could be maintained in G1 cell cycle arrest status by activation of Sic1 gene transcription, induced by the introduction of galactose into the growth media when depleted of glucose. Yeast strains were grown in universal tubes containing YPAD media at 30°C for 16-20 hours with shaking. The cells were harvested by centrifugation for 2 minutes at 2231 g. The cells were re-suspended in 1mL YEPR and transferred into 1.5mL tubes. The cells were harvested by

centrifugation for 30 seconds at 20,238 x g. The supernatant was removed and the cells were re-suspended using 1mL of YEPR. This wash step was repeated three times to remove traces of glucose. The cells were re-suspended in 1mL of MQ water and the O.D. was measured. 100mL of YEPR media was inoculated with the target OD of 60, using a doubling time of 1.7 hours. The culture was incubated at 30°C with shaking until the target OD was achieved. The culture was diluted to 10 OD in 50mL of YEPR. 1mL of culture was transferred into a 1.5mL tube. The cells were harvested by centrifugation for 30 seconds at 20,238 x g. The supernatant was removed and the cells were re-suspended in 1mL of 70% ethanol before storage at -20°C for later FACS analysis. 20µL of 5mg/mL yeast mating alpha factor (Zymo Research) was added to the 50mL culture and incubated at 30°C with shaking. After 1 hour, 10µL of alpha factor was added and returned to incubation. After 30 minutes, 10µL of alpha factor + 5mL of 20% galactose was added and returned to incubation. After 30 minutes, 10µL of alpha factor was added and returned to incubation. After 30-40 minutes, the cells were checked under the microscope. When more than 85% of the cells had shmoo, this indicated that the mating hormone had taken effect on the a mating type cells; successfully synchronising the cells at a stage of arrest. 1mL of culture was transferred into a 1.5mL tube. The cells were harvested by centrifugation for 30 seconds at 14,680 g. The supernatant was removed and the cells were re-suspended in 1mL of 70% ethanol before storage at -20°C for later FACS analysis. The rest of the culture was washed 3 times with YPAD media to remove traces of the alpha factor using centrifugation and re-suspension. The cells were re-suspended in 50mL YPAD media with 1mg/mL alpha factor protease (Sigma Aldrich). The culture was incubated for 1 hour at 30°C with shaking. 1mL of culture was transferred into a 1.5mL tube. The cells were harvested by centrifugation for 30 seconds at 20,238 x g. The supernatant was

removed and the cells were re-suspended in 1mL of 70% ethanol before storage at -20°C for later FACS analysis. The rest of the culture was used to perform BMOE crosslinking as described in 3.2.3.17.

3.2.3.21 Nocodazole cell cycle arrest

Arrest in G2 phase for yeast strains was achieved by the addition of nocodazole 5mg/mL dissolved in DMSO (Sigma). Yeast strains were grown in universal tubes containing YPAD media at 30°C for 16-20 hours with shaking. The cells were harvested by centrifugation for 2 minutes at 2231 g. The cells were re-suspended in 1mL of MQ water and the O.D. was measured. 100mL of YPAD media was inoculated with the target OD of 60, using a doubling time of 1.5 hours. The culture was incubated at 30°C with shaking until the target OD was achieved. The culture was diluted to 10 OD in 50mL of YPAD. 1mL of culture was transferred into a 1.5mL tube. The cells were harvested by centrifugation for 30 seconds at 20,238 x g. The supernatant was removed and the cells were re-suspended in 1mL of 70% ethanol before storage at -20°C for later FACS analysis. 20µL of 5mg/mL yeast mating alpha factor (Zymo Research) was added to the 50mL culture and incubated at 30°C with shaking. After 1 hour, 10µL of alpha factor was added and returned to incubation. After 30 minutes, 10µL of alpha factor was added and returned to incubation. After 30 minutes, 10µL of alpha factor was added and returned to incubation. After 30-40 minutes, the cells were checked under the microscope. When more than 85% of the cells had shmoo, this indicated that the mating hormone had taken effect on the a mating type cells; successfully synchronising the cells at a stage of arrest. 1mL of culture was transferred

into a 1.5mL tube. The cells were harvested by centrifugation for 30 seconds at 14,680 g. The supernatant was removed and the cells were re-suspended in 1mL of 70% ethanol before storage at -20°C for later FACS analysis. The rest of the culture was washed 3 times with YPAD media to remove traces of the alpha factor using centrifugation and re-suspension. The cells were re-suspended in 50mL YPAD media with 50µL of 5mg/mL nocodazole (Sigma Aldrich). The culture was incubated for 1 hour at 30°C with shaking. 1mL of culture was transferred into a 1.5mL tube. The cells were harvested by centrifugation for 30 seconds at 20,238 x g. The supernatant was removed and the cells were re-suspended in 1mL of 70% ethanol before storage at -20°C for later FACS analysis. The rest of the culture was used to perform BMOE crosslinking as described in 3.2.3.17.

3.2.3.22 Fluorescence activated cell sorting (FACS)

Samples for FACS were prepared by harvesting 0.5 OD of cells in 1.5mL tubes via centrifugation at 20,238 x g for 30 seconds. The supernatant was removed and 1mL of MQ H₂O was added before re-suspending the cells. The tubes were centrifuged at 20,238 x g for 30 seconds and the supernatant was removed. 1mL of 70% ethanol in MQ H₂O was added to the tubes which fixed the cells. The tubes were centrifuged at 3,381 x g for 5 minutes and the supernatant was removed. The cells were re-suspended with 1ml of 50mM Tris pH 7.5 containing 0.2mg/mL RNase. The cell suspensions were incubated with shaking for 2 hours at 37°C to allow RNA digestion. The cells were then centrifuged at 3,381 x g for 5 minutes and the supernatant was removed. The cells were re-suspended with 400µL FACS buffer which contained:

0.18M Tris pH 7.5, 0.19M NaCl, 0.07M MgCl₂ and 0.05mg/mL propidium iodide in MQ H₂O. The cells were sonicated at 10 μ M amplitude for 5 seconds. 100 μ L of each cell suspension was diluted in 900 μ L of 1M Tris pH 7.5 and mixed. The samples were then run in a BD FACSCalibur flow cytometer, measuring 10,000 events at a rate of 300 events per second.

3.2.3.23 Bradford protein assay

The protein assay used in this study involved establishing a protein standard using bovine serum albumin (NEB). Dilutions of bovine serum albumin (BSA) were prepared at 0, 2, 4, 6, 8, and 10mg/mL using x1 protein assay buffer (BioRad) and MQ H₂O in 1mL cuvettes (Thermo Fisher). The OD of the protein standard was measured at 595nm using a Helios Delta spectrophotometer (Thermo Electron). The OD measurements were plotted on a graph using Microsoft Excel and a line of best fit was drawn. The equation of this line was used to find the protein concentration of samples for testing. These were prepared by adding 1 μ L of sample into a cuvette containing 1mL of x1 protein assay buffer (Biorad) before vortexing.

4.0 Results

4.1 Chapter 1

4.1.1 Introduction

Once sister chromatid cohesion is created during DNA replication, Smc3 acetylation is required to maintain cohesion by stabilising cohesin on DNA until the metaphase/anaphase transition. This is achieved by preventing Rad61-Pds5 dependent releasing activity, which triggers the opening of Smc3-Scc1 interface and allows the escape of entrapped sister chromatids from cohesin ring. Smc3 acetylation may also inhibit the Scc2-Scc4 dependent loading of cohesin and therefore prevent the establishment of cohesion. The molecular mechanism underlying this inhibitory effect is still unknown. A technical challenge to the study of this phenomenon is that acetylation of Smc3 is a post-translational modification that cannot be studied directly. This is because there are no efficient systems available in molecular biology to trigger acetylation at will, or, assay which can track acetylated cohesin *in vivo* at the molecular level without significantly interfering with normal function of cohesin. To model acetylation more easily, the mimicking form smc3K112Q, K113Q (QQ or smc3QQ) was employed instead as a continuation of Dr Bin Hu's work. It has been demonstrated that acetylation of cohesin causes cohesion defects in the following cell cycle of $\Delta hos1$ cells (Beckouët et al., 2016; Borges et al., 2010). In tandem, the QQ mutation is known to greatly reduce the interaction between cohesin and DNA as shown by chromatin immunoprecipitation (ChIP) experiments (Hu et al., 2015). Therefore it may be

possible that acetylation prevents effective loading onto the DNA. Lysine is positively charged whereas glutamine is neutral, thus removing the positive charge much like acetylation which may be connected to the phenotype of *smc3QQ* and pre-acetylated cohesin. This is supported by other experiments which tested the mutation *smcK112N*, *K113N* for viability and found that this is also lethal. In addition, asparagine substitution also causes cohesion defects verified by ChIP (Borges et al., 2010). ATP hydrolysis is required for loading and releasing processes. Because acetylation of cohesin may abrogate loading and releasing activity, it is hypothesised in this study that acetylation may interfere with ATP hydrolysis activity at some stage in loading or releasing processes. In order to understand the effect of acetylation on the structure or interaction sites of Smc3; the suppressor mutants of QQ may provide insight into possible changes. This was the rationale for a genetic screen examining QQ suppressor mutations. By producing a catalogue of various suppressor mutants, these may be later studied for changes to Smc3 structure or interactions as part of further experiments.

A genetic screen can be performed by introducing random mutations via error prone PCR into a plasmid containing the gene of interest; in this case *SMC3* (McCullum et al., 2010; Wilson and Keefe, 2001). By combining these mutations with *smc3QQ*, these plasmids may be transformed into a haploid strain possessing deletion of *SMC3* supplemented with a plasmid containing a functional copy of *SMC3*. As the only functional copy of *SMC3* is the mutant version once the plasmid is lost, the strain viability is a direct assay of Smc3 functionality. As the QQ mutation itself is lethal, only plasmids containing QQ suppressors will generate viable strains (Hu et al., 2015). The mutations *smc3R1008I* and *E199A* are both able to rescue *smc3QQ*. This was a

finding by the Nasmyth laboratory (personal communication). A genetic screen was performed by Jessica McMaster, University of Sheffield, UK, in an attempt to find suppressor mutations for the poor viability phenotype of *smc3QQ, R1008I* using error-prone PCR on the *SMC3* gene of a plasmid. However, this screen yielded multiple mutations per copy of *SMC3*, any of which could have been responsible for improved viability of *smc3QQ, R1008I*. Transforming strains with a mix of error-prone produced *SMC3* on plasmids may cause selection pressures that allow transformants to grow which possess mutations in other parts of the genome, thus masking the real suppressor mutations. Therefore, another more robust albeit less extensive viability test was performed which tested single candidate suppressor mutations.

4.1.2 Chapter 1 part 1: *smc3K112Q*, *K113Q*, *R1008I* suppressor screen

In order to test whether mutations from the McMaster screen were indeed suppressors of *QQ*, *R1008I*; the diploid strain 981, containing one wild type allele of *SMC3* and a deletion of the other via interruption with the *HIS3* marker was transformed with YIplac211 plasmids containing the *SMC3* candidate suppressor mutant and the *QQ*, *R1008I* mutations. The *HIS3* marker is a gene which encodes a protein involved in histidine biosynthesis. YIplac211 is a integrative plasmid, designed to modify the genome, and was used to integrate the *QQ* suppressor mutant gene into the *ura3* locus, marked with a functional copy of *URA3*. Sporulation and tetrad dissection then produced four haploids with the following possible genotypes:

Table 3: All possible haploid genotypes with “mutation” representing a candidate *smc3QQ* suppressor mutation.

	Genotype
Haploid 1	<i>SMC3</i> <i>ura3</i>
Haploid 2	<i>SMC3</i> <i>ura3::smc3K112Q,K113Q, R1008I,</i> <i>mutation:: URA3</i>
Haploid 3	<i>smc3Δ::HIS3</i> <i>ura3</i>

Haploid 4	<i>smc3Δ::HIS3</i> <i>ura3::smc3K112Q,K113Q, R1008I,</i> <i>mutation:: URA3</i>
-----------	---

With these possible genotypes, the segregation of viability is the assay for QQ, *R1008I* rescue. If the candidate mutation indeed rescues QQ, *R1008I*, then the spore containing the suppressor mutation will grow faster and present a larger colony than the spore without. This method allows for the easy tracking of $\Delta smc3$ and mutant *SMC3* as they have separate genetic markers which can be tested by replica plating. In addition, there are no plasmids that can be lost during replication, which may affect results.

Single candidate QQ suppressor mutations were provided on plasmids by Jessica McMaster after her genetic screen using error prone PCR. The backbone of these plasmids were changed from YCplac111 to Ylplac211 using the restriction enzyme Bgl1 and the cloning methods described in 3.2.3.5-6. YCplac plasmids contain centromeric sequences and exhibit chromosomal behaviour when transformed. Ylplac plasmids can be cleaved to form linear DNA which have homologous sequences to a specific gene at either end, allowing incorporation into the genome via the homologous recombination pathway. As the purpose of the plasmids were to modify the genome of yeast, the backbone was changed to fit this need. Afterwards, the construct was verified by restriction enzyme digest and gel electrophoresis by comparing the plasmid to the parental vector using methods described in 3.2.3.3 (see figure 18). The plasmid was then sequenced using methods described in 3.2.3.8.

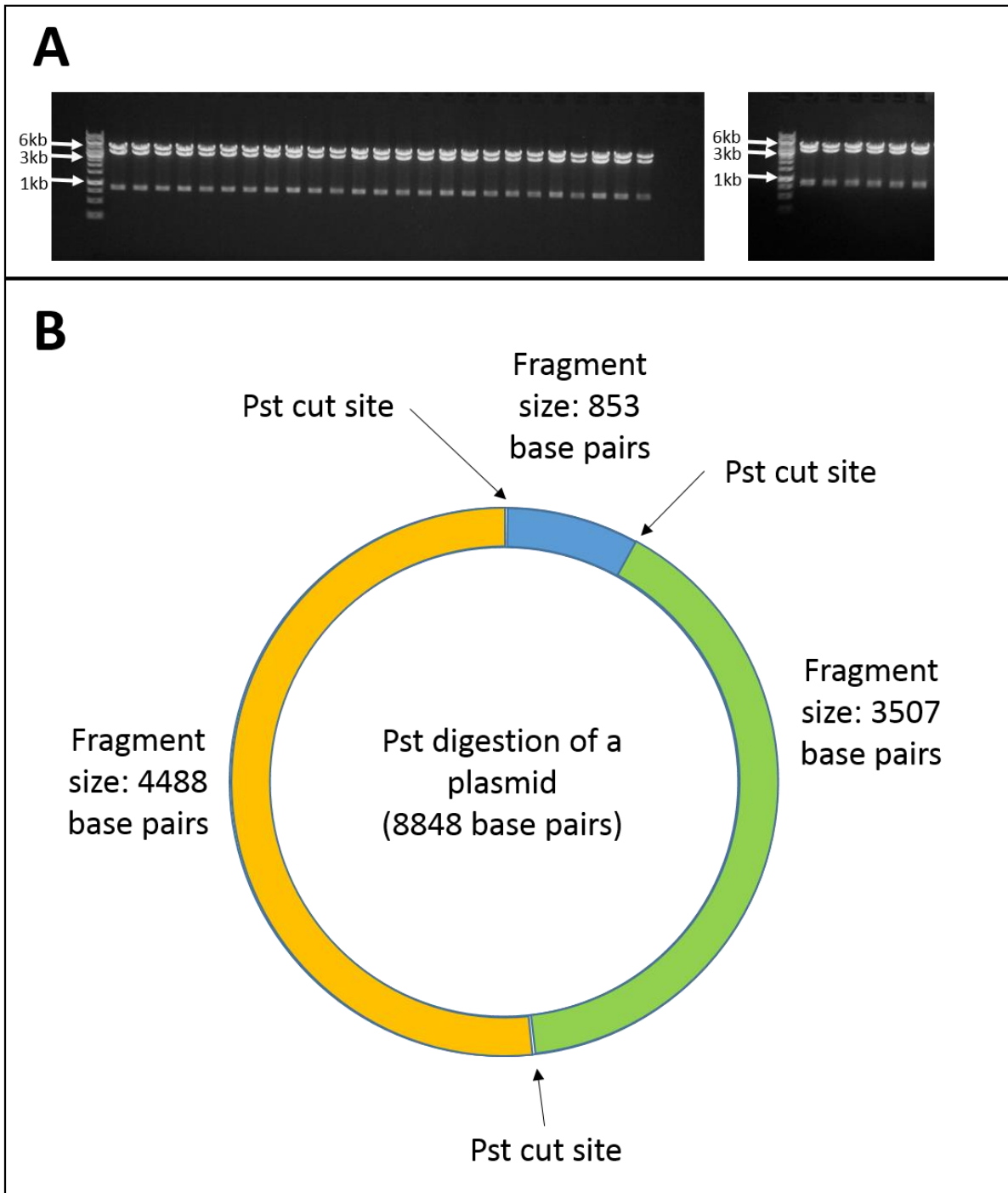


Figure 18: Agarose gel image of Pst1 restriction enzyme digested plasmids and plasmid map.

(A): Agarose gel (0.8% in x1 TAE buffer). Lane 1: 1kb GeneRuler DNA ladder (Thermo Fisher),

lane 2-25: plasmids 592-622. Gel photo, right: Lane 1: 1kb DNA ladder (Thermo Fisher), lane

2-7: plasmid 635-639, 547. The DNA was stained by the agarose gel itself which contained 0.005% ethidium bromide. The image was taken using the G:BOX (Syngene) imaging system with automatic exposure conditions. (B): Plasmid map of Pst1 digestion, yielding product sizes of: 4488, 3507 and 853 base pairs. These three bands are visible in the agarose image of (A) and are in the expected locations relative to the DNA ladder.

Yeast strain 981 was then transformed with the integrative plasmids carrying the mutant forms of *SMC3*. The strains were dissected to find haploids that had better viability than those containing only the *smc3QQ*, *R1008I* mutations. A rating system was used to describe the quality of survival on a scale of 0 to 4 where 0 denotes lethality (*smc3K112Q*, *K113Q* control) and 4 denotes growth equivalent to wild type *SMC3* haploids (see figure 19). For reference, *smc3QQ*, *R1008I* has a survival rating of 1.

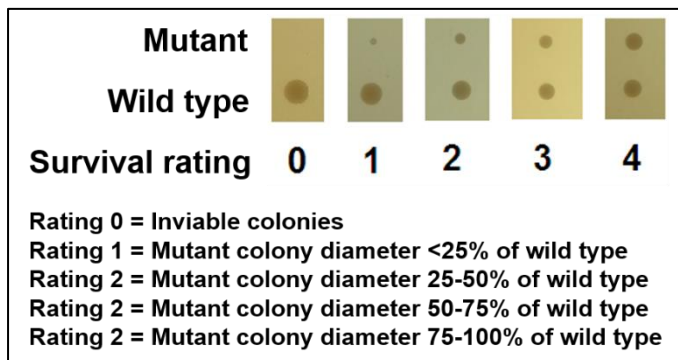


Figure 19: Survival ratings given to mutant *Smc3* carriers in comparison to wild type *Smc3* and the rating criteria.

The results of the viability test showed a wide distribution of suppressors across the Smc3 protein. Rescue ratings of the tested mutations can be found in tabular form under 7.4.1. In order to analyse the distribution of suppressors according to position within Smc3, particular domains were identified. The four areas of interest were the head, hinge, coiled coil and break regions. The head domain was identified using the crystal structure and amino acid alignment from Gligoris and co-workers, and the hinge from Haering and co-workers (Gligoris et al., 2014; Haering et al., 2002). As full length eukaryotic Smc3-Smc1 have not been resolved, coiled coil prediction software was used to predict these regions along with breaks which occur in between where the alpha helix structure is disrupted. The software used was an online tool derived from Lupas and co-workers (Lupas et al., 1991). This software was used with a scanning window of 21 and a probability threshold of 0.7. The reason this software was used is because Dr Bin Hu used this software to insert tobacco etch virus cleavage sites into Smc3 in break regions successfully to avoid coiled coil disruption. Mutation of the coiled coil regions may cause cohesion defects (Orgil et al., 2016). Known coiled coil regions were subsequently added according to known structure around the head and hinge domains. The locations with high suppressor density may represent locations of interest which involve protein interactions or notable structures which are essential to cohesin function (see figure 20).

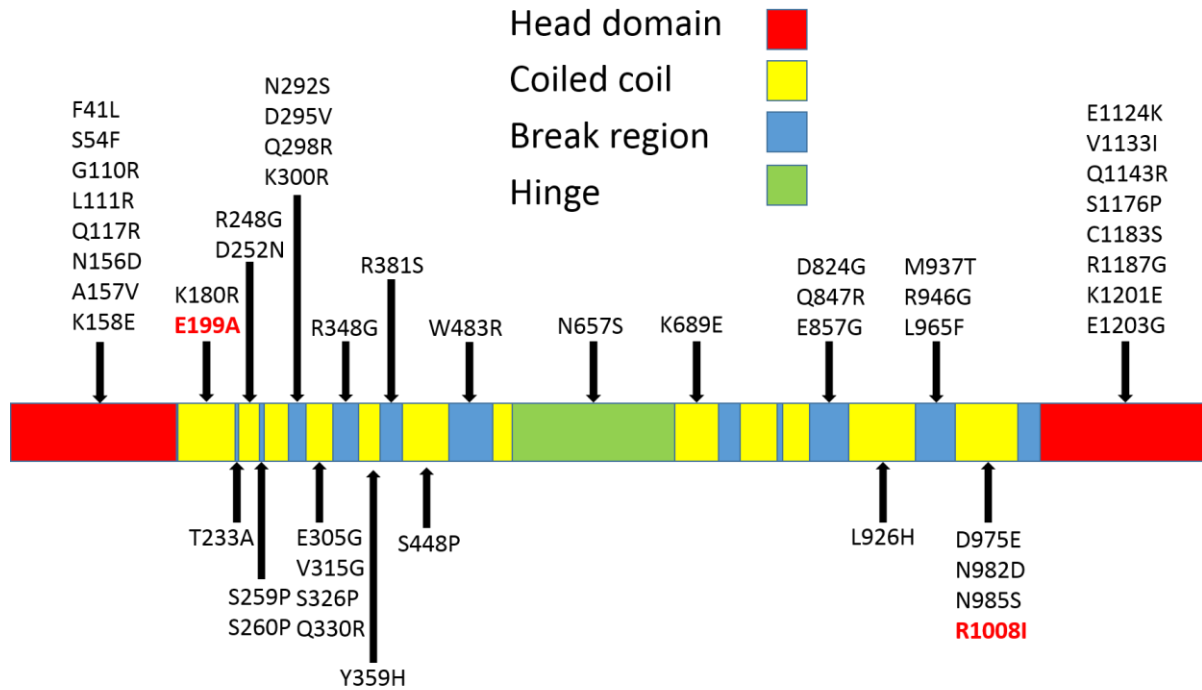


Figure 20: Diagram showing the relative locations of the *smc3QQ* suppressor mutations.

The map shows that the 48 tested suppressor mutations are found all over Smc3. Of these 48, 16 are found in the head domain (33%), 15 in the coiled coil regions (31%), 16 in the break region (33%), and only 1 suppressor (2%) was located in the hinge domain. Proportionally, the head domain occupies 341 residues of 1230 (28%), the hinge 168 (14%), coiled coil 539 (44%), and break regions 182 (15%). The head domain and break regions are disproportionately overrepresented with the break regions accounting for more than twice the expected incidence.

Without the structure of the break regions, positional analysis cannot be performed. Positional analysis of suppressors in the head domain however, was achievable as essential ATP related motifs can be identified within the structure of the head domain using protein alignment with other fully resolved ATPases. From these, five essential

motifs were identified and can be seen in figure 21: the Walker A, Walker B, Q-loop, H-loop and C motif (Diederichs, 2000; Gaudet and Wiley, 2001; Löwe et al., 2001; Neuwald et al., 1999).

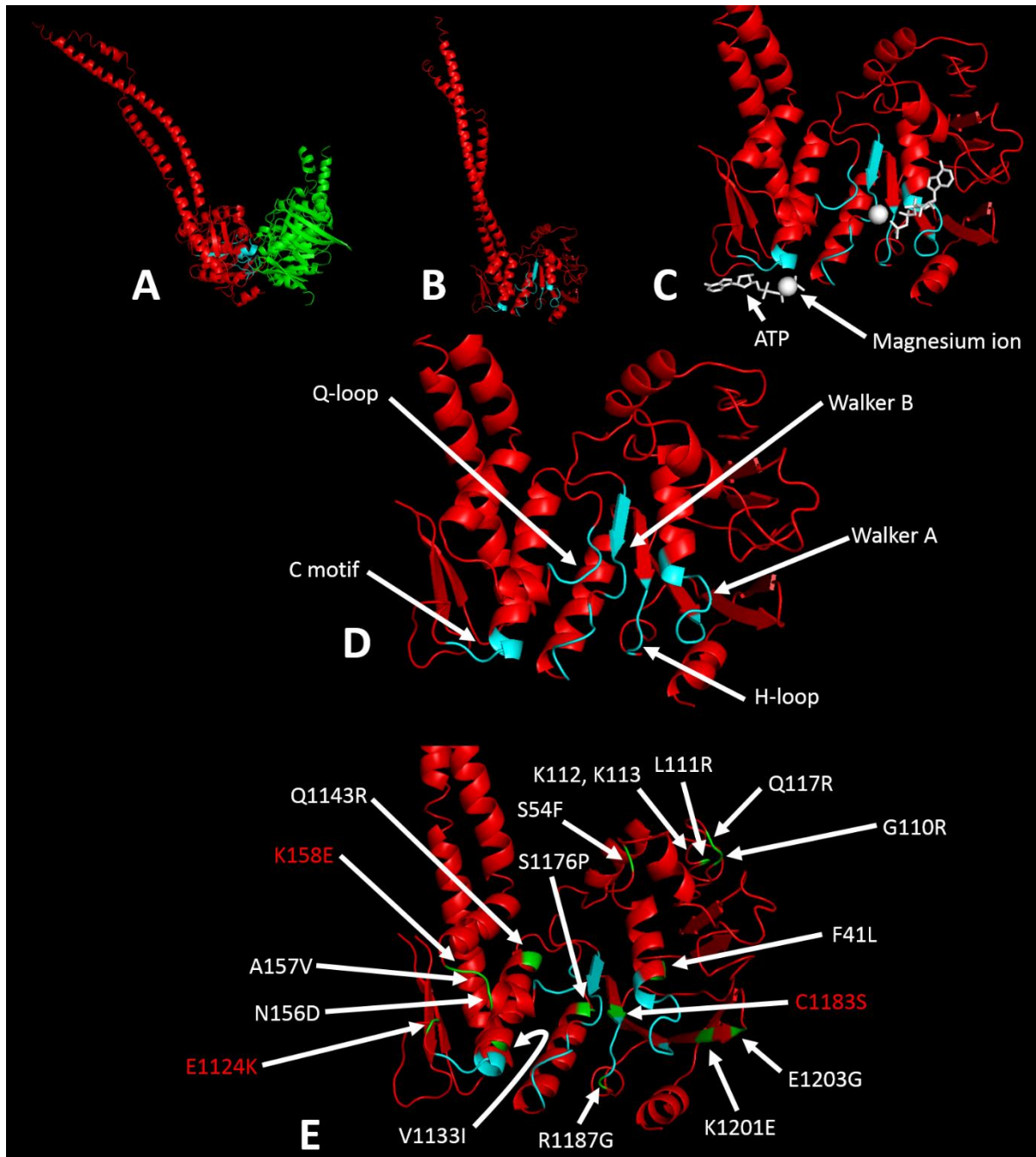


Figure 21: Cartoons of Smc3 head domain structure along with essential motifs and locations of QQ suppressor mutants.

Colour code: Smc3 (red), Smc1 (green), ATPase domain motifs (cyan), ATP and Magnesium (white), suppressor mutants (green against red Smc3). (A) View of Smc3 and Smc1 in the head engagement position. (B) View of Smc3 without Smc1 and rotated to expose the Smc1 interface. (C) Zoom image of the Smc1 interface with ATPase essential motifs in cyan and the position of ATP along with magnesium in white. (D) Annotated zoom image of the Smc1 interface with labelled motifs. (E) Annotated zoom image of the Smc1 interface with labelled QQ, *R1008I* suppressor mutations and location of acetylation targets K112, K113. True QQ suppressors are highlighted in red font. Smc3R1008 (not featured) is located in the coiled coil and not the head domain. Structures adapted from Gligoris and co-workers (Gligoris et al., 2014).

The overall distribution of the QQ, *R1008I* suppressor mutants does not appear to indicate a particular site of Smc3 which may be responsible for rescue activity. There are many sites in the coiled coil and break regions along with further sites within the vicinity of all five motifs in the head domain. This suggests that QQ may cause a defect that is remediable by many possible changes all over Smc3 structure which may be due to global structural change rather than local.

Another screen was performed to examine whether any of the tested candidate mutations were able to suppress *smc3QQ* without *R1008I*. Only three mutants were able to do so: *K158E*, *Q1143R* and *C1183S* (highlighted in figure 21 with red font). All of these mutations are located in the head domain. *K158E* is situated close to the Q-loop, a structure required to bind the magnesium ion. *Q1143R* has side chains that

extend towards others in the Walker B motif which contains a glutamate residue that performs the nucleophilic attack on ATP using a water molecule. *C1183S* immediately precedes the H-loop; the structure which may polarise the involved water molecule prior to hydrolysis (Hollenstein et al., 2007). The result from this test shows more clearly that structural changes in the head domain alone are sufficient for QQ suppression. All of these suppressors however, suffer from noticeably slow growth, and have a survival rating of no more than 2 in the QQ background without *R1008I* (see table 9).

The *smc3R1008I* mutation is required for the rescue of *smc3QQ* in most candidate mutations tested and therefore may have heightened importance in rescuing the fatal QQ phenotype. By combining the effect of *smc3R1008I* and some of the more effective candidate suppressors such as *smc3M937T*, complete rescue of *smc3QQ* can be achieved. However, without *smc3R1008I*, *smc3M937T* cannot suppress *smc3QQ* at all. This result may suggest that *smc3R1008I* facilitates an essential function of cohesin that is blocked by QQ leading to cell death but is fully restored when combined with other mutations. In addition, all of the true QQ suppressors in the head domain have improved viability when combined with *smc3R1008I*, possibly due to an additive effect from a common mode of rescue.

The results from this part suggest two possible mechanisms of action which may explain the function of acetylation via study of the mimic, *smc3QQ*. Either, *smc3QQ* may affect ATP hydrolysis function, or affect the interaction with other proteins in some way. To test this, two methods were attempted. The first aimed at testing the proposed

method of ATP hydrolysis abrogation described by Gligoris and co-workers (Gligoris et al., 2014). The second method is to test the effect of a particular Scc2 mutant on rescuing *smc3QQ*.

4.1.3 Chapter 1 part 2: Testing the effects of mutations in the vicinity of smc3QQ.

Gligoris and co-workers claimed that *smc3R61Q* is lethal due to effects on an alpha helix structure opposite Smc3K112, K113 which may affect ATPase machinery (Gligoris et al., 2014). Figure 22 below shows the position of *smc3R61Q* in close proximity to the acetylation sites K112, K113. The supposed mechanism of action was described as being the removal of positive charge by acetylation which indirectly deforms the ATPase machinery as this structure may be supported by repulsive positive charges in the opposing alpha helix. By confirming this finding, further study of the exact structural change may be instigated. Strains were made to test this hypothesis by mutagenesis and cloning methods (3.2.3.5-6) followed by transformation (3.2.3.9) and mating procedures before being dissected (3.2.1.1).

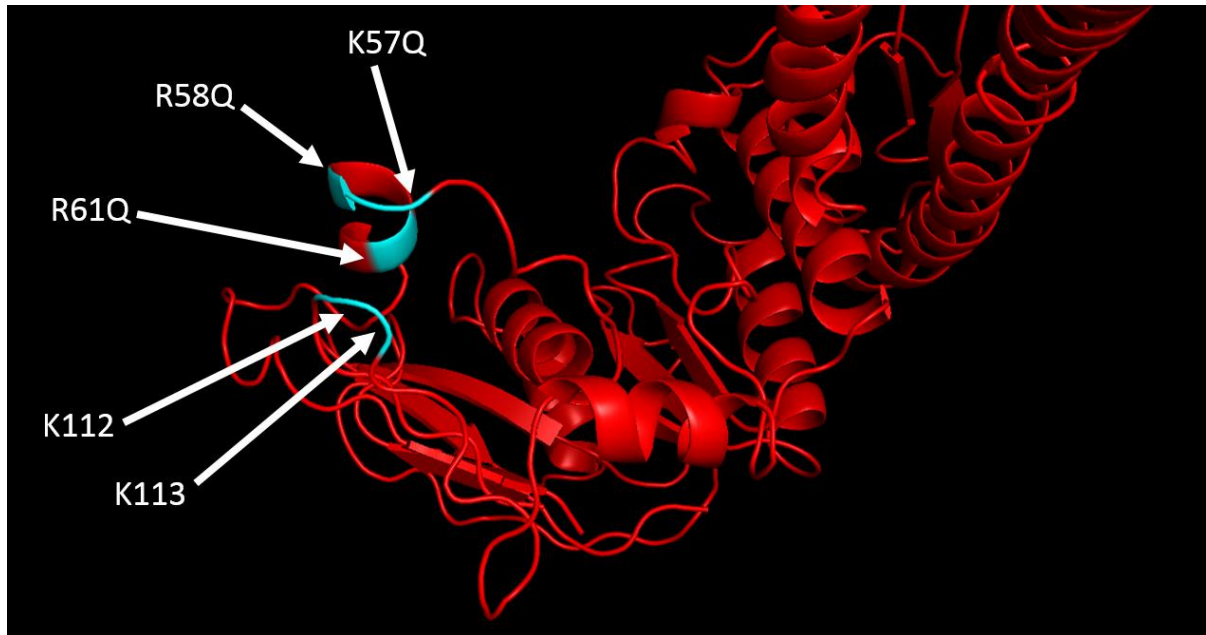


Figure 22: Smc3 head domain structure cartoon showing the location of acetylation sites (K112, K113) and residues that have been mutated.

The viability assay results in table 4 show that *smc3R61Q* is not lethal, nor are other mutations close by which remove the positive charge from the alpha helix opposing the acetylation site strand. This suggests that acetylation does not dramatically affect the ATPase machinery this particular way. This evidence also refutes the result of the fluorescent microscopy results in Gligoris and co-workers which show *smc3R61Q*-GFP mutants failing to accumulate at the kinetochores because failure to do so would be lethal (Gligoris et al., 2014).

Table 4: Viability of mutations in the KKD strand opposing helix.

Smc3 mutation	Rescue rating (+ <i>smc3R1008I</i>)	Rescue rating (- <i>smc3R1008I</i>)	Strains
<i>R58Q</i>	3	4	1384, 1395
<i>K57Q + R58Q</i>	3	4	1385, 1396
<i>R61Q</i>	4	3	1386, 1397
<i>R61Q + K57Q + R58Q</i>	3	3	1387, 1398
<i>K57Q</i>	4	4	1391, 1399

The viability results also examined the effect of *smc3R1008I*. Table 4 shows that these mutations have a small impact on viability and *smc3R1008I* may slightly improve viability in the case of *R58Q* and *K57Q + R58Q* but not *R61Q*. To conclude, mutations removing the positive charge in the alpha helix opposing the acetylation sites are not lethal and do not cause dramatic changes to ATPase machinery or recruitment to chromatin.

4.1.4 Chapter 1 part 3: Testing the effects of mutations in the cohesin loader Scc2.

The alternative method described briefly at the end of 4.1.2 outlined testing the effect of *smc3QQ* on interactions with other proteins, examining whether the mutant *scc2E822K, L937F* (*scc2EKLF*) could rescue *smc3QQ* or *smc3QQ, R1008I*. To further examine recruitment to DNA defects, the Nasmyth laboratory performed a genetic screen to find suppressors for *SCC4* deletion, a protein which interacts with Scc2, critical for recruiting cohesin to DNA. A mutant of Scc2 was found, *scc2E822K, L937F* (*scc2EKLF*) which could survive *SCC4* deletion, indicating that these two mutations are somehow hypermorphic, allowing recruitment of cohesin to DNA without Scc4 in the arm regions of the chromosomes but not the centromere (Petela et al., 2018). This mutation was put onto a plasmid and transformed into yeast before being delivered and added to the yeast strain collection as 1265. The *scc2EKLF* mutant also may have the property of interacting with cohesin more strongly. The *scc2EKLF* mutant protein was found to interact with cohesin even after loading onto the DNA, which would otherwise dissociate, a result found by ChIP sequencing (Petela et al., 2018). The mutant *scc2EKLF* allows the testing of QQ cohesin to examine whether any Scc4 related DNA recruitment defects occur. The rationale behind testing this particular mutant is because this study has the focus of studying the effect of acetylation on loading functions of cohesin. Scc2-Scc4 is responsible for this loading process. The mutant *scc2EKLF* has supposed enhanced cohesin binding ability, thus if *smc3QQ* or *smc3QQ, R1008I* is defective in Scc2 interaction or DNA recruitment then *scc2EKLF* might be able to rescue either.

The *scc2EKLF* mutant was tested for its ability to rescue the QQ mutation and QQ, *R1008I*. Yeast strains 1392 and 1393 were produced by cloning (3.2.3.5), transformation (3.2.3.9) and mating procedures before being dissected and shown below in figure 23 (3.2.1.1).

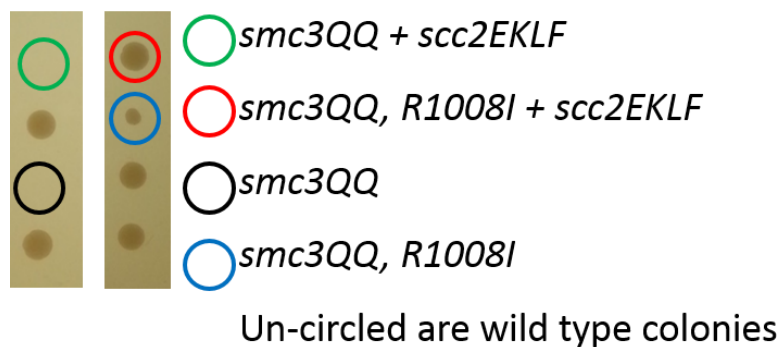


Figure 23: Tetrad dissection results showing that *scc2EKLF* is able to rescue *smc3QQ, R1008I* to normal viability but not *smc3QQ*.

The two photos show suppression with high viability, confirmed by replica plating, indicating that *smc3QQ, R1008I* can be rescued to high viability by *scc2EKLF* (rating 4). The red circle shows a single colony with high viability of a haploid strain containing *smc3QQ, R1008I* rescued by *scc2EKLF*. This colony has the *HIS, URA, and NATMX* genetic markers confirmed by replica plating. The blue circle shows the low viability of *smc3QQ, R1008I*. The black and green circles show that *smc3QQ* and *smc3QQ + scc2EKLF* are inviable.

The dissections shows that *scc2EKLF* cannot rescue the QQ mutation but can fully rescue QQ + *smc3R1008I*. This indicates two possibilities or a combination of both. The first is that *smc3R1008I* may increase interaction with Scc2 because *scc2EKLF* may interact more strongly with cohesin and this property may be linked with its ability

to fully rescue QQ + *smc3R1008I* cohesin compared to wild type Scc2 in figure 23. Like many of the suppressors found in 4.1.2, *smc3R1008I* is essential in allowing *scc2EKLF* rescue in an additive manner suggesting that however *scc2EKLF* acts on QQ cohesin, R1008I may play a supplementary role. The second possibility is that QQ may cause a defect with DNA recruitment and that is rescued by *smc3R1008I* and *scc2EKLF*. Either possibility however, involves some kind of detectable change to the Scc2-Scc4 interaction as this is the complex responsible for loading and DNA recruitment.

Cohesin may interact with Scc2 in a variety of locations. These locations may be where many of the suppressor mutants were found, however R1008I may be a more important interaction platform. QQ may reduce Scc2 interaction which is partially restored by R1008I, and dramatically restored by *scc2EKLF*. Chao and co-workers show through protein crosslinking and mass-spectrometry that Scc2 may contact cohesin at multiple sites (Chao et al., 2017a). Possibly, *scc2EKLF* may rescue the supposed Scc2 recruitment defect of *smc3QQ* by enhancing some of these interactions. Alternatively, these sites may be involved in correcting the QQ-caused cohesin-Scc2 configuration defect for DNA recruitment as part of the loading process.

4.1.5 Chapter 1: Summary

The QQ suppressor mutation *smc3R1008I* appears to restore essential function of cohesin minimally, which is displayed by very poor viability from 7.4.1, table 9. Positional analysis of *smc3QQ*, *R1008I* suppressors shows that these are distributed all over the length of the protein, but overrepresented in the break regions of the Smc3 coiled coil and the head domain. The restorative effect of *smc3R1008I* can be improved dramatically, but not replaced with the introduction of most other suppressor mutants. A few true QQ suppressor mutants were found that can suppress QQ without *R1008I* but these suffered significant growth defects and were all located in the head domain near to key ATPase motifs. This result, along with the mostly indispensable *R1008I*, instigated two separate methods of testing the possible QQ mechanism. The first was to test and build upon the acetylation mode of action outlined in literature. Acetylation was proposed by Gligoris and co-workers to affect the ATPase machinery by structurally changing the position of an alpha helix in close proximity to the location of *smc3QQ* via neutralising positive charges (Gligoris et al., 2014). Results in this study have shown this to be false; the mutations removing positive charges from this region are not lethal as claimed. The second method of testing was to examine whether a Scc2 mutant (*scc2E822K, L937F*) which bypasses $\Delta scc4$ and may possibly interact with cohesin more strongly could rescue QQ or QQ, *R1008I* (figure 23). As *scc2EKLF* was found to require *smc3R1008I* in order to fully restore viability, it is possible that either hypermorphism of *scc2EKLF* may contribute to QQ, *R1008I* rescue.

4.2 Chapter 2

4.2.1 Introduction

Chapter 1 attempted to produce various lines of investigation to answer how acetylation may affect loading. After testing the model of acetylation effect in 4.1.3 and possessing no further testable models, this line of investigation was abandoned. The two other lines described at the end of 4.1.4 involved either further examining cohesin interactions with Scc2 or recruitment to DNA.

As per chapter 1, the mutation *smc3R1008I* was shown to be critical in facilitating the rescue of the QQ viability defect by other mutations. Because of the dramatic effect *R1008I* has on viability when in combination with QQ suppressor mutants, there may be a change in protein interactions which allows QQ to be suppressed. That change was proposed to be the restoration/modification of Scc2 interaction implied by the results of figure 23 mentioned previously. To further test this hypothesis, Scc2 is predicted to interact with the area of the coiled coil immediately around R1008I. By characterising the cohesin-Scc2 interaction, the change caused by the QQ mutation may be found.

To assay potential protein interactions occurring in this region, the method of benzoyl-L-phenylalanine (BPA) photo-reactive crosslinking was selected. BPA is a synthetic amino acid, belonging to a group of chemicals known as benzophenones which have

the remarkable ability to form covalent bonds with any carbon-hydrogen bonds that are in within 9.6 Ångström distance if subjected to UV light between 320 and 360nm. This property allows BPA incorporated proteins to form crosslinks with other proteins. BPA may be incorporated at any position in a protein when paired with mutant aminoacyl tRNA synthetase (aaRS) that recognises the TAG stop codon. A visual aid to the BPA crosslinking system can be found below in figure 24. A plasmid may carry the aaRS sequence and be transformed into *S. cerevisiae* growing in BPA present media. BPA will be incorporated into any protein sequence containing a TAG stop codon. Therefore, the sequence of any protein may be modified for BPA incorporation. However, as BPA incorporation is less efficient than release factor 1 which terminates translation at a TAG stop codon, TAG incorporated proteins may be more suitably carried by 2 micron vectors (YEplac) in yeast which allow for high expression and copy number to ensure plenty of complete protein production (Chin et al., 2002; Forné et al., 2012).

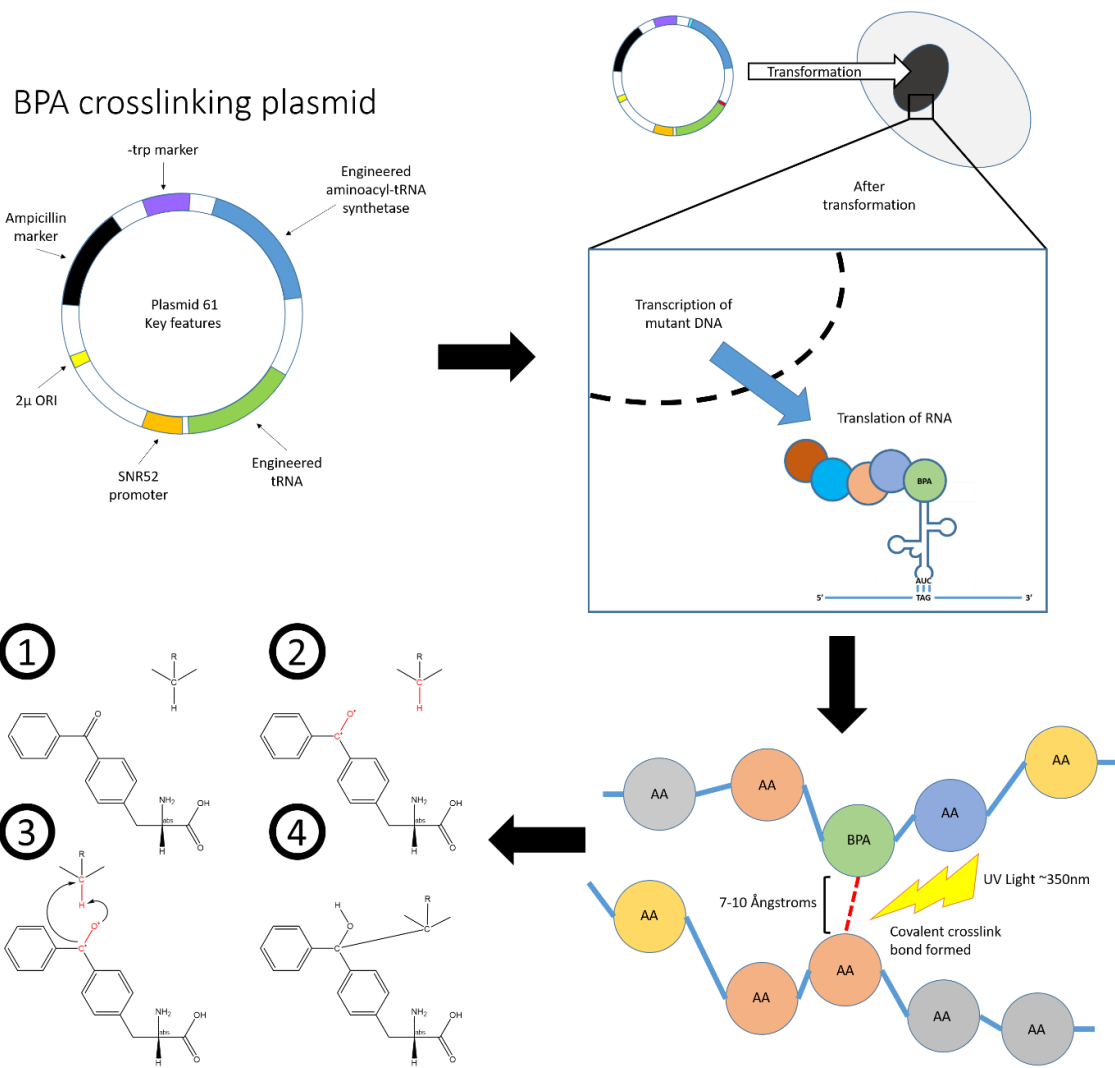


Figure 24: Diagram showing the mechanism behind the BPA crosslinking system.

The system involves BPA incorporation and crosslinking, using mutant tRNA synthetase and UV light. BPA photo-reactive crosslinking occurs by two radicals attacking the C-H bond in an adjacent amino acid within a 7-10 Ångström radius. A covalent bond is formed between the carbon atom of BPA and the carbon atom of the amino acid. This crosslink is physiologically irreversible (Chen et al., 2007; Galardy et al., 1973; Kauer et al., 1986; Pham et al., 2013).

The following chapter involved the use of this method extensively to uncover protein interactions with cohesin.

4.2.2 Chapter 2 part 1: Investigating interactions near *smc3R1008I*

4.2.2.1 Establishing the BPA crosslinking system

The BPA crosslinking plasmid used in these experiments was sourced from Shawn Chen, The Scripps Research Institute, USA (Chen et al., 2007). When incorporating BPA into protein, a protein function assay must be performed to assess that incorporation does not significantly impair protein function. The assay used in these experiments was the 5-fluoroorotic acid (5-FOA) shuffling technique. This involves producing a strain containing two plasmids. The first plasmid encodes the mutant protein to be tested. The second plasmid encodes the wild type version of that protein with a *URA3* marker. The strain also has deletion of the endogenous wild type gene. The protein product of *URA3* converts 5-FOA into the toxic by-product, 5-fluorouracil. Cells which lose the plasmid with the *URA3* marker can only grow if they possess the plasmid encoding the mutant protein, given that mutation yields a functional protein (Boeke et al., 1987). An example of this growth can be seen in figure 25.

5-FOA plasmid shuffling

Testing the functionality of BPA incorporated mutant *smc3*.

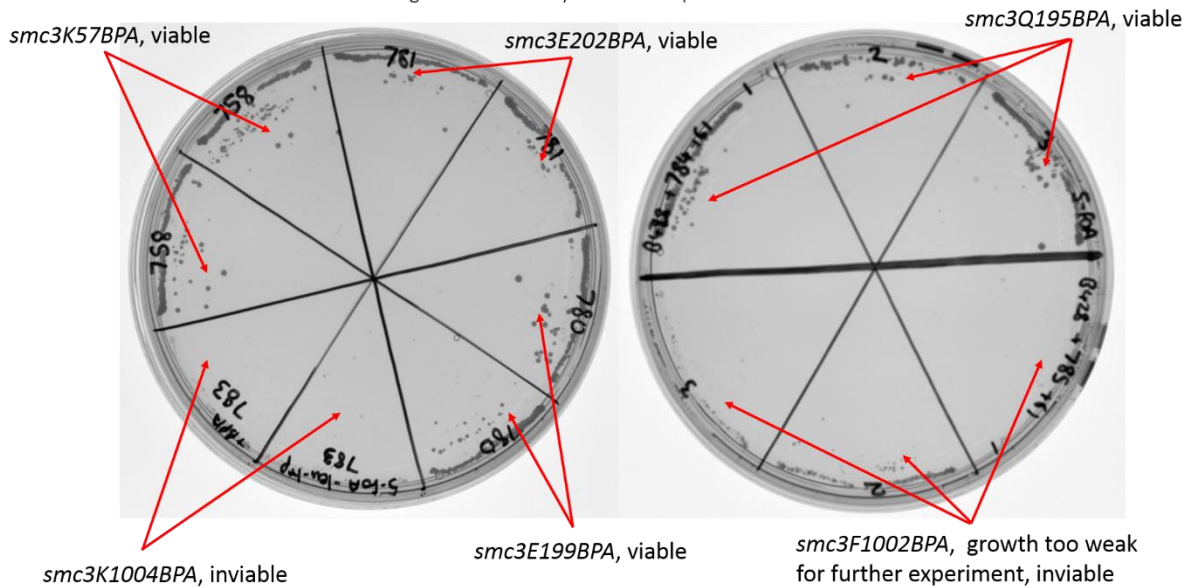


Figure 25: Streak to single colonies of various strains containing plasmids testing for functionality on two +5-FOA, +BPA, -leucine, -tryptophan plates.

The proteins tested require the presence of BPA in the media for expression, along with the plasmid 61 (details can be found in 7.2) containing the genes for the modified tRNA and tRNA synthetase. Cells carrying the wild type *SMC3* gene on the *URA3* marked plasmid will die on the 5-FOA plate. Only cells which have lost this plasmid but retain the mutant BPA-incorporated *smc3* gene plasmid will survive, given that the tested mutation yields a functional protein. (Left): The mutant strains carrying *smc3K57BPA*, *E199BPA*, or *E202BPA* expressed a functional mutant *smc3* protein. *K1004BPA* did not yield a functional protein. (Right): *Q195BPA* yielded functionality, whereas *F1002BPA* did not.

As the nature of the Scc2-cohesin interaction may be weak or transient, little direct evidence of Scc2-cohesin interaction has been found. BPA crosslinking was selected

as the ideal tool to further determine the nature of this interaction. In order to test whether *R1008I* may act as a Scc2 interacting platform, BPA was incorporated in possible interaction sites around this region along with other sites in Smc3. A screen was performed to find amino acids near *R1008I* and around the head domain of Smc3 which when substituted with the amber stop codon, TAG, still maintained normal SMC protein function. The candidates were selected by looking at the crystal structure of the Smc3-Smc1 head domain interaction produced by Gligoris and co-workers before choosing residues at regular intervals in the vicinity of *smc3R1008I* using the structural rendering software, PyMOL (DeLano Scientific).

Before testing the viable screen candidates, a BPA photo-reactive crosslinking control experiment was conducted (see figure 26). The design of the experiment involved testing the BPA crosslinking system to ensure that crosslinking only occurs due to the incorporation of BPA from growth in BPA media and with UV treatment exclusively.

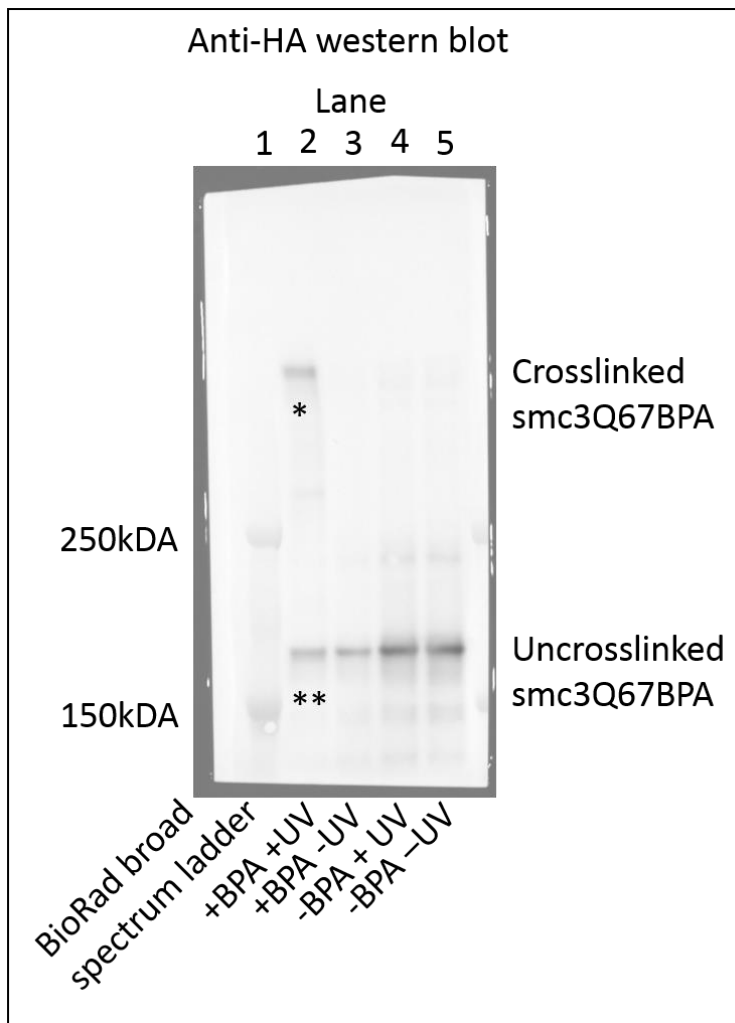


Figure 26: Western blot showing a BPA crosslinking control experiment.

The western blot shows that crosslinking can only occur with the presence of both BPA in the growth medium and treatment with UV light as the expected high molecular weight crosslink band only exists when the strain is treated with both UV light and BPA growth media (indicated by a single “*”). The BioRad broad-spectrum ladder was run in lane 1, alongside with anti-PK immunoprecipitation samples from the smc3Q67BPA mutant strain (listed as 1505 under 7.3) under the listed treatment conditions in lanes 2-5. The protein band sizes of the ladder ranged from 10-250kDA. The un-crosslinked 170kDA Smc3-HA bands are in the expected position between the 150 and 250kDA protein standard bands (indicated by double “**”). This control was also used to establish the validity of the BPA crosslinking system in the

publication listed under 7.5 (Bürmann et al., 2019). Further details regarding methods and materials can be found under 3.2.3.15-16.

The strain used in figure 26 was produced by Caitlyn O'Clarey (personal communication, University of Sheffield, UK, 2018) using mutagenesis methods described in 3.2.3.6, allowing the introduction of the mutation *smc3Q67BPA* onto a high expression YEplac plasmid which would allow large amount of protein expression to account for the low probability of BPA incorporation. This along with plasmid 61 was transformed into strain 1474, which already had been transformed using integrative plasmids to tag Scc1 with PK and Scc2 with FLAG. PK is the name for a peptide representing a 14 amino acid long chain which is part of the RNA polymerase alpha subunit of Simian virus 5 against which specific antibodies have been developed (Randall et al., 1987). FLAG is the name of an artificial 8 amino acid long peptide chain against which highly specific antibodies were developed (Hopp et al., 1988). This crosslink control experiment used the *smc3Q67BPA* mutation tagged with HA, which was also previously established by Caitlyn O'Clarey (personal communication, University of Sheffield, UK, 2018). The immunoprecipitation was performed by capturing Scc1-PK with anti-PK antibody, which retrieved the entire cohesin complex using methods described in 3.2.3.14. This ensures that the collected Smc3 proteins are in the cohesin complex as the Smc3-Smc1 dimer is required for the recruitment of Scc1 (Haering et al., 2002). The experiments conducted by Caitlyn O'Clarey deduced that *smc3Q67BPA* crosslinks with Scc2. This is consistent with the western blot pictured in figure 26 as the crosslink band is expected to be 312 kDA (Scc2 171kDA + Smc3 141kDA) which is the combined molecular weight of Smc3 and Scc2. The

crosslink band indicated by a single "*" is placed much higher than the 250 kDA protein standard band suggesting that the crosslink band is over 250 kDA as expected.

4.2.2.2 Cohesin BPA crosslinking screen

After establishing the validity of the BPA crosslinking system, the viable candidate mutations from the Smc3 screen were tested using BPA crosslinking to find if any proteins interact in these locations (see figure 27). To prepare the strains for this experiment, the same strategy was utilised as the BPA controlled experiment illustrated by figure 26.

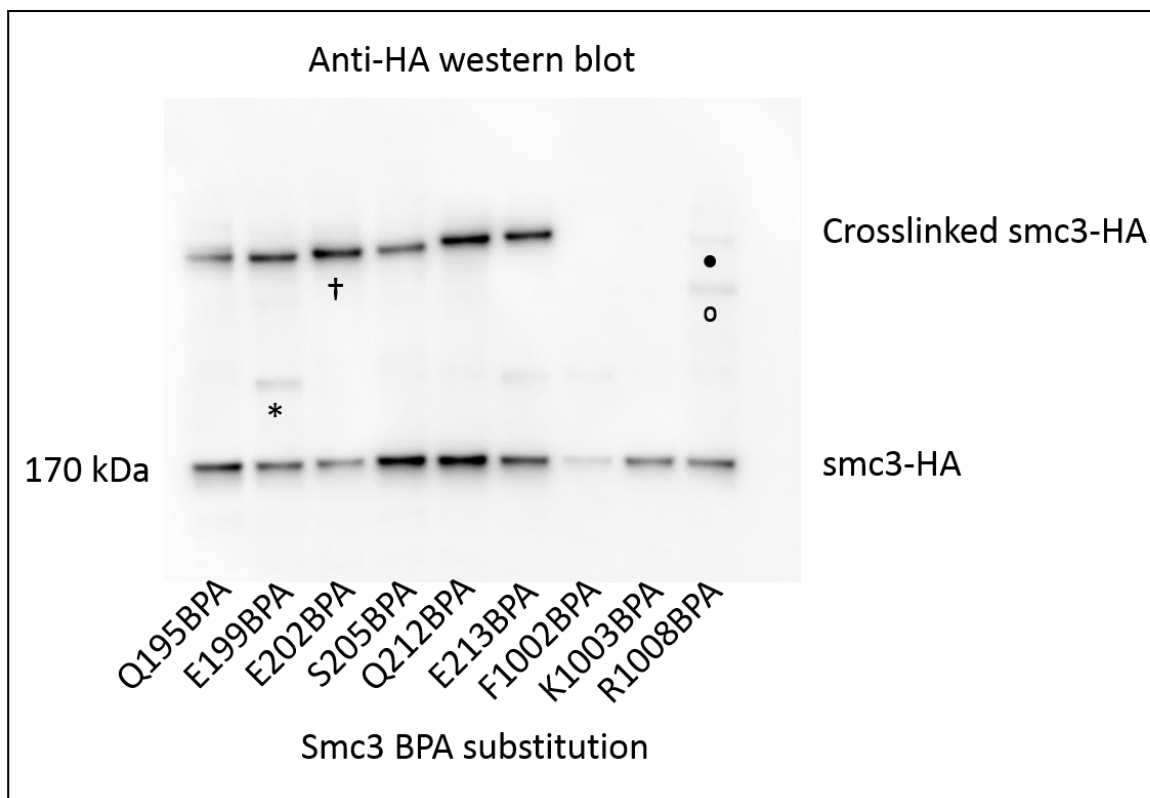


Figure 27: Anti-HA western blot of the cohesin coiled coil BPA crosslink screen.

As the control western blot has already established the expected band sizes; for ease of viewing, the western blot images shown hence forth will be the inverted dark images, rather than the composite images which possess considerable background due to excess light. This results in loss of visibility with regards to the protein standard ladder as it does not contain

the primary antibody required to produce a signal during image capture. The results show that smc3Q195BPA, E199BPA, E202BPA, S205BPA, Q212BPA and E213BPA, all tagged with HA strongly crosslink a protein all in line with the marker “+”. Smc3-HA has mobility of around 170kDa supported by Strunnikov and co-workers with Smc1 running at 165kDa (Strunnikov et al., 1993). Despite performing a Bradford protein concentration assay as described in 3.2.3.23 before conducting the immunoprecipitation, the total signal from each lane differs considerably, most notably in the lane of smc3F1002BPA. This may be caused by different levels of expression and BPA incorporation of the mutant protein. The western blot does show however, that a number of residues near smc3R1008I are within close proximity to other proteins. The residue smc3E199BPA appears to have crosslinked with a protein of a much lower molecular weight and intensity marked by “*”; these kind of bands also exist in the lane of E213BPA. It may be possible that these represent degraded crosslink products or smaller cohesin associated proteins. The lanes containing smc3K1003BPA and F1002BPA did not form a crosslink at all. The last lane with the residue smc3R1008BPA shows two very weak crosslinks bands which may be due to two separate proteins marked by “•” and “o”. As the strains used did not have additional cohesin associated proteins tagged other than Scc1 and Smc3, it is not possible to determine the identity of any other potential crosslinked proteins. The strains used were: 1861, 1903, 1881, 1953, 1949, 1950, 1904, 1954, and 1877.

The next step of the investigation was to identify the proteins crosslinked by the tested residues. This was attempted by epitope tagging other known cohesin associated proteins and testing whether these can be detected by western blot.

4.2.2.3 Finding participating proteins of BPA crosslinking at specific residues of cohesin

Two residues of interest that were found in the screen were smc3Q195BPA and smc3E202BPA. Both of these variants were found to form intermolecular crosslinks. In order to identify other proteins potentially involved in the crosslink product, another western blot with multiple tagged cohesin associated proteins was performed (see figure 28). The additional proteins selected were other cohesin associated proteins such as Scc2, Scc3, Pds5 and Smc1.

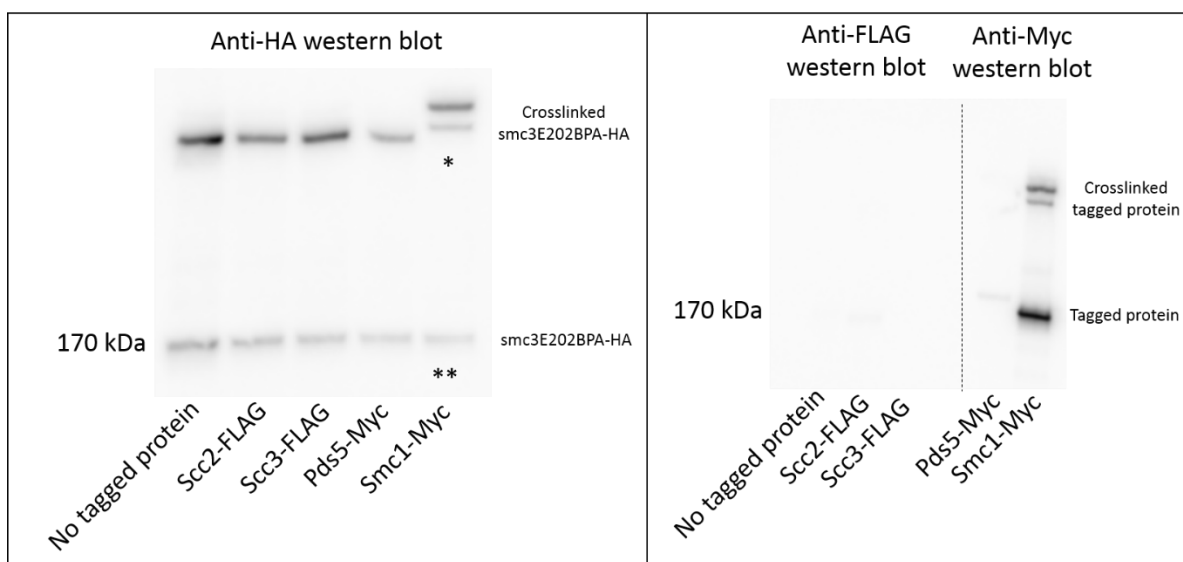


Figure 28: Three western blots showing the proteins crosslinked to smc3E202BPA.

The lower upshifted high molecular weight crosslink band indicated by a single “*” indicates that the crosslink of smc3E202BPA occurs with Smc1 as this upshift is explained by the addition of the Myc epitope tag. The higher band is likely to be caused by smc3E202BPA crosslinking with Smc1 in a secondary location as a result of the Myc tag. This is supported by the anti-Myc western blot which shows both high molecular weight crosslink bands clearly. In

addition, the absence of high molecular weight crosslink bands in the entire anti-FLAG or Pds5-Myc western blots confirms that no significant crosslinking occurs between smc3E202BPA and Scc2, Scc3 or Pds5. By introducing a no tagged protein sample control, it can be ascertained that all the proteins tested were expressed as normal. The un-crosslinked bands of Scc2, Scc3 and Pds5 in the anti-FLAG and anti-Myc western blots are very faint but are present in the expected locations and can be viewed under higher contrasts. As the western blotting technique itself is very sensitive, crosslinked protein should still be detectable in the case of Scc2, Scc3 and Pds5; however none were detected regardless of contrast. The dotted line between the anti-FLAG and anti-Myc western blot indicates the site where the membrane was cut to produce the two separate western blots. The strains used in this experiment were: 1881, 1849, 1883, 1873, and 1882.

As smc3E202BPA and smc3Q195BPA lie very close to each other, there is a distinct possibility that smc3Q195BPA may also crosslink with Smc1 and other cohesin complex proteins. A similar preparation of strains were used to find possible additional proteins that crosslink with smc3Q195BPA (see figure 29).

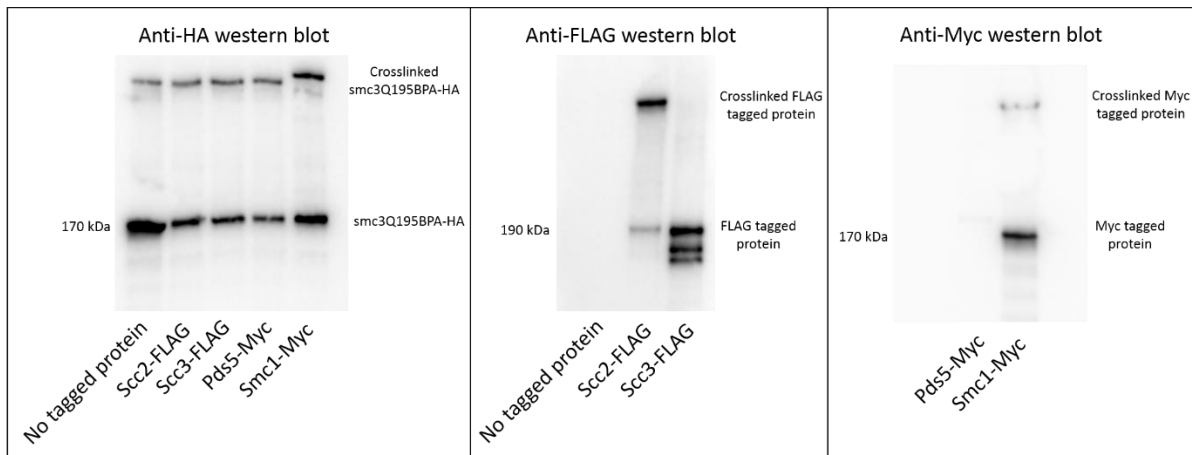


Figure 29: Three western blots showing the crosslink profile of smc3Q195BPA.

The results show that smc3Q195BPA crosslinks to both Scc2 and Smc1, but not to Scc3 or Pds5, as shown by the crosslink bands found in the anti-FLAG and anti-Myc western blots. The western blots shows that smc3Q195BPA forms less crosslink product with Smc1 but more with Scc2, and almost none with the other proteins tested. There are a number of bands in the Scc3-FLAG lane. This is likely degradation of the protein Scc3 which would create a number of protein products of a lower molecular weight that may still have the FLAG tag intact. As the strains used were haploid, there are no other copies of Scc3-FLAG which could interfere. The un-crosslinked Pds5 protein band in the anti-Myc western blot is of low intensity but is visible under high contrast. The crosslink formed by smc3Q195BPA and Scc2 is the first evidence of interaction between the coiled coil domain of cohesin and the Scc2-Scc4 loading complex. The region surrounding *smc3R1008I* may be a key interaction site with Scc2 that is modified by *smc3R1008I* to allow rescue from the QQ phenotype. The strains used in this experiment were: 1861, 1851, 1901, 1902, and 1893.

The results from the western blots of smc3E202BPA and Q195BPA are intriguing as they both interact with Smc1 and Q195BPA even crosslinks Scc2, lending support to the idea that Scc2 may interact with the coiled coil in this region. To plan further crosslink experiments and produce a structural basis for these interactions, the positions of all tested BPA residues were mapped *in silico*.

4.2.2.4 Positional analysis of Smc3 BPA crosslink mutants

After finding many crosslink sites in Smc3 and around smc3R1008I, the locations of these were studied for clustering of potential activity shown in figure 30 and 31.

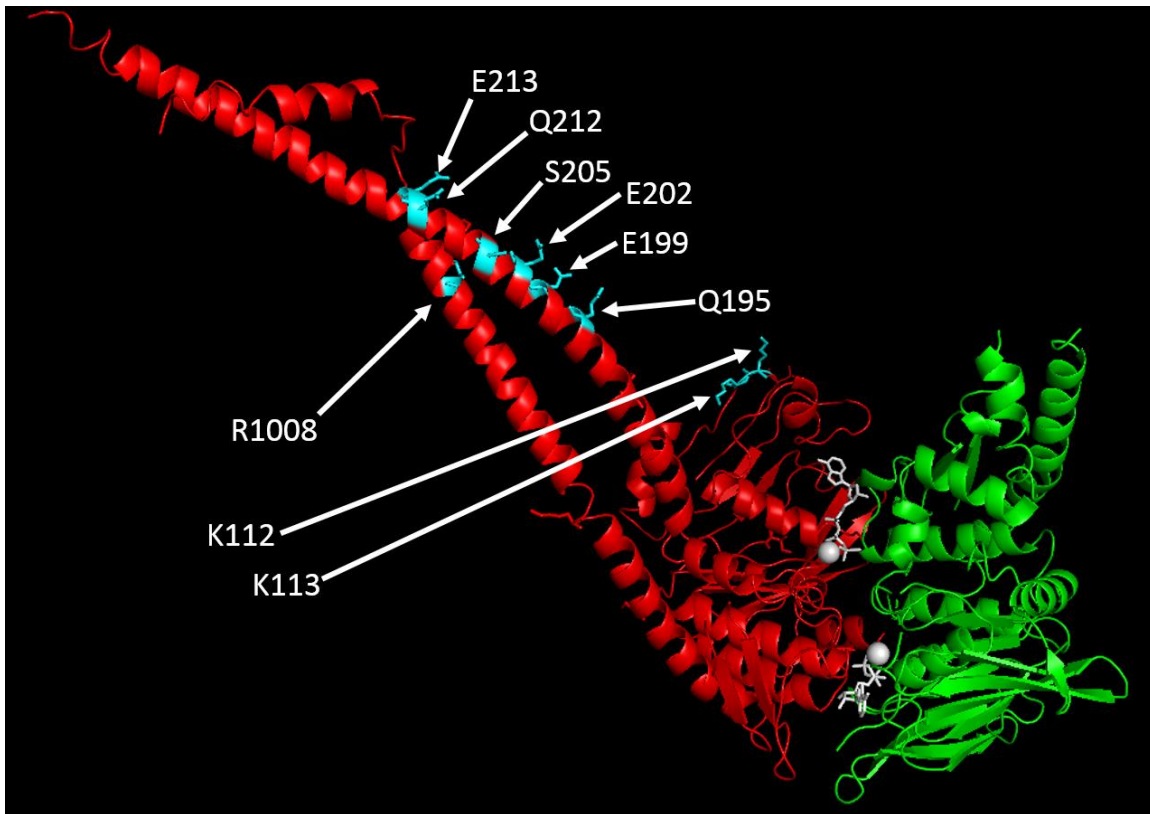


Figure 30: A cartoon diagram of partial cohesin structure as resolved by Gligoris and co-workers with marked crosslink and acetylation sites smc3K112 and K113.

The head domains of both Smc3 (red) and Smc1 (green) are pictured in the engaged position where the Walker motifs of each domain are in a position to facilitate the hydrolysis of ATP. In this state, it is suggested that this is the position which is represented by the ring configuration of cohesin which may be responsible for the topological entrapment of sister chromatids (Gligoris et al., 2014).

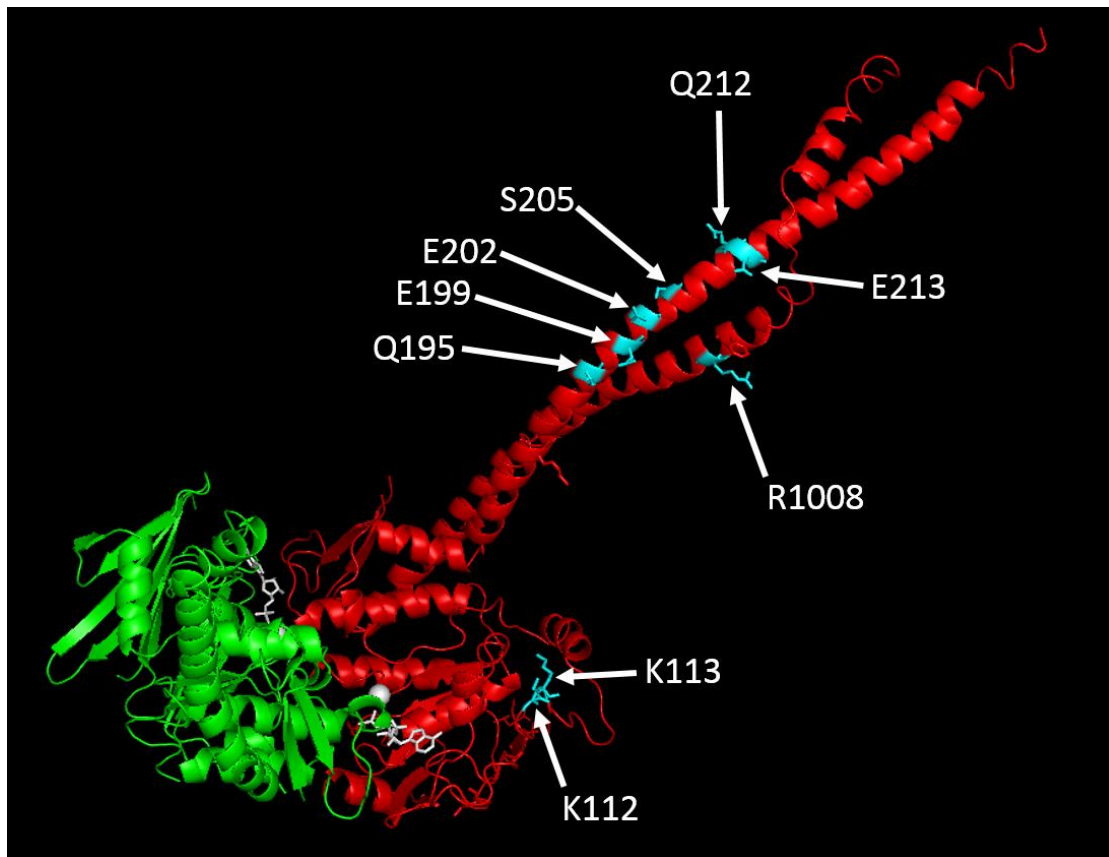


Figure 31: Alternate view (180 degree rotation about the Y axis) of a cartoon diagram depicting partial cohesin structure as resolved by Gligoris and co-workers with marked crosslink and acetylation sites smc3K112 and K113 (Gligoris et al., 2014).

Figure 30 shows that the crosslink sites are clustered around the N terminal coiled coil region opposite smc3R1008I. In order to find out what effect QQ has on protein interactions, the structural implications of these crosslinks must be first be elucidated before assaying the effect of QQ on these configurations.

From low resolution EM images of cohesin in figure 5, it can be seen that cohesin is a flexible complex but with a configuration that can be generalised into two categories,

a discernible lumen or lack thereof. This feature may be determined by the state of head domain engagement which provides some form of mechanical support to the lumen. The case for this is supported by X-ray crystallography data from Gligoris and co-workers which is shown in figure 30 and also figure 6 by the distance between the coiled coil sections of Smc1 and Smc3, creating a lumen in between. There must be some stability associated with this configuration as it would be otherwise impossible to determine. Protein structures with high degrees of flexibility are very difficult to determine accurately. The residues Q195BPA and E202BPA crosslink with Smc1, however, the participating residues in Smc1 are not known. These residues may conceivably crosslink with the coiled coil region of Smc1 given some flexibility. There are two possible configurations supported by literature. The first is a position where the coiled coil domains of Smc1 and Smc3 are in close proximity and head domains are juxtaposed (Chapard et al., 2019; Diebold-Durand et al., 2017). The second position is where the cohesin folds at an especially flexible region known as the elbow where part of Smc1 could possibly contact the tested residues in 4.2.2.3 (Bürmann et al., 2019). Figure 8 provides a visual aid to the folded configuration and figure 9 provides this for engaged head domain configurations (E state) and juxtaposed head domain configurations (J state). To distinguish all of these configurations experimentally, a cleavage system was employed to produce fragments of expected size which can be detected by western blot and then analysed to deduce the position of these crosslinks.

4.2.2.5 Establishing the BPA crosslinking TEV cleavage system

In order to clarify the quaternary structure of cohesin under the conditions of the crosslink sites found, a screen was performed to search for Smc3-Smc1 coiled coil crosslink sites to provide sufficient data for a structural prediction model to be produced. BPA photo-reactive crosslinking is inadequate for this task as BPA will crosslink with any compound containing C-H bonds within a 7-10 Ångström radius, providing only information regarding what protein is crosslinked, but not where. To narrow down the range of possible sites, the BPA photo-reactive crosslinking was combined with another technique; tobacco etch virus (TEV) protease cleavage (see figure 32). The TEV protease is a protein encoded in the tobacco etch virus and cleaves amino acid chains strictly at a specific 7 amino acids sequence: glutamic acid, asparagine, leucine, tyrosine, phenylalanine, glutamine (cleavage site), glycine. Therefore, by introducing this sequence, a cleavage site is created. The TEV protease cleavage technique involves the insertion of multiple TEV protease cleavage site sequences within a protein which then are the target of the TEV protease (Frew et al., 2012; Wehr et al., 2006).

The Nasmyth lab, University of Oxford, UK performed the screen for TEV cleavage site viability in Smc1 and Scc2 as part of this study.

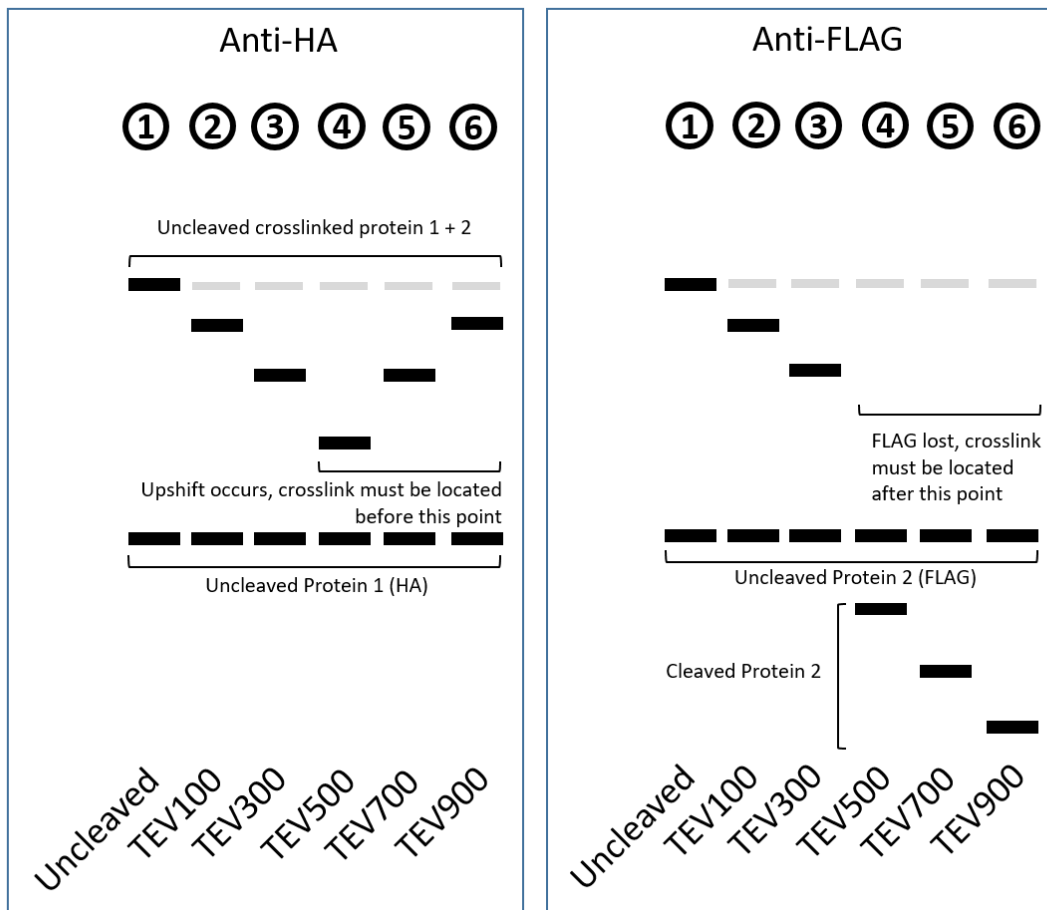
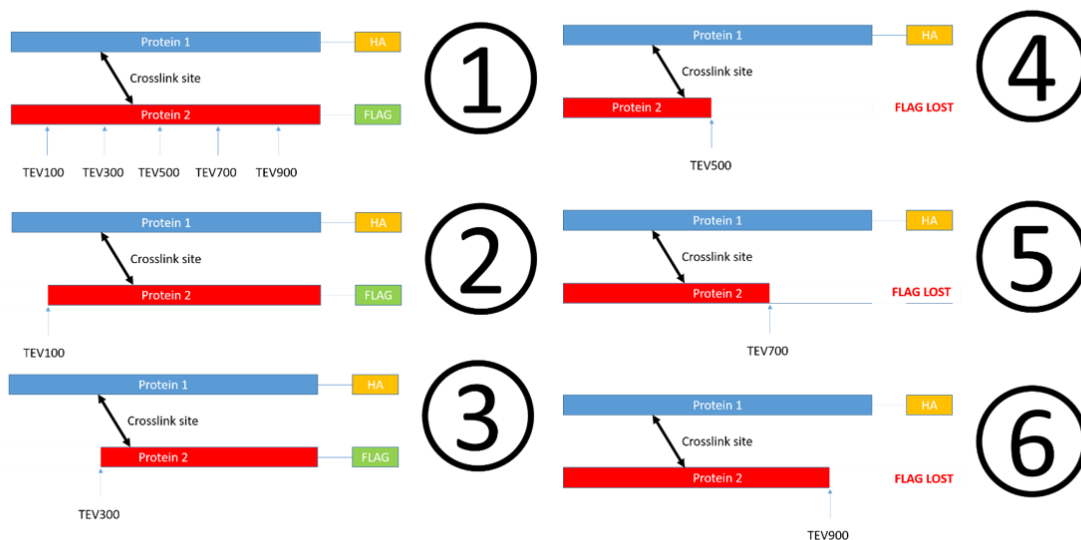


Figure 32: A diagram showing how the TEV protease cleavage system allows the detection of a crosslink site by analysing the pattern produced by the western blot.

The hallmark feature used to determine the range within which a crosslink exists is the beginning of the upshift on the anti-HA western blot and the location of the FLAG loss along with smaller cleavage fragments on the anti-FLAG western blot. From the example western blot cartoon, it is shown that the crosslink can be determined to exist between TEV300 and 500.

Strains were constructed using the CRISPR-Cas9 system adapted for use in *S. cerevisiae* developed by Daniels and co-workers (Daniels et al., 2018). The CRISPR-Cas9 system is a form of rudimentary acquired immunity found in prokaryotes. CRISPR-Cas9, facilitates resistance against attack from viruses by preventing viral proteins from being expressed. This is achieved by cleaving the foreign DNA. Cas9 is a RNA-guided DNA endonuclease enzyme which performs the double strand DNA cleavage activity found in the CRISPR-Cas9 system. Foreign DNA is detected by binding with template RNA, itself bound to the Cas9 protein. This allows recognition of specific sites in DNA. The template RNA is composed of two parts; the guide RNA (gRNA) scaffold sequence, and the variable spacer. The gRNA scaffold sequence, upon binding with Cas9, creates a conformational change which activates the DNA cleaving activity of Cas9. At the end of the gRNA scaffold sequence is a short, 20 base pair sequence known as the spacer. This sequence is what dictates the cleavage site of Cas9, and can be modified to be complementary to any desired cut site on the condition that wherever the target site is located, there exists a protospacer adjacent motif (PAM) sequence immediately afterward. The PAM sequence is essential for the localisation of Cas9 to the target cut site. This is an intrinsic property of the Cas9 protein and this specificity cannot be changed without modifying Cas9. Upon

localisation to the PAM sequence and binding of the complementary spacer to the target cleavage site, Cas9 performs the DNA cleavage. By cutting viral DNA, viral proteins cannot be expressed. The CRISPR-Cas9 system has been adapted to modify genes in eukaryotic organisms such as *S. cerevisiae* (Dicarlo et al., 2013; DiCarlo et al., 2015). By designing an appropriate spacer, a gene may be cut and replaced with any other gene transfected into *S. cerevisiae* via the homologous recombination repair pathway. This technique was adapted in novel vectors to operate in *S. cerevisiae* as part of this study as seen in figure 33 (Daniels et al., 2018).

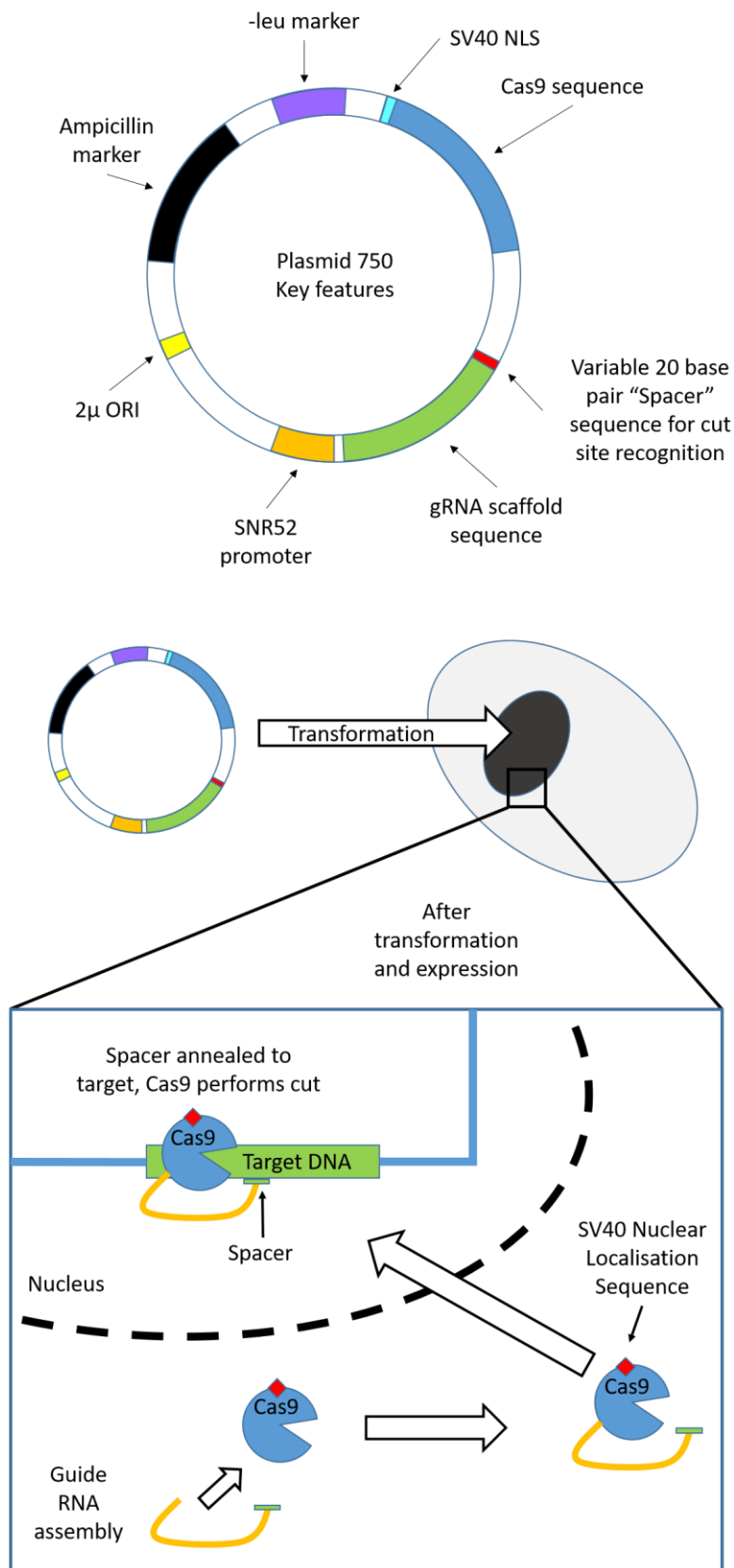


Figure 33: A diagram highlighting the key features of the CRISPR-Cas9 plasmid used for transforming yeast.

The plasmid pictured in figure 33 contains the Cas9 protein sequence with the SV40 nuclear localisation sequence attached at the end. This allows Cas9 to be translocated to the nucleus in order for it to perform the double stranded break at the target location. Cas9 requires a guide RNA (gRNA) scaffold in order to produce a conformational change that activates the DNA cleavage function of Cas9. This is present on the plasmid along with a *SNR52* promoter which recruits RNA polymerase III, adding no modifications, thus allowing RNA transcription but avoiding protein expression (Dicarlo et al., 2013). The “Spacer” is added at the end of the gRNA to allow the cut recognition site to be customised, with the obligatory PAM following. The plasmid also has an origin of replication (2 micron ORI) which allows higher copy numbers for increased Cas9 expression. The ampicillin and *LEU* markers allow the plasmid to be selected in *E. coli* and *S. cerevisiae* respectively. Another plasmid was used in later experiments of this study, listed as plasmid 263 which had a spacer targeting the *LYS2* gene.

The Cas9 vectors were provided by Dr Bin Hu on 2 micron plasmids; 750 and 263. Transformations involving the CRISPR-Cas9 system were performed as described in 3.2.3.9 and were used to integrate TEV-incorporated *smc1* into the *MET15* gene which codes for a protein involved in methionine biosynthesis. This was performed along with deletion of endogenous *SMC1* by interruption with *NATMX* to allow functionality to be determined using tetrad dissection, as the BPA mutation combined with TEV may be synthetically lethal. *NATMX* is a gene used as a marker which codes for a protein essential for nourseothricin resistance, being an antibiotic used in yeast growth media.

4.2.2.6 Finding crosslink sites in Smc1 with BPA substituted Smc3 residues

TEV protease cleavage was performed on strains containing a known BPA substitution residue which formed a crosslink, and a Smc1 TEV cleavage site, allowing identification of the Smc1 crosslink site within an arbitrary range depending on how many sites are tested (see figure 34). The mutations tested were obtained from the coiled coil crosslink screen found in figure 27. These were three residues that produced very strong crosslink bands which was expected to make the detection of cleaved fragments from crosslink products easier. By virtue of their position relative to E202BPA these were also expected to crosslink Smc1.

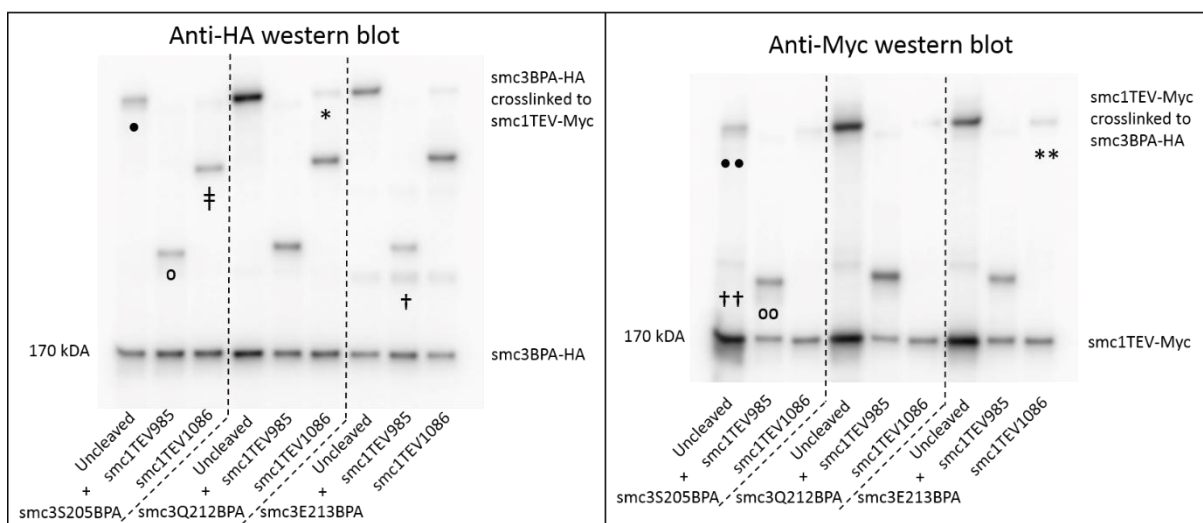


Figure 34: Western blots of TEV cleaved BPA crosslinked proteins with BPA substitutions in the coiled coil region of Smc3.

The western blots reveal the possible range that the crosslink site of the tested Smc3 residues may crosslink with Smc1. The crosslinks produced by smc3S205BPA, Q212BPA and E213BPA all include Smc1 as this is detected in the crosslink band of the anti-Myc western blot and

these crosslinks can also be seen in figure 27. All of the crosslink sites lie between smc1TEV985 and TEV1086 as the hallmark upshift of TEV cleavage occurs between these two cut sites. This is shown in the anti-HA western blot by the crosslink band of smc1TEV1086 samples being higher than smc11TEV985 in all samples tested. An example is highlighted by the symbols “•”, “°”, and “‡” in the smc3S205BPA lanes. The band indicated by the single “•” shows the position of the uncleaved crosslink band. The cleaved crosslink band at Smc1 position 985 is shown by “°”. This band is considerably downshifted due to the loss molecular weight from cleavage at position 985. The cleaved crosslink band at position 1086 is shown by “‡”. This band is upshifted compared to the cleavage at position 985 because the crosslink is located between 985 and 1086 and this is the distinguishing hallmark discussed in figure 32. This pattern is repeated with smc3Q212BPA and E213BPA. There are uncleaved crosslink bands which exist in the cleavage lanes, with an example being highlighted with “*”. This was expected as TEV cleavage is not 100% effective. In addition, there may be some non-specific crosslinking/degradation products highlighted by “†”. The TEV cleavage sites 985 and 1086 in Smc1 were selected because this is one of the range of residues expected if the juxtaposed configuration of cohesin was implicated. This is because if Smc3 residues in positions 190-210 are in close proximity to smc3R1008 as pictured in figure 30-31, the same must also be true of Smc1 as the two proteins have very high similarity. If the Smc1-Smc3 coiled coil domains are indeed within close proximity then a crosslink can be expected to form between positions 190-210 or 990-1010. Therefore, the TEV cleavage experiment was designed with a cleavage site at position 985 and 1086 in anticipation for a crosslink occurring in this range. The anti-Myc western blot shows that the protein crosslinked by the BPA substituted Smc3 variants must be Smc1 because both the anti-HA and anti-Myc western blots show one crosslink band in the same position, highlighted by “••”. The results show that all of the tested sites crosslink

with the adjacent coiled coil domain of Smc1 near the C-terminal. The anti-Myc western blot supports this conclusion as the crosslink band is downshifted when cleaved at smc1TEV985 highlighted by “oo”, and disappears completely when testing smc1TEV1086 in all three samples. There are also bands that represent undigested crosslinked protein which exist as lower intensity bands in the lanes of smc1TEV985 and smc1TEV1086 tested samples. An example of these undigested bands is highlighted with “***”. In addition, there may be some non-specific crosslinking/degradation products highlighted by “††”. The strains used in this experiment were: 2192, 2188, 2190, 2186, 2191, and 2187.

The TEV cleavage experiments show that the configuration of the Smc3 to Smc1 crosslinks is very likely to be the juxtaposed state as the range containing the crosslink site matches the prediction of coiled coil interactions occurring near the juxtaposed heads. This is supported by Chapard and co-workers in which crosslinking was also achieved near this location (Chapard et al., 2019). As the Smc1 and Smc3 coiled coils come into close contact, this interaction may be affected by QQ suppressor mutations which may alter the configuration, possibly affecting Scc2 interaction. To test the change on cohesin coiled coil configuration, Smc3 BPA crosslinking residues may now be combined with QQ suppressors to assay the effect on Smc3-Smc1 interactions. Effects on Scc2 interaction were tested later, being the topic of chapter 3.

4.2.3 Chapter 2 part 2: Testing the effect of *smc3QQ* suppressors on coiled coil configuration

The suppression of the *smc3QQ* phenotype by suppressor mutants occurs by an unknown mechanism of action. It may be possible that QQ suppressor mutations may slightly modify the structure of cohesin or change key interaction sites to produce this effect. To test this hypothesis, two QQ suppressor mutations, *smc3R1008I* and *E199A*, which are located in the Smc3 coiled coil were combined with nearby known BPA crosslink residues, E202BPA and Q195BPA (see figures 35 and 36). The purpose of this experiment was to test whether a QQ suppressor mutation has the ability change cohesin protein interactions. As *smc3E202BPA* is known to crosslink with Smc1 in the J state configuration (Chapard et al., 2019), any changes to crosslinking efficiency would indicate that this interaction is affected by the suppressor mutation.

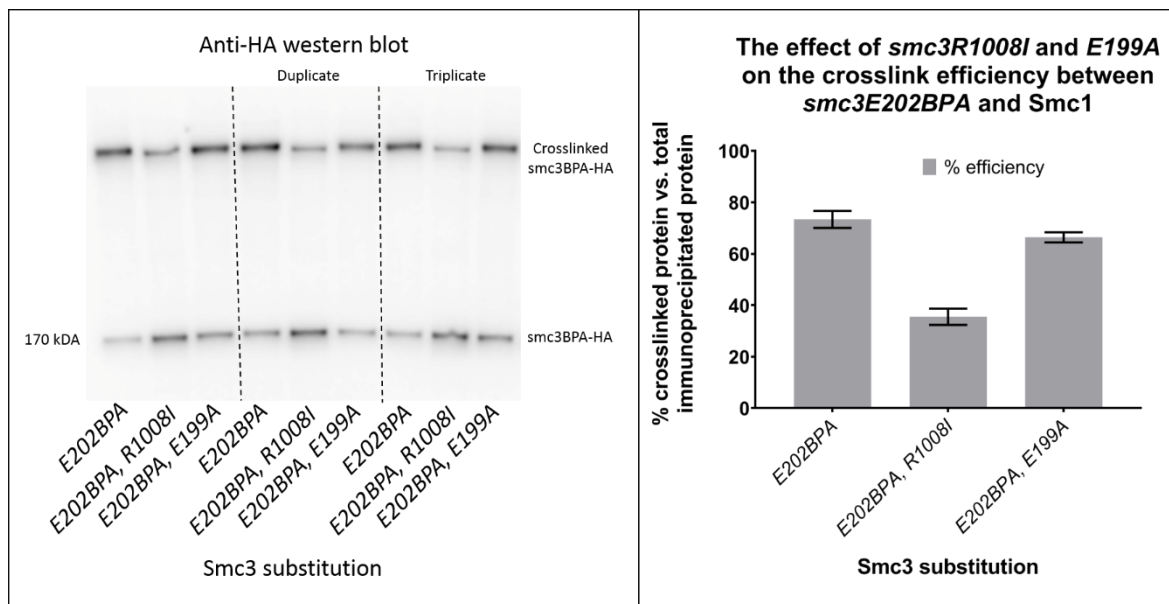


Figure 35: Western blot and graph showing the effect of two coiled coil mutations, *smc3R1008I* and *E199A* on *smc3E202BPA* crosslinking efficiency.

The western blot pictured left shows that the introduction of the suppressor mutants, *smc3R1008I* or *smc3E199A* affects the crosslinking efficiency of *smc3E202BPA*. The crosslinking efficiency is reduced when *smc3R1008I* is introduced but only marginally with *smc3E199A*. The graph pictured right confirms this by plotting the % efficiency of each crosslink (n=3) showing a difference between the strains containing the *smc3R1008I* or *E199A* mutations compared to without. The introduction of *smc3E199A* only marginally decreases crosslink efficiency, whereas *smc3R1008I* approximately halves it. Kruskal-Wallis statistical testing (jamovi software) shows that there is a significant difference between the mean averages of the three mutant strains tested (chi-squared = 7.2, degrees of freedom = 2, probability value = 0.02732). However, as the sample size is too small, statistical significance cannot be established between each mean by the Dwass-Steel-Critchlow-Fligner test. The graph was produced by manually quantifying the bands of the western blot using GeneTools (Syngene) software. The software measured the signal intensity of each band by comparing it

to parts of the western blot where there is no signal and assigning a numerical value. The total immunoprecipitated protein was calculated by adding the signal intensity of the uncrosslinked band to the crosslinked band of each sample. The crosslink efficiency was determined by dividing the crosslinked band intensity by the total immunoprecipitated protein which provided the ratio of crosslink product to total protein which was then converted to a percentage. The strains used in this experiment were: 1881, 1957, and 1960.

To further test affected coiled coil interactions, *smc3Q195BPA* was also tested with *R1008I* and *E199A*.

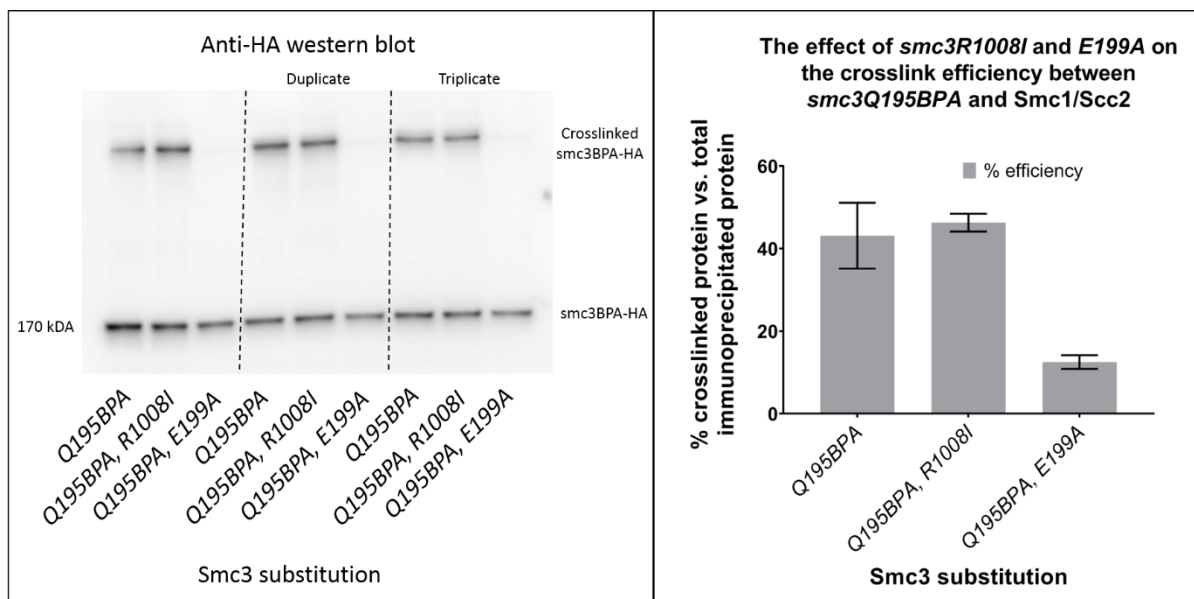


Figure 36: Western blot and graph showing the effect of two coiled coil mutations, *smc3R1008I* and *E199A* on *smc3Q195BPA* crosslinking efficiency.

The western blot shows that the introduction of the suppressor mutant, *smc3E199A* may affect the crosslinking efficiency of *smc3Q195BPA*. The crosslinking efficiency appears to be reduced when *smc3E199A* is introduced but not with *smc3R1008I*. The graph pictured right

shows this by plotting the % efficiency of each crosslink (n=3) showing a difference between the strains containing the *smc3R1008I* or *E199A* mutations compared to without. Kruskal-Wallis statistical testing shows that there is a not significant difference between the mean averages of the three mutant strains tested (chi-squared = 5.6, degrees of freedom = 2, p-value = 0.061). The sample size is too small so statistical significance cannot be established between each mean by the Dwass-Steel-Critchlow-Fligner test. The introduction of *smc3R1008I* only marginally decreases crosslink efficiency, whereas *smc3E199A* reduces it by approximately two thirds. The strains used in this experiment were: 1861, 1956, and 1958.

These results suggests that both *smc3E199A* and *smcR1008I* impact coiled coil interactions, albeit in perhaps different ways in order to achieve QQ suppression. Continuing this line of investigation, a structural model of cohesin based on crosslinking is required which can be used to determine the effects of QQ on the configuration of cohesin. Two such configurations are supported by literature, engaged head domains of Smc1-Smc3, and the other is juxtaposed (E and J state). Hence, to produce these structural models, a more specific form of crosslinking was selected to produce enough crosslink data.

4.2.4 Chapter 2 part 3: Producing a novel structural model of cohesin

4.2.4.1 Establishing the BMOE crosslinking system

Producing a structural model of cohesin requires manipulation of the known crystal structures of Smc1-Smc3 *in silico*. To accomplish this, distances between residues must be known which produces constraints to narrow the possible configurations. BPA crosslinking is indiscriminate and attacks any C-H bond within a small radius. This does not provide any information about where the other crosslink site is. TEV cleavage may narrow the range of possible residues, but to produce an accurate model specific residue distances are necessary. For this purpose, a sulfhydryl-reactive crosslink system using BMOE (bismaleimidoethane) was selected (see figure 37). The BMOE crosslinking system involves substitution of amino acid residues in a protein for cysteine. BMOE has the ability to create a physiologically irreversible crosslink between cysteine residues that are within 8.0 Ångströms (Giron-Monzon et al., 2004).

BMOE crosslinking system

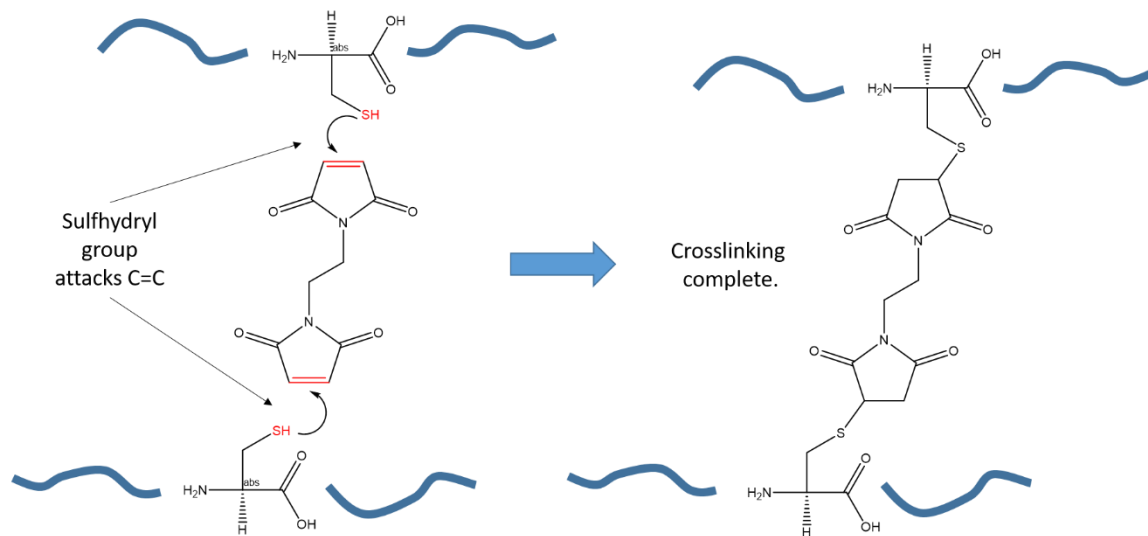
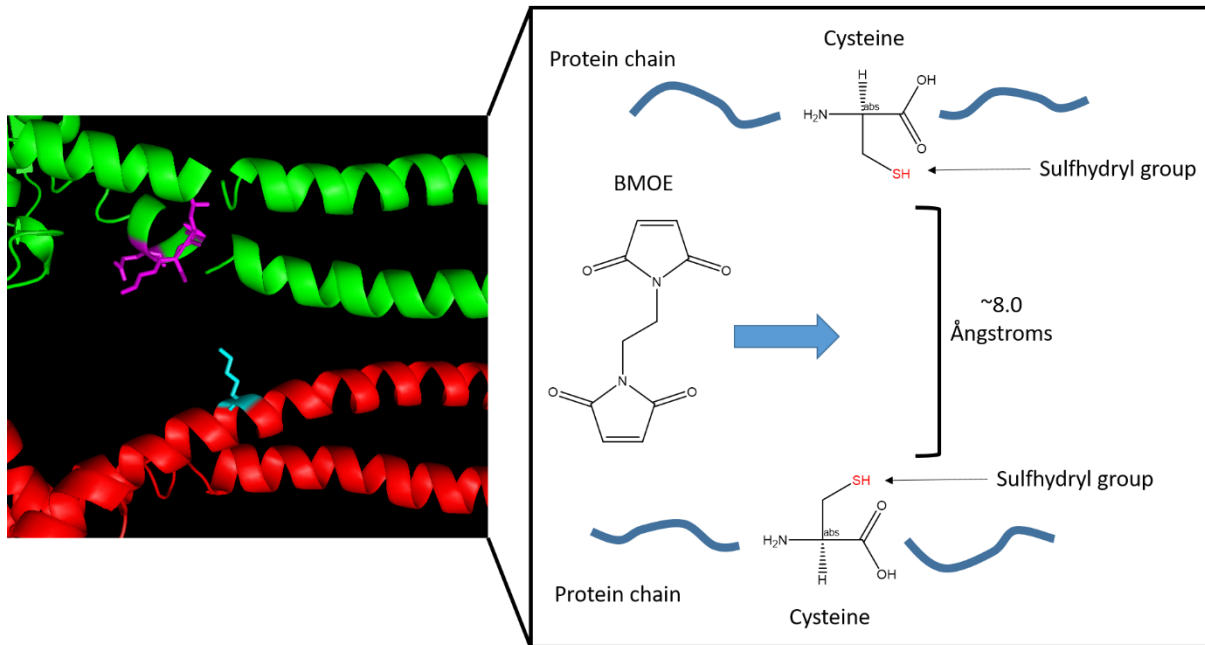


Figure 37: A diagram showing how BMOE crosslinks cysteine residues within 8.0 Ångströms *in vivo*.

Cysteine residues can be integrated anywhere in any protein by mutagenesis. BMOE is a small, hydrophobic molecule which may diffuse through the cell membrane freely and can therefore be applied directly to yeast cells as a treatment solution. These two properties combined

allow the production of a robust assay which may be used to crosslink different proteins in the cohesin complex together, given a small region containing crosslink activity which can be screened (Chen et al., 1991).

4.2.4.2 BMOE crosslinking screen between the coiled coil domains of Smc1 and Smc3

As per figures 27-29 and 34, the area of crosslink interest is known between Smc1 and Smc3. A screen was performed to find amino acid sites in the coiled coil domains of Smc3 and Smc1 which when substituted with cysteine, maintained normal SMC protein function. This was achieved using the tetrad dissection viability assay mentioned in chapter 1. Five sites near the N-terminal of Smc3 were identified: smc3E188C, K184C, Q195C, E202C and E213C. The range of the Smc1 screen was determined by simply testing the amino acid positions between the TEV cleavage positions of smc1TEV985 to smc1TEV1086 and around the adjacent N terminal coiled coil as found in crystallography data (Gligoris et al., 2014). Nineteen sites across Smc1 were identified: (near N-terminal) smc1E190C, S193C, S195C, S199C, K201C, N202C, R205C, E209C, Y213C, (near C-terminal) N1013C, R1020C, R1024C, A1028C, R1031C, I1035C, T1039C, L1042C, E1046C, I1049C. The following BMOE crosslink experiments were performed with these mutations using methods described in 3.2.3.17 (see figure 38-40).

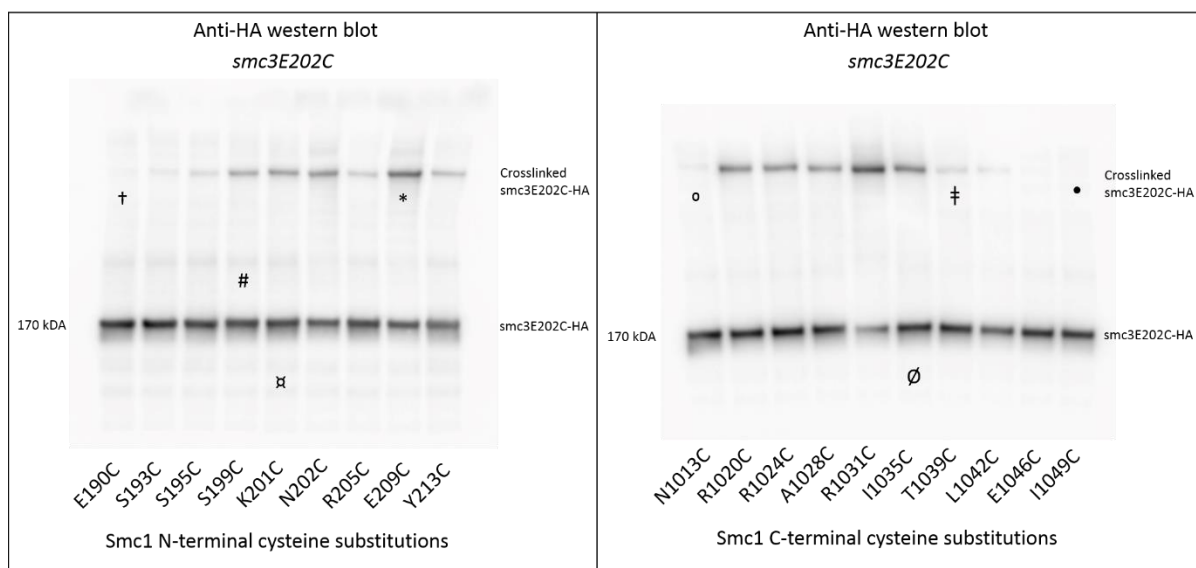


Figure 38: Western blots showing Smc1 cysteine residues which crosslink with smc3E202C near to both the N and C terminals.

In the Smc1-N terminal crosslink western blot, a single “*” marks the position of a particularly strong crosslink band. This indicates that at this position, the crosslink efficiency between smc1E209C and smc3E202C is higher. This may be due to a closer proximity between the two residues. There is a general trend of decreasing crosslink band intensities present between smc1E209C and smc1E190C, going right to left. The “†” marks the residue where the crosslink becomes undetectable, smc1E190C. This shows that the crosslink intensity depends on the position of the Smc1 cysteine residue. The ability of smc3E202C to crosslink a range of residues in the Smc1 coiled coil suggest that there may be a particularly large range of motion between Smc1 and Smc3 where these residues may come within the 8 Ångström range of the BMOE crosslinking system. The results also show that smc3E202C may also crosslink both coiled coil regions near the N and C terminal of Smc1 with similar efficiency. The “#” and “α” marks the positions where all the tested residues possess a non-specific crosslink band, or possible degradation products. The C-terminal crosslinks show similar results with the

crosslink efficiency appearing to peak at smc1R1031 and tapering off quickly; dropping to low efficiency at smc1N1013C and smc1T1039C marked by “o” and “‡” respectively. The single “•” shows a Smc1 residue which does not crosslink with smc3E202C, while the “∅” marks the presence of some potential non-specific bands or degradation products. The strains used in this experiment were: 2313, 2316, 2300, 2304, 2306, 2302, 2312, 2311, 2310, 2230, 2121, 2231, 2232, 2233, 2234, 2314, 2315, 2308, and 2309.

The next Smc3 site tested was smc3Q195C. A slightly smaller range of Smc1 residues were tested in this case.

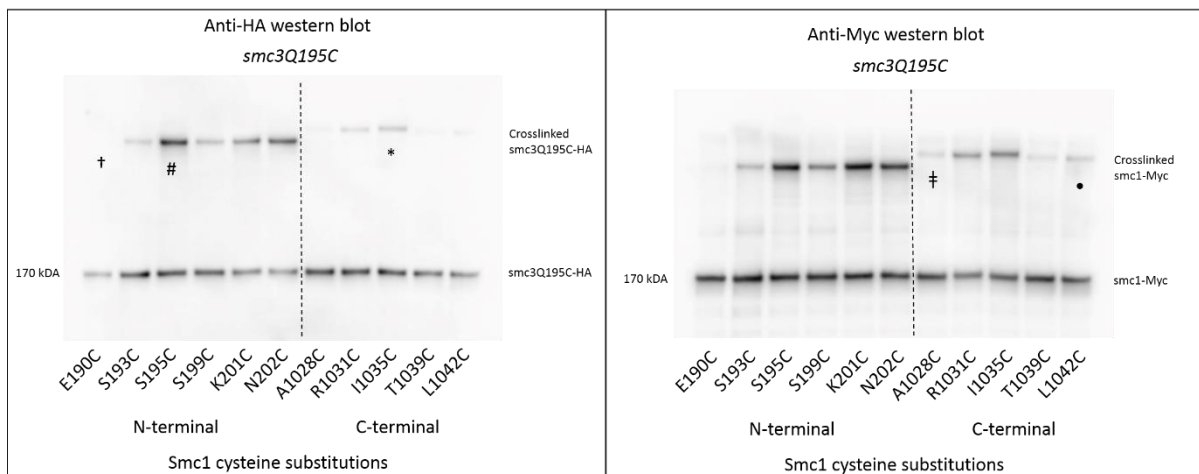


Figure 39: Western blots showing Smc1 cysteine residues which crosslink with smc3Q195C near to both the N and C terminals.

For smc3Q195C, an anti-Myc western blot was performed because unlike smc3E202C, the smc3Q195 BPA experiment showed that this residue may crosslink Scc2 too. To discount the possibility that smc3Q195C may crosslink with an endogenous cysteine residue in Scc2, the anti-Myc western blot will show that the crosslinks in anti-HA western blot contain Smc1-Myc as only one crosslink band will appear on either blot and it will be in the same position. In the

anti-HA western blot, a single “#” marks the position of a particularly strong crosslink band. The “+” marks the residue where the crosslink becomes undetectable, smc1E190C. The C-terminal crosslinks show much lower crosslink efficiency than the N terminal, appearing to peak at smc1I1035 and tapering off quickly; dropping to very low efficiency at smc1A1028C and smc1L1042C marked by “‡” and “•”, respectively. The results show that smc3Q195C crosslinks to the Smc1 coiled coil near the N terminal more efficiently than near the C terminal. This suggests that at this position, this residue is closer to the Smc1 N terminal coiled coil than the C terminal. The anti-Myc western blot shows that all the crosslink bands detected in the anti-HA western blot contain Smc1-Myc. The strains used in this experiment were: 2417, 2404, 2423, 2421, 2425, 2427, 2406, 2431, 2408, 2410, and 2435.

The final Smc3 site tested was smc3E213C. A modified range of Smc1 residues were tested in this case, as per crystallography data.

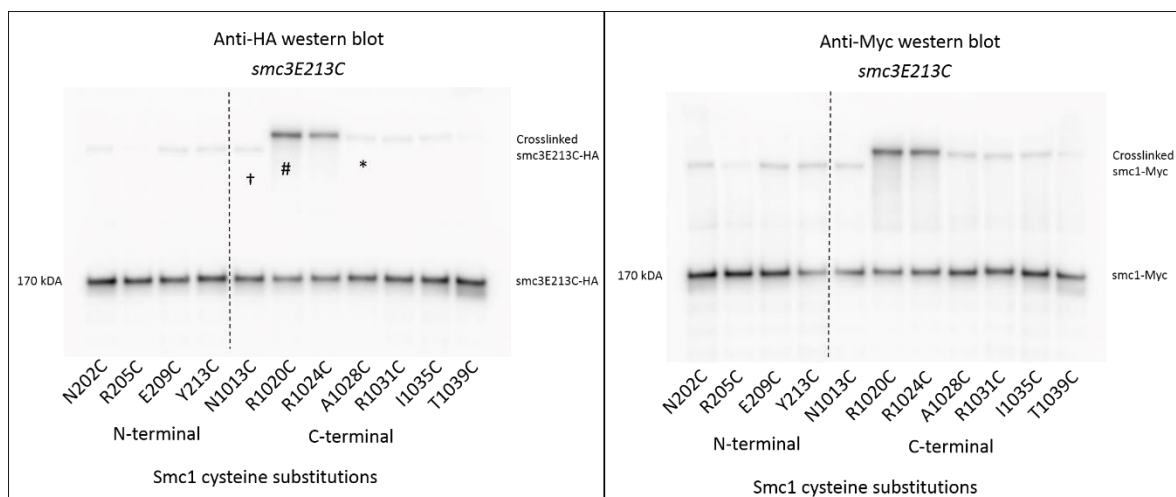


Figure 40: Western blots showing Smc1 cysteine residues which crosslink with smc3E213C near to both the N and C terminals.

Like smc3Q195C, an anti-Myc western blot was performed because there is a chance that this residue may crosslink with another protein. In the anti-HA western blot, a single “#” marks the position of a particularly strong crosslink band. The “+” and “*” marks the residues where the crosslinks becomes low efficiency. The N-terminal crosslinks are of much lower efficiency and do not show a clear peak of where the crosslink occurs most efficiently. The results show that smc3E213C crosslinks to the Smc1 coiled coil near the C terminal more efficiently than near the N terminal. The anti-Myc western blot shows that all the crosslink bands detected in the anti-HA western blot contain Smc1-Myc. The strains used in this experiment were: 2363, 2367, 2369, 2371, 2374, 2376, 2378, 2380, 2386, 2387, and 2389.

The data collected from the numerous Smc3-Smc1 coiled coil BMOE crosslink experiments were sufficient for the production of a predicted structural model of Smc3-Smc1 configuration which was constructed by Dr John Rafferty, Reader in Structural Biology, University of Sheffield, UK (see figure 41 and 42).

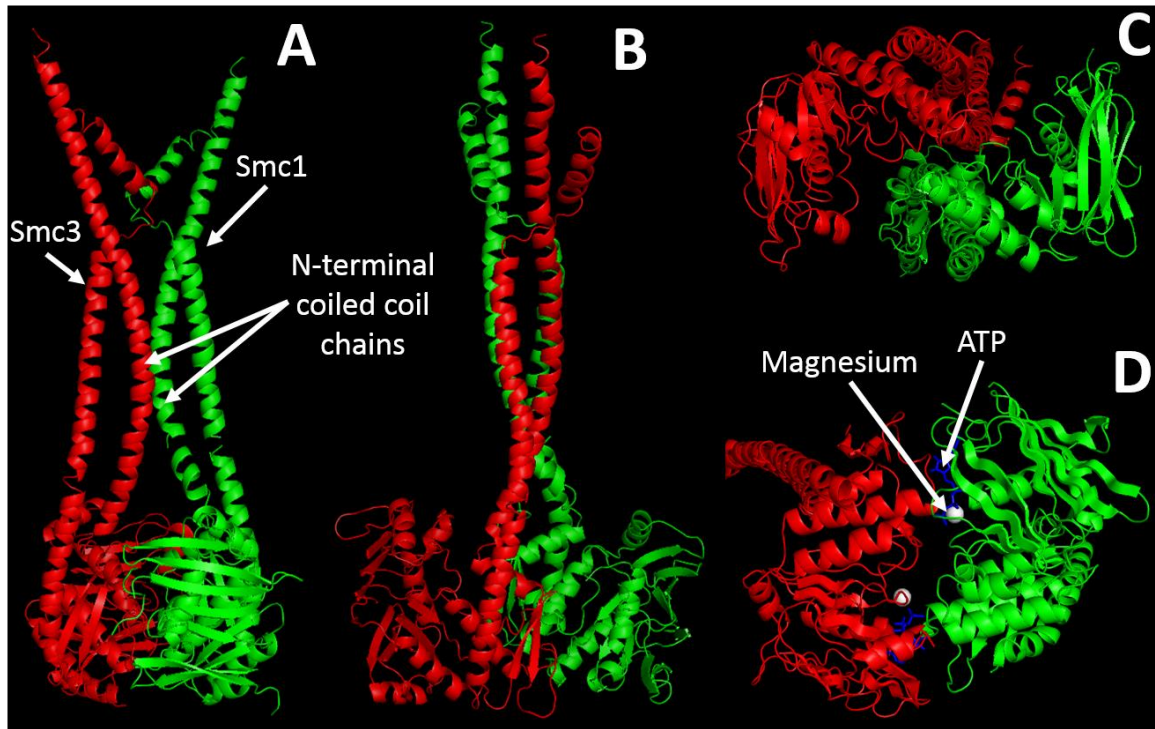


Figure 41: Cartoon diagram showing the structural model of cohesin using the data collected from the coiled coil BMOE crosslink data.

Dr John Rafferty produced a model of Smc3-Smc1 configuration which is consistent with all the crosslink data available as pictured in figure 32. These images show: (A) front view of Smc3 (red) and Smc1 (green), (B) side view of Smc3-Smc1, (C) view from below of the Smc3-Smc1 head domains, and (D) comparison of the engaged head position view from below. The N-terminal coiled coil regions of both Smc3 and Smc1 come closest to intersecting at positions 190 to 210, with respect to the crosslink data.

The predicted model shows that Smc3 and Smc1 form a rod structure while the ATP binding head regions are disengaged. This may be the configuration pictured by EM as found in figure 5.

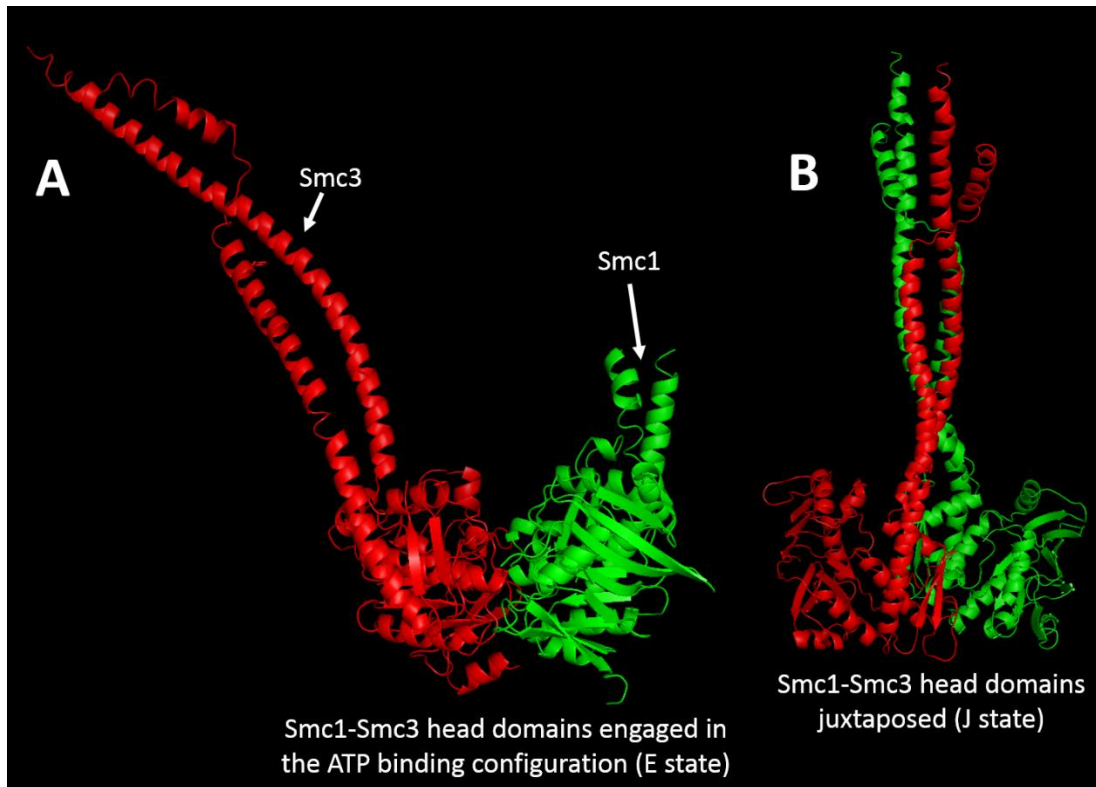


Figure 42: Cartoon diagram comparing the head engaged model as resolved by Gligoris and co-workers with the predicted structural model produced in this study.

The two models were named the E and J state of cohesin. The E state represents the model on the left (A) and stands for the engaged state of the Smc protein heads (Gligoris et al., 2014). The J state (B) represents the model on the right and stands for the juxtaposed state of the Smc3 protein heads.

In order to refine the J state model, further BMOE crosslink sites were examined to test the predictive accuracy.

4.2.4.3 Refining the J state coiled coil model

By adding more crosslink data, more constraints can be placed on the model, thus improving its reliability. Two further Smc3 residues were tested for crosslinking to select Smc1 cysteine residues: smc3E188C and K184C (see figure 43 and 44).

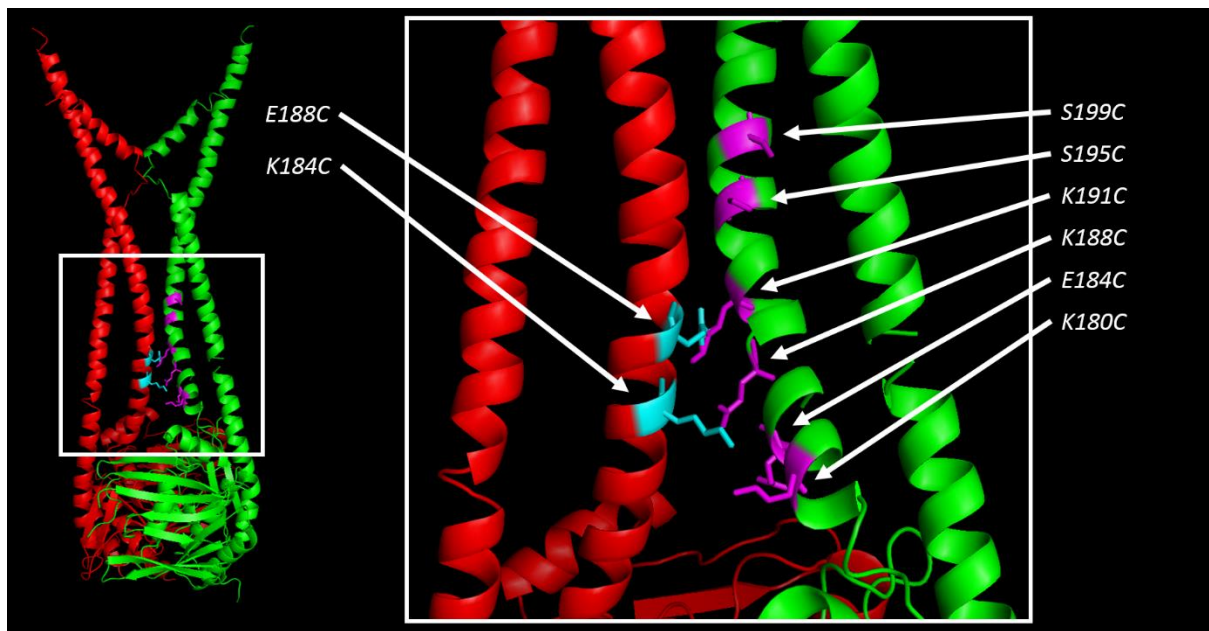


Figure 43: A cartoon showing the structural model of cohesin J state with predicted potential BMOE crosslink sites.

The diagram shows sites of cysteine substituted residues of Smc1 which may crosslink to smc3E188C and smc3K184C. Smc3 is coloured red while Smc1 is coloured green.

The residues highlighted in figure 43 were then tested for crosslinking using the BMOE system (see figure 44).

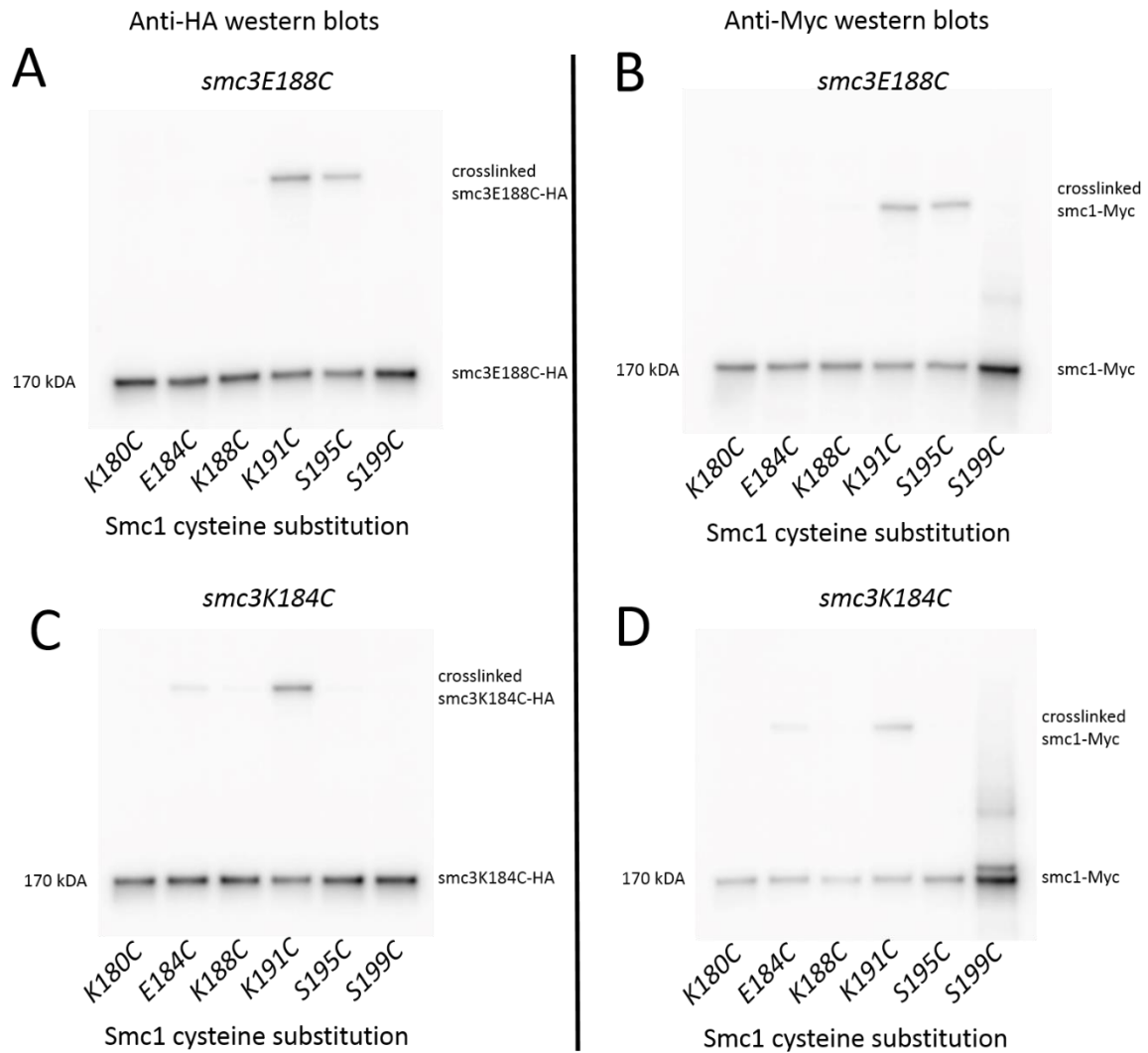


Figure 44: Four western blots showing crosslink products between smc3E188C and smc3K184C with various cysteine substituted residues in Smc1.

(A): The smc3E188C anti-HA western blot shows crosslinking occurs between smc1K191C and smc1S195C. The absence of other crosslinks shows that smc3E188C does not crosslink with any endogenous Smc1 cysteine residues. This is confirmed by the same crosslink results on (B) the anti-Myc western blot. (C): The smc3K184C anti-HA western blot shows that crosslinking occurs with smc1E184C and more efficiently with smc1K191C. This is confirmed by the same crosslink results on (D) the anti-Myc western blot. The strains used in this

experiment were: 2629, 2654, 2631, 2612, 2639, 2632, 2650, 2655, 2648, 2656, 2649, and 2664.

The introduction of smc1S199C may cause crosslinking with another protein as there is a lower molecular weight crosslink band present in both instances of anti-Myc western blot, albeit of low efficiency. All of the tested residue locations in 4.2.4.3 can be found in figure 45.

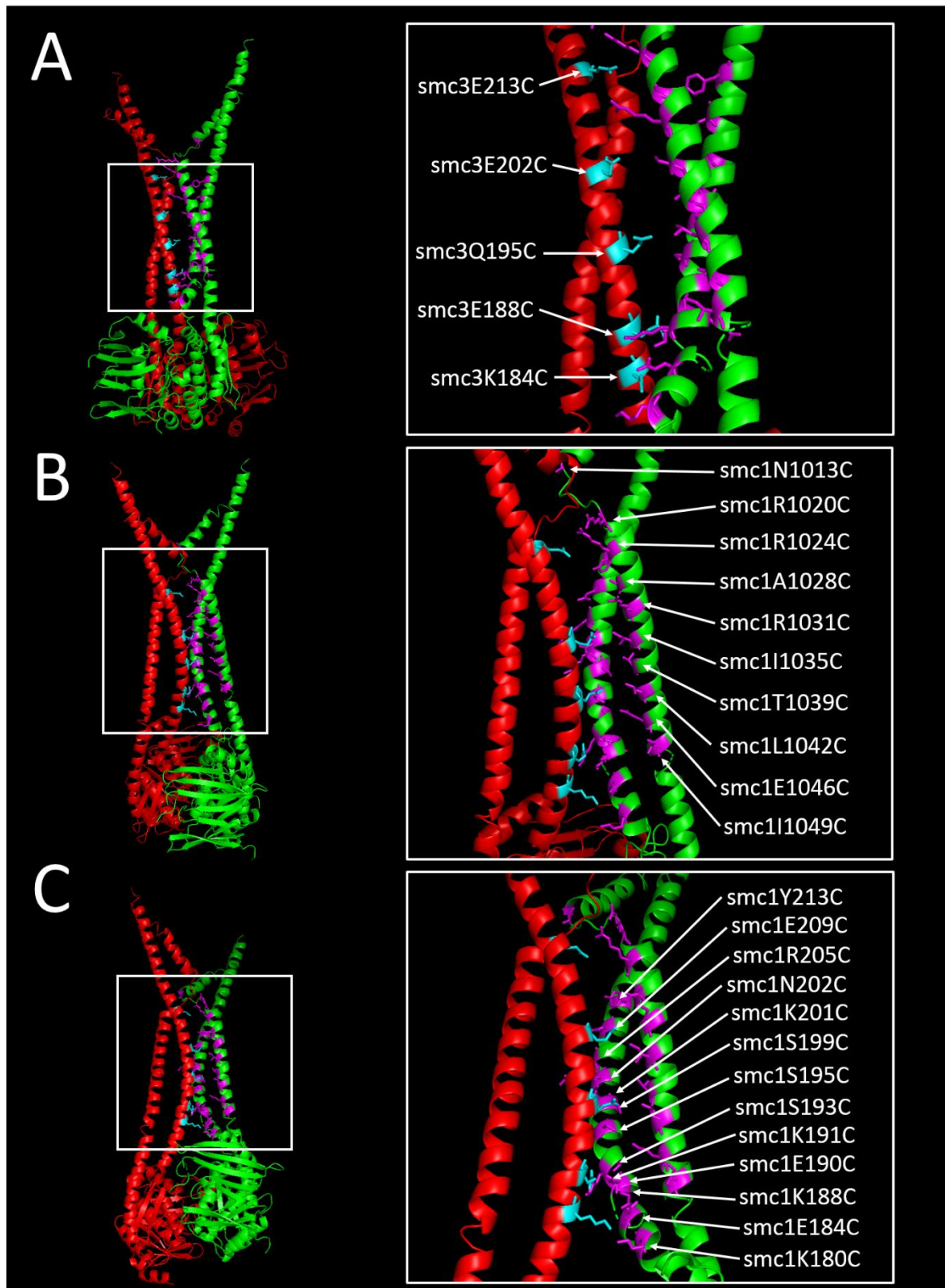


Figure 45: Cartoon showing the locations of all the cysteine-substituted residues tested with the BMOE crosslinking system thus far.

(A): Locations of all five Smc3 cysteine-substituted residues tested for crosslink formation using the BMOE crosslinking system. (B): Locations of all the Smc1 C terminal cysteine-substituted residues. (C): Locations of all the Smc1 N terminal cysteine-substituted residues.

With now five constraints on the Smc3-Smc1 coiled coil interaction pictured in figure 45, further crosslink pairs in the head domain were designed to ensure that the head domain configuration was also accurately represented *in silico*.

4.2.4.4 Refining the J state head configuration

To further test the predicted model, a BMOE crosslink experiment was designed where particular residues in the Smc3 and Smc1 head domains that are predicted to be within 8 Ångströms apart were substituted with cysteine so a variety of possible BMOE crosslinks may be detected which can be seen below in figure 46 and 47.

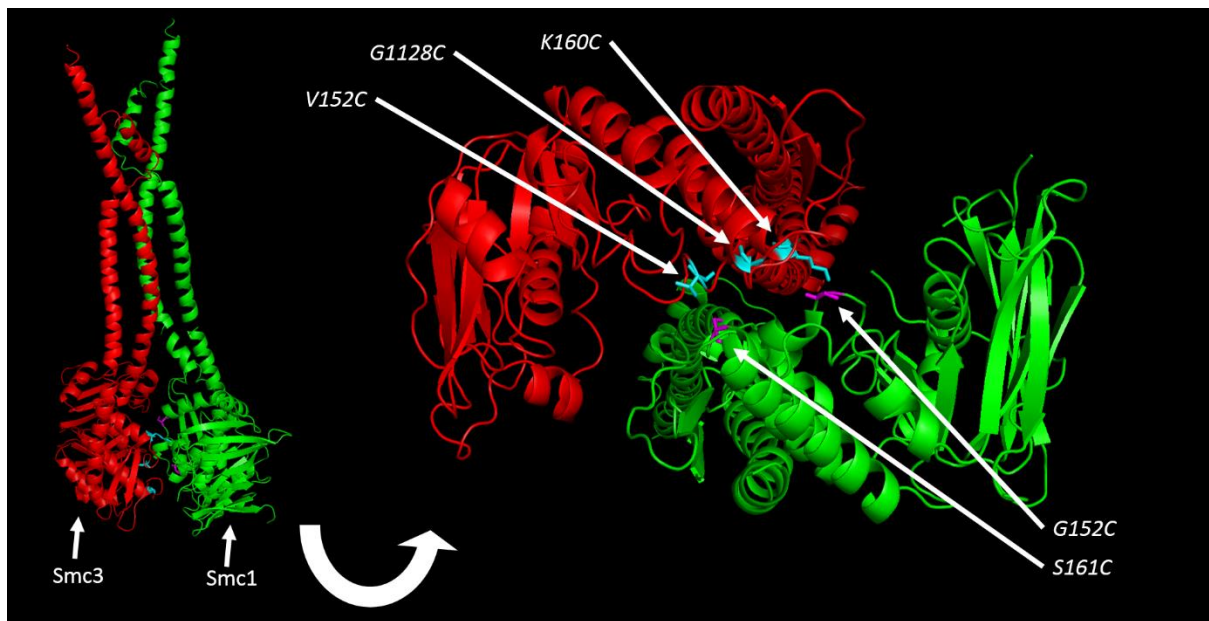


Figure 46: Cartoon showing cysteine substituted residues in the Smc3 and Smc1 head domain.

Smc3 is coloured red while Smc1 is coloured green.

The residues highlighted in figure 46 were tested for crosslinking using the BMOE crosslinking system (see figure 47).

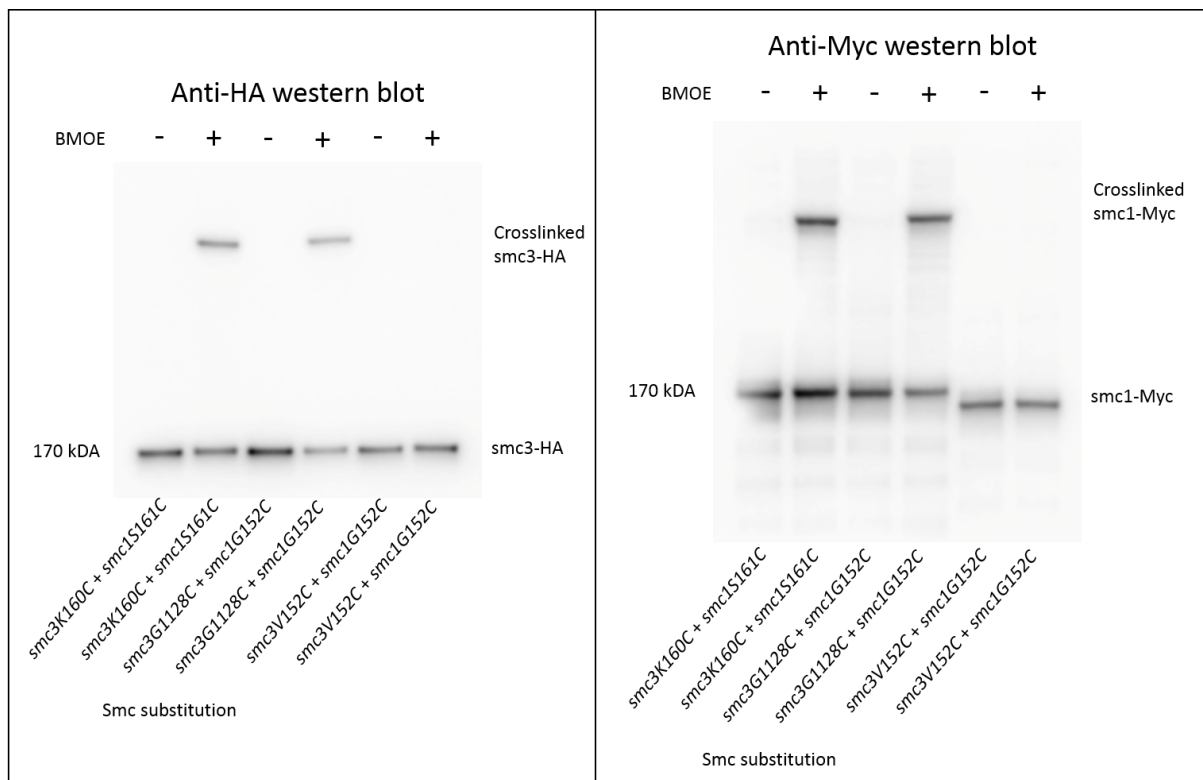


Figure 47: Western blots showing the crosslinking of various cysteine substituted residues in the Smc1 and Smc3 head domain.

The anti-HA western blot shows that crosslinking occurs between smc3K160C and smc1S161C as well as between smc3G1128C and smc1G152C. This is confirmed in the anti-Myc western blot which shows the crosslink bands contain Smc1. The cysteine pair smc3V152C and smc1G152C appear to have downshifted uncrosslinked smc1G152C-Myc bands. Due to the methods used to construct the strains, it is possible that homologous recombination has caused the loss of some Myc tag repeats, thus lowering the molecular weight. The strains used in this experiment were: 2643, 2647, and 2642.

The J state model, having sufficient accuracy to predict crosslinking over a small range of residues as per figures 43-44 and 46-47, was not yet tested to accurately predict

crosslinking of individual amino acids or predict the orientation of possible crosslinking amino acid side chains. To make sure that the model is robust enough to detect small changes in structure which can be found from changes to crosslinking efficiencies, very specific crosslink pairs were selected for testing.

4.2.4.5 Testing the refined model of the J state

Using the data from figures 43-47, the J state model was modified with these extra constraints, producing the refined model shown below in figure 48.

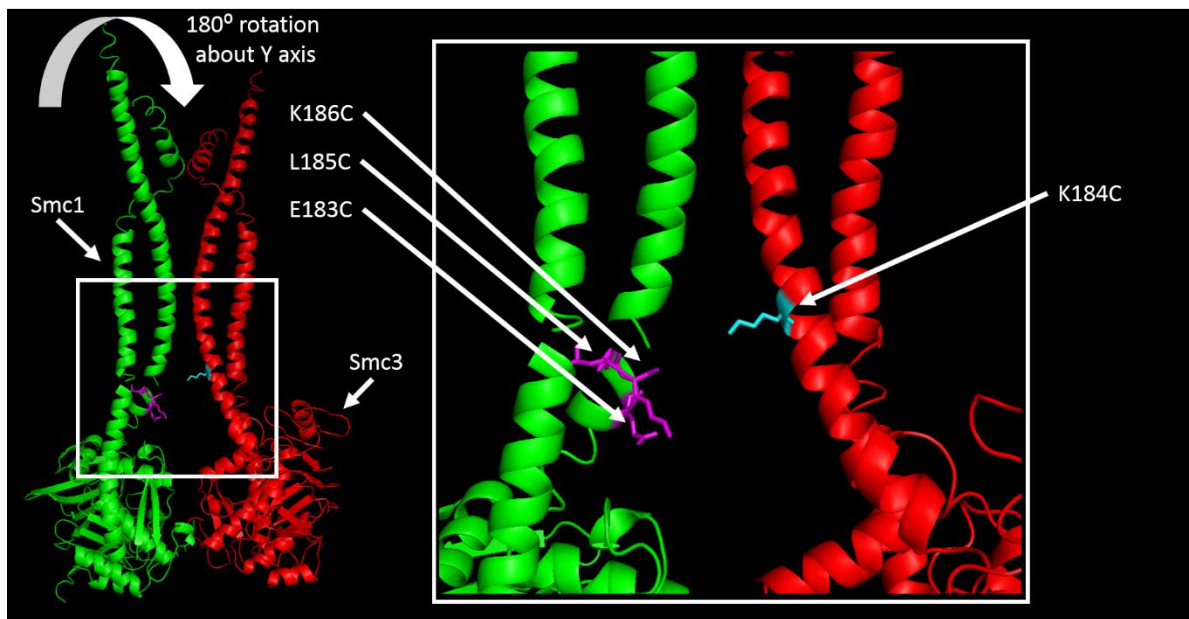


Figure 48: A cartoon showing the refined J state model, highlighting cysteine substituted residues in the Smc1 and Smc3 coiled coil domain.

The point of view for this cartoon has been rotated to allow better view of the highlighted residues and now shows Smc1 on the left and Smc3 on the right. The residues labelled were predicted not to crosslink strongly in the refined model as displayed, but were predicted to crosslink strongly in the previous model, due to small changes in the orientation of the Smc1-Smc3 head domains. The three additional Smc1 residues: E183C, L185C and K186C are estimated to be in range of crosslinking, but due to the rotation of Smc1-Smc3 are predicted not to crosslink. In other words, the centre of rotation for these residues is within 8 Ångström, however the rotational orientation brings the crosslinking side chains out of range. Thus, this

test was performed to calibrate the model spacing and rotational position of residues accurately. Smc3 is coloured red while Smc1 is coloured green.

The residues displayed in figure 48 were tested alongside the previously tested Smc1 residues in figure 44 (see figure 49).

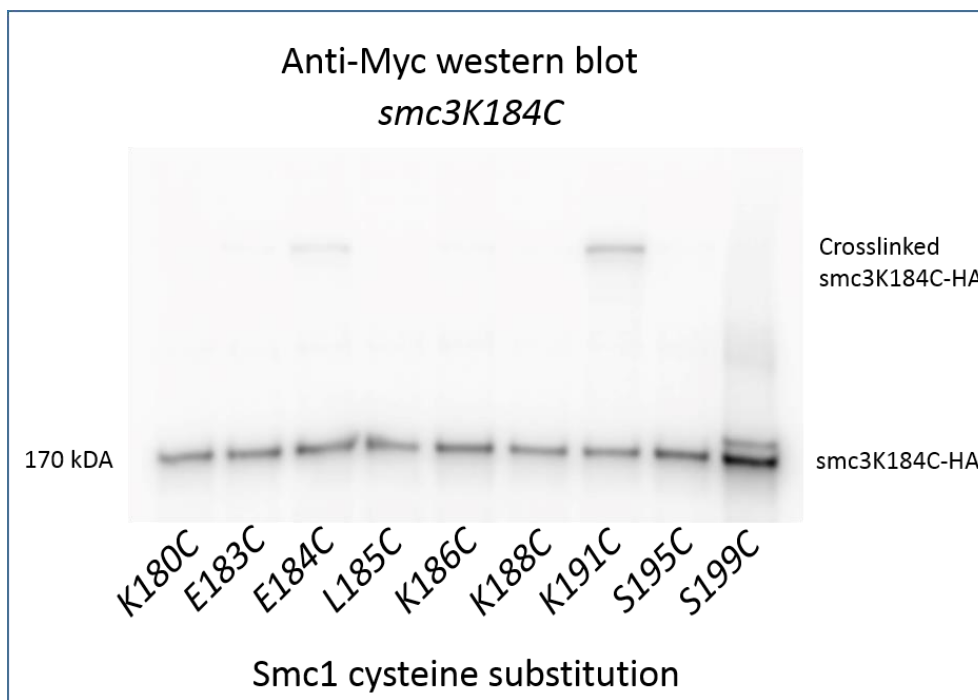


Figure 49: Western blot showing crosslink between *smc3K184C* and various cysteine substituted residues in Smc1.

The anti-Myc western blot shows that as predicted, the crosslinking efficiency between *smc3K184C* and Smc1 is very low with the residues *smc1E183C*, *L185C* and *K186C*. There is significant crosslinking occurring with *smc1K191C* as demonstrated previously. There is a modest amount of crosslink product with *smc1K184C*. This is because, as predicted, this residue is orientated more in the direction of *smc3K184C*. This shows that orientation of the

residues are correct and absolute distance between them is likely to be accurate. The strains used in this experiment were: 2650, 2698, 2655, 2700, 2702, 2648, 2656, 2649, and 2665.

With a calibrated J state model, it was now possible to produce crosslink pairs which represent the possibility of mutually exclusive states, being the E and J state. After this was achieved, a crosslink assay was produced which examined the crosslink products of each state and the effects of mutations on their formation, such as QQ.

4.3.4.6 Resolving E and J state crosslink products

To prove with biochemical evidence that the E and J states of cohesin are mutually exclusive, a pair of Smc3-Smc1 cysteine residues from the E and J state were combined in a single strain to test for a crosslink product band not identifiable as E or J state; hence a crosslink product with both sites crosslinked simultaneously. The selected residues are shown in figure 50.

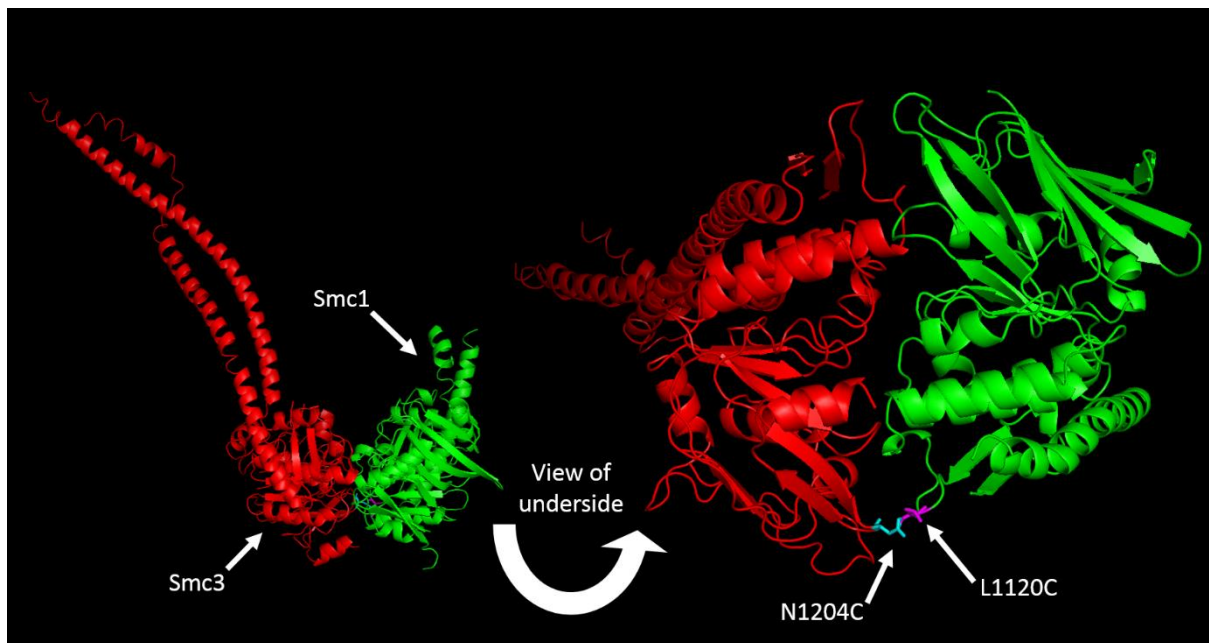


Figure 50: A cartoon showing a pair of cysteine residues predicted to crosslink in the resolved structure of Smc1 and Smc3 fragments.

Smc3 is coloured red while Smc1 is coloured green with structures as resolved by Gligoris and co-workers (Gligoris et al., 2014)

The E state pair smc3N1204C and smc1L1120C were tested along with the J state pair smc3K160C and smc1S161C established in figure 47 (see figure 51).

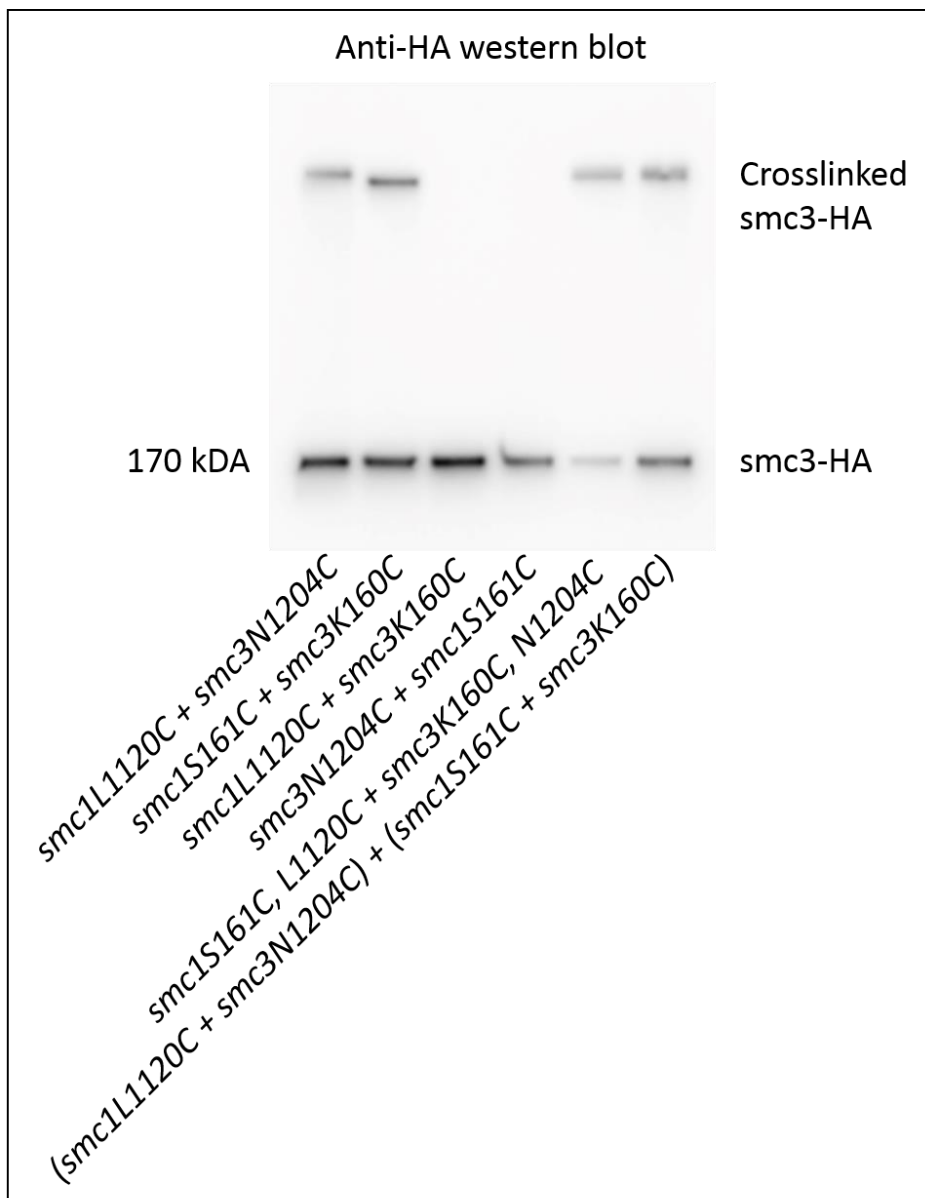


Figure 51: Western blot showing crosslink products made between cysteine pairs in Smc1 and Smc3.

The anti-HA western blot shows that crosslinking may only occur when the E and J cysteines are correctly paired up. The E state cysteine pair, smc1L1120C and smc3N1204C form significant crosslink products, but not when they are separated and combined with J state cysteines. Likewise, the J state pair, smc1K161C and smc3K160C behave in the same way. In order for an E and J state assay to be developed, the crosslink products must be

distinguishable on the western blot, forming two separate bands when combined. When the E and J state pairs are introduced into a single strain, the crosslink products have such similar electrophoretic properties that they merge to form a single band. This effect is also seen when mixing together the two samples after immunoprecipitation in the last lane of the blot. As a result, this experiment does not prove that the E and J state are mutually exclusive. For this claim to be substantiated, the two different crosslink products would have to be distinguished with the assay confirming or excluding the presence of a third crosslink product. The strains used in this experiment were: 2734, 2730, 2728, 2733, and 2731.

As the experiment did not yield the expected result of two distinct bands representing the E and J state respectively, a change in experimental design was required to change electrophoretic mobility of the E and J state crosslink products to allow differentiation.

4.2.4.7 Testing J state coiled coil configuration compatibility with E state head engagement

As the previous experiment failed to yield evidence of E and J state mutual exclusivity, another strategy was developed. During the construction of the strains used, the HA tag was removed from the C terminal and a FLAG tag was inserted at the N terminal of Smc3 using cloning and transformation methods (3.2.3.5 and 3.2.3.9) This was in an attempt to test how moving and changing the type of tag may change the electrophoretic dynamics of crosslink products and thus improve resolution.

Furthermore, to strengthen the case of the E and J state being mutually exclusive due to coiled coil configuration, this could be tested by producing strains which yield crosslink products between the E state in the head and coiled coil simultaneously (via a double crosslink). This could produce an assay where another coiled coil cysteine pair further away from the head domain may fail to produce double crosslink products, providing evidence suggesting that there are coiled coil configurations which are incompatible with the E state head domain configuration, allowing the distinct possibility of a mutually exclusive E and J state existing. This experiment used two pairs of previously established coiled coil crosslinks to show that some flexibility exists in the region to allow some J state crosslinks to coexist with E state but not those close to the head domain (see figure 52).

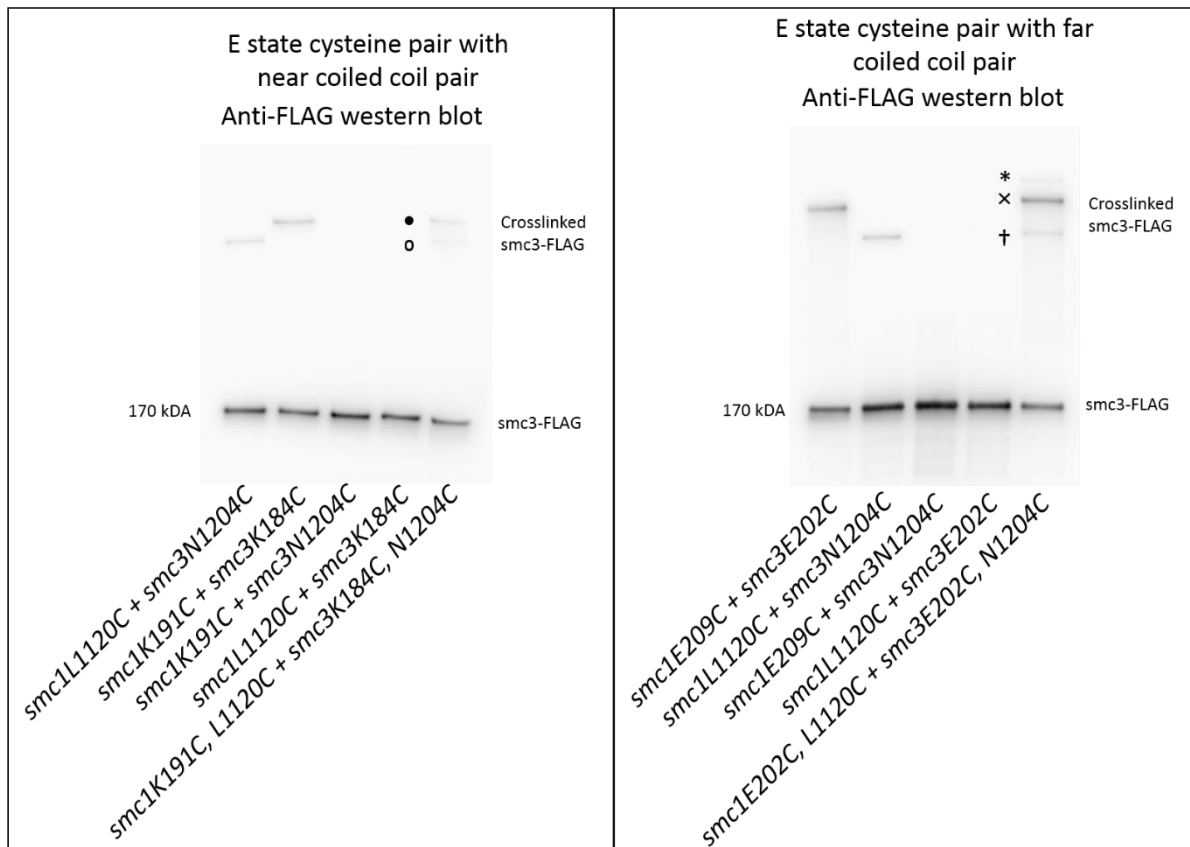


Figure 52: Western blots showing the crosslinks formed between the coiled coil of Smc1-Smc3 and the head domains.

The western blots show the differences in crosslink product electrophoretic dynamics between E state cysteine pairs combined with coiled coil cysteine pairs of a varying distance from the head domain. The anti-FLAG western blot pictured left, shows that a previously established J state coiled coil cysteine pair is incompatible with the E state pair. The coiled coil cysteine pair, smc1K191C and smc3K184C, named the near pair, forms a crosslink product as expected when independent. The same is also true of the E state pair, smc1L1120C and smc3N1204C. However when paired together, both crosslink products are formed, (marked by “•” for coiled coil and “o” for the E state product) without a third crosslink product which would represent the two crosslinks occurring simultaneously. This is in direct contrast with

the anti-FLAG western blot pictured right, showing that another previously established J state coiled coil cysteine pair is compatible with the E state pair. The coiled coil cysteine pair, smc1E209C and smc3E202C, named the far pair, forms a crosslink product as expected when independent. The same is also true of the E state pair, smc1L1120C and smc3N1204C. However when paired together, both crosslink products are formed, (marked by “*” for coiled coil and “+” for the E state product) with an additional third crosslink product, representing the two crosslinks occurring simultaneously (marked by “**”). The results of the experiment show that two distinct states of cohesin are likely to exist as the coiled coil is not flexible enough to allow full mobility of the head domains. The strains used in this experiment were: 2787, 2866, 2864, 2865, 2867, 2894, 2787, 2895, 2896, and 2897.

Although this experiment does provide evidence of mutually exclusive E and J states, it does not correlate them with any particular function of cohesin. However, it does show that there is a limit to the flexibility of the coiled coil and its configuration does directly impact the configuration of the head domains. It is therefore possible that a global effect on the coiled coil may be the primary driver of head engagement as suggested by Bürmann and co-workers which describes a folding region in a bacterial homologue of cohesin, MukBEF (Bürmann et al., 2019). This folding “elbow” action may be driven by ATP hydrolysis or facilitated by action of other proteins. In the next part of this chapter, this study tested the QQ mutation to examine its effect on the coiled coil configuration of cohesin and the possible reasons and outcomes of these effects. As moving the FLAG epitope tag to the Smc3 N terminal proved viable and also possibly beneficial in differentiating crosslink products, the same strategy was employed to produce a working E and J state assay.

4.2.5 Chapter 2 part 4: The effect of QQ on the E and J configurations

4.2.5.1 Establishing an E and J state assay

To develop an assay which probes for the effect of mutations on the E and J state crosslink efficiency, the FLAG tag was moved to the N terminal of Smc3 variants which was expected to solve the problem of the two separate crosslink products merging to form a single band as found in figure 51. The experiment was then repeated in a similar manner, with the exception of also testing the E and J state strain with the QQ mutation (see figure 53).

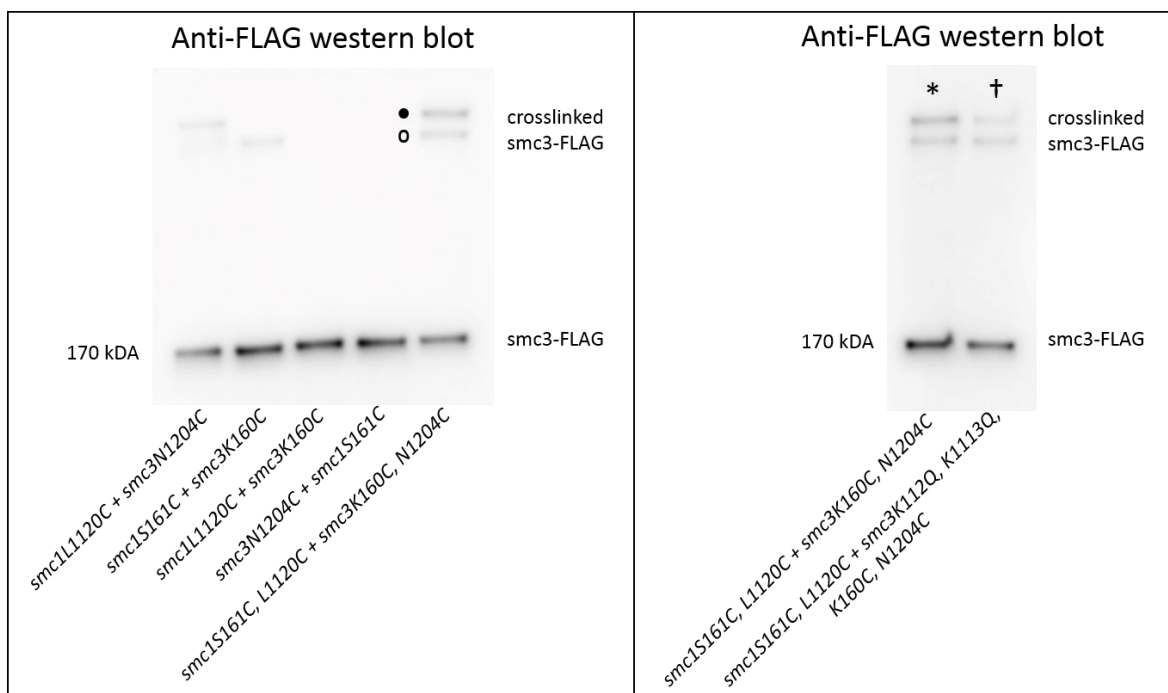


Figure 53: Western blots showing resolution of crosslink products produced by the E and J state cysteine pairs with and without smc3K112Q, K113Q.

The anti-FLAG western blot pictured left shows that the crosslinks are not interchangeable between the E and J state and also that the E and J state crosslinks are mutually exclusive, in support of figure 52 as there is no detectable third crosslink product. The E and J state crosslink products are represented by the bands marked with “•” and “o” respectively. The anti-FLAG western blot pictured right shows a comparison between the E and J state crosslink products produced with and without the QQ mutation marked by “+” and “*” respectively. It appears that the top band representing the J state with the QQ mutation (marked by “+”) may be of reduced efficiency compared to without (marked by “*”). The strains used in this experiment were: 2783, 2787, 2785, 2777, 2780, 2781, and 2788.

Although the E and J state represent different configurations of cohesin, it is still unknown exactly what functions these configurations perform *in vivo*. To shed light on this further, the proportions of the E and J state could be examined at particular stages of the cell cycle as it is known that cohesin performs specific functions during these stages. For example, the highest level of cohesin loaded on to chromatin is found after S phase and throughout G2. The E and J state assay may show a large bias to one of these states during these particular phases of the cell cycle and may provide circumstantial evidence for the function of cohesin represented by either the E or J state. In order to quantitatively ascertain whether the QQ mutation significantly affects the proportion of E and J state crosslink products, repeats of the experiment are required. In addition, the experiments can be performed with the arrest of the cells in particular phases of the cell cycle via mating pheromone intervention. Yeast mating involves the secretion of small pheromone peptides which signal physiological changes to facilitate sexual reproduction. As a consequence, when haploid yeast are

subjected to their complementary pheromone (a factor for alpha cells and alpha factor for a cells) they are arrested in the G1 phase of the cell cycle.

Sic1 is a protein which inhibits the function of Cdk1, a cyclin kinase responsible for the advancement of the cell cycle into S phase. By controlling the expression of Sic1, entry into S phase is blocked. This is achieved by introducing a *SIC1* incorporated *GAL* regulon into a *leu* locus of a yeast strain which makes the strain express Sic1 whenever galactose is present in the growth medium, allowing Sic1 expression at will (Barberis et al., 2005). The *GAL* regulon works via expressing the galactose receptor Gal3p, a stoichiometric sensor, which by binding to galactose increases binding affinity to inhibit the repressor Gal80p. With Gal80p inhibited, Gal4 is available to dimerise and bind to a upstream activating sequence, thus activating the transcription of *GAL* genes which allow the metabolism of galactose (Malakar and Venkatesh, 2014). Overexpression of Sic1 via the *GAL* regulon is necessary because Sic1 is phosphorylated and becomes a target for ubiquitination by Cdc34 before being digested at the transition of G1 to S phase. By overexpressing Sic1, this action is overcome and the abundance of Sic1 continues to inhibit Cdk1 to prevent entry into S phase (Verma et al., 1997).

As G1 phase arrest can be achieved by manipulation of Sic1 expression, G2 phase arrest can be introduced by nocodazole, a spindle fibre poison. Nocodazole disrupts the polymerisation of microtubules which are critical in producing the spindle fibres that generate proper disjunction of chromosomes during mitosis. This is shown by the complete disruption of cytoskeleton formation and inhibition of microtubule mediated

axonal transport (Salas et al., 1986; Samson et al., 1979; Zegers et al., 1998). Lack of spindle fibres connected to the spindle pole body causes a phenomenon known as the spindle assembly checkpoint (SAC) where anaphase is delayed until all chromosomes are aligned on the metaphase plate, shown by targeted spindle destruction via ultraviolet-microbeam (Zirkle, 1970). Mutant *S. cerevisiae* strains which possess mutations in particular genes known as mitotic arrest deficient (MAD) genes, allow cells to continue through G2 phase into mitosis despite the lack of properly assembled spindle fibres (disrupted by anti-microtubule drugs) before finally dying afterwards due to non-disjunction (Li and Murray, 1991). This is further supported by manual activation of the SAC by overexpressing the kinase responsible for MAD phosphorylation, a known response critical for the activation of the checkpoint (Hardwick et al., 1996). Thus, the introduction of nocodazole into growth media can reliably cause G2/M arrest via activation of the SAC.

4.2.5.2 Testing the effect of *smc3QQ* on the E and J state dynamics during various stages of the cell cycle

By producing strains combined with the *GAL* regulon, E and J state cysteine pairs and the QQ mutation, the experiment was conducted comparing three samples of two strains (see figure 54). The first strain, 2779, did not have the QQ mutation whereas the second strain, 2788, did. The three samples were prepared by running a standard BMOE crosslink experiment with cells growing normally (cycling cells), a Sic1 G1 arrest method of preparation as described in 3.2.3.20 and another G2 arrest method of combining the protocols of 3.2.3.20 and 3.2.3.21.

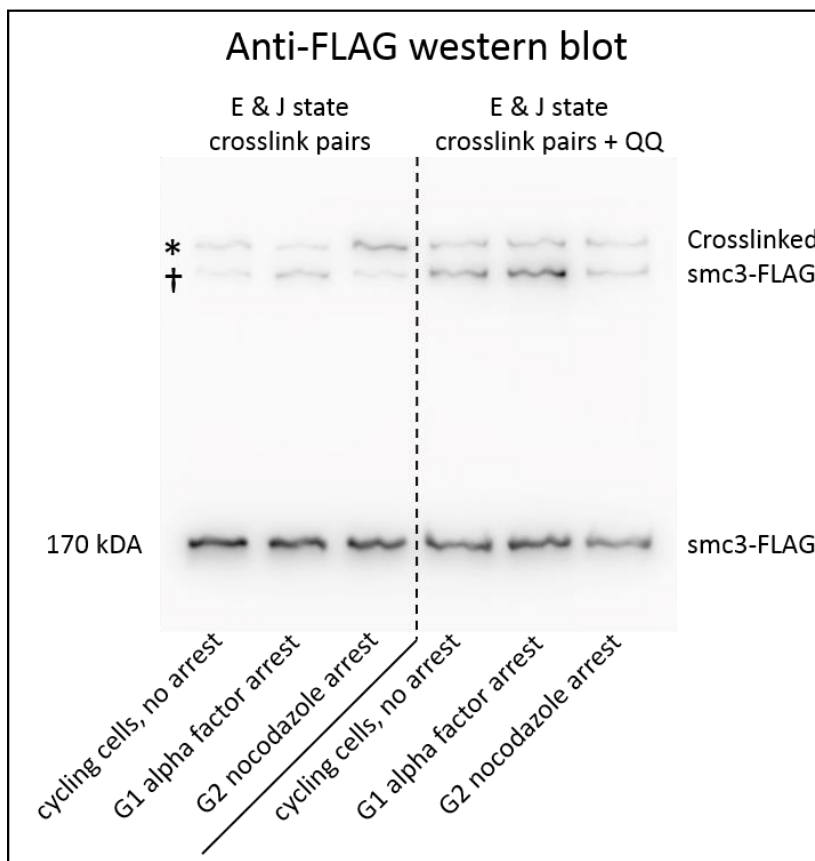


Figure 54: Western blot showing the effect of the QQ mutation on the formation of E and J state crosslink products at various stages of the cell cycle.

G1 alpha factor arrest refers to the use of alpha factor and Sic1 overexpression via the *GAL* regulon system, and G2 nocodazole arrest refers to release of G1 arrest through S phase by growth in galactose-free media before addition of nocodazole. The anti-FLAG western blot pictured left, shows that without the *QQ* mutation: the E and J state crosslink products appear close to equal in proportion from cycling cells, more E state crosslink product was formed than J state from G1 arrest cells, and more J state crosslink product was formed than E state from G2 arrest cells. With the *QQ* mutation however, there appears to be: more E state crosslink product than J state from cycling cells and G1 arrest cells, with close to equal proportion of E and J state crosslink product from G2 arrest cells. The strains used in this experiment were: 2779 and 2788.

After the above experiment was repeated three times, the western blots were used to manually quantify the bands as was done with the blots in figure 35 and 36 to produce a graph (see figure 55).

The effect of K112Q, K113Q on the E and J state of cohesin during various phases of the cell cycle

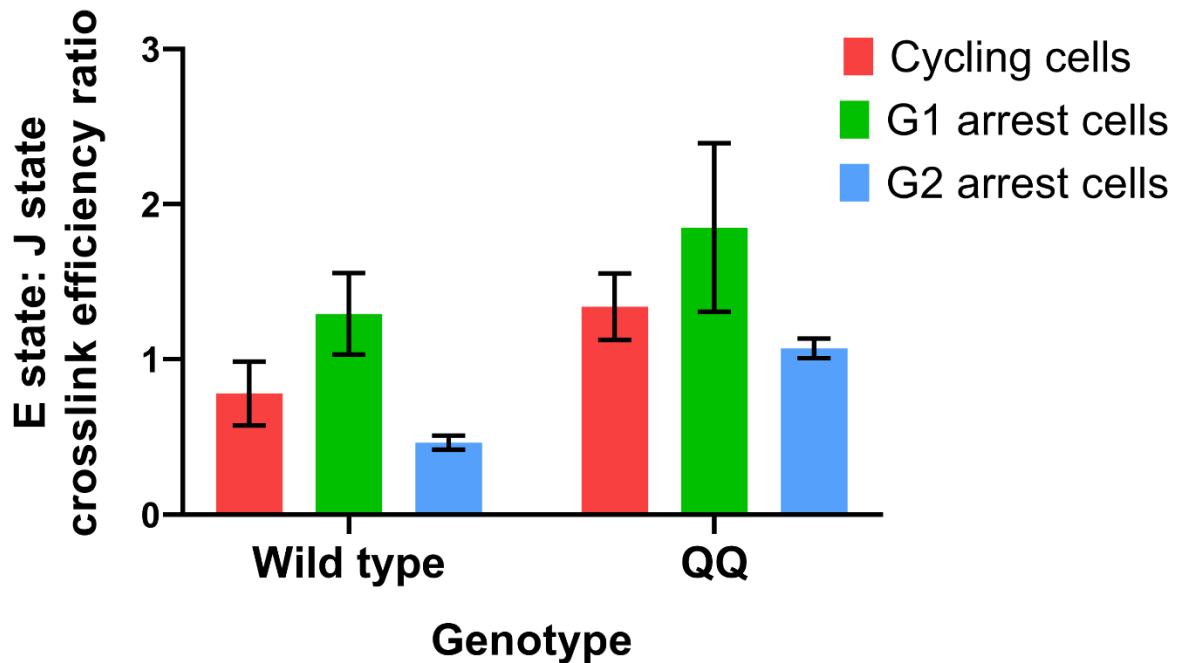


Figure 55: Graph showing the effect of *smc3QQ* on the E and J state crosslink product formation of cohesin during various phases of the cell cycle.

The graph (n=3) shows the E state crosslink product of the total immunoprecipitated protein as a ratio with the J state crosslink product. The graph shows that the total J state crosslink product from cycling, G1 and G2 arrest cells was reduced by the introduction of the QQ mutation. Statistical analysis shows that QQ significantly reduced J state crosslink product formation compared to wild type in cycling and G2 arrest cells (non-parametric one-way ANOVA, chi squared: 3.86/3.86, degrees of freedom: 1/1, probability value: 0.05/0.05, respectively). QQ did not significantly reduce E state crosslink product formation compared to wild type in G1 arrest cells however (non-parametric one-way ANOVA, chi squared: 2.33,

degrees of freedom: 1, probability value: 0.127). Fluorescent automatic cell sorting (FACS) data confirming the cell phases in this experiment may be found in 7.4.3.

As cohesin is loaded on the DNA by G2 phase, it is likely that the J state of cohesin represents this configuration as this product is more abundant from G2 arrest cells. This is supported by experiments in the literature which have captured DNA in the J state of cohesin (Chapard et al., 2019; Vazquez Nunez et al., 2019). Therefore, the E state conversely may represent unloaded cohesin.

4.2.6 Chapter 2: Summary

The region around smc3R1008I yielded BPA crosslink sites with the coiled coil region of Smc1, and Scc2 (figures 27 and 29). Combining BPA crosslinking and TEV cleavage revealed that sites in the Smc3 coiled coil crosslinked to an adjacent region of Smc1 coiled coil. This may be indicative of the rod conformations described in literature (Bürmann et al., 2019; Chapard et al., 2019; Diebold-Durand et al., 2017; Vazquez Nunez et al., 2019). Many BMOE crosslink sites exist between the coiled coil region of Smc3 and Smc1, indicating that they are within very close proximity (figures 38-40). The numerous crosslinks in the region provide biochemical evidence of the rod conformation as seen in EM imaging (Hons *et al.*, 2016). This configuration is affected by introducing QQ and its suppressors, as crosslinking efficiency of known residues are demonstrably enhanced or diminished (figures 35, 36, 54 and 55). By testing the possible combinations of crosslinks between the head domains and coiled coil domains of Smc1 and Smc3, it can be shown it is likely that due to inflexibility of the coiled coil region proximal to the head domain, the engaged configuration cannot occur if the coiled coil domains of Smc1 and Smc3 are in close proximity within about 200 residues away from the head domain. This supports a further result which showed that crosslinks in the head domain reveal two mutually exclusive arrangements, called the E (engaged) and J (juxtaposed) states (figure 53). It is expected that these two distinct states have biological significance that is to be tested further; however it was found that QQ reduced the proportion of J state in all stages of the cell cycle which is the state implicated in DNA capture by studies in literature (figure 54 and 55). To conclude, it is not understood why QQ may affect the incidence of E and J state.

4.3 Chapter 3

4.3.1 Introduction

As per the experimental strategy outlined at the end of 4.1.4, experimental efforts were made to find the changes in cohesin structure which would explain why QQ may prevent loading activity. Results in chapter 2 found that QQ had the effect of increasing the E to J state ratio in cycling cells and those arrested at the G1 or G2 phase of the cell cycle. For this to occur, a change in the coiled coil configuration of cohesin is necessary to explain why QQ affects the formation of particular states, however no data have been collected explaining the mechanism. The other line of investigation previously described in 4.1.4, was to examine the effect of QQ on cohesin-Scc2 interaction. One possibility is that the transition between the E and J state is facilitated by the loading complex Scc2-Scc4, via specific interaction sites in cohesin and that QQ may inhibit such activity. This could explain the ability of *smc3R1008I* and other suppressor mutants that suppress QQ. Scc2 has also been crosslinked at a site proximal to R1008I. If this hypothesis is true, then it should be demonstrable that QQ abolishes Scc2 interaction with cohesin and that QQ suppressors restore this interaction. To continue this line of investigation, the following chapter will utilise techniques previously established in chapters 1 and 2 along with data obtained during the collaborative efforts with the Nasmyth laboratory to test this hypothesis.

4.3.2 Chapter 3 part 1: Finding Smc3 / Smc1 interaction sites in Scc2

4.3.2.1 Finding Scc2 BPA crosslinking sites in Smc3 and Smc1

In order to test the hypothesis that QQ abolishes or reduces Scc2 interaction with cohesin, an assay must be used to measure the affinity of cohesin for Scc2 interaction. The strategy to accomplish this was to use the BPA crosslinking system established previously along with manual band quantification as used in figures 35 and 36 to measure the Scc2 crosslink product. Furthermore, mapping possible Scc2 interaction sites around cohesin may reveal how Scc2 interacts with the rod or ring form of cohesin by producing a model which can highlight particular features of the configuration that may be disrupted by the QQ mutation. This would help elucidate the precise mechanism by which QQ prevents loading of cohesin onto the DNA, which could be accomplished in a similar way as done in 4.2.4.

Due to the lack of a predictive model of Scc2 interaction, BPA photo-reactive crosslinking was used in addition with TEV protease cleavage. Screens were performed in the head, hinge and coiled coil domains of Smc3 and Smc1 looking for viable BPA substitution sites that crosslink with Scc2 (see figure 56).

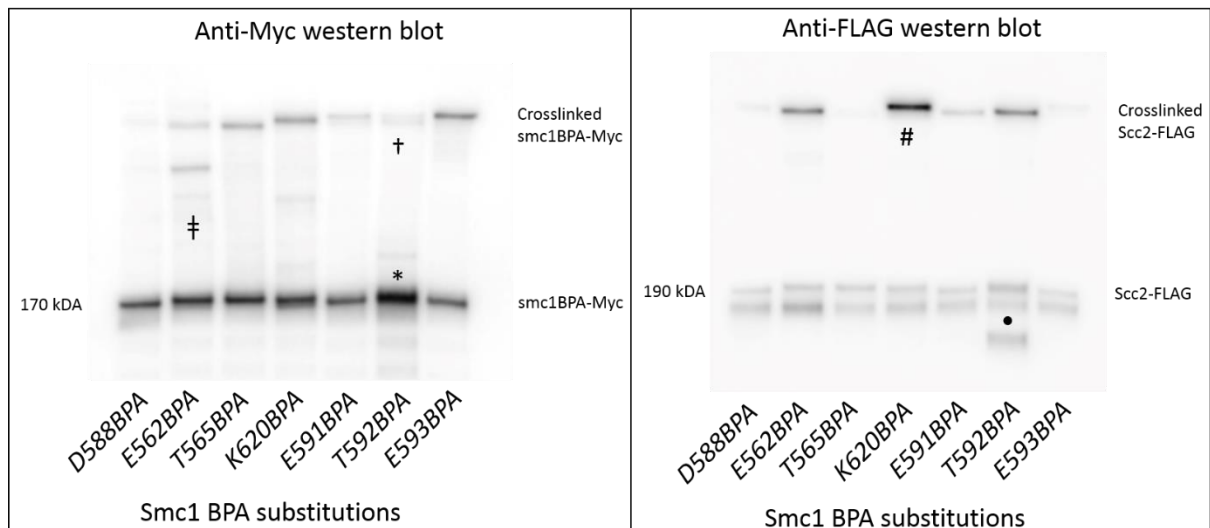


Figure 56: Western blots showing crosslink products of BPA substituted residues near the hinge region of Smc1.

The anti-Myc western blot shows that all the of tested residues crosslink with another protein, in line with the marked “+”. There are also crosslink products of lower molecular weight marked by “‡” and “*”. The anti-FLAG western blot however, shows that many of the crosslink bands found on the anti-Myc western contain Scc2-FLAG. There is a particularly strong crosslink band marked by “#”, smc1K620BPA. The anti-FLAG western blot also has non-specific bands marked by “•” which are not in line with the expected weight of 190 kDa for Scc2-FLAG. The strains used in this experiment were: 1966, 1967, 1968, 1969, 1970, 1971, and 1972.

As smc1K620BPA produced the strongest crosslink with Scc2, this residue was further tested for its ability to crosslink other proteins associated with cohesin (see figure 57).

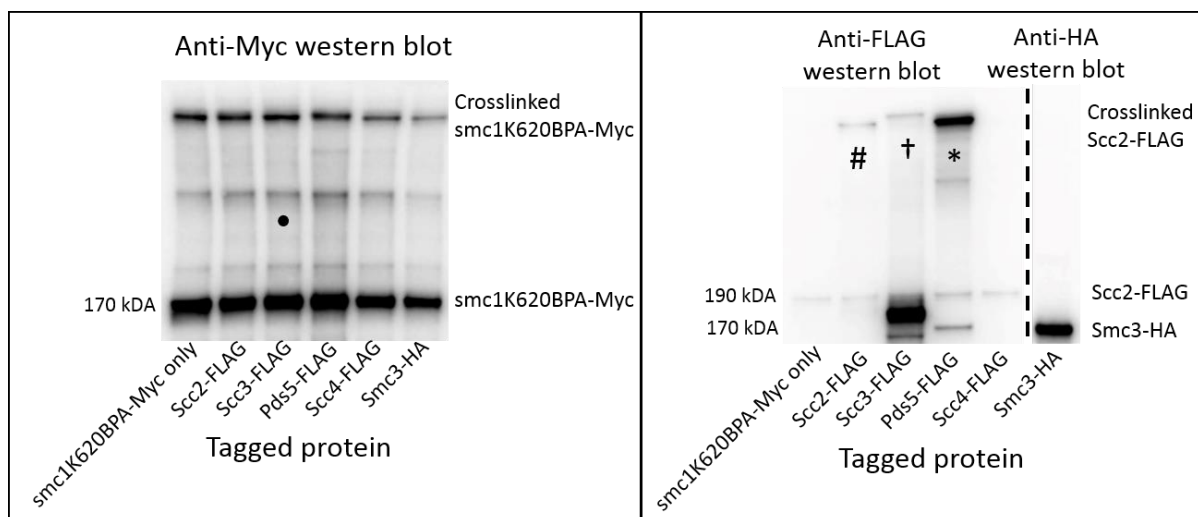


Figure 57: Western blots showing crosslink products of smc1K620BPA in strains containing various tagged proteins.

The anti-Myc along with the anti-FLAG and anti-HA western blots, show that smc1K620BPA crosslinks with a number of proteins, but very efficiently with Pds5. This is supported by the fact that in the anti-FLAG western blot, the most intense band marked by “*” contains Pds5-FLAG. Two other crosslinks found are Scc2 and Scc3 marked by “#” and “†” respectively. There is a crosslink band present in every lane which can be found around the marker “•”. This band may contain a smaller protein than Pds5-FLAG as it exists at a lower position, however despite efforts, the identity of this protein was never found in this study. Scc2 is involved with loading processes, and Scc3 is required for stable association with DNA after loading. The presence of these crosslinks support the notion that the hinge may be involved with loading via an opening mechanism. The strains used in this experiment were: 1983, 1969, 1976, 2072, 2079, and 2020.

To find the Smc3 residue which produced the strongest crosslink with Scc2, a screen was performed comparing crosslinks sites in Smc3 (see figure 58).

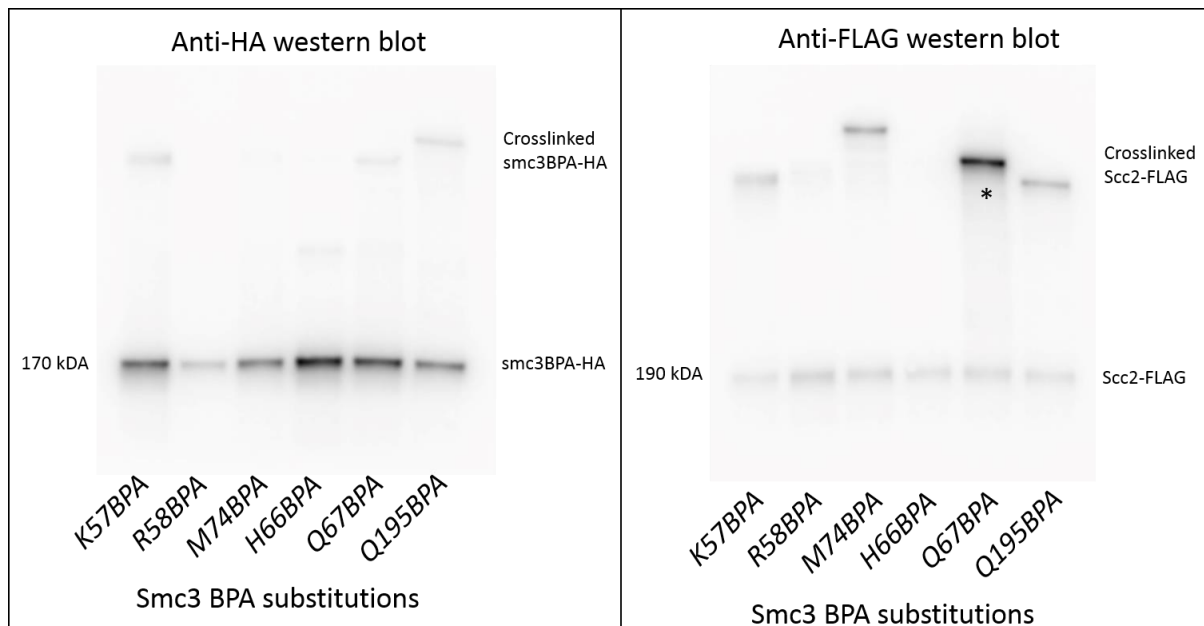


Figure 58: Western blot showing crosslink products of various Smc3 residues that are known to crosslink Scc2 or are possible candidates.

It is very apparent that smc3Q67BPA produces the most efficient crosslinking ability by the much higher intensity crosslink band compared to other residues tested, marked by “*”. The strains used in this experiment were: 1850, 1900, 1854, 1878, 1505, and 1851.

As two of the strongest available crosslinks in the hinge and head domains of cohesin have been found in smc1K620BPA and smc3Q67BPA, TEV cleavage of Scc2 with BPA crosslinking would reveal how Scc2 interacts with these two sites separated at distance. This has been discussed previously in figure 8, regarding how the elbow region must bend in order for shorter proteins such as Pds5 to interact with the head and hinge domain simultaneously. In preparation for the TEV cleavage experiment for

smc3Q67BPA, a test was conducted to examine which proteins smc3Q67BPA crosslinked to (see figure 59). This was performed to identify any non-specific bands that may appear on the TEV cleavage western blot as was done with smc1K620BPA.

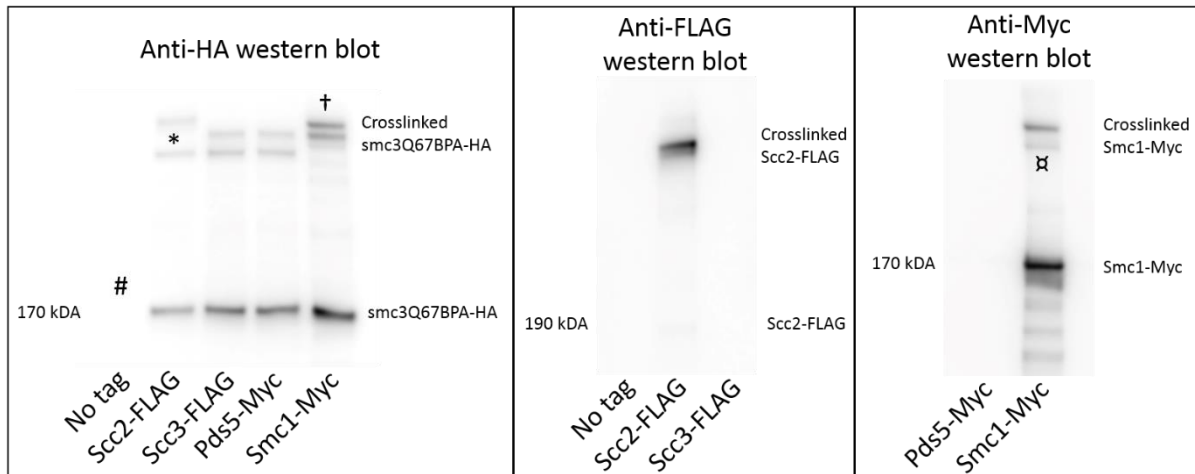


Figure 59: Western blots showing the proteins crosslinked by smc3Q67BPA.

The anti-HA western blot shows that without the HA tag, there is no signal and there are no non-specific bands which allow the binding of the anti-HA antibody, marked by “#”. The next lane shows two crosslink bands, with the marker “*” placed in between. The crosslink band above the marker “*” is upshifted in comparison with the crosslink band in the next adjacent lane. This is likely caused by the FLAG tag of Scc2 and suggests that Scc2 is crosslinked by smc3Q67BPA. The band below the marker “*” likely contains Smc1 as the marker “†” is placed above the upshifted band which is so positioned due to the addition of the Myc tag to Smc1. This suggests that smc3Q67BPA crosslinks to Smc1 and Scc2. The anti-FLAG western blot shows that the crosslink band contains Scc2-FLAG and that Scc3 does not crosslink with smc3Q67BPA, indicated by the lack of crosslink band. The uncrosslinked Scc3-FLAG band is present, albeit only visibly under high contrast. The anti-Myc western blot shows two crosslink

bands, suggesting that smcQ67BPA may crosslink with Smc1 in two different locations, marked by “ α ”. The strains used in this experiment were: 1189, 1505, 1504, 1506, and 1196.

4.3.2.2 BPA crosslinking and TEV cleavage of Scc2 crosslinked to Smc3 and Smc1

With the screening complete, BPA crosslinking with TEV cleavage experiments were conducted on smc3Q67BPA and smc1K620BPA (see figures 60-62).

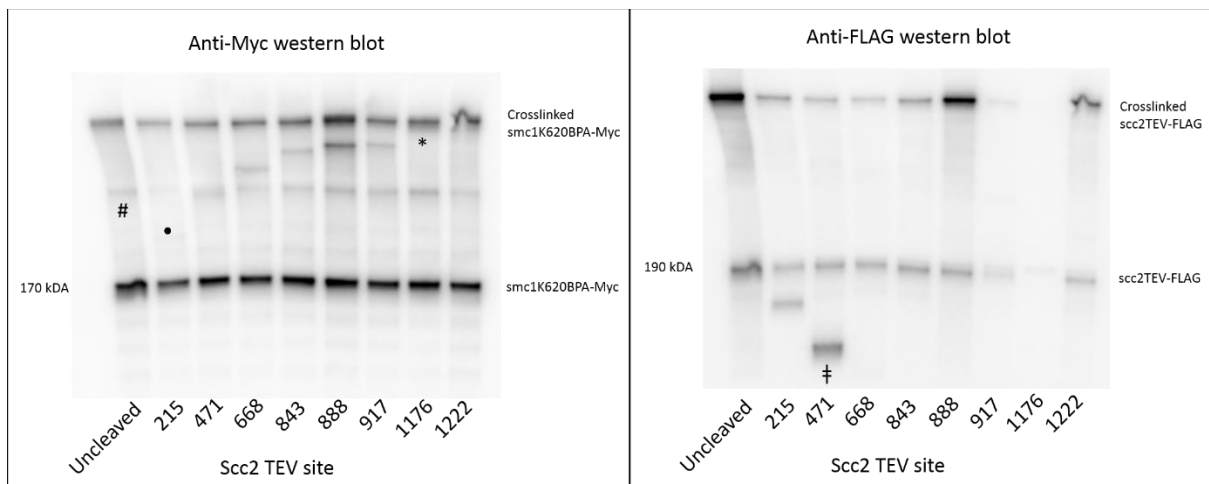


Figure 60: Western blots showing TEV cleavage products of Scc2 crosslinked by smc1K620BPA.

The anti-Myc western blot shows that the crosslink of smc1K620BPA to Scc2 is likely to lie before position 215. This is supported by a series of gradually upshifting bands starting from position 215 and rising consistently all the way to 1222. The “#” marks the position of a non-specific band which is present across all the samples. The “•” marks the position of a low intensity band which is a cleavage product clearly visible at high contrast. The cleavage product of each sample is upshifted, moving from position 215 to 1176 where it merges with the uncleaved crosslink band, marked by “*”. This result would only be possible if the crosslink site was before position 215, as after would cause the series to begin with a smaller downshift from the uncleaved crosslink band. The anti-FLAG western blot shows that the cleavage of uncrosslinked Scc2 is efficient, as the marker “†” shows a cleavage product band. After

scc2TEV471, the cleavage products become too small and are run off the gel during the SDS-PAGE. Downshifted crosslink bands are expected to be visible if the crosslink of smc1K620BPA occurs within the range 217-1222. No downshifted crosslink bands are visible on the blot. This indicates that the crosslink may occur before scc2TEV215 because cleavage at this point and beyond will cause loss of the FLAG tag which is located at the C terminal, rendering the crosslink bands undetectable. The conclusion that can be drawn from these results is that smc1K620BPA may crosslink to Scc2 before position 215. The strains used in this experiment were: 2143, 2144, 2145, 2149, 2153, 2150, 2142, and 2151.

In order to reduce the range further, an additional BPA crosslinking with TEV cleavage experiment was performed with more Scc2 TEV sites closer to the N terminal (see figure 61).

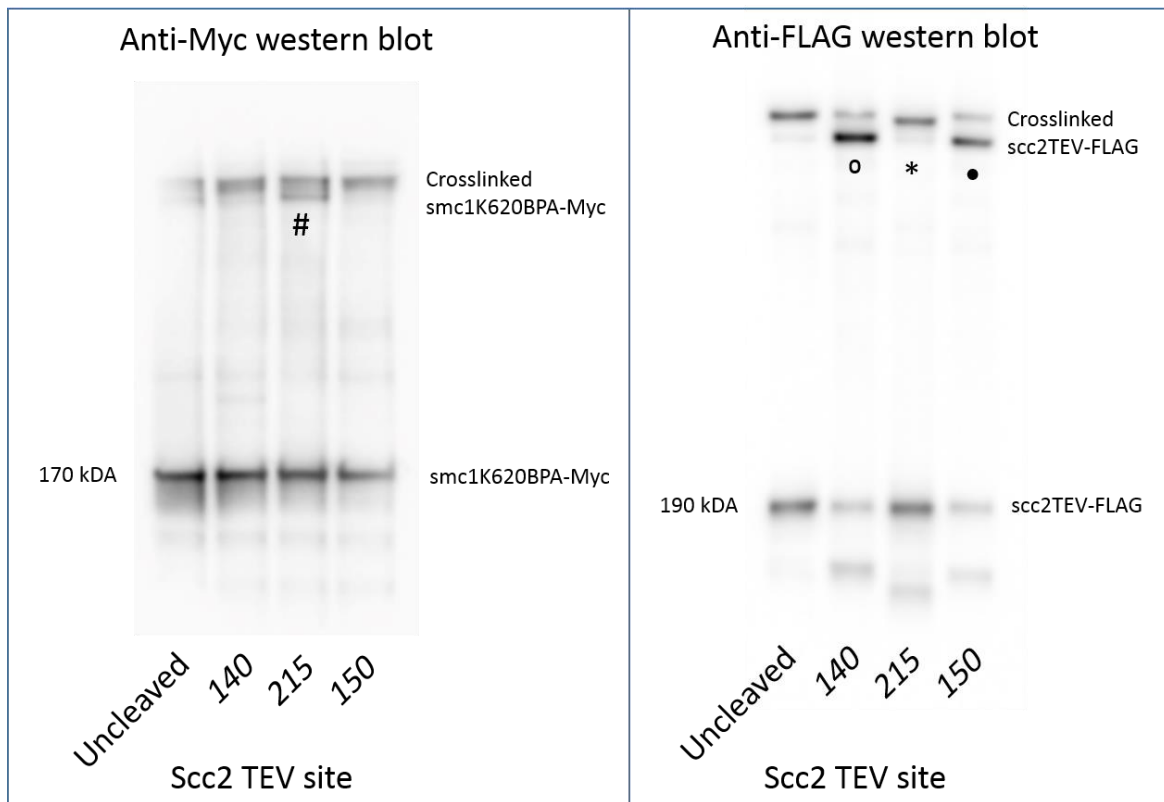


Figure 61: Western blots showing TEV cleavage products of Scc2 crosslinked by smc1K620BPA within a smaller range.

The anti-FLAG western blot shows that the crosslink site of smc1K620BPA occurs between position 150 and 215. This is supported by the presence of a downshifted cleavage product band when testing scc2TEV140 and scc2TEV150, indicated by “o” and “•” respectively. This downshifted band is lost when testing scc2TEV215, indicated by “*”. This is because if the crosslinked protein is cleaved after the crosslink site, the FLAG tag will be lost. The anti-Myc western blot suffers from high background. The predicted band pattern is to see slightly downshifted cleavage products from the uncleaved crosslink band. This is not easily discernible in the cases of scc2TEV140 or 150 but can be seen in scc2TEV215 indicated by “#”. The strains used in this experiment were: 2295, 2296, and 2298.

Following the discovery of the smc1K620BPA crosslink with Scc2 between Scc2 positions 150 and 215, the smc3Q67BPA crosslink TEV cleavage experiment was performed (see figure 62).

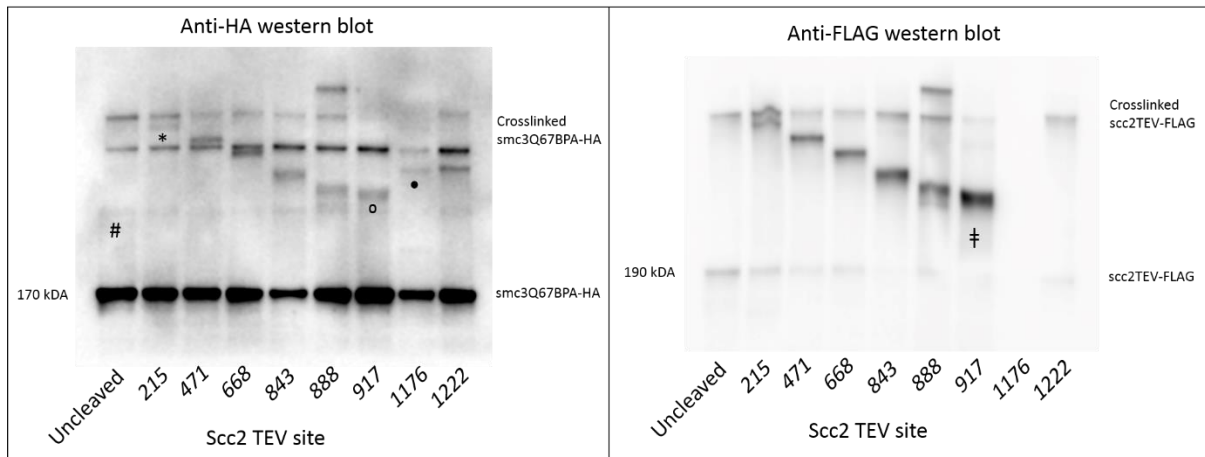


Figure 62: Western blots showing TEV cleavage products of Scc2 crosslinked by smc3Q67BPA.

The anti-HA western blot shows that the crosslink of smcQ67BPA to Scc2 is likely to lie between position 917 and 1176. This is supported by a series of gradually downshifting bands starting from position 215 (marked by “*”) and dropping consistently all the way to 917 (marked by “o”) before the hallmark upshift occurring at 1176 (marked by “•”). The “#” marks the position of a non-specific band which is present across all the samples. The anti-FLAG western blot also shows that the crosslink of smcQ67BPA to Scc2 is likely to lie between position 917 and 1176. This is shown by the gradually downshifting cleavage product bands. As the scc2TEV1176 strain does not contain the FLAG tag due to lethality, it does not provide signal. The cleavage product band is absent from the scc2TEV1222 sample as cleaving after the crosslink site causes the loss of the FLAG tag. The strains used in this experiment were: 2152, 2171, 2172, 2173, 2146, 2152, 2147, 2170, and 2148.

There were no more viable Scc2 TEV cleavage sites found between position 917 and 1176 which could be used to further narrow the crosslink site range. However the TEV cleavage experiments for both residues (smc3Q67BPA and smc1K620BPA) show that Scc2 may be crosslinked in the hinge and head domains of cohesin. Scc2 may therefore connect both regions together as part of the loading processes. It is already known that cohesin may fold at a “elbow” region which may allow this configuration to exist (Bürmann et al., 2019).

Further experiments were planned to map BMOE crosslink sites and create structural models between Scc2 and resolved cohesin sites, however these were not completed due to time constraints of this project. The discovery of the smc3Q67BPA crosslink site to Scc2, did however allow the construction of a crosslink assay to determine the effect of QQ on Scc2 interaction. Figure 63 below contains a map of the crosslink sites found using TEV cleavage.

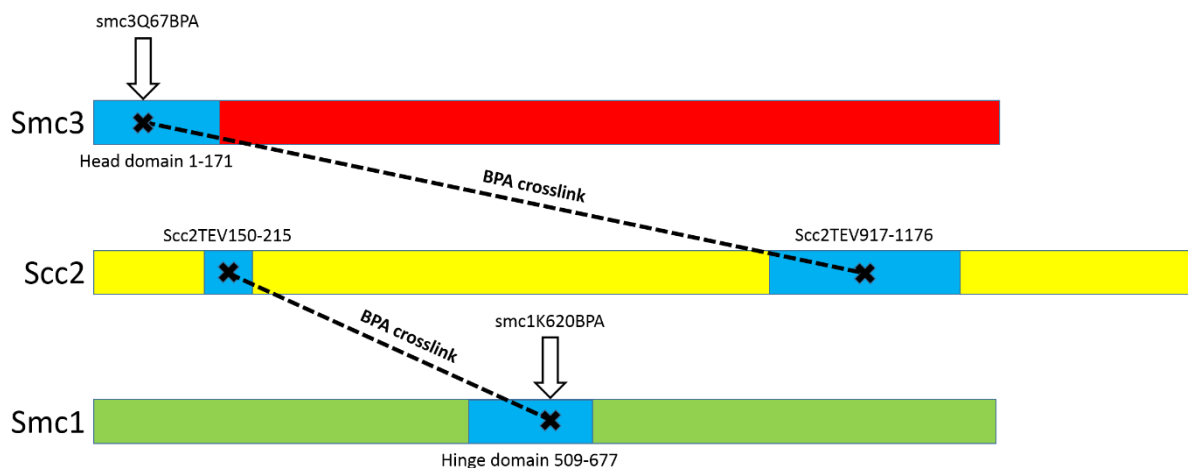


Figure 63: Map of the BPA crosslinking sites between Smc1, Smc3 and Scc2 found by TEV cleavage.

4.3.3 Chapter 3 part 2: Testing the effect of *smc3QQ* and suppressor mutations on cohesin interactions with *Scs2*

The known *Scs2* BPA crosslinking residue, *smc3Q67BPA*, was combined with the QQ mutation, *smc3R1008I*, and *scc2E822K*, *L937F* (*scc2EKLF*) and tested for its crosslinking of *Scs2* (see figure 64). This is because these mutants are all known to restore viability to QQ mutants and therefore may impact *Scs2* interaction.

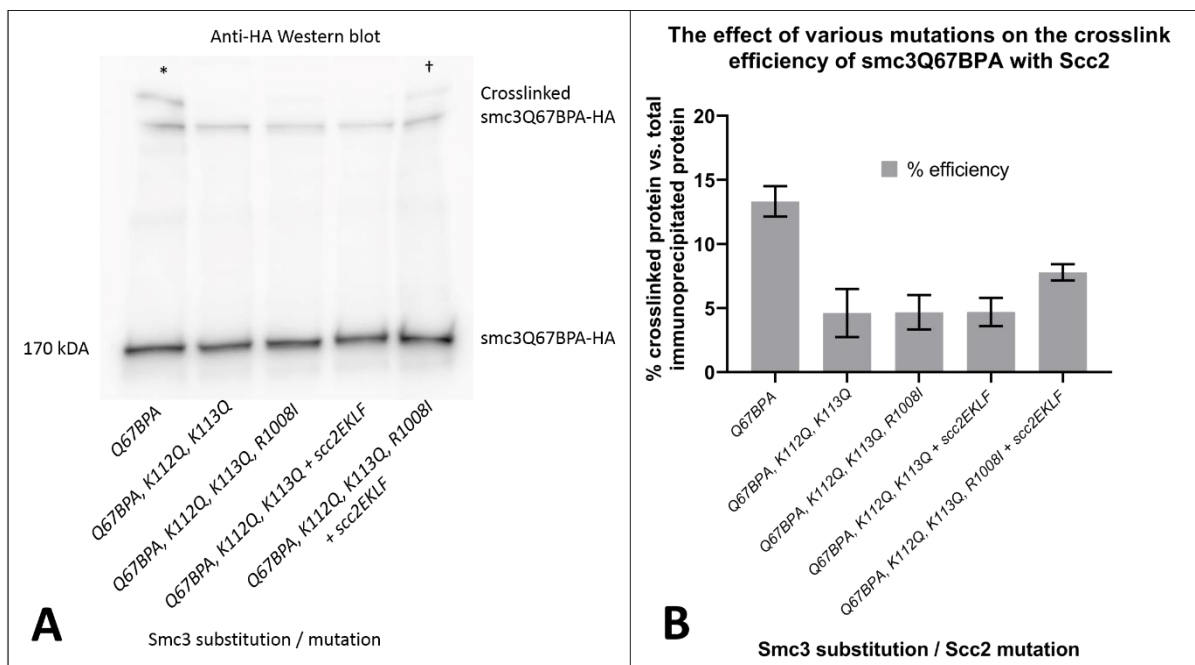


Figure 64: Western blot and a graph showing the effect of various mutations on the crosslinking efficiency of *smc3Q67BPA* with *Scs2*.

(A): The western blot shows that *smc3Q67BPA* produces two crosslink bands. Both bands have been identified; one containing *Smc1* being the lower of the two high molecular weight bands, and the other containing *Scs2* being the upper band as described in figure 59. The introduction of the QQ mutation dramatically reduces the crosslink efficiency of *smc3Q67BPA* to *Scs2*, but not *Smc1*. However, when the QQ mutation is combined with a number of

suppressor mutants, notable for their QQ phenotype rescue, the Scc2 crosslink band is somewhat restored. This can be seen by visual comparison of the band marked with “*” and the bands of the adjacent three lanes, and finally the band marked with “†”. (B): The graph (n=2) pictured right, shows that when the bands are quantified, *smc3Q67BPA* combined with the QQ mutation, *smc3R1008I* and *scc2EKLf* produce more crosslink product than other mutation combinations, but still lower than without the QQ mutation. This result correlates well with the suppressor screen performed in chapter 1 part 1, where the QQ mutation had to be combined with *smc3R1008I* and *scc2EKLf* for a higher level of growth defect rescue. It is likely that the inability to interact with Scc2 at the position *smc3Q67* is a critical function for cohesin loading. Therefore, the data so far suggest that the QQ mutation may reduce Scc2 interaction at the very least in a specific location of the Smc3 head domain. Due to small sample size of n=2, statistical analysis was not possible to establish with significance. The strains used in this experiment were: 1505, 2678, 2679, 2684, and 2685.

Now that the effect of the QQ phenotype can be connected with a reduction of Scc2 interaction, possibly explaining the loading defect of QQ; this may be expanded by testing the effect of QQ on ATP hydrolysis activity of cohesin.

4.3.4 Chapter 3 part 3: Investigating ATP hydrolysis activity of cohesin

It is known that Scc2-Scc4 along with Smc1-Smc3 head engagement, and ATP hydrolysis activity are all required for entrapment of DNA (Ciosk et al., 2000; Murayama and Uhlmann, 2014; Petela et al., 2018). ATP hydrolysis activity assays performed by collaborators from the Nasmyth laboratory (unpublished data) showed that cohesin has strong ATP hydrolysis activity when combined with Scc2 and DNA, but no significant activity without Scc2. Cohesin with only Scc2 has significant activity but much less than when combined with DNA. This assay showed that Scc2 is the major contributing factor for cohesin to produce ATP hydrolysis activity. To investigate the effect of the QQ mutation on ATP hydrolysis activity, another assay from the Nasmyth laboratory was performed, showing that QQ negatively affected ATP hydrolysis activity compared to wild type cohesin in the presence of Scc2 and DNA. Tetramer wild type cohesin when paired with Scc2 had significantly higher ATP hydrolysis activity than tetramer QQ cohesin, which had no significant activity. The addition of DNA greatly improved activity for both wild type and QQ cohesin when combined with Scc2, however QQ cohesin still appeared to have a minor defect compared to wild type. Comparing ATP hydrolysis results of Scc2 with cohesin, wild type produced significant activity, unlike QQ which produced almost none. This could be because QQ cohesin is somewhat defective in Scc2 interaction as found in 4.3.3. This defect likely does not abolish Scc2 interaction completely as strong ATP hydrolysis is still produced by further adding DNA. As this improves overall hydrolysis activity, it is possible that DNA further supplements or stabilises ATP hydrolysis configurations of cohesin.

To test what conditions restores the QQ cohesin defect in Scc2 interaction, another assay was performed with the addition of smc3R1008I and W483R, both were suppressors found in this study. R1008I did not restore activity lost by QQ, however the addition of both smc3R1008I and W483R, showed minor rescue of Scc2-dependent ATP hydrolysis activity which is otherwise completely abrogated by QQ alone. This result showed that QQ suppressor mutations may somewhat restore Scc2 interaction as found in 4.3.3.

QQ paired with scc2EKLF was also tested to find out whether potentially stronger cohesin interaction can restore activity, as scc2EKFL does not significantly increase ATP hydrolysis *in vitro* compared to wild type Scc2 but yet remains associated with cohesin after loading (Petela et al., 2018). The results showed that *scc2EKLF* produced activity better than wild type Scc2 when paired with QQ cohesin. Despite the strong ATP hydrolysis activity produced by QQ paired with scc2EKLF, this combination is still not viable *in vivo*; therefore ATP hydrolysis activity alone cannot explain the lethal effect of QQ. The data so far suggest that a reduction ATP hydrolysis activity may not be the exclusive or even principle mechanism of abrogating entrapment and releasing activity by the QQ mutation.

The last set of ATP hydrolysis tests focused on the role of the coiled coil domains of cohesin on activity. This was achieved by testing truncated forms of cohesin by deleting sections of coiled coil sequence from the genome. Two forms were tested, a slightly reduced form which was named 224 cohesin, and a short form. 224 cohesin possessed higher baseline activity compared to wild type without Scc2 or DNA and

was enhanced when Scc2 and DNA were introduced. Short cohesin also had higher baseline activity than wild type, however the difference in enhancement between adding Scc2 and Scc2 with DNA was less pronounced. This suggests that short coiled coil regions somehow increase ATP hydrolysis activity while reducing the need for further stimulation by DNA. A summary of all the ATP hydrolysis activity assays can be found below in table 5.

Table 5: Factors affecting *in vitro* ATP hydrolysis activity in tabular form.

Cohesin type	DNA	Scc2	scc2EKLF	ATP hydrolysis activity
Trimer	x	x	x	No detectable activity
	✓	x	x	No detectable activity
	x	✓	x	No detectable activity
	✓	✓	x	Very high
Tetramer	x	x	x	No detectable activity
	✓	x	x	No detectable activity
	x	✓	x	Moderate
	✓	✓	x	Very high
	x	x	✓	Very high
QQ Tetramer	x	x	x	No detectable activity
	✓	x	x	No detectable activity
	x	✓	x	No detectable activity
	✓	✓	x	High
	x	x	✓	Very high
QQ, R1008I Tetramer	x	x	x	No detectable activity
	✓	x	x	No detectable activity
	x	✓	x	No detectable activity
	✓	✓	x	Very high
	x	x	✓	Very high
QQ, R1008I, W483R Tetramer	x	x	x	No detectable activity
	✓	x	x	No detectable activity
	x	✓	x	Low
	✓	✓	x	Moderate
224 Trimer	x	x	x	Low
	✓	x	x	Low
	x	✓	x	High
	✓	✓	x	Very High
224 Tetramer	x	x	x	Low
	✓	x	x	Low
	x	✓	x	High
	✓	✓	x	Very High
	x	x	x	No detectable activity

224 QQ Tetramer	✓	x	x	No detectable activity
	x	✓	x	Very low
	✓	✓	x	High
224 QQ Trimer	x	x	x	No detectable activity
	✓	x	x	Very low
	x	✓	x	Very low
Short	✓	✓	x	High
	x	x	x	Moderate
	✓	x	x	Moderate
	x	✓	x	Very high
	✓	✓	x	Very high

ATP hydrolysis activity was rated according to the following scale: very high, high, moderate, low, very low, or no detectable activity. Very high was considered to be the reaction rate of wild type cohesin with Scc2 and DNA. High was considered as no less than 75% of wild type activity. Moderate was considered to be between 50-75% of wild type activity. Low was considered to be 25-50% of wild type activity. Very low was considered to be below 25% of wild type activity.

4.3.5 Chapter 3: Summary

The Scc2 interaction with cohesin at smc3Q67BPA was shown to be significantly impaired by QQ but partially rescued by smc3R1008I and scc2EKLF (figure 64). As this rescue effect correlates with viability data, it is likely that this may be the rescue mechanism of QQ suppressors (table 9). These two results completed the second objective of this study as suppressor mutants and smc3QQ have demonstrated evidence of changes to cohesin configuration and associated protein interactions. The *in vitro* assays performed by the Nasmyth laboratory mentioned in 4.3.4 have found that tetramer cohesin had little endogenous ATP hydrolysis activity compared to when paired with its loader, Scc2. Hydrolysis activity was maximised when both DNA and Scc2 were combined with cohesin. The mutations smc3K112Q, K113Q greatly reduced the resultant ATP hydrolysis activity when compared to wild type only when tested with Scc2 and not DNA. This defect may be partially restored with the addition of suppressor mutants such as *smc3W483R*, *R1008I* and *scc2EKLF*. Also, hydrolysis activity is increased when engineered versions of cohesin with short coiled coil domains were tested (table 5). These results collectively suggest that QQ affects Scc2 interaction and that the coiled coil regulates head domain configuration and ATP hydrolysis activity.

5.0 Discussion

5.1 General discussion

The data collected in this study support a number of mechanisms by which QQ may affect loading activity. These can be summarised into four separate effects:

- A.) QQ causes an interaction defect between Scc2 and cohesin.
- B.) QQ causes a change in the Smc3-Smc1 coiled coil interactions.
- C.) QQ causes a defect in the ATP hydrolysis machinery.
- D.) QQ causes a DNA recruitment defect.

Each effect is supported by some data from this study and will be assessed separately before concluding the most probable mechanism of acetylation-mediated loading abrogation.

Effect A is supported by figure 64 which shows that QQ reduces Scc2 interaction at the site of smc3Q67BPA and is partially restored by QQ suppressor mutations such as smc3R1008I and scc2EKLF. Unpublished results from Dr Bin Hu has shown that smc1E1102BPA also crosslinks with Scc2 but this crosslink site is not affected by the addition of QQ. This suggests that Scc2 interaction is not abolished but rather, becomes locally defective in the vicinity of QQ, sufficient for disrupting loading activity. It is known from Hu and co-workers that QQ cohesin does not accumulate on the chromatin, suggesting some defect which ultimately prevents successful loading (Hu

et al., 2015). There are numerous possible explanations for this result. The first is that a defect in Scc2 binding prevents the facilitation of ATP hydrolysis. This is supported by the abrogation of activity in the ATP hydrolysis assays described in 4.3.4, where Scc2 alone may stimulate activity in wild type cohesin but not QQ cohesin *in vitro*. In addition, if QQ cohesin is indeed defective in binding to Scc2, then it may be possible that *smc3R1008I* is a critical interaction platform for Scc2 interaction which partially corrects the defect caused by QQ. As *smc3R1008I* is required by most of the QQ suppressor mutations found in order to rescue the QQ mutation, this was predicted to increase Scc2 interaction to oppose this effect which was confirmed by the findings in figure 64, showing that *smc3R1008I* is important in partially rescuing the Scc2 interaction defect caused by QQ, restoring crosslinking efficiency. Furthermore, Srinivasan and co-workers found that a temperature sensitive allele of Scc2 caused viability defects at the permissive temperature and required *smc3R1008I* for survival with $\Delta wapl$ (Srinivasan et al., 2019). This can be explained by *smc3R1008I* improving Scc2 interaction to account for the temperature sensitive mutation. ATP hydrolysis assays however, show that R1008I does not significantly restore activity facilitated by Scc2 which is abrogated by QQ. Despite this, *smc3QQ, R1008I* is viable which implies that the reduction of ATP hydrolysis activity is not the principle cause of lethality. Total abrogation of ATP hydrolysis activity by a mutation such as *smc3E1155Q* does confer lethality (Gruber et al., 2006). To reconcile these two facts, the introduction of DNA with Scc2 stimulates strong ATP hydrolysis activity even in QQ cohesin, suggesting that the ATP machinery in QQ suffers only a minor defect as per effect C. Thus, a defect in Scc2 interaction caused by QQ but reparable by DNA interaction is more likely. In support, QQ cohesin with *scc2EKLF* has greater ATP hydrolysis activity than wild type cohesin with wild type Scc2 or *scc2EKLF*, yet is still not viable. QQ cohesin

with smc3R1008I and W483R partially restores ATP hydrolysis activity facilitated by Scc2 but has viability indistinguishable from wild type despite the defect. These results do not support ATP hydrolysis activity with Scc2 being the correlate for viability. As scc2EKLF is not defective in stimulating ATP hydrolysis activity, then there must be another function lost by QQ which is not rescued. This function is proposed to be correctly binding to Scc2 forming a special configuration with cohesin which enables Scc2-Scc4 dependent recruitment to the centromere. Petela and co-workers shows with ChIP sequencing that Scc2 localisation to chromatin is dramatically reduced when S phase is completed without Scc1 expression, suggesting that cohesin is required for Scc2 localisation (Petela et al., 2018). This may be explained by effect D which suggests the DNA association defect of QQ as an explanation for the QQ phenotype. If QQ causes a DNA recruitment defect along with/as a result of Scc2 binding then this would explain smc3R1008I combined with scc2EKLF fully restoring viability. Heidinger-Pauli and co-workers states that overexpression of smc3E1155Q is lethal but this can be rescued by expressing QQ with smc3E1155Q (Heidinger-Pauli et al., 2010). This may be explained by smc3E1155Q cohesin being stuck at the centromere as it cannot be loaded without ATP hydrolysis, but competes with wild type cohesin as shown by ChIP sequencing (Hu et al., 2015). The QQ mutation appears to have a recruitment defect as it does not localise on the chromatin. This ability may prevent the build-up of smc3E1155Q cohesin at the centromere. The potential mechanism of the QQ mediated Scc2 defect may be due to a small change in the flexibility of the head or coiled coil domain of Smc3. The positive charges of lysine may contribute to stabilisation of some kind which are neutralised by acetylation. The evidence for this are the results of an ATP hydrolysis assay which tested truncated forms of cohesin with shorter coiled coil domains. These possessed higher baseline activity without

Scc2 or DNA than wild type cohesin. However when QQ is introduced, this activity falls to levels typical of wild type (table 5). Therefore, the effect of QQ on ATP hydrolysis in truncated cohesin cannot be due to Scc2 or DNA binding defects as these were not present in the assay. The reasoning behind this deduction is that it is known that the coiled coil domains of SMC protein dimers likely form a configuration lined up in parallel (Diebold-Durand et al., 2017; Hons et al., 2016). It is also known that this configuration is reversible and may be regulated by acetylation sites in the coiled coil (Kulemzina et al., 2016). The head configuration of the Smc1-Smc3 dimer is also dependent on the coiled coil configuration as per crosslinking results from figure 52. It is therefore a reasonable suggestion that QQ may produce a conformational change which affects this configuration independently from Scc2 and DNA interaction, supporting effect C. At the very least it is known that this change is probably not as dramatic as claimed by Gligoris and co-workers which were rebutted by the viability results in table 4, however the actual changes may be of a similar premise (Gligoris et al., 2014). These suggested changes by QQ may also cause subsequent changes to the coiled coil configuration as it is linked to the head domain. This change to the coiled coil configuration may be similar to the changes caused by a mutation found by Orgil and co-workers, *smc3L217P* (Orgil et al., 2016). This mutation is lethal, does not support sister chromatid cohesion, inhibits loading of cohesin, and does not interfere with Scc2 co-immunoprecipitation or other cohesin subunits. The mutation does however cause a conformational change detected by state-selective cleavage and improves cleavage in an ATP bound state (Onn et al., 2007; Orgil et al., 2016). This is reflected in figures 54 and 55 where E state relative to J state was increased. The reason this may be significant is because unpublished results from Dr Bin Hu's laboratory show that *smc3E1102BPA* crosslinks with Scc2 and this product formation

is incompatible with E state crosslinks but not J state. This supports the finding that Scc2 dissociates from cohesin immediately after loading and does not translocate (Petela et al., 2018). This also explains why there is a hydrolysis defect without DNA association as described by hydrolysis assays in 4.3.4, as E state would cause Scc2 dissociation before recruitment to DNA. Cell cycle arrest experiments in figure 54 and 55 show that the J state crosslink efficiency is highest during G2 phase. This reflects data in literature which suggests that DNA is captured in the J state within the space enclosed by Scc1 (Chapard et al., 2019; Diebold-Durand et al., 2017; Vazquez Nunez et al., 2019). As Pds5 is necessary for acetylation and protection from Hos1, Pds5 may bind to J state cohesin for this purpose, while binding to E state during releasing processes with Rad61 (Chan et al., 2013).

Scc2 is implicated in the loading of cohesin onto DNA and it is assumed that Scc2 temporarily boosts ATP activity during loading. The way by which this occurs is unclear, however by comparing various results from this study and in the literature from both published and unpublished sources, there is a case for Scc2 mediated configuration change which allows cohesin to transition into the E state. This could be due to these areas around smc3QQ and R1008I being critical for dissociation of the supercoiling in the conversion process to the ring configuration (E state) from the rod form (J state). These sites could be involved in producing an alteration in coiled coil configuration as described by Kulemzina and co-workers which showed that acetylation of lysine residues in the coiled coil were necessary to form a rod conformation of cohesin that is required for cohesin assembly and association with DNA (Kulemzina et al., 2016). None of these exist in the hinge region. A potential explanation is that the multitude of the lysine residues in the coiled coils of Smc1/Smc3

repel each other due to their positive charge and without head engagement, the heterodimers may form any configuration as found by electron microscopy (Haering et al., 2002). Once these lysine residues have been neutralised by acetylation, the heterodimer may then form the rod conformation by other attracting residues in the coiled coil which leads to Scc1 association. The suppressor mutants found do not coincide with the conserved lysine residues in the coiled coil found by Kulemzina and co-workers with the exception of *smc3K180R* which is a very poor suppressor anyway (Kulemzina et al., 2016). These acetylation sites may be conserved and important much like the residues for Scc1 interaction in Smc3 (Gligoris et al., 2014). This study has found that QQ suppressors do in fact affect the configuration of the coiled coil by changing the distances between residues of the Smc1-Smc3 interface as shown by BMOE crosslinking in figure 35 and 36. The QQ suppressor mutants may therefore complement the lysine acetylation system in the coiled coil to promote loading. Scc2 may unzip the supercoiling of the Smc1-Smc3 interface, beginning the interaction in the vicinity of Smc3K112, K113.

If the hinge is the entry gate for cohesin loading onto the chromatid, then Scc2 must somehow assist in the transmission of energy supplied by ATP hydrolysis to the hinge, thereby opening it. As the coiled coil regions of Smc1/Smc3 are very flexible, it is proposed that Scc2 interacts with the coiled coil domains in order to act as a platform for the transmission of energy during loading. This study has shown that Scc2 interacts with cohesin at a minimum of two locations. The N terminal of Scc2 interacts with *smc1K620BPA* and C terminal with *smc3Q67BPA* (figures 60-63). This distance can be bridged by the folding of cohesin (Bürmann et al., 2019). This finding also supports data published by Petela and co-workers showing Scc2 and Pds5 binding is mutually

exclusive as both are now known to bridge the hinge and surrounding head region through the folding of the elbow (Petela et al., 2018). Scc2 may unzip the J state into the E state via conserved interaction sites and secure this configuration via the elbow region, beginning in the vicinity of smc3QQ. If Scc2 interacts in a variety of locations as suggested by Chao and co-workers then Scc2 should be able to perform its role using all the other sites (Chao et al., 2017a). The QQ phenotype and hydrolysis activity assays show that this is probably not the case and QQ is an essential site. Changing the configuration from E to J state in a zip-like manner is consistent with these results as a zip must be operated strictly from the start and not elsewhere. It is hypothesised that the folded elbow conformation is where ATP hydrolysis occurs and transmits energy into either the hinge or Smc3-Scc1 interface, driving loading or releasing activity (Bürmann et al., 2019). Interaction with Pds5 may transmit the energy downward into the Smc3-Scc1 interface by interacting with the coiled coil and hinge while Scc2 transmits energy upwards into the hinge.

As there is evidence supporting each effect, it is likely that the true mechanism of how QQ may abrogate loading processes is a combination of these. Thus, to summarise the data in literature, both published and unpublished, including those obtained from this study; the following proposed model of loading affected by QQ is recapped:

1. Normal loading involves Scc2 interaction with the J state at numerous places of cohesin in the head and coiled coil domains. The complex formed by cohesin and Scc2-Scc4 is an intermediary between E and J state.

2. This intermediary configuration allows effective recruitment of cohesin to DNA where contact further promotes E state formation which allows maximal ATP hydrolysis activity. Cohesin is then loaded topologically onto DNA.
3. The loading process itself briefly involves E state which causes Scc2 to dissociate from cohesin.
4. The QQ mutation prevents loading by causing a small change in cohesin configuration, probably by introducing some local flexibility which destabilises the Scc2 interaction and a further minor impact on Smc1-Smc3 coiled coil interaction.
5. As the nature of the Scc2 interaction with cohesin is changed by QQ, the configuration required for effective recruitment to DNA is impaired, thus loading activity is abrogated. A visual aid to this description can be found in figure 65.

There are a number of questions that have been left unanswered from the results of this study. First of all, the physiological significance of the E and J state is not fully understood. The main issue is that the E and J state crosslinks are not known to absolutely represent a state of cohesin during a function. If it can be proven for example, that the J state represents only cohesin that has been successfully loaded onto the DNA then figures 54 and 55 show that QQ reduces successful loading of cohesin. However, the J state crosslink study only represents cohesin which may have entered the J state position for any reason at all. To improve the assay, crosslink states must be found which only occur during loading or when cohesin is already loaded. Nevertheless, this study has produced an alternative way to study the conformational changes of cohesin that would be difficult to achieve by crystallography analysis.

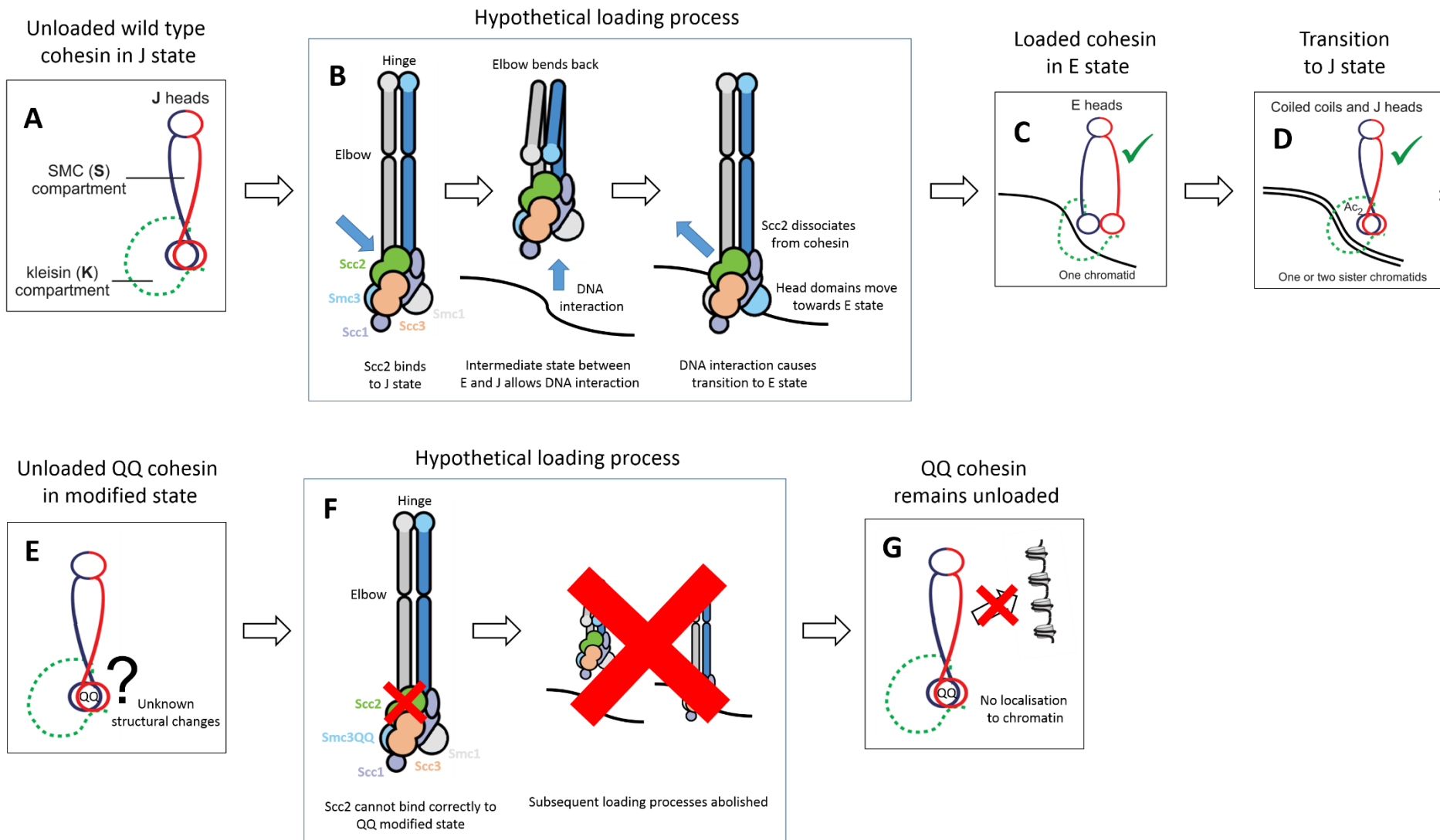


Figure 65: Diagram of the proposed loading mechanism and effect of QQ.

(A): Cohesin exists primarily in J state when unbound to ATP. (B): Scc2 binds to J state cohesin and causes a change in configuration by interacting with the hinge, coiled coil, and head domains simultaneously. This interaction bends the elbow region of cohesin back towards the head domains, causing a change to an intermediate head domain configuration. This intermediate state allows DNA localisation and binding which causes another transition to E state. The transition to E state causes Scc2 to dissociate. (C): DNA is successfully loaded in the kleisin compartment of cohesin (D): Loaded cohesin may transition into J state during the capture of sister chromatids. (E): The QQ mutations of Smc3 may cause a small but significant structural change to cohesin which impairs function. (F): Scc2 cannot bind correctly to QQ cohesin due to the slight structural modification caused by the mutations. This prevents the further proposed steps to the loading process. (G): QQ cohesin cannot be localised to the chromatin because it cannot interact properly with Scc2 which is critical for this process. Diagram adapted from: (Bürmann et al., 2019; Chapard et al., 2019).

5.2 Future topics of research

5.2.1 Resolving Scc2 and Pds5 interaction with cohesin

Scc2 could be crosslinked at multiple sites with cohesin and then electron microscopy could be used to resolve the pre-loading complex as was attempted by Hons and co-workers with Pds5 (Hons et al., 2016). By performing a BMOE crosslink screen as was performed with the Smc1-Smc3 coiled coils in this study, crosslinking Scc2 at many locations could provide the stability required for higher resolutions than the achieved 35 Ångströms using cryogenic electron microscopy. Not only would this reveal the nature of Scc2 interaction, this method may provide the structural support necessary to finally allow the resolution of the cohesin complex in action. Mapping how Scc2 interacts with the ring and rod configuration may also help explain the roles performed after loading which appear to oppose some kind of Rad61-Pds5 independent mechanism found by Srinivasan and co-workers (Srinivasan et al., 2019). Testing how the E and J states are affected by Scc2 BMOE crosslinks would be of great interest along with testing mutants which affect head engagement or hydrolysis.

The same strategy could be used with studying Pds5 as it is already known that Pds5 may traverse the head and hinge domains (Bürmann et al., 2019). Further BMOE crosslink screening could also make electron microscopy work more effectively. Pds5 protects Smc3 against deacetylation from Hos1 (Chan et al., 2013). There is likely to be at least two different interaction configurations that cohesin accommodates with Pds5 because this protection is moderated by Scc1 cleavage (Beckouët et al., 2010).

This supposedly removes Pds5 interaction but Pds5 is still necessary for Rad61-Pds5 mediated dissociation of the Scc1 fragment (Murayama and Uhlmann, 2015). It is possible that like QQ and the smc3Q67BPA crosslinking, the nature of the interaction is changed rather than completely abolished as mentioned in 5.1. Further crosslinking screens could reveal this alternate interaction during the removal of the N terminal Scc1 fragment.

5.2.2 Pre-loading complex

The pre-loading complex is known to contain cohesin and Scc2-Scc4, however other proteins may be involved at the point of loading. Because loading may involve very transient interactions between a multitude of proteins, it has not yet been fully described *in vivo* (Uhlmann, 2016). As per the ATP hydrolysis assay results mentioned in 4.3.4, there appears to be an increase of activity stimulated by DNA when combined with Scc2. This suggest that DNA may further facilitate ATP hydrolysis when presented with cohesin bound to Scc2. This configuration is unknown, however by combining the potential data from experiments outlined in 5.2.1, it may be possible to identify the configuration of cohesin at the point of loading. QQ may then be tested for its effect on Scc2 binding configuration to cohesin and the further change it may have on the DNA binding configuration. This may provide the clearest picture yet of the mechanism behind loading. A strategy to achieve this may involve the use of mini-chromosomes and the hydrolysis mutant *smc3E1155Q*; this mutation is known to accumulate at the site of loading in the centromere as seen by ChIP sequencing (Hu et al., 2015). This accumulation may be caused by stalled loading machinery which is

an ideal target for formaldehyde crosslinking at the point of loading. After native protein extraction and immunoprecipitation, it may be possible to capture and purify the complex. The complex due to its size may prove very difficult to image, however even at low resolutions it is possible to find the general locations of each protein subunit. From this point, mass spectrometry and targeted cleavage may further reveal more detail from cryogenic electron microscopy. The method could also reveal any *in vivo* loading activities of Rad61 as suggested by Murayama and co-workers, identifying any additional proteins that have not been previously found to be involved in loading processes (Murayama and Uhlmann, 2015). When testing QQ cohesin however, the DNA recruitment defect may prevent this strategy from working. To combat this, there is a suitable artificial recruitment system available. More specifically, the Tet-Off system involves introducing tetracycline operons (Tet-O) sequences into the genome of *S. cerevisiae* along with the sequence for the tetracycline repressor (Tet-R) which binds to the Tet operon. The Tet-R can be incorporated into the sequence of Scc4 which is known to interact with DNA, or Scc3. The interaction between Scc4-Tet-R and the Tet-O sequences may occur at the point of loading. Formaldehyde may crosslink the pre-loading complex and the proteins involved may be detected using western blot. This system has been used to study the Smc3-Scc1 interface (Beckouët et al., 2016). The system could be used to examine the minimal requirements of loading, excluding any recruitment machinery in the centromere as the Tet-O/R system allows recruitment in the absence of these.

5.2.3 Future topics of research summary

- Electron microscopy of Scc2 and Pds5 crosslinked with cohesin, and Smc3/Smc1 coiled coil crosslinks to resolve the various interactions that these proteins may have which contribute to loading and releasing processes.
- Identifying the configuration of cohesin at the point of DNA loading using the hydrolysis mutation, smc3E1155Q, along with formaldehyde crosslinking and cryogenic electron microscopy.

6.0 References

Adams, D.E., Shekhtman, E.M., Zechiedrich, E.L., Schmid, M.B., and Cozzarelli, N.R. (1992). The role of topoisomerase IV in partitioning bacterial replicons and the structure of catenated intermediates in DNA replication. *Cell* 71, 277–288.

Arumugam, P., Gruber, S., Tanaka, K., Haering, C.H., Mechtler, K., and Nasmyth, K. (2003). ATP Hydrolysis Is Required for Cohesin's Association with Chromosomes. *Curr. Biol.* 13, 1941–1953.

Barberis, M., De Gioia, L., Ruzzene, M., Sarno, S., Coccetti, P., Fantucci, P., Vanoni, M., and Alberghina, L. (2005). The yeast cyclin-dependent kinase inhibitor Sic1 and mammalian p27 Kip1 are functional homologues with a structurally conserved inhibitory domain. *Biochem. J.* 387, 639–647.

Beckouët, F., Hu, B., Roig, M.B., Sutani, T., Komata, M., Uluocak, P., Katis, V.L., Shirahige, K., and Nasmyth, K. (2010). An Smc3 Acetylation Cycle Is Essential for Establishment of Sister Chromatid Cohesion. *Mol. Cell* 39, 689–699.

Beckouët, F., Srinivasan, M., Roig, M.B., Chan, K.L., Scheinost, J.C., Batty, P., Hu, B., Petela, N., Gligoris, T., Smith, A.C., et al. (2016). Releasing Activity Disengages Cohesin's Smc3/Scc1 Interface in a Process Blocked by Acetylation. *Mol. Cell* 61, 563–574.

Ter Beek, J., Guskov, A., and Slotboom, D.J. (2014). Structural diversity of ABC transporters. *J. Gen. Physiol.* 143, 419–435.

Ben-Shahar, T.R., Heeger, S., Lehane, C., East, P., Flynn, H., Skehel, M., and

Uhlmann, F. (2008). Eco1-dependent cohesin acetylation during establishment of sister chromatid cohesion. *Science* (80-.). 321, 563–566.

Boeke, J.D., Trueheart, J., Natsoulis, G., and Fink, G.R. (1987). [10] 5-Fluoroorotic acid as a selective agent in yeast molecular genetics. *Methods Enzymol.* 154, 164–175.

Borges, V., Lehane, C., Lopez-Serra, L., Flynn, H., Skehel, M., Ben-Shahar, T.R., and Uhlmann, F. (2010). Hos1 Deacetylates Smc3 to Close the Cohesin Acetylation Cycle. *Mol. Cell* 39, 677–688.

Bose, T., and Gerton, J.L. (2010). Cohesinopathies, gene expression, and chromatin organization. *J. Cell Biol.* 189, 201–210.

Bürmann, F., Lee, B.G., Than, T., Sinn, L., O'Reilly, F.J., Yatskevich, S., Rappsilber, J., Hu, B., Nasmyth, K., and Löwe, J. (2019). A folded conformation of MukBEF and cohesin. *Nat. Struct. Mol. Biol.* 26, 227–236.

Çamdere, G., Guacci, V., Stricklin, J., and Koshland, D. (2015). The ATPases of cohesin interface with regulators to modulate cohesin-mediated DNA tethering. *Elife* 4.

Chan, K.L., Roig, M.B., Hu, B., Beckouët, F., Metson, J., and Nasmyth, K. (2012). Cohesin's DNA exit gate is distinct from its entrance gate and is regulated by acetylation. *Cell* 150, 961–974.

Chan, K.L., Gligoris, T., Upcher, W., Kato, Y., Shirahige, K., Nasmyth, K., and Beckouët, F. (2013). Pds5 promotes and protects cohesin acetylation. *Proc. Natl. Acad. Sci. U. S. A.* 110, 13020–13025.

Chao, W.C.H., Murayama, Y., Muñoz, S., Costa, A., Uhlmann, F., and Singleton, M.R. (2015). Structural Studies Reveal the Functional Modularity of the Scc2-Scc4 Cohesin Loader. *Cell Rep.* 12, 719–725.

Chao, W.C.H., Murayama, Y., Muñoz, S., Jones, A.W., Wade, B.O., Purkiss, A.G., Hu, X.W., Borg, A., Snijders, A.P., Uhlmann, F., et al. (2017a). Structure of the cohesin loader Scc2. *Nat. Commun.* 8, 6–13.

Chao, W.C.H., Wade, B.O., Bouchoux, C., Jones, A.W., Purkiss, A.G., Federico, S., O'Reilly, N., Snijders, A.P., Uhlmann, F., and Singleton, M.R. (2017b). Structural basis of Eco1-mediated cohesin acetylation. *Sci. Rep.* 7.

Chapard, C., Jones, R., van Oepen, T., Scheinost, J.C., and Nasmyth, K. (2019). Sister DNA Entrapment between Juxtaposed Smc Heads and Kleisin of the Cohesin Complex. *Mol. Cell* 75, 224-237.e5.

Chen, L.L., Rosa, J.J., Turner, S., and Pepinsky, R.B. (1991). Production of multimeric forms of CD4 through a sugar-based cross-linking strategy. *J. Biol. Chem.* 266, 18237–18243.

Chen, S., Schultz, P.G., and Brock, A. (2007). An Improved System for the Generation and Analysis of Mutant Proteins Containing Unnatural Amino Acids in *Saccharomyces cerevisiae*. *J. Mol. Biol.* 371, 112–122.

Chin, J.W., Martin, A.B., King, D.S., Wang, L., and Schultz, P.G. (2002). Addition of a photocrosslinking amino acid to the genetic code of *Escherichia coli*. *Proc. Natl. Acad. Sci. U. S. A.* 99, 11020–11024.

Choudhary, C., Kumar, C., Gnad, F., Nielsen, M.L., Rehman, M., Walther, T.C., Olsen, J. V., and Mann, M. (2009). Lysine acetylation targets protein complexes and co-

regulates major cellular functions. *Science* (80-.). 325, 834–840.

Chuang, P.T., Albertson, D.G., and Meyer, B.J. (1994). DPY-27: A chromosome condensation protein homolog that regulates *C. elegans* dosage compensation through association with the X chromosome. *Cell* 79, 459–474.

Ciosk, R., Shirayama, M., Shevchenko, A., Tanaka, T., Toth, A., Shevchenko, A., and Nasmyth, K. (2000). Cohesin's binding to chromosomes depends on a separate complex consisting of Scc2 and Scc4 proteins. *Mol. Cell* 5, 243–254.

Cortés-Ledesma, F., and Aguilera, A. (2006). Double-strand breaks arising by replication through a nick are repaired by cohesin-dependent sister-chromatid exchange. *EMBO Rep.* 7, 919–926.

Dadam, P., and Reichert, M. (2009). The ADEPT project: A decade of research and development for robust and flexible process support: Challenges and Achievements. *Comput. Sci. - Res. Dev.* 23, 81–97.

Daniels, P.W., Mukherjee, A., Goldman, A.S., and Hu, B. (2018). A set of novel CRISPR-based integrative vectors for *Saccharomyces cerevisiae*. *Wellcome Open Res.* 3, 72.

Dicarlo, J.E., Norville, J.E., Mali, P., Rios, X., Aach, J., and Church, G.M. (2013). Genome engineering in *Saccharomyces cerevisiae* using CRISPR-Cas systems. *Nucleic Acids Res.* 41, 4336–4343.

DiCarlo, J.E., Chavez, A., Dietz, S.L., Esvelt, K.M., and Church, G.M. (2015). Safeguarding CRISPR-Cas9 gene drives in yeast. *Nat. Biotechnol.* 33, 1250–1255.

Diebold-Durand, M.L., Lee, H., Ruiz Avila, L.B., Noh, H., Shin, H.C., Im, H., Bock, F.P.,

Bürmann, F., Durand, A., Basfeld, A., et al. (2017). Structure of Full-Length SMC and Rearrangements Required for Chromosome Organization. *Mol. Cell* 67, 334-347.e5.

Diederichs, K. (2000). Crystal structure of MalK, the ATPase subunit of the trehalose/maltose ABC transporter of the archaeon *Thermococcus litoralis*. *EMBO J.* 19, 5951–5961.

Eijpe, M., Offenberg, H., Jessberger, R., Revenkova, E., and Heyting, C. (2003). Meiotic cohesin REC8 marks the axial elements of rat synaptonemal complexes before cohesins SMC1 β and SMC3. *J. Cell Biol.* 160, 657–670.

Elbatsh, A.M.O., Haarhuis, J.H.I., Petela, N., Chapard, C., Fish, A., Celie, P.H., Stadnik, M., Ristic, D., Wyman, C., Medema, R.H., et al. (2016). Cohesin Releases DNA through Asymmetric ATPase-Driven Ring Opening. *Mol. Cell* 61, 575–588.

Fernius, J., and Marston, A.L. (2009). Establishment of cohesion at the pericentromere by the Ctf19 kinetochore subcomplex and the replication fork-associated factor, Csm3. *PLoS Genet.* 5.

Forné, I., Ludwigsen, J., Imhof, A., Becker, P.B., and Mueller-Planitz, F. (2012). Probing the conformation of the ISWI ATPase domain with genetically encoded photo-reactive crosslinkers and mass spectrometry. *Mol. Cell. Proteomics* 11, M111.012088.

Foster, D.A., Yellen, P., Xu, L., and Saqcena, M. (2010). Regulation of G1 cell cycle progression: Distinguishing the restriction point from a nutrient-sensing cell growth checkpoint(s). *Genes and Cancer* 1, 1124–1131.

Frew, B.C., Joag, V.R., and Mogridge, J. (2012). Proteolytic processing of Nlrp1b is required for inflammasome activity. *PLoS Pathog.* 8.

Galardy, R.E., Craig, L.C., and Printz, M.P. (1973). Benzophenone triplet: A new photochemical probe of biological ligand-receptor interactions. *Nat. New Biol.* 242, 127–128.

Ganji, M., Shaltiel, I.A., Bisht, S., Kim, E., Kalichava, A., Haering, C.H., and Dekker, C. (2018). Real-time imaging of DNA loop extrusion by condensin. *Science* (80-.). 360, 102–105.

Gaudet, R., and Wiley, D.C. (2001). Structure of the ABC ATPase domain of human TAP1, the transporter associated with antigen processing. *EMBO J.* 20, 4964–4972.

Giron-Monzon, L., Manelyte, L., Ahrends, R., Kirsch, D., Spengler, B., and Friedhoff, P. (2004). Mapping protein-protein interactions between MutL and MutH by cross-linking. *J. Biol. Chem.* 279, 49338–49345.

Gligoris, T.G., Scheinost, J.C., Bürmann, F., Petela, N., Chan, K.L., Uluocak, P., Beckouët, F., Gruber, S., Nasmyth, K., and Löwe, J. (2014). Closing the cohesin ring: Structure and function of its Smc3-kleisin interface. *Science* (80-.). 346, 963–967.

Gruber, S., Haering, C.H., and Nasmyth, K. (2003). Chromosomal cohesin forms a ring. *Cell* 112, 765–777.

Gruber, S., Arumugam, P., Katou, Y., Kuglitsch, D., Helmhart, W., Shirahige, K., and Nasmyth, K. (2006). Evidence that Loading of Cohesin Onto Chromosomes Involves Opening of Its SMC Hinge. *Cell* 127, 523–537.

Guacci, V., Koshland, D., and Strunnikov, A. (1997). A direct link between sister chromatid cohesion and chromosome condensation revealed through the analysis of MCD1 in *S. cerevisiae*. *Cell* 91, 47–57.

Hadjur, S., Williams, L.M., Ryan, N.K., Cobb, B.S., Sexton, T., Fraser, P., Fisher, A.G., and Merckenschlager, M. (2009). Cohesins form chromosomal cis-interactions at the developmentally regulated IFNG locus. *Nature* *460*, 410–413.

Haering, C.H., Löwe, J., Hochwagen, A., and Nasmyth, K. (2002). Molecular Architecture of SMC Proteins and the Yeast Cohesin Complex C-terminal domains forming a head would be part of. *Mol. Cell* *9*, 773–788.

Haering, C.H., Schoffnegger, D., Nishino, T., Helmhart, W., Nasmyth, K., and Löwe, J. (2004). Structure and stability of cohesin's Smc1-kleisin interaction. *Mol. Cell* *15*, 951–964.

Haering, C.H., Farcas, A.M., Arumugam, P., Metson, J., and Nasmyth, K. (2008). The cohesin ring concatenates sister DNA molecules. *Nature* *454*, 297–301.

Hardwick, K.G., Weiss, E., Luca, F.C., Winey, M., and Murray, A.W. (1996). Activation of the budding yeast spindle assembly checkpoint without mitotic spindle disruption. *Science* (80-.). *273*, 953–956.

Hartman, T., Stead, K., Koshland, D., and Guacci, V. (2000). Pds5p is an essential chromosomal protein required for both sister chromatid cohesion and condensation in *Saccharomyces cerevisiae*. *J. Cell Biol.* *151*, 613–626.

Heidinger-Pauli, J.M., Onn, I., and Koshland, D. (2010). Genetic evidence that the acetylation of the Smc3p subunit of cohesin modulates its ATP-bound state to promote cohesion establishment in *Saccharomyces cerevisiae*. *Genetics* *185*, 1249–1256.

Hinshaw, S.M., Makrantoni, V., Kerr, A., Marston, A.L., and Harrison, S.C. (2015). Structural evidence for Scc4-dependent localization of cohesin loading. *Elife* *4*, 1–15.

Hinshaw, S.M., Makrantoni, V., Harrison, S.C., and Marston, A.L. (2017). The Kinetochore Receptor for the Cohesin Loading Complex. *Cell* 171, 72-84.e13.

Hiraga, S., Niki, H., Ogura, T., Ichinose, C., Mori, H., Ezaki, B., and Jaffe, A. (1989). Chromosome partitioning in *Escherichia coli*: Novel mutants producing anucleate cells. *J. Bacteriol.* 171, 1496–1505.

Hirano, T., and Mitchison, T.J. (1994). A heterodimeric coiled-coil protein required for mitotic chromosome condensation in vitro. *Cell* 79, 449–458.

Hirano, T., Kobayashi, R., and Hirano, M. (1997). Condensins, chromosome condensation protein complexes containing XCAP- C, XCAP-E and a *Xenopus* homolog of the *Drosophila* Barren protein. *Cell* 89, 511–521.

Hollenstein, K., Dawson, R.J., and Locher, K.P. (2007). Structure and mechanism of ABC transporter proteins. *Curr. Opin. Struct. Biol.* 17, 412–418.

Holm, C., Goto, T., Wang, J.C., and Botstein, D. (1985). DNA topoisomerase II is required at the time of mitosis in yeast. *Cell* 41, 553–563.

Hons, M.T., Huis Int Veld, P.J., Kaesler, J., Rombaut, P., Schleiffer, A., Herzog, F., Stark, H., and Peters, J.M. (2016). Topology and structure of an engineered human cohesin complex bound to Pds5B. *Nat. Commun.* 7.

Hopp, T.P., Prickett, K.S., Price, V.L., Libby, R.T., March, C.J., Cerretti, D.P., Urdal, D.L., and Conlon, P.J. (1988). A short polypeptide marker sequence useful for recombinant protein identification and purification. *Bio/Technology* 6, 1204–1210.

Horsfield, J.A., Print, C.G., and Mönnich, M. (2012). Diverse developmental disorders from the one ring: Distinct molecular pathways underlie the cohesinopathies. *Front.*

Genet. 3.

Hu, B., Liao, C., Millson, S.H., Mollapour, M., Prodromou, C., Pearl, L.H., Piper, P.W., and Panaretou, B. (2005). Qri2/Nse4, a component of the essential Smc5/6 DNA repair complex. *Mol. Microbiol.* 55, 1735–1750.

Hu, B., Itoh, T., Mishra, A., Katoh, Y., Chan, K.L., Upcher, W., Godlee, C., Roig, M.B., Shirahige, K., and Nasmyth, K. (2011). ATP hydrolysis is required for relocating cohesin from sites occupied by its Scc2/4 loading complex. *Curr. Biol.* 21, 12–24.

Hu, B., Petela, N., Kurze, A., Chan, K.L., Chapard, C., and Nasmyth, K. (2015). Biological chromodynamics: A general method for measuring protein occupancy across the genome by calibrating ChIP-seq. *Nucleic Acids Res.* 43.

Huber, R.G., Kulemzina, I., Ang, K., Chavda, A.P., Suranthran, S., Teh, J.T., Kenanov, D., Liu, G., Rancati, G., Szmyd, R., et al. (2016). Impairing Cohesin Smc1/3 Head Engagement Compensates for the Lack of Eco1 Function. *Structure* 24, 1991–1999.

Ivanov, D., and Nasmyth, K. (2005). A topological interaction between cohesin rings and a circular minichromosome. *Cell* 122, 849–860.

Kanke, M., Tahara, E., Huis in't Veld, P.J., and Nishiyama, T. (2016). Cohesin acetylation and Wapl-Pds5 oppositely regulate translocation of cohesin along DNA. *EMBO J.* 35, 2686–2698.

Klein, F., Mahr, P., Galova, M., Buonomo, S.B.C., Michaelis, C., Nairz, K., and Nasmyth, K. (1999). A central role for cohesins in sister chromatid cohesion, formation of axial elements, and recombination during yeast meiosis. *Cell* 98, 91–103.

Koshland, D., and Hartwell, L.H. (1987). The structure of sister minichromosome DNA

before anaphase in *Saccharomyces cerevisiae*. *Science* (80-). 238, 1713–1716.

Kouprina, N.Y., Pashina, O.B., Nikolaishwili, N.T., Tsouladze, A.M., and Larionov, V.L. (1988). Genetic control of chromosome stability in the yeast *Saccharomyces cerevisiae*. *Yeast* 4, 257–269.

Kousholt, A.N., Menzel, T., and Sørensen, C.S. (2012). Pathways for genome integrity in G2 phase of the cell cycle. *Biomolecules* 2, 579–607.

Kulemzina, I., Ang, K., Zhao, X., Teh, J.T., Verma, V., Suranthran, S., Chavda, A.P., Huber, R.G., Eisenhaber, B., Eisenhaber, F., et al. (2016). A Reversible Association between Smc Coiled Coils Is Regulated by Lysine Acetylation and Is Required for Cohesin Association with the DNA. *Mol. Cell* 63, 1044–1054.

Kurlandzka, A., Rytka, J., Gromadka, R., and Murawski, M. (1995). A new essential gene located on *Saccharomyces cerevisiae* chromosome IX. *Yeast* 11, 885–890.

Ladstätter, S., and Tachibana-Konwalski, K. (2016). A Surveillance Mechanism Ensures Repair of DNA Lesions during Zygotic Reprogramming. *Cell* 167, 1774-1787.e13.

Larionov, V.L., Karpova, T.S., Kouprina, N.Y., and Jouravleva, G.A. (1985). A mutant of *Saccharomyces cerevisiae* with impaired maintenance of centromeric plasmids. *Curr. Genet.* 10, 15–20.

Lee, B.G., Roig, M.B., Jansma, M., Petela, N., Metson, J., Nasmyth, K., and Löwe, J. (2016). Crystal Structure of the Cohesin Gatekeeper Pds5 and in Complex with Kleisin Scc1. *Cell Rep.* 14, 2108–2115.

Lehmann, A.R., Walicka, M., Griffiths, D.J., Murray, J.M., Watts, F.Z., McCready, S.,

and Carr, A.M. (1995). The rad18 gene of *Schizosaccharomyces pombe* defines a new subgroup of the SMC superfamily involved in DNA repair. *Mol. Cell. Biol.* 15, 7067–7080.

Lengronne, A., McIntyre, J., Katou, Y., Kanoh, Y., Hopfner, K.P., Shirahige, K., and Uhlmann, F. (2006). Establishment of Sister Chromatid Cohesion at the *S. cerevisiae* Replication Fork. *Mol. Cell* 23, 787–799.

Li, R., and Murray, A.W. (1991). Feedback control of mitosis in budding yeast. *Cell* 66, 519–531.

Li, S., Yue, Z., and Tanaka, T.U. (2017). Smc3 Deacetylation by Hos1 Facilitates Efficient Dissolution of Sister Chromatid Cohesion during Early Anaphase. *Mol. Cell* 68, 605-614.e4.

Lopez-Serra, L., Lengronne, A., Borges, V., Kelly, G., and Uhlmann, F. (2013). Budding yeast Wapl controls sister chromatid cohesion maintenance and chromosome condensation. *Curr. Biol.* 23, 64–69.

Losada, A. (2014). Cohesin in cancer: Chromosome segregation and beyond. *Nat. Rev. Cancer* 14, 389–393.

Löwe, J., Cordell, S.C., and Van Den Ent, F. (2001). Crystal structure of the SMC head domain: An ABC ATPase with 900 residues antiparallel coiled-coil inserted. *J. Mol. Biol.* 306, 25–35.

Lupas, A., Van Dyke, M., and Stock, J. (1991). Predicting coiled coils from protein sequences. *Science* (80-.). 252, 1162–1164.

Luttinger, A.L., Springer, A.L., and Schmid, M.B. (1991). A cluster of genes that affects

nucleoid segregation in *Salmonella typhimurium*. *New Biol.* 3, 687–697.

Maine, G.T., Sinha, P., and Tye, B.W. (1984). Mutants of *S. cerevisiae* defective in the maintenance of minichromosomes. *Genetics* 106, 365–385.

Malakar, P., and Venkatesh, K. V. (2014). GAL regulon of *Saccharomyces cerevisiae* performs optimally to maximize growth on galactose. *FEMS Yeast Res.* 14, 346–356.

Marko, J.F., De Los Rios, P., Barducci, A., and Gruber, S. (2019). DNA-segment-capture model for loop extrusion by structural maintenance of chromosome (SMC) protein complexes. *Nucleic Acids Res.* 47, 6956–6972.

Mc Intyre, J., Muller, E.G.D., Weitzer, S., Snyderman, B.E., Davis, T.N., and Uhlmann, F. (2007). In vivo analysis of cohesin architecture using FRET in the budding yeast *Saccharomyces cerevisiae*. *EMBO J.* 26, 3783–3793.

McCullum, E.O., Williams, B.A.R., Zhang, J., and Chaput, J.C. (2010). Random mutagenesis by error-prone PCR. *Methods Mol. Biol.* 634, 103–109.

Michaelis, C., Ciosk, R., and Nasmyth, K. (1997). Cohesins: Chromosomal proteins that prevent premature separation of sister chromatids. *Cell* 91, 35–45.

Muñoz, S., Minamino, M., Casas-Delucchi, C.S., Patel, H., and Uhlmann, F. (2019). A Role for Chromatin Remodeling in Cohesin Loading onto Chromosomes. *Mol. Cell* 74, 664-673.e5.

Murayama, Y., and Uhlmann, F. (2014). Biochemical reconstitution of topological DNA binding by the cohesin ring. *Nature* 505, 367–371.

Murayama, Y., and Uhlmann, F. (2015). DNA Entry into and Exit out of the Cohesin Ring by an Interlocking Gate Mechanism. *Cell* 163, 1628–1640.

Nasmyth, K. (2001). Disseminating the Genome: Joining, Resolving, and Separating Sister Chromatids During Mitosis and Meiosis. *Annu. Rev. Genet.* 35, 673–745.

Nasmyth, K., and Haering, C.H. (2009). Cohesin: Its Roles and Mechanisms. *Annu. Rev. Genet.* 43, 525–558.

Nativio, R., Wendt, K.S., Ito, Y., Huddleston, J.E., Uribe-Lewis, S., Woodfine, K., Krueger, C., Reik, W., Peters, J.M., and Murrell, A. (2009). Cohesin is required for higher-order chromatin conformation at the imprinted IGF2-H19 locus. *PLoS Genet.* 5.

Neuwald, A.F., Aravind, L., Spouge, J.L., and Koonin, E. V. (1999). AAA+: A class of chaperone-like ATPases associated with the assembly, operation, and disassembly of protein complexes. *Genome Res.* 9, 27–43.

Niki, H., Jaffe, A., Imamura, R., Ogura, T., and Hiraga, S. (1991). coiled-coil domains involved in chromosome partitioning of *E. coli*. *EMBO J.* 10, 183–193.

Niki, H., Imamura, R., Kitaoka, M., Yamanaka, K., Ogura, T., and Hiraga, S. (1992). *E. coli* MukB protein involved in chromosome partition forms a homodimer with a rod-and-hinge structure having DNA binding and ATP/GTP binding activities. *EMBO J.* 11, 5101–5109.

Oliveira, R.A., Kotadia, S., Tavares, A., Mirkovic, M., Bowlin, K., Eichinger, C.S., Nasmyth, K., and Sullivan, W. (2014). Centromere-Independent Accumulation of Cohesin at Ectopic Heterochromatin Sites Induces Chromosome Stretching during Anaphase. *PLoS Biol.* 12.

Onn, I., Aono, N., Hirano, M., and Hirano, T. (2007). Reconstitution and subunit geometry of human condensin complexes. *EMBO J.* 26, 1024–1034.

Orgil, O., Mor, H., Matityahu, A., and Onn, I. (2016). Identification of a region in the coiled-coil domain of Smc3 that is essential for cohesin activity. *Nucleic Acids Res.* *44*, 6309–6317.

Palecek, J.J., and Gruber, S. (2015). Kite Proteins: A Superfamily of SMC/Kleisin Partners Conserved Across Bacteria, Archaea, and Eukaryotes. *Structure* *23*, 2183–2190.

Palecek, J., Vidot, S., Feng, M., Doherty, A.J., and Lehmann, A.R. (2006). The Smc5-Smc6 DNA repair complex: Bridging of the Smc5-Smc6 heads by the kleisin, nse4, and non-kleisin subunits. *J. Biol. Chem.* *281*, 36952–36959.

Panizza, S., Tanaka, T., Hochwagen, A., Eisenhaber, F., and Nasmyth, K. (2000). Pds5 cooperates with cohesion in maintaining sister chromatid cohesion. *Curr. Biol.* *10*, 1557–1564.

Petela, N.J., Gligoris, T.G., Metson, J., Lee, B.G., Voulgaris, M., Hu, B., Kikuchi, S., Chapard, C., Chen, W., Rajendra, E., et al. (2018). Scc2 Is a Potent Activator of Cohesin's ATPase that Promotes Loading by Binding Scc1 without Pds5. *Mol. Cell* *70*, 1134-1148.e7.

Pham, N.D., Parker, R.B., and Kohler, J.J. (2013). Photocrosslinking approaches to interactome mapping. *Curr. Opin. Chem. Biol.* *17*, 90–101.

Ralser, M., Kuhl, H., Ralser, M., Werber, M., Lehrach, H., Breitenbach, M., and Timmermann, B. (2012). The *Saccharomyces cerevisiae* W303-K6001 cross-platform genome sequence: Insights into ancestry and physiology of a laboratory mutt. *Open Biol.* *2*.

Randall, R.E., Young, D.F., Goswami, K.K., and Russell, W.C. (1987). Isolation and

characterization of monoclonal antibodies to simian virus 5 and their use in revealing antigenic differences between human, canine and simian isolates. *J. Gen. Virol.* 68 (Pt 11), 2769–2780.

Rao, H., Uhlmann, F., Nasmyth, K., and Varshavsky, A. (2001). Degradation of a cohesin subunit by the N-end rule pathway is essential for chromosome stability. *Nature* 410, 955–959.

Rao, S.S.P., Huang, S.C., Glenn St Hilaire, B., Engreitz, J.M., Perez, E.M., Kieffer-Kwon, K.R., Sanborn, A.L., Johnstone, S.E., Bascom, G.D., Bochkov, I.D., et al. (2017). Cohesin Loss Eliminates All Loop Domains. *Cell* 171, 305-320.e24.

Roig, M.B., Löwe, J., Chan, K.L., Beckouët, F., Metson, J., and Nasmyth, K. (2014). Structure and function of cohesin's Scc3/SA regulatory subunit. *FEBS Lett.* 588, 3692–3702.

Rowland, B.D., Roig, M.B., Nishino, T., Kurze, A., Uluocak, P., Mishra, A., Beckouët, F., Underwood, P., Metson, J., Imre, R., et al. (2009). Building Sister Chromatid Cohesion: Smc3 Acetylation Counteracts an Antiestablishment Activity. *Mol. Cell* 33, 763–774.

Saitoh, N., Goldberg, I.G., Wood, E.R., and Earnshaw, W.C. (1994). Scll: An abundant chromosome scaffold protein is a member of a family of putative ATPases with an unusual predicted tertiary structure. *J. Cell Biol.* 127, 303–318.

Salas, P.J.I., Misek, D.E., Vega-Salas, D.E., Gundersen, D., Cereijido, M., and Rodriguez-Boulan, E. (1986). Microtubules and actin filaments are not critically involved in the biogenesis of epithelial cell surface polarity. *J. Cell Biol.* 102, 1853–1867.

Samson, F., Donoso, J.A., Heller-Bettinger, I., Watson, D., and Himes, R.H. (1979). Nocodazole action on tubulin assembly, axonal ultrastructure and fast axoplasmic transport. *J. Pharmacol. Exp. Ther.* 208, 411–417.

Sansbury, B.M., Hewes, A.M., and Kmiec, E.B. (2019). Understanding the diversity of genetic outcomes from CRISPR-Cas generated homology-directed repair. *Commun. Biol.* 2, 1–10.

Schleiffer, A., Kaitna, S., Maurer-Stroh, S., Glotzer, M., Nasmyth, K., and Eisenhaber, F. (2003). Kleisins: A superfamily of bacterial and eukaryotic SMC protein partners. *Mol. Cell* 11, 571–575.

Shero, J.H., Koval, M., Spencer, F., Palmer, R.E., Hieter, P., and Koshland, D. (1991). Analysis of chromosome segregation in *Saccharomyces cerevisiae*. *Methods Enzymol.* 194, 749–773.

Sjögren, C., and Nasmyth, K. (2001). Sister chromatid cohesion is required for postreplicative double-strand break repair in *Saccharomyces cerevisiae*. *Curr. Biol.* 11, 991–995.

Srinivasan, M., Scheinost, J.C., Petela, N.J., Gligoris, T.G., Wissler, M., Ogushi, S., Collier, J.E., Voulgaris, M., Kurze, A., Chan, K.L., et al. (2018). The Cohesin Ring Uses Its Hinge to Organize DNA Using Non-topological as well as Topological Mechanisms. *Cell* 173, 1508-1519.e18.

Srinivasan, M., Petela, N.J., Scheinost, J.C., Collier, J., Voulgaris, M., B Roig, M., Beckouët, F., Hu, B., and Nasmyth, K.A. (2019). Scc2 counteracts a Wapl-independent mechanism that releases cohesin from chromosomes during G1. *Elife* 8.

Strunnikov, A. V., Larionov, V.L., and Koshland, D. (1993). SMC1: An essential yeast

gene encoding a putative head-rod-tail protein is required for nuclear division and defines a new ubiquitous protein family. *J. Cell Biol.* 123, 1635–1648.

Strunnikov, A. V., Hogan, E., and Koshland, D. (1995). SMC2, a *Saccharomyces cerevisiae* gene essential for chromosome segregation and condensation, defines a subgroup within the SMC family. *Genes Dev.* 9, 587–599.

Sutani, T., Kawaguchi, T., Kanno, R., Itoh, T., and Shirahige, K. (2009). Budding Yeast Wpl1(Rad61)-Pds5 Complex Counteracts Sister Chromatid Cohesion-Establishing Reaction. *Curr. Biol.* 19, 492–497.

Takeda, D.Y., and Dutta, A. (2005). DNA replication and progression through S phase. *Oncogene* 24, 2827–2843.

Tanaka, T., Fuchs, J., Loidl, J., and Nasmyth, K. (2000). Cohesin ensures bipolar attachment of microtubules to sister centromeres and resists their precocious separation. *Nat. Cell Biol.* 2, 492–499.

Terakawa, T., Bisht, S., Eeftens, J.M., Dekker, C., Haering, C.H., and Greene, E.C. (2017). The condensin complex is a mechanochemical motor that translocates along DNA. *Science* (80-.). 358, 672–676.

Tóth, A., Ciosk, R., Uhlmann, F., Galova, M., Schleiffer, A., and Nasmyth, K. (1999). Yeast cohesin complex requires a conserved protein, Eco1p(Ctf7), to establish cohesion between sister chromatids during DNA replication. *Genes Dev.* 13, 320–333.

Uhlmann, F. (2016). SMC complexes: From DNA to chromosomes. *Nat. Rev. Mol. Cell Biol.* 17, 399–412.

Uhlmann, F., Lottspelch, F., and Nasmyth, K. (1999). Sister-chromatid separation at

anaphase onset is promoted by cleavage of the cohesin subunit Scc1. *Nature* 400, 37–42.

Uhlmann, F., Wernic, D., Koonin, E. V, and Nasmyth, K. (2000). *Uhlmann_Cell02*. 103, 12.

Ünal, E., Heidinger-Pauli, J.M., Kim, W., Guacci, V., Onn, I., Gygi, S.P., and Koshland, D.E. (2008). A molecular determinant for the establishment of sister chromatid cohesion. *Science* (80-.). 321, 566–569.

Vargas-Trinidad, A.S., Lerena, M.C., Alonso-del-Real, J., Esteve-Zarzoso, B., Mercado, L.A., Mas, A., Querol, A., and Combina, M. (2020). Effect of transient thermal shocks on alcoholic fermentation performance. *Int. J. Food Microbiol.* 312.

Vazquez Nunez, R., Ruiz Avila, L.B., and Gruber, S. (2019). Transient DNA Occupancy of the SMC Interarm Space in Prokaryotic Condensin. *Mol. Cell* 75, 209-223.e6.

Verma, R., Annan, R.S., Huddleston, M.J., Carr, S.A., Reynard, G., and Deshaies, R.J. (1997). Phosphorylation of Sic1p by G1 Cdk required for its degradation and entry into S phase. *Science* (80-.). 278, 455–460.

Vermeulen, K., Van Bockstaele, D.R., and Berneman, Z.N. (2003). The cell cycle: A review of regulation, deregulation and therapeutic targets in cancer. *Cell Prolif.* 36, 131–149.

Watrín, E., Schleiffer, A., Tanaka, K., Eisenhaber, F., Nasmyth, K., and Peters, J.M. (2006). Human Scc4 Is Required for Cohesin Binding to Chromatin, Sister-Chromatid Cohesion, and Mitotic Progression. *Curr. Biol.* 16, 863–874.

Wehr, M.C., Laage, R., Bolz, U., Fischer, T.M., Grünewald, S., Scheek, S., Bach, A., Nave, K.A., and Rossner, M.J. (2006). Monitoring regulated protein-protein interactions using split TEV. *Nat. Methods* 3, 985–993.

Weickert, M.J., and Adhya, S. (1993). The galactose regulon of *Escherichia coli*. *Mol. Microbiol.* 10, 245–251.

Weitzer, S., Lehane, C., and Uhlmann, F. (2003). A Model for ATP Hydrolysis-Dependent Binding of Cohesin to DNA. *Curr. Biol.* 13, 1930–1940.

Wells, J.N., Gligoris, T.G., Nasmyth, K.A., and Marsh, J.A. (2017). Evolution of condensin and cohesin complexes driven by replacement of Kite by Hawk proteins. *Curr. Biol.* 27, R17–R18.

Wilson, D.S., and Keefe, A.D. (2001). Random Mutagenesis by PCR. In *Current Protocols in Molecular Biology*, p.

Yamanaka, K., Ogura, T., Niki, H., and Hiraga, S. (1996). Identification of two new genes, *mukE* and *mukF*, involved in chromosome partitioning in *Escherichia coli*. *Mol. Gen. Genet.* 250, 241–251.

Zegers, M.M.P., Zaal, K.J.M., Van IJzendoorn, S.C.D., Klappe, K., and Hoekstra, D. (1998). Actin filaments and microtubules are involved in different membrane traffic pathways that transport sphingolipids to the apical surface of polarized HepG2 cells. *Mol. Biol. Cell* 9, 1939–1949.

Zhang, N., Kuznetsov, S.G., Sharan, S.K., Li, K., Rao, P.H., and Pati, D. (2008). A handcuff model for the cohesin complex. *J. Cell Biol.* 183, 1019–1031.

Zhang, N., Jiang, Y., Mao, Q., Demeler, B., Tao, Y.J., and Pati, D. (2013).

Characterization of the Interaction between the Cohesin Subunits Rad21 and SA1/2.
PLoS One 8.

Zirkle, R.E. (1970). Ultraviolet-Microbeam Irradiation of Newt-Cell Cytoplasm: Spindle Destruction, False Anaphase, and Delay of True Anaphase. *Radiat. Res.* 41, 516.

7.0 Appendix

7.1 Primer list

Table 6: Primer list. All primers listed are sourced from this study.

Primer name	Sequence 3'-5'
<i>smc3E79KF</i>	CAGTGATGAGTGCCTCGGTAAAAATTGTGTTCCACGATCCAG
<i>smc3E79KR</i>	CTGGATCGTGGAACACAATTTTTACCGAGGCACTCATCACTG
<i>smc3A157VF</i>	ATAGTCGCCTTAACTAATGTCAAGGATAAGGAAAGATTG
<i>smc3A157VR</i>	CAATCTTTCCTTATCCTTGACATTAGTTAAGGCGACTAT
<i>smc3K158EF</i>	GTCGCCTTAACTAATGCCGAGGATAAGGAAAGATTGCAG
<i>smc3K158ER</i>	CTGCAATCTTTCCTTATCCTCGGCATTAGTTAAGGCGAC
<i>smc3D252NF</i>	ATGGAAAGACTGGACGGTAATTATAATAACACGGTATAC
<i>smc3D252NR</i>	GTATACCGTGTTATTATAATTACCGTCCAGTCTTTCCAT
<i>smc3S260PF</i>	AATAACACGGTATACTCTCCCGAACAAATACATCCAGGAG
<i>smc3S260PR</i>	CTCCTGGATGTATTGTTCCGGGAGAGTATACCGTGTTATT
<i>smc3N292SF</i>	GCTTCACTGAAGATCAAAAGTGCGACTGATTTACAACAG
<i>smc3N292SR</i>	CTGTTGTAATCAGTCGCACTTTTTGATCTTCAGTGAAGC
<i>smc3D295GF</i>	GAAGATCAAAAATGCGACTGTTTTACAACAGGCCAAAACACTACG
<i>smc3D295GR</i>	CGTAGTTTTGCCTGTTGTA AACAGTCGCATTTTTGATCTTC
<i>smc3Q298RF</i>	AATGCGACTGATTTACAACGGGCAAAACTACGGGAATCTG
<i>smc3Q298RR</i>	CAGATTCCTGAGTTTTGCCCCGTTGTAATCAGTCGCATT
<i>smc3K300RF</i>	CGACTGATTTACAACAGGCAAGACTACGGGAATCTGAGATTTTC
<i>smc3K300RR</i>	GAAATCTCAGATTCCTGAGTCTTGCCTGTTGTAATCAGTCG
<i>smc3E305GF</i>	GCAAAACTACGGGAATCTGGGATTTCTCAGAAATTAACAAACG
<i>smc3E305GR</i>	CGTTTGTTAATTTCTGAGAAATCCCAGATTCCTGATTTTTGC
<i>smc3L926HF</i>	CGATTACTATTAAGAAGCATGACAATTTCCAAAAAAGTG
<i>smc3L926HR</i>	CACTTTTTTGGAAATTGTCATGCTTCTTTAATAGTAATCG
<i>smc3M937TF</i>	CAAAAAAGTGTTGAAAAAACGACGATTAAGAAAACAACCTTTG
<i>smc3M937TR</i>	CAAAGTTGTTTTCTTAATCGTCGTTTTTTCAACACTTTTTTG
<i>smc3R946GF</i>	GAAAACAACCTTTGGTTACTGGAAGAGAAGAATTACAGCAAAG
<i>smc3R946GR</i>	CTTTGCTGTAATCTTCTCTTCCAGTAACCAAAGTTGTTTTTC
<i>smc3N982DF</i>	CAGCTATTACAAAGACTGGATGATATGAACACAGAGATTTTC
<i>smc3N982DR</i>	GAAATCTCTGTGTTTCATATCATCCAGTCTTTGTAATAGCTG
<i>smc3E1124KF</i>	CAAAACGAACAACCTGCATGTTAAACAGCTCTCAGGTGGTCAG
<i>smc3E1124KR</i>	CTGACCACCTGAGAGCTGTTTAAACATGCAGTTGTTCCGTTTTG
<i>smc3V1133IF</i>	CTCAGGTGGTCAGAAGACTATATGTGCCATTGCTTTGATTCTG
<i>smc3V1133IR</i>	CAGAATCAAAGCAATGGCACATATAGTCTTCTGACCACCTGAG
<i>smc3Q1143RF</i>	GCTTTGATTCTGGCAATCCGAATGGTTGACCCTGCTTCC
<i>smc3Q1143RR</i>	GGAAGCAGGGTCAACCATTCCGATTGCCAGAATCAAAGC
<i>smc3S1176PF</i>	CTACACTTCTAAAAGAAGCTGCCAAAAAATGCCAGTTTATTTG
<i>smc3S1176PR</i>	CAAATAAACTGGGCATTTTTTTGGCAGTTCTTTTAGAAGTGTAG
<i>smc3R1187GF</i>	GTTTATTTGTACGACGTTCCGGAACAGATATGTTGCAAGTTG
<i>smc3R1187GR</i>	CAACTTGCAACATATCTGTTCCGAACGTCGTACAAATAAAC

<i>smc3C1183SF</i>	CAAAAAATGCCAGTTTATTTCTACGACGTTCCAGAACAGATATG
<i>smc3C1183SR</i>	CATATCTGTTCTGAACGTCGTAGAAATAAACTGGGCATTTTTTG
<i>smc3L965FF</i>	CTTCTGCCAGAGGATGCTTTTGTAATGATTTTAGCGAC
<i>smc3L965FR</i>	GTCGCTAAAATCATTACAAAAGCATCCTCTGGCAGAAG
<i>smc3D975EF</i>	GATTTTAGCGACATCACAAGTGAACAGCTATTACAAAGACTG
<i>smc3D975ER</i>	CAGTCTTTGTAATAGCTGTTCACTTGTGATGTCGCTAAAATC
<i>smc3N985SF</i>	CAAAGACTGAATGATATGAGCACAGAGATTTCTGGTTTG
<i>smc3N985SR</i>	CAAACCAGAAATCTCTGTGCTCATATCATTCAAGTCTTTG
<i>smc3Q67TAGF</i>	GAAAGGCAAGGGCTTATCCACTAGGGTTCTGGTGGTTCAGTG
<i>smc3Q67TAGR</i>	CACTGAACCACCAGAACCCTAGTGGATAAGCCCTTGCCTTTC
<i>smc3I1008RF</i>	CTTCAAAAAGTTTAAACGAAAGACGCAAAGACCTTGC GGAGAG
<i>smc3I1008RR</i>	CTCTCCGCAAGGTCTTTGCGTCTTTGTTAAACTTTTTGAAG
<i>smc3N156DF</i>	GTAANAATAGTCGCCTTAACTGATGCCAAGGATAAGGAAAG
<i>smc3N156DR</i>	CTTTCCTTATCCTTGGCATCAGTTAAGGCGACTATTTTAC
<i>smc3K180RF</i>	CATTTGAAGTAAAATTGAGAGCTTCATTGAAAAAATG
<i>smc3K180RR</i>	CATTTTTTTCAATGAAGCTCTCAATTTTACTTCAAATG
<i>smc3T233AF</i>	CAGAAAGATCTACCAGTTCGCATTGTATGATCGAGAATTAATG
<i>smc3T233AR</i>	CATTTAATTCTCGATCATACAATGCGAACTGGTAGATCTTTCTG
<i>smc3R248GF</i>	GTTATCAATCAAATGGAAGGACTGGACGGTGATTATAATAAC
<i>smc3R248GR</i>	GTTATTATAATCACCGTCCAGTCTTCCATTTGATTGATAAC
<i>smc3S259PF</i>	GATTATAATAACACGGTATACCCTTCCGAACAATACATCCAG
<i>smc3S259PR</i>	CTGGATGTATTGTTCCGGAAGGGTATACCCTGTTATTATAATC
<i>smc3V315GF</i>	GAAATTAACAAACGTCAACGGAAAAATAAAGGATGTTCAAC
<i>smc3V315GR</i>	GTTGAACATCCTTTATTTTTCCGTTGACGTTTGTTAATTTTC
<i>smc3Y359HF</i>	CTAAAATTTTACCTAGACACCAAGAACTCACAAAGGAAG
<i>smc3Y359HR</i>	CTTCCTTTGTGAGTCTTGGTGTCTAGGTAAAATTTTAG
<i>smc3V1200GF</i>	GCAGACAAATTTTTCCGTGGTAAGTACGAGAATAAGATTTTC
<i>smc3V1200GR</i>	GAAATCTTATTCTCGTACTTACCACGGAAAAATTTGTCTGC
<i>smc3K1201EF</i>	CAGACAAATTTTTCCGTGTTGAGTACGAGAATAAGATTTCCACG
<i>smc3K1201ER</i>	CGTGGAATCTTATTCTCGTACTCAACACGGAAAAATTTGTCTG
<i>smc3E1203GF</i>	CAAATTTTTCCGTGTTAAGTACGGTAATAAGATTTCCACGG
<i>smc3E1203GR</i>	CCGTGGAATCTTATTACCCTACTTAACACGGAAAAATTTG
<i>smc3K112R,K113QF</i>	CATTAGAAGAACAGTAGGGCTGAGACAAGATGACTATCAATTAATG
<i>smc3K112R,K113QR</i>	CATTTAATTGATAGTCATCTTGTCTCAGCCCTACTGTTCTTCTAATG
<i>smc3K112Q,K113RF</i>	GAAGAACAGTAGGGCTGCAAAGAGATGACTATCAATTAATG
<i>smc3K112Q,K113RR</i>	CATTTAATTGATAGTCATCTCTTTGCAGCCCTACTGTTCTTC
<i>smc3W483RF</i>	GACTCTCGTAAGGAATTGAGGAGAAAGGAGCAAAAATTAC
<i>smc3W483RR</i>	GTAATTTTTGCTCCTTTCTCCTCAATTCTTACGAGTGTC
<i>smc3Q195TAGF</i>	CAGAGCAGAAAAAGATTTAGATTAACAAGGAAATG
<i>smc3Q195TAGR</i>	CATTTCTTGTTAATCTAAATCTTTTTCTGCTCTG
<i>smc3E199TAGF</i>	GATTCAAATTAACAAGTAGATGGGTGAACTAAACTC
<i>smc3E199TAGR</i>	GAGTTTAGTTCACCCATCTACTTGTTAATTTGAATC
<i>smc3E202TAGF</i>	CAAATTAACAAGGAAATGGGTTAGCTAAACTCTAAATTGAGTG
<i>smc3E202TAGR</i>	CACTCAATTTAGAGTTTAGCTAACCCATTTCTTGTTAATTTG
<i>smc3F999TAGF</i>	GAATGTAACAAGAGAGCTTAGGAAAACCTCAAAAAGTTTAAC
<i>smc3F999TAGR</i>	GTTAAACTTTTTGAAGTTTTCCCTAAGCTCTTGTTTACATTC
<i>smc3F1002TAGF</i>	CAAGAGAGCTTTTGAAAAGTAAAGTTTAAACGAAAGAC
<i>smc3F1002TAGR</i>	GTCTTTCGTTAAACTTTTTCTAGTTTTCAAAGCTCTCTTG
<i>smc3K57TAGF</i>	GACGATTACTCTAATCTTTAGAGGGAAGAAAGGCAAGGG
<i>smc3K57TAGR</i>	CCCTTGCCTTTCTCCCTCTAAAGATTAGAGTAATCGTC
<i>smc3R61TAGF</i>	AATCTTAAGAGGGAAGAATAGCAAGGGCTTATCCACCAAG
<i>smc3R61TAGR</i>	CTTGGTGGATAAGCCCTTGCTATTCTTCCCTCTTAAGATT

<i>smc3M74TAGF</i>	GGTTCTGGTGGTTCAGTGTAGAGTGCCTCGGTAGAAATTG
<i>smc3M74TAGR</i>	CAATTTCTACCGAGGCACTCTACACTGAACCACCAGAACC
<i>smc3G110TAGF</i>	GACCATTAGAAGAACAGTATAGCTGAAGAAGGATGACTATC
<i>smc3G110TAGR</i>	GATAGTCATCCTTCTTCAGCTATACTGTTCTTCTAATGGTC
<i>smc3L111TAGF</i>	CATTAGAAGAACAGTAGGGTAGAAGAAGGATGACTATCAA
<i>smc3L111TAGR</i>	TTGATAGTCATCCTTCTTCTACCCTACTGTTCTTCTAATG
<i>smc3Q117TAGF</i>	CTGAAGAAGGATGACTATTAGTTAAATGACAGAAACGTG
<i>smc3Q117TAGR</i>	CACGTTTCTGTCATTAACTAATAGTCATCCTTCTTCAG
<i>smc3H66TAGF</i>	GAAAGGCAAGGGCTTATCTAGCAAGGTTCTGGTGGTTCAG
<i>smc3H66TAGR</i>	CTGAACCACCAGAACCTTGCTAGATAAGCCCTTGCCCTTC
<i>smc1D588YF</i>	CTGCATCTTTCATACCACTATACACAATTGAGACAGAGTTAC
<i>smc1D588YR</i>	GTA ACTCTGTCTCAATTGTGTATAGTGGTATGAAAGATGCAG
<i>smc1E562TAGR</i>	CTTTGATTCCGTCATTGTATAGAATTTAACCGTAGCTCAAG
<i>smc1E562TAGF</i>	CTTGAGCTACGGTTAAATTCTATACAATGACGGAATCAAAG
<i>smc1T565TAGF</i>	CGTCATTGTAGAAAATTTATAGGTAGCTCAAGAATGCATTG
<i>smc1T565TAGR</i>	CAATGCATTCTTGAGCTACCTATAAATTTTCTACAATGACG
<i>smc1K620TAGF</i>	CTACGAGCCGGAATATGAATAGGCGATGCAATATGTGTGTG
<i>smc1K620TAGR</i>	CACACACATATTGCATCGCCTATTCATATTCCGGCTCGTAG
<i>smc1E591TAGF</i>	CATACCACTAGACACAATTTAGACAGAGTTACCTACATTATC
<i>smc1E591TAGR</i>	GATAATGTAGGTA ACTCTGTCTAAATTGTGTCTAGTGGTATG
<i>smc1T592TAGF</i>	CCACTAGACACAATTGAGTAGGAGTTACCTACATTATCATTG
<i>smc1T592TAGR</i>	CAATGATAATGTAGGTA ACTCCTACTCAATTGTGTCTAGTGG
<i>smc1E593TAGF</i>	CTAGACACAATTGAGACATAGTTACCTACATTATCATTG
<i>smc1E593TAGR</i>	CAATGATAATGTAGGTA ACTATGTCTCAATTGTGTCTAG
<i>scc2TEV843F</i>	GATATTAAGGTACATGAAGGTACCGGATCCGTATTGGACCAGCCC GAAAAG
<i>scc2TEV843R</i>	CTTTTCGGGCTGGTCCAATACGGATCCGGTACCTTCATGTACCTTTA ATATC
<i>scc2TEV888F</i>	CTTTTATCTCCTAAACAAAGAAGGTACCGGATCCGCGCATTCAAAG AAGCATA C
<i>scc2TEV888R</i>	GTATGCTTCTTTTGAATGCGCGGATCCGGTACCTTCTTTGTTTAGGA GATAAAAG
<i>scc2TEV917F</i>	CAAAAAATTGTCGAGCTCAACGGTACCGGATCCTCAGATGACACAA ATGAAAAG
<i>scc2TEV917R</i>	CTTTTCATTTGTGTCATCTGAGGATCCGGTACCGTTGAGCTCGACAA TTTTTTG
<i>smc3R58TAGF</i>	GATTACTCTAATCTTAAAGTAGGAAGAAAGGCAAGGGCTT
<i>smc3R58TAGR</i>	AAGCCCTTGCCCTTCTTCTACTTAAAGATTAGAGTAATC
<i>scc2TEV843F2</i>	GATATTAAGGTACATGAAGCTAGCGCATGCGTATTGGACCAGCCC GAAAAG
<i>scc2TEV843R2</i>	CTTTTCGGGCTGGTCCAATACGCATGCGCTAGCTTCATGTACCTTTA ATATC
<i>scc2TEV888F2</i>	CTTTTATCTCCTAAACAAAGAAGCTAGCGCATGCGCGCATTCAAAG AAGCATA C
<i>scc2TEV888R2</i>	GTATGCTTCTTTTGAATGCGCGCATGCGCTAGCTTCTTTGTTTAGGA GATAAAAG
<i>scc2TEV917F2</i>	CAAAAAATTGTCGAGCTCAACGCTAGCGCATGCTCAGATGACACAA ATGAAAAG
<i>scc2TEV917R2</i>	CTTTTCATTTGTGTCATCTGAGCATGCGCTAGCGTTGAGCTCGACAA TTTTTTG
<i>scc2TEV1244F</i>	GATTTTGAAATTTGGTTACACAGCTAGCGCATGCAATCCCTCTCATT CAATTCCAAC
<i>scc2TEV1244R</i>	GTTGGAATTGAATGAGAGGGATTGCATGCGCTAGCTGTGTAACCAA ATTTCAAATC
<i>scc2TEV1222F</i>	CTCCA ACTATGTCTCCTAGCTAGCGCATGCCGTGATCTAAAGAATTC TC

<i>scc2TEV1222R</i>	GAGAATTCTTTAGATCACGGCATGCGCTAGCTAGGAGACATAGTTG GAG
<i>scc2TEV1181F</i>	CACTGGCGTTAATAGCACTGCTAGCGCATGCTCGAACTCCATTTTGA AAAAG
<i>scc2TEV1181R</i>	CTTTTTCAAATGGAGTTCGAGCATGCGCTAGCAGTGCTATTAACGC CAGTG
<i>smc3Q195TAGE199A F</i>	GATTTAGATTAACAAGGCTATGGGTGAACTAAAC
<i>smc3Q195TAGE199A R</i>	GTTTAGTTCACCCATAGCCTTGTTAATCTAAATC
<i>smc3Q195TAGE199Y F</i>	GATTTAGATTAACAAGTACATGGGTGAACTAAAC
<i>smc3Q195TAGE199Y R</i>	GTTTAGTTCACCCATGTACTTGTTAATCTAAATC
<i>smc3E202TAGE199A F</i>	GATTCAAATTAACAAGGCTATGGGTAGCTAAAC
<i>smc3E202TAGE199A R</i>	GTTTAGCTAACCCATAGCCTTGTTAATTTGAATC
<i>smc3E202TAGE199Y F</i>	GATTCAAATTAACAAGTACATGGGTAGCTAAAC
<i>smc3E202TAGE199Y R</i>	GTTTAGCTAACCCATGTACTTGTTAATTTGAATC
<i>smc3E202CF</i>	CAAATTAACAAGGAAATGGGTGTCTAAACTCTAAATTGAGTG
<i>smc3E202CR</i>	CACTCAATTTAGAGTTTAGACAACCCATTTCTTGTTAATTTG
<i>smc3E213CF</i>	ATTGAGTGAATGGAACAGTGTCGTAAGGAATTAGAGAAATAC
<i>smc3E213CR</i>	GTATTTCTCTAATTCCTTACGACACTGTTCCATTTCACTCAAT
<i>smc3Q212CF</i>	CTAAATTGAGTGAATGGAATGTGAACGTAAGGAATTAGAG
<i>smc3Q212CR</i>	CTCTAATTCCTTACGTTACATTCCATTTCACTCAATTTAG
<i>smc3Q195CF</i>	GAAACAGAGCAGAAAAAGATTTGTATTAACAAGGAAATGGGTG
<i>smc1G152CF</i>	AATTTTCTAGTGTTCCAGTGTGATGTTGAGCAAATTG
<i>smc1G152CR</i>	CAATTTGCTCAACATCACACTGGAACACTAGAAAATT
<i>smc1A159CF</i>	GATGTTGAGCAAATTGCATGTCAATCTCCCGTAGAATTATC
<i>smc1A159CR</i>	GATAATTCTACGGGAGATTGACATGCAATTTGCTCAACATC
<i>smc3E188CF</i>	CTTCATTGAAAAAATGGAGGTACAGAGCAGAAAAAGATTC
<i>smc3E188CR</i>	GAATCTTTTTCTGCTCTGTACACTCCATTTTTTCAATGAAG
<i>smc3K185CR</i>	ATTGAAAGCTTCATTGAAATGTATGGAGGAAACAGAGCAG
<i>smc3K185CF</i>	CTGCTCTGTTTCCTCCATACATTTCAATGAAGCTTTCAAT
<i>smc1K191CF</i>	GTTGAAGGAAAAGATTGAGTGTTAAGCAAATCTGCAACCG
<i>smc1K191CR</i>	CGGTTGCAGATTTGCTTAAACACTCAATCTTTTCCTTCAAC
<i>smc1K188CF</i>	GTATGAAGAGTTGAAGGAATGTATTGAGAAATTAAGCAAATC
<i>smc1K188CR</i>	GATTTGCTTAATTTCTCAATACATTCCTTCAACTCTTCATAC
<i>smc1E185CF</i>	CAATACAAAAAGGAGTATGAATGTTTGAAGGAAAAGATTGAG
<i>smc1E185CR</i>	CTCAATCTTTTCCTTCAAACATTCATACTCCTTTTTGTATTG
<i>smc1K180CF</i>	GGTTCTATCCAATACAAATGTGAGTATGAAGAGTTGAAG
<i>smc1K180CR</i>	CTTCAACTCTTCATACTCACATTTGTATTGGATAGAACC
<i>smc3K184CR</i>	GTAAAATTGAAAGCTTCATTGTGTAAAATGGAGGAAACAGAG
<i>smc3K184CF</i>	CTCTGTTTCCTCCATTTTACACAATGAAGCTTTCAATTTTAC
<i>smc3K160CF</i>	CTTAACATAATGCCAAGGATTGTGAAAGATTGCAGTTATTG
<i>smc3K160CR</i>	CAATAACTGCAATCTTTACAATCCTTGGCATTAGTTAAG
<i>smc3V152CF</i>	GTACCACAAGGTAATAATGTGCCTTAACTAATGCCAAG
<i>smc3V152CR</i>	CTTGGCATTAGTTAAGGCACATATTTTACCTTGTTGGTAC
<i>smc3G1128CF</i>	GCATGTTGAACAGCTCTCATGTGGTCAGAAGACTGTATG
<i>smc3G1128CR</i>	CATACAGTCTTCTGACCACATGAGAGCTGTTCAACATGC
<i>smc1S161CF</i>	GAGCAAATTGCAGCACAAATGTCCCGTAGAATTATCAAG
<i>smc1S161CR</i>	CTTGATAATTCTACGGGACATTGTGCTGCAATTTGCTC

<i>smc1outF</i>	ACGTTAAGAAGTTGATTCTGCTG
<i>smc1outF2</i>	ATCCCGTAAACTCCTCGTCGTCG
<i>smc1outF3</i>	TTGTCATGATAAACACGTACGG
<i>smc1seq1</i>	GGAAAACTGTCTCCTATAAGG
<i>smc1seq2</i>	CGGATTTACGGCTCATAAAGG
<i>smc1seq3</i>	CTGAACGTTTGCACGAGCTG
<i>smc1seq4</i>	AATCGATGAACCTTCCAACGG
<i>smc1seq5</i>	ATGAAAATCGGATCAATAGAG
<i>smc1seq6</i>	GCTTTGGAGAGATACGACGAG
<i>smc1seq7</i>	GGACGCAGCCCTAGACATTA
<i>smc1seq8</i>	CTTGGCAGTGTCTACCATCTTAG
<i>smc1seqR1</i>	ATATGTCTTCAATTCTCCATGG
<i>smc1seqR2</i>	TACCTAAGATGGTAGACACTG
<i>smc1seqR3</i>	TCTGGTCACCACTTTTAGTTGTG
<i>smc1seqR4</i>	TTTAGTTCAGTTATCTTCGGTTG
<i>smc1seqR5</i>	CCAAAGTTATGATCTTCGACGAG
<i>smc1outR</i>	CCACCACAATTGGGTTACCCTG
<i>smc1outR1</i>	GAGCTCGGTACCGCTAGCTAACG
<i>smc1outR2</i>	CCTGTCACTAACATAATCCAGCG
<i>smc3outF</i>	GACGCGACGCGTTAGGAAATG
<i>smc3outF2</i>	CACTTGCTGGATCCGCAGTCATG
<i>smc3outF3</i>	TTTACAAGACGACCTGCTGG
<i>smc3seq1</i>	GGACATAGTCAGAATGTTGG
<i>smc3seq2</i>	TACTCTTCCGAACAATACATCCAG
<i>smc3seq3</i>	AGTCAATTGCAAATGGATCG
<i>smc3seq4</i>	AATGAATCAAGAAGTCAACAC
<i>smc3seq5</i>	TTTGGTCTACAAGATGAGTTG
<i>smc3seq6</i>	TGAAAGATTAGTTCCAGAGG
<i>smc3seq7</i>	CGACGTTCAGAACAGATATG
<i>smc3seqF9</i>	CTGGTTTGAAGAATGTAAAC
<i>smc3seq10</i>	TACAACCATTGACTCGTTGAATGC
<i>smc3seq11</i>	AACGGCCACTTTGATTATG
<i>smc3outR</i>	AACATTATTGTTTAGTAACAG
<i>smc3R2</i>	GTACTGCTTCCTTAAAGAAGTACG
<i>smc3R3</i>	CGTATCGCGTTCATCCTTTG
<i>smc3R4</i>	GTTTCGTTTGTGCTGGTCAAG
<i>smc3R5</i>	AAGCATCCTCTGGCAGAAG
<i>YlpF</i>	ACATTAACCTATAAAAAATAGGCG
<i>YlpR</i>	CACCGTCATACCGAAACGCGCG
<i>URA3F</i>	CAAAGAAGGTTAATGTGG
<i>URA3R</i>	CGTCATTATAGAAATCATTACGACCG
<i>KanF</i>	GATCTTGCCATCCTATGGAACCTG
<i>KanR</i>	CAATCGATAGATTGTCGCACCTG
<i>M13F</i>	TGTAAAACGACGGCCAGT
<i>M13R</i>	CAGGAAACAGCTATGACC
<i>scc2seq1F</i>	CCAAAACCTCTGCTGAAATTGG
<i>scc2seq1R</i>	TATCAAGATCGTACCGAGCC
<i>scc2seq2F</i>	GAAGAGTATACAAAGGATGCC
<i>scc2seq2R</i>	AACCTGGCAAACCGGTGG
<i>scc2seq3F</i>	GTAGGCTACCAAAGATGAATG
<i>scc2seq3R</i>	CCCAAATCCTGTAAGCTTAAC
<i>scc2seqF5</i>	TCCCTCTCATTCAATTCCAACCTG

<i>scc2outR2</i>	GGTTTGCTATCGTAGCTGAGCCG
<i>smc3K1201TAGF</i>	CAGACAAATTTTTCCGTGTTTAGTACGAGAATAAGATTTCC
<i>smc3K1201TAGR</i>	GGAAATCTTATTCTCGTACTAAACACGGAAAAATTTGTCTG
<i>smc3E1203TAGF</i>	CAAATTTTTCCGTGTTAAGTACTAGAATAAGATTTCCACGG
<i>smc3E1203TAGR</i>	CCGTGGAAATCTTATTCTAGTACTTAACACGGAAAAATTTG
<i>smc3F41LF</i>	CAATGGTTCAGGTAATCGAATCTCTTCGCTGCGATTAGATTTG
<i>smc3F41LR</i>	CAAATCTAATCGCAGCGAAGAGATTTCGATTTACCTGAACCATTG
<i>smc3S54F</i>	GATTTGTTCTTAGTGACGATTACTTTAATCTTAAGAGGGAAGAAAG
<i>smc3S54R</i>	CTTTCTTCCCTCTTAAGATTAAGTAATCGTCACTAAGAACAATC
<i>smc3L111RK112QK113QF</i>	CATTAGAAGAACAGTAGGGCGGCAACAAGATGACTATCAATTAATG
<i>smc3L111RK112QK113QR</i>	CATTTAATTGATAGTCATCTTGTTGCCGCCCTACTGTTCTTCTAATG
<i>smc3K112QK113QQ117RF</i>	CTGCAACAAGATGACTATCGATTAATGACAGAAACGTG
<i>smc3K112QK113QQ117RR</i>	CACGTTTCTGTCAATTAATCGATAGTCATCTTGTTGCAG
<i>smc3G110RK112QK113QR</i>	GACCATTAGAAGAACAGTACGGCTGCAACAAGATGACTATC
<i>smc3G110RK112QK113QF</i>	GATAGTCATCTTGTTGCAGCCGTAAGTCTTCTTCTAATGGTC
<i>smc3E857GF</i>	CTAGAATCCAAGATGTCAGGAGTAGGTGACGCATTTAT
<i>smc3E857GR</i>	ATAAATGCGTCACCTACTCCTGACATCTTGGATTCTAG
<i>smc3Q847RF</i>	GAGTCCAACTTATCCCACGAGAAAATGATCTAGAATCCAAG
<i>smc3Q847RR</i>	CTTGGATTCTAGATCATTTTTCTCGTGGGATAAGTTTGGACTC
<i>smc3D824GF</i>	GCTAAATATTACATCAGGCGCCCTAGAAGGTATAACTAC
<i>smc3D824GR</i>	GTAGTTATACCTTCTAGGGCGCCTGATGTAATATTTAGC
<i>smc3K689EF</i>	GAATCAAGAAGTCAACACGAAAAAATACTGGAAGAATTAG
<i>smc3K689ER</i>	CTAATCTTCCAGTATTTTTTTCGTGTTGACTTCTTGATTG
<i>smc3N657SF</i>	GCTAAGAAACACAACTCAGTGCCATCACTTTAGATGGTG
<i>smc3N657SR</i>	CACCATCTAAAGTGATGGCACTGAGTTTGTGTTTCTTAGC
<i>smc3S448PF</i>	GATTGAAGAGCTAATTGATCCTATCAATGGACCAGATACC
<i>smc3S448PR</i>	GGTATCTGGTCCATTGATAGGATCAATTAGCTCTTCAATC
<i>smc3R381SF</i>	CTCCTTGCAACAAAAGCAGAGCGATCTTATCTTAAGAAAG
<i>smc3R381SR</i>	CTTTCTTTAAGATAAGATCGCTCTGCTTTTGTGCAAGGAG
<i>smc3R348GF</i>	CAAATCTATAATTGAGCAAGGGAAACAAAAGTTGTCTAAA
<i>smc3R348GR</i>	TTTAGACAACTTTTGTTCCCTTGCTCAATTATAGATTTG
<i>smc3Q330RF</i>	CAAATTGAGTCAAATGAGGAGCGGAGAAATTTGGATAGTGCAAC
<i>smc3Q330RR</i>	GTTGCACTATCCAAATTTCTCCGCTCCTCATTTGACTCAATTTG
<i>smc3S326PF</i>	GTTCAACAGCAAATTGAGCCAAATGAGGAGCAGAGAAATTTG
<i>smc3S326PR</i>	CAAATTTCTCTGCTCCTCATTTGGCTCAATTTGCTGTTGAAC

7.2 Plasmid list

All plasmids listed were sourced from this study with exception to 61, which was from pLH157; Nat Struct Mol Biol. 2007, 14(8):696-703

Table 7: Plasmid list.

Name	Genotype	Origin	Yeast Marker
61	<i>BPA Crosslink vector tRNA/Bpa-tRNA synthetase plasmid</i>	pLH157	TRP1
84	<i>Ylplac211</i>	Ylplac211	URA3
92	<i>YCplac33</i>	YCplac33	URA3
263	<i>Cas9-LYS2</i>	pRS425	LEU2
332	<i>smc3(K112Q_K113Q_R1008I)</i>	YCplac111	LEU2
429	<i>SMC1-MYC9</i>	YCplac22	TRP1
547	<i>smc3(K112Q_K113Q_R1008I)</i>	Ylplac211	URA3
592	<i>smc3(K112Q_K113Q_R1008I_A157V)</i>	Ylplac211	URA3
593	<i>smc3(K112Q_K113Q_R1008I_K158E)</i>	Ylplac211	URA3
594	<i>smc3(K112Q_K113Q_R1008I_D252N)</i>	Ylplac211	URA3
595	<i>smc3(K112Q_K113Q_R1008I_S260P)</i>	Ylplac211	URA3
596	<i>smc3(K112Q_K113Q_R1008I_N292S)</i>	Ylplac211	URA3
597	<i>smc3(K112Q_K113Q_R1008I_Q298R)</i>	Ylplac211	URA3
598	<i>smc3(K112Q_K113Q_R1008I_K300R)</i>	Ylplac211	URA3
599	<i>smc3(K112Q_K113Q_R1008I_M937T)</i>	Ylplac211	URA3
600	<i>smc3(K112Q_K113Q_R1008I_R946G)</i>	Ylplac211	URA3
601	<i>smc3(K112Q_K113Q_R1008I_N982D)</i>	Ylplac211	URA3
602	<i>smc3(K112Q_K113Q_R1008I_E1124K)</i>	Ylplac211	URA3
603	<i>smc3(K112Q_K113Q_R1008I_V1133I)</i>	Ylplac211	URA3
604	<i>smc3(K112Q_K113Q_R1008I_Q1143R)</i>	Ylplac211	URA3
605	<i>smc3(K112Q_K113Q_R1008I_S1176P)</i>	Ylplac211	URA3
606	<i>smc3(K112Q_K113Q_R1008I_R1187G)</i>	Ylplac211	URA3
607	<i>smc3(K112Q_K113Q_R1008I_L965F)</i>	Ylplac211	URA3
608	<i>smc3(K112Q_K113Q_R1008I_D975E)</i>	Ylplac211	URA3
609	<i>smc3(K112Q_K113Q_R1008I_N985S)</i>	Ylplac211	URA3
610	<i>smc3(K112Q_K113Q_R1008I_E305G)</i>	Ylplac211	URA3
611	<i>smc3(K112Q_K113Q_R1008I_D295V)</i>	Ylplac211	URA3
612	<i>smc3(K112Q_K113Q_R1008I_L926H)</i>	Ylplac211	URA3
613	<i>smc3(K112Q_K113Q_R1008I_C1183S)</i>	Ylplac211	URA3
621	<i>smc3(K112Q_K113Q_R1008I_N156D)</i>	Ylplac211	URA3
622	<i>smc3(K112Q_K113Q_R1008I_K180R)</i>	Ylplac211	URA3
628	<i>smc3(K112Q_K113Q_R1008I_E1203G)</i>	Ylplac211	URA3
635	<i>smc3(K112Q_K113Q_R1008I_T233A)</i>	Ylplac211	URA3
636	<i>smc3(K112Q_K113Q_R1008I_R248G)</i>	Ylplac211	URA3
637	<i>smc3(K112Q_K113Q_R1008I_S259P)</i>	Ylplac211	URA3
638	<i>smc3(K112Q_K113Q_R1008I_V315G)</i>	Ylplac211	URA3
639	<i>smc3(K112Q_K113Q_R1008I_Y359H)</i>	Ylplac211	URA3
643	<i>smc3(K112Q_K113Q_K1201E_R1008I)</i>	Ylplac211	URA3
644	<i>smc3(F41L_K112Q_K113Q_R1008I)</i>	Ylplac211	URA3

645	<i>smc3(S54F_K112Q_K113Q_R1008I)</i>	YIplac211	URA3
646	<i>smc3(K112Q_K113Q_A157V)</i>	YIplac211	URA3
647	<i>smc3(K112Q_K113Q_K158E)</i>	YIplac211	URA3
648	<i>smc3(K112Q_K113Q_D252N)</i>	YIplac211	URA3
649	<i>smc3(K112Q_K113Q_S260P)</i>	YIplac211	URA3
650	<i>smc3(K112Q_K113Q_N292S)</i>	YIplac211	URA3
651	<i>smc3(K112Q_K113Q_Q298R)</i>	YIplac211	URA3
652	<i>smc3(K112Q_K113Q_K300R)</i>	YIplac211	URA3
653	<i>smc3(K112Q_K113Q_E1124K)</i>	YIplac211	URA3
654	<i>smc3(K112Q_K113Q_V1133I)</i>	YIplac211	URA3
655	<i>smc3(K112Q_K113Q_Q1143R)</i>	YIplac211	URA3
656	<i>smc3(K112Q_K113Q_S1176P)</i>	YIplac211	URA3
657	<i>smc3(K112Q_K113Q_R1187G)</i>	YIplac211	URA3
658	<i>smc3(K112Q_K113Q_E305G)</i>	YIplac211	URA3
659	<i>smc3(K112Q_K113Q_D295V)</i>	YIplac211	URA3
660	<i>smc3(K112Q_K113Q_C1183S)</i>	YIplac211	URA3
661	<i>smc3(K112Q_K113Q_N156D)</i>	YIplac211	URA3
662	<i>smc3(K112Q_K113Q_K180R)</i>	YIplac211	URA3
663	<i>smc3(K112Q_K113Q)</i>	YIplac211	URA3
664	<i>smc3(K112Q_K113Q_T233A)</i>	YIplac211	URA3
665	<i>smc3(K112Q_K113Q_R248G)</i>	YIplac211	URA3
666	<i>smc3(K112Q_K113Q_Y359H)</i>	YIplac211	URA3
667	<i>smc3(L111R_K112Q_K113Q_R1008I)</i>	YIplac211	URA3
668	<i>smc3(K112Q_K113Q_Q117R_R1008I)</i>	YIplac211	URA3
669	<i>smc3(K112Q_K113Q_R946G)</i>	YIplac211	URA3
670	<i>smc3(K112Q_K113Q_N982D)</i>	YIplac211	URA3
671	<i>smc3(K112Q_K113Q_D975E)</i>	YIplac211	URA3
672	<i>smc3(K112Q_K113Q_L926H)</i>	YIplac211	URA3
673	<i>smc3(K112Q_K113Q_S259P)</i>	YIplac211	URA3
674	<i>smc3(K112Q_K113Q_V315G)</i>	YIplac211	URA3
675	<i>smc3(K112Q_K113Q_M937T)</i>	YIplac211	URA3
676	<i>smc3(K112Q_K113Q_N985S)</i>	YIplac211	URA3
683	<i>smc3(K112Q_K113Q_K1201E)</i>	YIplac211	URA3
684	<i>smc3(K112Q_K113Q_E1203G)</i>	YIplac211	URA3
685	<i>smc3(K112Q_K113Q_L965F)</i>	YIplac211	URA3
686	<i>smc3(K57Q_G110R_K112Q_K113Q_R1008I)</i>	YIplac211	URA3
700	<i>smc3(K112Q_K113R_R1008I)</i>	YIplac211	URA3
702	<i>smc3(K112Q_K113R)</i>	YIplac211	URA3
703	YCplac33-Eco1	YCplac33	URA3
709	<i>smc3(K689E_K112Q_K113Q_R1008I)</i>	YIplac211	URA3
709	<i>smc3(K689E_K112Q_K113Q_R1008I)</i>	YIplac211	URA3
710	<i>smc3(S448P_K112Q_K113Q_R1008I)</i>	YIplac211	URA3
710	<i>smc3(S448P_K112Q_K113Q_R1008I)</i>	YIplac211	URA3
711	<i>smc3(Q330R_K112Q_K113Q_R1008I)</i>	YIplac211	URA3
711	<i>smc3(Q330R_K112Q_K113Q_R1008I)</i>	YIplac211	URA3
713	<i>smc3(R348G_K112Q_K113Q_R1008I)</i>	YIplac211	URA3
713	<i>smc3(R348G_K112Q_K113Q_R1008I)</i>	YIplac211	URA3
714	<i>smc3(S326P_K112Q_K113Q_R1008I)</i>	YIplac211	URA3
714	<i>smc3(S326P_K112Q_K113Q_R1008I)</i>	YIplac211	URA3
717	<i>smc3(Q847R_K112Q_K113Q_R1008I)</i>	YIplac211	URA3
718	<i>smc3(D824G_K112Q_K113Q_R1008I)</i>	YIplac211	URA3
719	<i>smc3(W483R_K112Q_K113Q_R1008I)</i>	YIplac211	URA3

723	YCplac111-Eco1	YCplac111	LEU2
728	smc3(E759K_K112Q_K113Q_R1008I)	YIplac211	URA3
729	smc3(E857G_K112Q_K113Q_R1008I)	YIplac211	URA3
729	smc3(E857G_K112Q_K113Q_R1008I)	YIplac211	URA3
731	smc3(N657S_K112Q_K113Q_R1008I)	YIplac211	URA3
731	smc3(N657S_K112Q_K113Q_R1008I)	YIplac211	URA3
732	smc3(R381S_K112Q_K113Q_R1008I)	YIplac211	URA3
732	smc3(R381S_K112Q_K113Q_R1008I)	YIplac211	URA3
737	smc3(E857G_K112Q_K113Q)	YIplac211	URA3
738	smc3(R381S_K112Q_K113Q)	YIplac211	URA3
739	smc3(R348G_K112Q_K113Q)	YIplac211	URA3
740	smc3(K689E_K112Q_K113Q)	YIplac211	URA3
741	smc3(W483R_K112Q_K113Q)	YIplac211	URA3
742	smc3(Q330R_K112Q_K113Q)	YIplac211	URA3
750	Cas9-Met15	pBH257	LEU2
751	YCplac33-Smc1	YCplac33	URA3
753	smc3D1011TAG-HA3	YEplac181	LEU2
754	YEplac181	YEplac181	LEU2
755	YCplac22	YCplac22	TRP1
755	YCplac22	YCplac22	TRP1
756	Met15 integration vector for Cas9-Met15 (pBH750)	pUC19	MET15
758	smc3K57TAG-HA3	YEplac181	LEU2
759	smc3M74TAG-HA3	YEplac181	LEU2
760	smc3L111TAG-HA3	YEplac181	LEU2
761	smc3Q117TAG-HA3	YEplac181	LEU2
768	Smc1-myc9	YEplac181	LEU2
769	smc3(N517D_K112Q_K113Q_R1008I)	YIplac211	URA3
770	smc3(S512G_K112Q_K113Q_R1008I)	YIplac211	URA3
771	smc3F1005TAG-HA3	YEplac181	LEU2
772	smc3G110TAG-HA3	YEplac181	LEU2
773	smc3R61TAG-HA3	YEplac181	LEU2
774	PDS5	YCplac22	TRP1
780	smc3E199TAG-HA3	YEplac181	LEU2
781	smc3E202TAG-HA3	YEplac181	LEU2
782	smc3F999TAG-HA3	YEplac181	LEU2
783	smc3K1004TAG-HA3	YEplac181	LEU2
784	smc3Q195TAG-HA3	YEplac181	LEU2
785	smc3F1002TAG-HA3	YEplac181	LEU2
786	smc3R1008TAG-HA3	YEplac181	LEU2
787	smc3H66TAG-HA3	YEplac181	LEU2
788	smc3(Q195TAG,R1008I)-HA3	YEplac181	LEU2
790	smc3(Q195TAG,K112Q,K113Q)-HA3	YEplac181	LEU2
791	smc3(Q195TAG,K112Q,K113Q,R1008I)-HA3	YEplac181	LEU2
795	smc3R58TAG in YCplac111	YCplac111	LEU2
796	smc3R58TAG in YEplac181	YEplac181	LEU2
803	smc3E202TAG,K112Q,K113Q-HA3	YEplac181	LEU2
810	Met15::smc1Myc9 integration vector for Cas9-Met15 (pBH750)	pUC19	MET15
811	smc3E202TAG,K112Q,K113Q,R1008I-HA3	YEplac181	LEU2
812	smc3E202TAG_R1008I-HA3	YEplac181	LEU2
817	smc3Q212TAG-HA3	YEplac181	LEU2
819	smc3I1206TAG-HA3	YEplac181	LEU2

820	<i>smc3P1147TAG-HA3</i>	YEplac181	LEU2
821	<i>smc3E213TAG-HA3</i>	YEplac181	LEU2
822	<i>smc3E209TAG-HA3</i>	YEplac181	LEU2
823	<i>smc3S1149TAG-HA3</i>	YEplac181	LEU2
836	<i>smc3S205TAG-HA3</i>	YEplac181	LEU2
837	<i>smc3K1201TAG-HA3</i>	YEplac181	LEU2
838	<i>smc3K1003TAG-HA3</i>	YEplac181	LEU2
839	<i>smc3A1148TAG-HA3</i>	YEplac181	LEU2
844	<i>smc3Q67TAG_E202TAG_E1155Q-HA3</i>	YEplac181	LEU2
845	<i>smc3Q195TAG_E1155Q-HA3</i>	YEplac181	LEU2
848	<i>smc3E1014TAG-HA3</i>	YEplac181	LEU2
866	<i>smc3N1178TAG-HA3</i>	YEplac181	LEU2
867	<i>smc3A1179TAG-HA3</i>	YEplac181	LEU2
868	<i>smc3E1203TAG-HA3</i>	YEplac181	LEU2
869	<i>smc3S208TAG-HA3</i>	YEplac181	LEU2
874	<i>smc3K1177TAG-HA3</i>	YEplac181	LEU2
883	<i>smc3E202TAG-E1155Q-HA3</i>	YEplac181	LEU2
952	<i>pds5R415C_His6_Flag6 integration vector</i>	pUC19	Caura3
971	<i>Met15::smc1S54CMyC9 integration vector for Cas9-Met15</i>	pUC19	MET15
973	<i>Met15::smc1G152CMyC9 integration vector for Cas9-Met15</i>	pUC19	MET15
974	<i>smc3E1124C_HA6_His3MX6 integration vector (not full-length smc3)</i>	pBlueScript SK	spHIS3
975	<i>smc3S1180C_HA6_His3MX6 integration vector (not full-length smc3)</i>	pBlueScript SK	spHIS3
976	<i>Met15::smc1K191CMyC9 integration vector for Cas9-Met15 (pBH750)</i>	pBlueScript SK	MET15
977	<i>Met15::smc1K188CMyC9 integration vector for Cas9-Met15 (pBH750)</i>	pBlueScript SK	MET15
978	<i>Met15::smc1E184CMyC9 integration vector for Cas9-Met15 (pBH750)</i>	pBlueScript SK	MET15
979	<i>Met15::smc1K180CMyC9 integration vector for Cas9-Met15 (pBH750)</i>	pBlueScript SK	MET15
981	<i>smc3E188C-HA3</i>	YIplac211	URA3
982	<i>smc3K185C-HA3</i>	YIplac211	URA3
998	<i>smc3Q67TAG_W483R_K112Q_K113Q-HA3</i>	YEplac181	LEU2
999	<i>smc3Q67TAG_W483R_K112Q_K113Q_R1008I-HA3</i>	YEplac181	LEU2
1006	<i>Met15::smc1E183C-MyC9 integration vector for Cas9-Met15 (pBH750)</i>	pUC19	MET15
1007	<i>Met15::smc1L185C-MyC9 integration vector for Cas9-Met15 (pBH750)</i>	pUC19	MET15
1008	<i>Met15::smc1K186C-MyC9 integration vector for Cas9-Met15 (pBH750)</i>	pUC19	MET15
1038	<i>scc2C978S_FLAG6_KanMX integration vector</i>	pBlueScript SK	KanMX
1039	<i>scc2C1100S_FLAG6_KanMX integration vector</i>	pBlueScript SK	KanMX
1063	<i>N-FLAG3-smc3K112Q_K113Q_K160C_N1204C</i>	YIplac211	URA3
1064	<i>Met15::smc1L597TEV5MyC9 integration vector for Cas9-Met15 (pBH750)</i>	pUC19	MET15
1065	<i>N-FLAG3-smc3K160C_R1008I_N1204C</i>	YIplac211	URA3
1066	<i>N-FLAG3-smc3K160C_W483R_R1008I_N1204C</i>	YIplac211	URA3
1067	<i>N-FLAG3-smc3K160C_K112Q,K113Q_R1008I_N1204C</i>	YIplac211	URA3
1068	<i>N-FLAG3-smc3K112Q_K113Q_K160C_W483R_R1008I_N1204C</i>	YIplac211	URA3
1069	<i>smc1(K191C) integration vector</i>	pUC19	NatMX

1070	<i>smc1(K191C, L1120C) integration vector</i>	pUC19	NatMX
1071	<i>N-FLAG3-smc3K184C</i>	YIplac211	URA3
1072	<i>N-FLAG3-smc3K184C_N1204C</i>	YIplac211	URA3
1089	<i>smc3(K112Q_K113Q_W483R_R1008I) integration cassette</i>	pBluScript SK	spHIS3

7.3 Yeast strain list

All yeast strains listed were sourced from this study with the exception of 1265, which was sourced from: The Nasmyth lab, University of Oxford, UK.

Table 8: Yeast strain list. Background: W303, *S. cerevisiae*

Name	Genotype
216	<i>MAT a, his1</i>
217	<i>MAT alpha, his1</i>
699	<i>MAT a, ade2-1, trp1-1, can1-100, leu2-3, 112, his3-11, 15, ura3, GAL, psi+</i>
700	<i>MAT alpha, ade2-1, trp1-1, can1-100, leu2-3, 112, his3-11, 15, ura3, GAL, psi+</i>
981	<i>MAT a/alpha, ade2-1, trp1-1, can1-100, leu2-3, 112, his3-11, 15, ura3, GAL, psi, Δsmc3::HIS3/SMC3</i>
1129	<i>MAT a/alpha, ade2-1, trp1-1, can1-100, leu2-3, 112, his3-11, 15, ura3, GAL, psi, Δsmc3::HIS3/SMC3 ura3::smc3(K112Q_K113Q_R1008I_A157V)::URA3 (single copy checked by PCR)</i>
1139	<i>MAT a/alpha, ade2-1, trp1-1, can1-100, leu2-3, 112, his3-11, 15, ura3, GAL, psi, Δsmc3::HIS3/SMC3 ura3::smc3(K112Q_K113Q_R1008I_K158E)::URA3 (single copy checked by PCR)</i>
1143	<i>MAT a/alpha, ade2-1, trp1-1, can1-100, leu2-3, 112, his3-11, 15, ura3, GAL, psi, Δsmc3::HIS3/SMC3 ura3::smc3(K112Q_K113Q_R1008I_N292S)::URA3 (single copy checked by PCR)</i>
1150	<i>MAT a/alpha, ade2-1, trp1-1, can1-100, leu2-3, 112, his3-11, 15, ura3, GAL, psi, Δsmc3::HIS3/SMC3 ura3::smc3(K112Q_K113Q_R1008I_N982D)::URA3 (single copy checked by PCR)</i>
1153	<i>MAT a/alpha, ade2-1, trp1-1, can1-100, leu2-3, 112, his3-11, 15, ura3, GAL, psi, Δsmc3::HIS3/SMC3 ura3::smc3(K112Q_K113Q_R1008I_E1124K)::URA3 (single copy checked by PCR)</i>
1168	<i>MAT a/alpha, ade2-1, trp1-1, can1-100, leu2-3, 112, his3-11, 15, ura3, GAL, psi, Δsmc3::HIS3/SMC3 ura3::smc3(K112Q_K113Q_R1008I_N985S)::URA3 (single copy checked by PCR)</i>
1170	<i>MAT a/alpha, ade2-1, trp1-1, can1-100, leu2-3, 112, his3-11, 15, ura3, GAL, psi, Δsmc3::HIS3/SMC3 ura3::smc3(K112Q_K113Q_R1008I_E305G)::URA3 (single copy checked by PCR)</i>

1173	<i>MAT a/alpha, ade2-1, trp1-1, can1-100, leu2-3, 112, his3-11, 15, ura3, GAL, psi, Δsmc3::HIS3/SMC3</i> <i>ura3::smc3(K112Q_K113Q_R1008I_D295V)::URA3 (single copy checked by PCR)</i>
1176	<i>MAT a/alpha, ade2-1, trp1-1, can1-100, leu2-3, 112, his3-11, 15, ura3, GAL, psi, Δsmc3::HIS3/SMC3</i> <i>ura3::smc3(K112Q_K113Q_R1008I_C1183S)::URA3 (single copy checked by PCR)</i>
1189	<i>MAT a, ade2-1, trp1-1, can1-100, leu2-3, 112, his3-11, 15, ura3, GAL, psi, Δsmc3::HIS3</i> <i>pBH585 (SMC3-Q67TAG-HA3 in YEplac181)</i> <i>pBH61 (BPA crosslink, Trp1)</i>
1196	<i>MAT a</i> <i>URA3::SMC1-Myc9::URA3</i> <i>SCC1-PK9::KanMX</i> <i>pBH585 (smc3-Q67TAG-HA3 in YEplac181)</i> <i>pBH61 (BPA crosslink, Trp1)</i>
1207	<i>MAT a, ade2-1, trp1-1, can1-100, leu2-3, 112, his3-11, 15, ura3, GAL, psi, Δsmc3::HIS3/SMC3</i> <i>ura3::smc3(K112Q_K113Q_R1008I_D252N)::URA3 (single copy checked by PCR)</i>
1209	<i>MAT a, ade2-1, trp1-1, can1-100, leu2-3, 112, his3-11, 15, ura3, GAL, psi, Δsmc3::HIS3</i> <i>ura3::smc3(K112Q_K113Q_R1008I_S260P)::URA3 (single copy checked by PCR)</i>
1265	<i>MAT alpha, ade2-1, trp1-1, can1-100, leu2-3, 112, his3-11, 15, ura3, GAL, psi+</i> <i>Scs2(E822K, L937F)::NatMX</i>
1301	<i>MAT a/alpha, ade2-1, trp1-1, can1-100, leu2-3, 112, his3-11, 15, ura3, GAL, psi, Δsmc3::HIS3/SMC3</i> <i>ura3::smc3(K112Q_K113Q_R1008I_R1187G)::URA3 (single copy checked by PCR)YCplac111 lost.</i>
1302	<i>MAT a/alpha, ade2-1, trp1-1, can1-100, leu2-3, 112, his3-11, 15, ura3, GAL, psi, Δsmc3::HIS3/SMC3</i> <i>ura3::smc3(K112Q_K113Q_R1008I_Q298R)::URA3 (single copy checked by PCR)YCplac111 lost.</i>
1303	<i>MAT a/alpha, ade2-1, trp1-1, can1-100, leu2-3, 112, his3-11, 15, ura3, GAL, psi, Δsmc3::HIS3/SMC3</i> <i>ura3::smc3(K112Q_K113Q_R1008I_V1133I)::URA3 (single copy checked by PCR)YCplac111 lost.</i>
1304	<i>MAT a/alpha, ade2-1, trp1-1, can1-100, leu2-3, 112, his3-11, 15, ura3, GAL, psi, Δsmc3::HIS3/SMC3</i> <i>ura3::smc3(K112Q_K113Q_R1008I_D975E)::URA3 (single copy checked by PCR)YCplac111 lost.</i>
1305	<i>MAT a/alpha, ade2-1, trp1-1, can1-100, leu2-3, 112, his3-11, 15, ura3, GAL, psi, Δsmc3::HIS3/SMC3</i> <i>ura3::smc3(K112Q_K113Q_R1008I_R946G)::URA3 (single copy checked by PCR)YCplac111 lost.</i>
1306	<i>MAT a/alpha, ade2-1, trp1-1, can1-100, leu2-3, 112, his3-11, 15, ura3, GAL, psi, Δsmc3::HIS3/SMC3</i> <i>ura3::smc3(K112Q_K113Q_R1008I_S1176P)::URA3 (single copy checked by PCR)YCplac111 lost.</i>
1307	<i>MAT a/alpha, ade2-1, trp1-1, can1-100, leu2-3, 112, his3-11, 15, ura3, GAL, psi, Δsmc3::HIS3/SMC3</i> <i>ura3::smc3(K112Q_K113Q_R1008I_K300R)::URA3 (single copy checked by PCR)YCplac111 lost.</i>
1308	<i>MAT a/alpha, ade2-1, trp1-1, can1-100, leu2-3, 112, his3-11, 15, ura3, GAL, psi, Δsmc3::HIS3/SMC3</i> <i>ura3::smc3(K112Q_K113Q_R1008I_Q1143R)::URA3 (single copy checked by PCR)YCplac111 lost.</i>
1309	<i>MAT a/alpha, ade2-1, trp1-1, can1-100, leu2-3, 112, his3-11, 15, ura3, GAL, psi, Δsmc3::HIS3/SMC3</i> <i>ura3::smc3(K112Q_K113Q_R1008I_M937T)::URA3 (single copy checked by PCR)YCplac111 lost.</i>

1310	<i>MAT a/alpha, ade2-1, trp1-1, can1-100, leu2-3, 112, his3-11, 15, ura3, GAL, psi, Δsmc3::HIS3/SMC3 ura3::smc3(K112Q_K113Q_R1008I_L965F)::URA3 (single copy checked by PCR)YCplac111 lost.</i>
1330	<i>MAT a/alpha, ade2-1, trp1-1, can1-100, leu2-3, 112, his3-11, 15, ura3, GAL, psi, Δsmc3::HIS3/SMC3 ura3::smc3(K112Q_K113Q_R1008I_N156D)::URA3 (single copy checked by PCR)</i>
1331	<i>MAT a/alpha, ade2-1, trp1-1, can1-100, leu2-3, 112, his3-11, 15, ura3, GAL, psi, Δsmc3::HIS3/SMC3 ura3::smc3(K112Q_K113Q_R1008I_K180R)::URA3 (single copy checked by PCR)</i>
1332	<i>MAT a/alpha, ade2-1, trp1-1, can1-100, leu2-3, 112, his3-11, 15, ura3, GAL, psi, Δsmc3::HIS3/SMC3 ura3::smc3(K112Q_K113Q_R1008I_T233A)::URA3 (single copy checked by PCR)</i>
1333	<i>MAT a/alpha, ade2-1, trp1-1, can1-100, leu2-3, 112, his3-11, 15, ura3, GAL, psi, Δsmc3::HIS3/SMC3 ura3::smc3(K112Q_K113Q_R1008I_R248G)::URA3 (single copy checked by PCR)</i>
1334	<i>MAT a/alpha, ade2-1, trp1-1, can1-100, leu2-3, 112, his3-11, 15, ura3, GAL, psi, Δsmc3::HIS3/SMC3 ura3::smc3(K112Q_K113Q_R1008I_Y359H)::URA3 (single copy checked by PCR)</i>
1335	<i>MAT a/alpha, ade2-1, trp1-1, can1-100, leu2-3, 112, his3-11, 15, ura3, GAL, psi, Δsmc3::HIS3 / Smc3 ura3::smc3(K112Q_K113Q_R1008I)::URA3 (single copy checked by PCR)</i>
1336	<i>MAT a/alpha, ade2-1, trp1-1, can1-100, leu2-3, 112, his3-11, 15, ura3, GAL, psi, Δsmc3::HIS3/SMC3 ura3::smc3(K112Q_K113Q_K158E)::URA3 (single copy checked by PCR)</i>
1337	<i>MAT a/alpha, ade2-1, trp1-1, can1-100, leu2-3, 112, his3-11, 15, ura3, GAL, psi, Δsmc3::HIS3/SMC3 ura3::smc3(K112Q_K113Q_D252N)::URA3 (single copy checked by PCR)</i>
1338	<i>MAT a/alpha, ade2-1, trp1-1, can1-100, leu2-3, 112, his3-11, 15, ura3, GAL, psi, Δsmc3::HIS3/SMC3 ura3::smc3(K112Q_K113Q_S260P)::URA3 (single copy checked by PCR)</i>
1339	<i>MAT a/alpha, ade2-1, trp1-1, can1-100, leu2-3, 112, his3-11, 15, ura3, GAL, psi, Δsmc3::HIS3/SMC3 ura3::smc3(K112Q_K113Q_K300R)::URA3 (single copy checked by PCR)</i>
1340	<i>MAT a/alpha, ade2-1, trp1-1, can1-100, leu2-3, 112, his3-11, 15, ura3, GAL, psi, Δsmc3::HIS3/SMC3 ura3::smc3(K112Q_K113Q_V1133I)::URA3 (single copy checked by PCR)</i>
1341	<i>MAT a/alpha, ade2-1, trp1-1, can1-100, leu2-3, 112, his3-11, 15, ura3, GAL, psi, Δsmc3::HIS3/SMC3 ura3::smc3(K112Q_K113Q_Q1143R)::URA3 (single copy checked by PCR)</i>
1342	<i>MAT a/alpha, ade2-1, trp1-1, can1-100, leu2-3, 112, his3-11, 15, ura3, GAL, psi, Δsmc3::HIS3/SMC3 ura3::smc3(K112Q_K113Q_S1176P)::URA3 (single copy checked by PCR)</i>
1343	<i>MAT a/alpha, ade2-1, trp1-1, can1-100, leu2-3, 112, his3-11, 15, ura3, GAL, psi, Δsmc3::HIS3/SMC3 ura3::smc3(K112Q_K113Q_R1187G)::URA3 (single copy checked by PCR)</i>
1344	<i>MAT a/alpha, ade2-1, trp1-1, can1-100, leu2-3, 112, his3-11, 15, ura3, GAL, psi, Δsmc3::HIS3/SMC3 ura3::smc3(K112Q_K113Q_D295V)::URA3 (single copy checked by PCR)</i>
1345	<i>MAT a/alpha, ade2-1, trp1-1, can1-100, leu2-3, 112, his3-11, 15, ura3, GAL, psi, Δsmc3::HIS3/SMC3 ura3::smc3(K112Q_K113Q_K180R)::URA3 (single copy checked by PCR)</i>
1346	<i>MAT a/alpha, ade2-1, trp1-1, can1-100, leu2-3, 112, his3-11, 15, ura3, GAL, psi, Δsmc3::HIS3/SMC3 ura3::smc3(K112Q_K113Q_A157V)::URA3 (single copy checked by PCR)</i>
1347	<i>MAT a/alpha, ade2-1, trp1-1, can1-100, leu2-3, 112, his3-11, 15, ura3, GAL, psi, Δsmc3::HIS3/SMC3 ura3::smc3(K112Q_K113Q_Q298R)::URA3 (single copy checked by PCR)</i>

1348	<i>MAT a/alpha, ade2-1, trp1-1, can1-100, leu2-3, 112, his3-11, 15, ura3, GAL, psi, Δsmc3::HIS3/SMC3 ura3::smc3(K112Q_K113Q_E305G)::URA3 (single copy checked by PCR)</i>
1349	<i>MAT a/alpha, ade2-1, trp1-1, can1-100, leu2-3, 112, his3-11, 15, ura3, GAL, psi, Δsmc3::HIS3/SMC3 ura3::smc3(K112Q_K113Q_N156D)::URA3 (single copy checked by PCR)</i>
1350	<i>MAT a/alpha, ade2-1, trp1-1, can1-100, leu2-3, 112, his3-11, 15, ura3, GAL, psi, Δsmc3::HIS3/SMC3 ura3::smc3(K112Q_K113Q_T233A)::URA3 (single copy checked by PCR)</i>
1351	<i>MAT a/alpha, ade2-1, trp1-1, can1-100, leu2-3, 112, his3-11, 15, ura3, GAL, psi, Δsmc3::HIS3/SMC3 ura3::smc3(K112Q_K113Q_R248G)::URA3 (single copy checked by PCR)</i>
1352	<i>MAT a/alpha, ade2-1, trp1-1, can1-100, leu2-3, 112, his3-11, 15, ura3, GAL, psi, Δsmc3::HIS3/SMC3 ura3::smc3(K112Q_K113Q_Y359H)::URA3 (single copy checked by PCR)</i>
1353	<i>MAT a/alpha, ade2-1, trp1-1, can1-100, leu2-3, 112, his3-11, 15, ura3, GAL, psi, Δsmc3::HIS3/SMC3 ura3::smc3(K112Q_K113Q_N292S)::URA3 (single copy checked by PCR)</i>
1354	<i>MAT a/alpha, ade2-1, trp1-1, can1-100, leu2-3, 112, his3-11, 15, ura3, GAL, psi, Δsmc3::HIS3/SMC3 ura3::smc3(K112Q_K113Q_E1124K)::URA3 (single copy checked by PCR)</i>
1355	<i>MAT a/alpha, ade2-1, trp1-1, can1-100, leu2-3, 112, his3-11, 15, ura3, GAL, psi, Δsmc3::HIS3/SMC3 ura3::smc3(K112Q_K113Q_C1183S)::URA3 (single copy checked by PCR)</i>
1356	<i>MAT a/alpha, ade2-1, trp1-1, can1-100, leu2-3, 112, his3-11, 15, ura3, GAL, psi, Δsmc3::HIS3 / Smc3 ura3::smc3(K112Q_K113Q)::URA3 (single copy checked by PCR)</i>
1363	<i>MAT a/alpha, ade2-1, trp1-1, can1-100, leu2-3, 112, his3-11, 15, ura3, GAL, psi, Δsmc3::HIS3/SMC3 ura3::smc3(K112Q_K113Q_K1201E)::URA3 (single copy checked by PCR)</i>
1364	<i>MAT a/alpha, ade2-1, trp1-1, can1-100, leu2-3, 112, his3-11, 15, ura3, GAL, psi, Δsmc3::HIS3/SMC3 ura3::smc3(K112Q_K113Q_E1203G)::URA3 (single copy checked by PCR)</i>
1365	<i>MAT a/alpha, ade2-1, trp1-1, can1-100, leu2-3, 112, his3-11, 15, ura3, GAL, psi, Δsmc3::HIS3/SMC3 ura3::smc3(K112Q_K113Q_M937T)::URA3 (single copy checked by PCR)</i>
1366	<i>MAT a/alpha, ade2-1, trp1-1, can1-100, leu2-3, 112, his3-11, 15, ura3, GAL, psi, Δsmc3::HIS3/SMC3 ura3::smc3(K112Q_K113Q_R946G)::URA3 (single copy checked by PCR)</i>
1367	<i>MAT a/alpha, ade2-1, trp1-1, can1-100, leu2-3, 112, his3-11, 15, ura3, GAL, psi, Δsmc3::HIS3/SMC3 ura3::smc3(K112Q_K113Q_N982D)::URA3 (single copy checked by PCR)</i>
1368	<i>MAT a/alpha, ade2-1, trp1-1, can1-100, leu2-3, 112, his3-11, 15, ura3, GAL, psi, Δsmc3::HIS3/SMC3 ura3::smc3(K112Q_K113Q_L965F)::URA3 (single copy checked by PCR)</i>
1369	<i>MAT a/alpha, ade2-1, trp1-1, can1-100, leu2-3, 112, his3-11, 15, ura3, GAL, psi, Δsmc3::HIS3/SMC3 ura3::smc3(K112Q_K113Q_N985S)::URA3 (single copy checked by PCR)</i>
1370	<i>MAT a/alpha, ade2-1, trp1-1, can1-100, leu2-3, 112, his3-11, 15, ura3, GAL, psi, Δsmc3::HIS3/SMC3 ura3::smc3(K112Q_K113Q_L926H)::URA3 (single copy checked by PCR)</i>
1371	<i>MAT a/alpha, ade2-1, trp1-1, can1-100, leu2-3, 112, his3-11, 15, ura3, GAL, psi, Δsmc3::HIS3/SMC3 ura3::smc3(K112Q_K113Q_S259P)::URA3 (single copy checked by PCR)</i>
1372	<i>MAT a/alpha, ade2-1, trp1-1, can1-100, leu2-3, 112, his3-11, 15, ura3, GAL, psi, Δsmc3::HIS3/SMC3 ura3::smc3(K112Q_K113Q_V315G)::URA3 (single copy checked by PCR)</i>

1374	<i>MAT a/alpha, ade2-1, trp1-1, can1-100, leu2-3, 112, his3-11, 15, ura3, GAL, psi, Δsmc3::HIS3/SMC3 ura3::smc3(K112Q_K113Q_R1008I_S259P)::URA3 (single copy checked by PCR)</i>
1375	<i>MAT a/alpha, ade2-1, trp1-1, can1-100, leu2-3, 112, his3-11, 15, ura3, GAL, psi, Δsmc3::HIS3/SMC3 ura3::smc3(K112Q_K113Q_R1008I_V315G)::URA3 (single copy checked by PCR)</i>
1378	<i>MAT a/alpha, ade2-1, trp1-1, can1-100, leu2-3, 112, his3-11, 15, ura3, GAL, psi, Δsmc3::HIS3/SMC3 ura3::smc3(K112Q_K113Q_R1008I_K1201E)::URA3 (single copy checked by PCR)</i>
1379	<i>MAT a/alpha, ade2-1, trp1-1, can1-100, leu2-3, 112, his3-11, 15, ura3, GAL, psi, Δsmc3::HIS3/SMC3 ura3::smc3(F41L_K112Q_K113Q_R1008I)::URA3 (single copy checked by PCR)</i>
1380	<i>MAT a/alpha, ade2-1, trp1-1, can1-100, leu2-3, 112, his3-11, 15, ura3, GAL, psi, Δsmc3::HIS3/SMC3 ura3::smc3(S54F_K112Q_K113Q_R1008I)::URA3 (single copy checked by PCR)</i>
1381	<i>MAT a/alpha, ade2-1, trp1-1, can1-100, leu2-3, 112, his3-11, 15, ura3, GAL, psi, Δsmc3::HIS3/SMC3 ura3::smc3(L111R_K112Q_K113Q_R1008I)::URA3 (single copy checked by PCR)</i>
1382	<i>MAT a/alpha, ade2-1, trp1-1, can1-100, leu2-3, 112, his3-11, 15, ura3, GAL, psi, Δsmc3::HIS3/SMC3 ura3::smc3(K112Q_K113Q_Q117R_R1008I)::URA3 (single copy checked by PCR)</i>
1383	<i>MAT a/alpha, ade2-1, trp1-1, can1-100, leu2-3, 112, his3-11, 15, ura3, GAL, psi, Δsmc3::HIS3/SMC3 ura3::smc3(K57Q_G110R_K112Q_K113Q_R1008I)::URA3 (single copy checked by PCR)</i>
1392	<i>MAT a/alpha, ade2-1, trp1-1, can1-100, leu2-3, 112, his3-11, 15, ura3, GAL, psi+Δsmc3::HIS3/Smc3 ura3/ura3::smc3(K112Q_K113Q_R1008I)::URA3 (single copy checked by PCR) scc2(E822K, L937F):: NatMX / SCC2</i>
1393	<i>MAT a/alpha, ade2-1, trp1-1, can1-100, leu2-3, 112, his3-11, 15, ura3, GAL, psi+Δsmc3::HIS3 ura3::smc3(K112Q_K113Q)::URA3 (single copy checked by PCR) Scc2(E822K, L937F):: NatMX</i>
1413	<i>MAT a, ade2-1, trp1-1, can1-100, leu2-3, 112, his3-11, 15, ura3, GAL, psi+Δsmc3::HIS3 ura3::smc3(K112Q_K113Q_R1008I)::URA3 (single copy checked by PCR) scc2(E822K, L937F):: NatMX</i>
1419	<i>MAT a/alpha, ade2-1, trp1-1, can1-100, leu2-3, 112, his3-11, 15, ura3, GAL, psi, Δsmc3::HIS3 / Smc3 ura3::smc3(K112Q_K113R_R1008I)::URA3 (single copy checked by PCR)</i>
1420	<i>MAT a/alpha, ade2-1, trp1-1, can1-100, leu2-3, 112, his3-11, 15, ura3, GAL, psi, Δsmc3::HIS3/SMC3 ura3::smc3(K112Q_K113R)::URA3 (single copy checked by PCR)</i>
1453	<i>MAT a, ade2-1, trp1-1, can1-100, leu2-3, 112, his3-11, 15, ura3, GAL, psi, Δsmc3::HIS3ura3::smc3(K112Q_K113Q_R1008I_E1203G)::URA3 (single copy checked by PCR)</i>
1454	<i>MAT alpha, ade2-1, trp1-1, can1-100, leu2-3, 112, his3-11, 15, ura3, GAL, psi, Δsmc3::HIS3ura3::smc3(K112Q_K113Q_R1008I_E1203G)::URA3 (single copy checked by PCR)</i>
1455	<i>MAT a/alpha, ade2-1, trp1-1, can1-100, leu2-3, 112, his3-11, 15, ura3, GAL, psi, Δsmc3::HIS3/SMC3 ura3::smc3(K112Q_K113Q_R1008I_S448P)::URA3 (single copy checked by PCR)</i>
1456	<i>MAT a/alpha, ade2-1, trp1-1, can1-100, leu2-3, 112, his3-11, 15, ura3, GAL, psi, Δsmc3::HIS3/SMC3 ura3::smc3(K112Q_K113Q_R1008I_R348G)::URA3 (single copy checked by PCR)</i>
1457	<i>MAT a/alpha, ade2-1, trp1-1, can1-100, leu2-3, 112, his3-11, 15, ura3, GAL, psi, Δsmc3::HIS3/SMC3 ura3::smc3(K112Q_K113Q_R1008I_Q330R)::URA3 (single copy checked by PCR)</i>

1458	<i>MAT a/alpha, ade2-1, trp1-1, can1-100, leu2-3, 112, his3-11, 15, ura3, GAL, psi, Δsmc3::HIS3/SMC3</i> <i>ura3::smc3(K112Q_K113Q_R1008I_S326P)::URA3 (single copy checked by PCR)</i>
1471	<i>MAT a/alpha, ade2-1, trp1-1, can1-100, leu2-3, 112, his3-11, 15, ura3, GAL, psi, Δsmc3::HIS3 / Smc3</i> <i>ura3::smc3(K112Q_K113Q_R1008I_W483R)::URA3 (single copy checked by PCR)</i> <i>SCC1-PK9::KanMX/SCC1</i>
1489	<i>MAT alpha, ade2-1, trp1-1, can1-100, leu2-3, 112, his3-11, 15, ura3, GAL, psi+ Δeco1::KanMX6pBH723 (Ycplac111-Eco1 leu marker)</i>
1500	<i>MAT a/alpha, ade2-1, trp1-1, can1-100, leu2-3, 112, his3-11, 15, ura3, GAL, psi, Δsmc3::HIS3/SMC3</i> <i>ura3::smc3(K112Q_K113Q_R1008I_K689E)::URA3 (single copy checked by PCR)</i>
1504	<i>MATa, ade2-1, trp1-1, can1-100, leu2-3, 112, his3-11, 15, ura3, GAL, psi+</i> <i>SCC1-PK9::KanMX</i> <i>SCC3_6His_6FLAG::KANMX</i> <i>pBH585 (smc3-Q67TAG-HA3 in YEplac181)</i> <i>pBH61 (BPA crosslink, Trp1)</i>
1505	<i>MATa, ade2-1, trp1-1, can1-100, leu2-3, 112, his3-11, 15, ura3, GAL, psi+</i> <i>SCC1-PK9::KanMX</i> <i>SCC2_6xHis_FLAG6::KANMX</i> <i>pBH585 (smc3-Q67TAG-HA3 in YEplac181)</i> <i>pBH61 (BPA crosslink, Trp1)</i>
1506	<i>MATa, ade2-1, trp1-1, can1-100, leu2-3, 112, his3-11, 15, ura3, GAL, psi+</i> <i>SCC1-PK9::KanMX</i> <i>PDS5myc18::URA (K lactis)</i> <i>pBH585 (smc3-Q67TAG-HA3 in YEplac181)</i> <i>pBH61 (BPA crosslink, Trp1)</i>
1555	<i>MAT a/alpha, ade2-1, trp1-1, can1-100, leu2-3, 112, his3-11, 15, ura3, GAL, psi, Δsmc3::HIS3 / Smc3</i> <i>ura3::smc3(K112R_K113Q_R1008I)::URA3 (single copy checked by PCR)</i>
1556	<i>MAT a/alpha, ade2-1, trp1-1, can1-100, leu2-3, 112, his3-11, 15, ura3, GAL, psi, Δsmc3::HIS3/SMC3</i> <i>ura3::smc3(K112Q_K113Q_R1008I_E857G)::URA3 (single copy checked by PCR)</i>
1557	<i>MAT a/alpha, ade2-1, trp1-1, can1-100, leu2-3, 112, his3-11, 15, ura3, GAL, psi, Δsmc3::HIS3/SMC3</i> <i>ura3::smc3(K112Q_K113Q_R1008I_N657S)::URA3 (single copy checked by PCR)</i>
1559	<i>MAT a/alpha, ade2-1, trp1-1, can1-100, leu2-3, 112, his3-11, 15, ura3, GAL, psi, Δsmc3::HIS3/SMC3</i> <i>ura3::smc3(K112Q_K113Q_R1008I_R381S)::URA3 (single copy checked by PCR)</i>
1590	<i>MAT a/alpha, ade2-1, trp1-1, can1-100, leu2-3, 112, his3-11, 15, ura3, GAL, psi, Δsmc3::HIS3 / Smc3</i> <i>ura3::smc3(K112R_K113Q)::URA3 (single copy checked by PCR)</i>
1694	<i>MAT a/alpha, ade2-1, trp1-1, can1-100, leu2-3, 112, his3-11, 15, ura3, GAL, psi, Δsmc3::HIS3/SMC3</i> <i>ura3::smc3(K112Q_K113Q_W483R)::URA3 (single copy checked by PCR)</i> <i>scc2(E822K, L937F)::NatMX</i>
1848	<i>MATa, ade2-1, trp1-1, can1-100, leu2-3, 112, his3-11, 15, ura3, GAL, psi+SCC1-PK9::KanMX</i> <i>SCC2_6xHis_FLAG6::KANMX</i> <i>pBH773 (smc3-R61TAG-HA3 in YEplac181)</i> <i>pBH61 (BPA crosslink, Trp1)</i>
1849	<i>MATa, ade2-1, trp1-1, can1-100, leu2-3, 112, his3-11, 15, ura3, GAL, psi+SCC1-PK9::KanMX</i> <i>SCC2_6xHis_FLAG6::KANMX</i> <i>pBH781 (smc3-E202TAG-HA3 in YEplac181)</i> <i>pBH61 (BPA crosslink, Trp1)</i>
1850	<i>MATa, ade2-1, trp1-1, can1-100, leu2-3, 112, his3-11, 15, ura3, GAL, psi+SCC1-PK9::KanMX</i> <i>SCC2_6xHis_FLAG6::KANMX</i>

	<i>pBH758 (smcK57TAG-HA3 in YEplac181)</i> <i>pBH61 (BPA crosslink, Trp1)</i>
1851	<i>MATa,ade2-1,trp1-1,can1-100,leu2-3,112,his3-11,15,ura3,GAL,psi+SCC1-PK9::KanMX</i> <i>SCC2_6xHis_FLAG6::KANMX</i> <i>pBH784 (smc3-Q195TAG-HA3 in YEplac181)</i> <i>pBH61 (BPA crosslink, Trp1)</i>
1852	<i>MATa,ade2-1,trp1-1,can1-100,leu2-3,112,his3-11,15,ura3,GAL,psi+SCC1-PK9::KanMX</i> <i>SCC2_6xHis_FLAG6::KANMX</i> <i>pBH760 (smc3-L111TAG-HA3 in YEplac181)</i> <i>pBH61 (BPA crosslink, Trp1)</i>
1853	<i>MATa,ade2-1,trp1-1,can1-100,leu2-3,112,his3-11,15,ura3,GAL,psi+SCC1-PK9::KanMX</i> <i>SCC2_6xHis_FLAG6::KANMX</i> <i>pBH780 (smc3-E199TAG-HA3 in YEplac181)</i> <i>pBH61 (BPA crosslink, Trp1)</i>
1854	<i>MATa,ade2-1,trp1-1,can1-100,leu2-3,112,his3-11,15,ura3,GAL,psi+SCC1-PK9::KanMX</i> <i>SCC2_6xHis_FLAG6::KANMX</i> <i>pBH759 (smc3-M74TAG-HA3 in YEplac181)</i> <i>pBH61 (BPA crosslink, Trp1)</i>
1855	<i>MATa,ade2-1,trp1-1,can1-100,leu2-3,112,his3-11,15,ura3,GAL,psi+SCC1-PK9::KanMX</i> <i>SCC2_6xHis_FLAG6::KANMX</i> <i>pBH761 (smc3-Q117TAG-HA3 in YEplac181)</i> <i>pBH61 (BPA crosslink, Trp1)</i>
1856	<i>MATa,ade2-1,trp1-1,can1-100,leu2-3,112,his3-11,15,ura3,GAL,psi+SCC1-PK9::KanMX</i> <i>SCC2_6xHis_FLAG6::KANMX</i> <i>pBH785 (smc3-F1002TAG-HA3 in YEplac181)</i> <i>pBH61 (BPA crosslink, Trp1)</i>
1861	<i>MATa,ade2-1,trp1-1,can1-100,leu2-3,112,his3-11,15,ura3,GAL,psi+SCC1-PK9::KanMX</i> <i>pBH784 (smc3-Q195TAG-HA3 in YEplac181)</i> <i>pBH61 (BPA crosslink, Trp1)</i>
1873	<i>MATa,ade2-1,trp1-1,can1-100,leu2-3,112,his3-11,15,ura3,GAL,psi+SCC1-PK9::KanMX</i> <i>PDS5myc18::URA (K lactis)</i> <i>pBH781 (smc3-E202TAG-HA3 in YEplac181)</i> <i>pBH61 (BPA crosslink, Trp1)</i>
1878	<i>MATa,ade2-1,trp1-1,can1-100,leu2-3,112,his3-11,15,ura3,GAL,psi+SCC1-PK9::KanMX</i> <i>SCC2_6xHis_FLAG6::KANMX</i> <i>pBH787 (smc3-H66TAG-HA3 in YEplac181)</i> <i>pBH61 (BPA crosslink, Trp1)</i>
1879	<i>MATa,ade2-1,trp1-1,can1-100,leu2-3,112,his3-11,15,ura3,GAL,psi+SCC1-PK9::KanMX</i> <i>pBH758 (smc3-K57TAG-HA3 in YEplac181)</i> <i>pBH61 (BPA crosslink, Trp1)</i>
1881	<i>MATa,ade2-1,trp1-1,can1-100,leu2-3,112,his3-11,15,ura3,GAL,psi+SCC1-PK9::KanMX</i> <i>pBH781 (smc3-E202TAG-HA3 in YEplac181)</i> <i>pBH61 (BPA crosslink, Trp1)</i>
1882	<i>MAT a, ade2-1,trp1-1,can1-100,leu2-3,112,his3-11,15,ura3,GAL,psi+</i> <i>leu2:SMC1-myc9::hphNT1</i> <i>Δsmc1::NatMX4</i> <i>SCC1-PK9::KanMX</i> <i>pBH781 (smc3-E202TAG-HA3 in YEplac181)</i> <i>pBH61 (BPA crosslink, Trp1)</i>
1883	<i>MATa,ade2-1,trp1-1,can1-100,leu2-3,112,his3-11,15,ura3,GAL,psi+SCC1-PK9::KanMX</i> <i>SCC3_6His_6FLAG::KANMX</i> <i>pBH781 (smc3-E202TAG-HA3 in YEplac181)</i> <i>pBH61 (BPA crosslink, Trp1)</i>
1893	<i>MAT a, ade2-1,trp1-1,can1-100,leu2-3,112,his3-11,15,ura3,GAL,psi+</i> <i>leu2:SMC1-myc9::hphNT1</i> <i>Δsmc1::NatMX4</i> <i>SCC1-PK9::KanMX</i>

	<i>pBH784 (smc3-Q195TAG-HA3 in YEplac181)</i> <i>pBH61 (BPA crosslink, Trp1)</i>
1900	<i>MATa,ade2-1,trp1-1,can1-100,leu2-3,112,his3-11,15,ura3,GAL,psi+SCC1-PK9::KanMX</i> <i>SCC2_6xHis_FLAG6::KANMX</i> <i>pBH796 (smc3-R58TAG-HA3 in YEplac181)</i> <i>pBH61 (BPA crosslink, Trp1)</i>
1901	<i>MATa,ade2-1,trp1-1,can1-100,leu2-3,112,his3-11,15,ura3,GAL,psi+SCC1-PK9::KanMX</i> <i>SCC3_6His_6FLAG::KANMX</i> <i>pBH784 (smc3-Q195TAG-HA3 in YEplac181)</i> <i>pBH61 (BPA crosslink, Trp1)</i>
1902	<i>MATa,ade2-1,trp1-1,can1-100,leu2-3,112,his3-11,15,ura3,GAL,psi+SCC1-PK9::KanMX</i> <i>PDS5myc18::URA (K lactis)</i> <i>pBH784 (smc3-Q195TAG-HA3 in YEplac181)</i> <i>pBH61 (BPA crosslink, Trp1)</i>
1949	<i>MATa,ade2-1,trp1-1,can1-100,leu2-3,112,his3-11,15,ura3,GAL,psi+SCC1-PK9::KanMX</i> <i>pBH817 (smc3-Q212TAG-HA3 in YEplac181)</i> <i>pBH61 (BPA crosslink, Trp1)</i>
1950	<i>MATa,ade2-1,trp1-1,can1-100,leu2-3,112,his3-11,15,ura3,GAL,psi+SCC1-PK9::KanMX</i> <i>pBH821 (smc3-E213TAG-HA3 in YEplac181)</i> <i>pBH61 (BPA crosslink, Trp1)</i>
1951	<i>MATa,ade2-1,trp1-1,can1-100,leu2-3,112,his3-11,15,ura3,GAL,psi+SCC1-PK9::KanMX</i> <i>pBH822 (smc3-E209TAG-HA3 in YEplac181)</i> <i>pBH61 (BPA crosslink, Trp1)</i>
1953	<i>MATa,ade2-1,trp1-1,can1-100,leu2-3,112,his3-11,15,ura3,GAL,psi+SCC1-PK9::KanMX</i> <i>pBH836 (smc3-S205TAG-HA3 in YEplac181)</i> <i>pBH61 (BPA crosslink, Trp1)</i>
1954	<i>MATa,ade2-1,trp1-1,can1-100,leu2-3,112,his3-11,15,ura3,GAL,psi+SCC1-PK9::KanMX</i> <i>pBH838 (smc3-K1003TAG-HA3 in YEplac181)</i> <i>pBH61 (BPA crosslink, Trp1)</i>
1956	<i>MATa,ade2-1,trp1-1,can1-100,leu2-3,112,his3-11,15,ura3,GAL,psi+SCC1-PK9::KanMX</i> <i>pBH788 (smc3Q195TAG,R1008I-HA3 in YEplac181)</i> <i>pBH61 (BPA crosslink, Trp1)</i>
1957	<i>MATa,ade2-1,trp1-1,can1-100,leu2-3,112,his3-11,15,ura3,GAL,psi+SCC1-PK9::KanMX</i> <i>pBH812 (smc3E202TAG_R1008I-HA3 in YEplac181)</i> <i>pBH61 (BPA crosslink, Trp1)</i>
1958	<i>MATa,ade2-1,trp1-1,can1-100,leu2-3,112,his3-11,15,ura3,GAL,psi+SCC1-PK9::KanMX</i> <i>pBH851 (smc3Q195TAG,E199A-HA3 in YEplac181)</i> <i>pBH61 (BPA crosslink, Trp1)</i>
1960	<i>MATa,ade2-1,trp1-1,can1-100,leu2-3,112,his3-11,15,ura3,GAL,psi+SCC1-PK9::KanMX</i> <i>pBH853 (smc3E202TAG,E199A-HA3 in YEplac181)</i> <i>pBH61 (BPA crosslink, Trp1)</i>
1966	<i>MATa,ade2-1,trp1-1,can1-100,leu2-3,112,his3-11,15,ura3,GAL,psi+SCC1-PK9::KanMX</i> <i>SCC2_6xHis_FLAG6::KANMX</i> <i>pBH826 (smc1D588TAG-Myc9 in YEplac181)</i> <i>pBH61 (BPA crosslink, Trp1)</i>
1967	<i>MATa,ade2-1,trp1-1,can1-100,leu2-3,112,his3-11,15,ura3,GAL,psi+SCC1-PK9::KanMX</i> <i>SCC2_6xHis_FLAG6::KANMX</i> <i>pBH827 (smc1E562TAG-Myc9 in YEplac181)</i> <i>pBH61 (BPA crosslink, Trp1)</i>
1968	<i>MATa,ade2-1,trp1-1,can1-100,leu2-3,112,his3-11,15,ura3,GAL,psi+SCC1-PK9::KanMX</i> <i>SCC2_6xHis_FLAG6::KANMX</i>

	<p>pBH828 (<i>smc1T565TAG-Myc9</i> in <i>YEplac181</i>) pBH61 (<i>BPA crosslink, Trp1</i>)</p>
1970	<p><i>MATa,ade2-1,trp1-1,can1-100,leu2-3,112,his3-11,15,ura3,GAL,psi+SCC1-PK9::KanMX</i> <i>SCC2_6xHis_FLAG6::KANMX</i> pBH830 (<i>smc1E591TAG-Myc9</i> in <i>YEplac181</i>) pBH61 (<i>BPA crosslink, Trp1</i>)</p>
1971	<p><i>MATa,ade2-1,trp1-1,can1-100,leu2-3,112,his3-11,15,ura3,GAL,psi+SCC1-PK9::KanMX</i> <i>SCC2_6xHis_FLAG6::KANMX</i> pBH831 (<i>smc1T592TAG-Myc9</i> in <i>YEplac181</i>) pBH61 (<i>BPA crosslink, Trp1</i>)</p>
1972	<p><i>MATa,ade2-1,trp1-1,can1-100,leu2-3,112,his3-11,15,ura3,GAL,psi+SCC1-PK9::KanMX</i> <i>SCC2_6xHis_FLAG6::KANMX</i> pBH832 (<i>smc1E593TAG-Myc9</i> in <i>YEplac181</i>) pBH61 (<i>BPA crosslink, Trp1</i>)</p>
1976	<p><i>MATa,ade2-1,trp1-1,can1-100,leu2-3,112,his3-11,15,ura3,GAL,psi+SCC1-PK9::KanMX</i> <i>SCC3_6xHis_FLAG6::KANMX</i> pBH829 (<i>smc1K620TAG-Myc9</i> in <i>YEplac181</i>) pBH61 (<i>BPA crosslink, Trp1</i>)</p>
1983	<p><i>MATa,ade2-1,trp1-1,can1-100,leu2-3,112,his3-11,15,ura3,GAL,psi+SCC1-PK9::KanMX</i> pBH829 (<i>smc1K620TAG-Myc9</i> in <i>YEplac181</i>) pBH61 (<i>BPA crosslink, Trp1</i>)</p>
1989	<p><i>MATa,ade2-1,trp1-1,can1-100,leu2-3,112,his3-11,15,ura3,GAL,psi+SCC1-PK9::KanMX</i> pBH869 (<i>smc3S208TAG-HA</i> in <i>YEplac181</i>) pBH61 (<i>BPA crosslink, Trp1</i>)</p>
2020	<p><i>MATa,ade2-1,trp1-1,can1-100,leu2-3,112,his3-11,15,ura3,GAL,psi+SMC3HA6::HIS3</i> <i>SCC1-PK9::KanMX</i> pBH829 (<i>smc1K620TAG-Myc9</i> in <i>YEplac181</i>) pBH61 (<i>BPA crosslink, Trp1</i>)</p>
2072	<p><i>MAT a, ade2-1, trp1-1, can1-100, leu2-3, 112, his3-11, 15, ura3, GAL, psi,</i> <i>PDS5_6xHis_FLAG6::KANMX</i> <i>SCC1-PK9::NatMX</i> pBH829 (<i>smc1K620TAG-Myc9</i> in <i>YEplac181</i>) pBH61 (<i>BPA crosslink, Trp1</i>)</p>
2079	<p><i>MAT a, ade2-1, trp1-1, can1-100, leu2-3, 112, his3-11, 15, ura3, GAL, psi,</i> <i>SCC4_6xHis_FLAG6::KANMX</i> <i>SCC1-PK9::NatMX</i> pBH829 (<i>smc1K620TAG-Myc9</i> in <i>YEplac181</i>) pBH61 (<i>BPA crosslink, Trp1</i>)</p>
2121	<p><i>MAT a, ade2-1, trp1-1, can1-100, leu2-3, 112, his3-11, 15, ura3, GAL, psi+</i> <i>Δsmc1::NatMX4</i> <i>smc3E202C-HA6::spHis5</i> <i>SCC1-PK9::KanMX</i> <i>Δmet15::Smc1R1020C-myc9</i></p>
2142	<p><i>MAT a, ade2-1, trp1-1, can1-100, leu2-3, 112, his3-11, 15, ura3, GAL, psi+</i> <i>SCC1-PK9::KanMX</i> <i>scc2TEV1176::NatMX</i> pBH61 (<i>BPA crosslink, Trp1</i>) pBH829 (<i>smc1K620TAG-Myc9</i> in <i>YEplac181</i>)</p>
2143	<p><i>MAT a, ade2-1, trp1-1, can1-100, leu2-3, 112, his3-11, 15, ura3, GAL, psi+</i> <i>SCC1-PK9::KanMX</i> <i>scc2TEV215_6xHis_FLAG6::KanMX</i> pBH61 (<i>BPA crosslink, Trp1</i>) pBH829 (<i>smc1K620TAG-Myc9</i> in <i>YEplac181</i>)</p>
2144	<p><i>MAT a, ade2-1, trp1-1, can1-100, leu2-3, 112, his3-11, 15, ura3, GAL, psi+</i></p>

	<p> SCC1-PK9::KanMX scc2TEV471_6xHis_FLAG6::KanMX pBH61 (BPA crosslink, Trp1) pBH829 (smc1K620TAG-Myc9 in YEplac181) </p>
2145	<p> MAT a, ade2-1, trp1-1, can1-100, leu2-3, 112, his3-11, 15, ura3, GAL, psi+ SCC1-PK9::KanMX scc2TEV668_6xHis_FLAG6::KanMX pBH61 (BPA crosslink, Trp1) pBH829 (smc1K620TAG-Myc9 in YEplac181) </p>
2146	<p> MAT a, ade2-1, trp1-1, can1-100, leu2-3, 112, his3-11, 15, ura3, GAL, psi+ scc2TEV843_6xHis_FLAG6::KanMX SCC1-PK9::NatMX pBH61 (BPA crosslink, Trp1) pBH585 (smc3-Q67TAG-HA3 in YEplac181) </p>
2147	<p> MAT a, ade2-1, trp1-1, can1-100, leu2-3, 112, his3-11, 15, ura3, GAL, psi+ scc2TEV917_6xHis_FLAG6::KanMX SCC1-PK9::NatMX pBH61 (BPA crosslink, Trp1) pBH585 (smc3-Q67TAG-HA3 in YEplac181) </p>
2148	<p> MAT a, ade2-1, trp1-1, can1-100, leu2-3, 112, his3-11, 15, ura3, GAL, psi+ scc2TEV1222_6xHis_FLAG6::KanMX SCC1-PK9::NatMX pBH61 (BPA crosslink, Trp1) pBH585 (smc3-Q67TAG-HA3 in YEplac181) </p>
2149	<p> MAT a, ade2-1, trp1-1, can1-100, leu2-3, 112, his3-11, 15, ura3, GAL, psi+ scc2TEV843_6xHis_FLAG6::KanMX SCC1-PK9::NatMX pBH61 (BPA crosslink, Trp1) pBH829 (smc1K620TAG-Myc9 in YEplac181) </p>
2150	<p> MAT a, ade2-1, trp1-1, can1-100, leu2-3, 112, his3-11, 15, ura3, GAL, psi+ scc2TEV917_6xHis_FLAG6::KanMX SCC1-PK9::NatMX pBH61 (BPA crosslink, Trp1) pBH829 (smc1K620TAG-Myc9 in YEplac181) </p>
2151	<p> MAT a, ade2-1, trp1-1, can1-100, leu2-3, 112, his3-11, 15, ura3, GAL, psi+ scc2TEV1222_6xHis_FLAG6::KanMX SCC1-PK9::NatMX pBH61 (BPA crosslink, Trp1) pBH829 (smc1K620TAG-Myc9 in YEplac181) </p>
2152	<p> MAT a, ade2-1, trp1-1, can1-100, leu2-3, 112, his3-11, 15, ura3, GAL, psi+ scc2TEV888_6xHis_FLAG6::KanMX SCC1-PK9::NatMX pBH61 (BPA crosslink, Trp1) pBH585 (smc3-Q67TAG-HA3 in YEplac181) </p>
2153	<p> MAT a, ade2-1, trp1-1, can1-100, leu2-3, 112, his3-11, 15, ura3, GAL, psi+ scc2TEV888_6xHis_FLAG6::KanMX SCC1-PK9::NatMX pBH61 (BPA crosslink, Trp1) pBH829 (smc1K620TAG-Myc9 in YEplac181) </p>
2170	<p> MAT a, ade2-1, trp1-1, can1-100, leu2-3, 112, his3-11, 15, ura3, GAL, psi+ SCC1-PK9::KanMX scc2TEV1176::NatMX pBH61 (BPA crosslink, Trp1) pBH585 (smc3-Q67TAG-HA3 in YEplac181) </p>

2171	<i>MAT a, ade2-1, trp1-1, can1-100, leu2-3, 112, his3-11, 15, ura3, GAL, psi+ SCC1-PK9::KanMX scc2TEV215_6xHis_FLAG6::KanMX pBH61 (BPA crosslink, Trp1) pBH585 (smc3-Q67TAG-HA3 in YEplac181)</i>
2172	<i>MAT a, ade2-1, trp1-1, can1-100, leu2-3, 112, his3-11, 15, ura3, GAL, psi+ SCC1-PK9::KanMX scc2TEV471_6xHis_FLAG6::KanMX pBH61 (BPA crosslink, Trp1) pBH585 (smc3-Q67TAG-HA3 in YEplac181)</i>
2173	<i>MAT a, ade2-1, trp1-1, can1-100, leu2-3, 112, his3-11, 15, ura3, GAL, psi+ SCC1-PK9::KanMX scc2TEV668_6xHis_FLAG6::KanMX pBH61 (BPA crosslink, Trp1) pBH585 (smc3-Q67TAG-HA3 in YEplac181)</i>
2186	<i>MAT a, ade2-1, trp1-1, can1-100, leu2-3, 112, his3-11, 15, ura3, GAL, psi, Δsmc1::NatMX4 SCC1-PK9::KanMX Δmet15::Smc1P1086TEV3-myc9 pBH817 (smc3-Q212TAG-HA3 in YEplac181) pBH61 (BPA crosslink, Trp1)</i>
2187	<i>MAT a, ade2-1, trp1-1, can1-100, leu2-3, 112, his3-11, 15, ura3, GAL, psi, Δsmc1::NatMX4 SCC1-PK9::KanMX Δmet15::Smc1P1086TEV3-myc9 pBH821 (smc3-E213TAG-HA3 in YEplac181) pBH61 (BPA crosslink, Trp1)</i>
2188	<i>MAT a, ade2-1, trp1-1, can1-100, leu2-3, 112, his3-11, 15, ura3, GAL, psi, Δsmc1::NatMX4 SCC1-PK9::KanMX Δmet15::Smc1P1086TEV3-myc9 pBH836 (smc3-S205TAG-HA3 in YEplac181) pBH61 (BPA crosslink, Trp1)</i>
2190	<i>MAT a, ade2-1, trp1-1, can1-100, leu2-3, 112, his3-11, 15, ura3, GAL, psi, Δsmc1::NatMX4 SCC1-PK9::KanMX Δmet15::Smc1L985TEV3-myc9 pBH817 (smc3-Q212TAG-HA3 in YEplac181) pBH61 (BPA crosslink, Trp1)</i>
2191	<i>MAT a, ade2-1, trp1-1, can1-100, leu2-3, 112, his3-11, 15, ura3, GAL, psi, Δsmc1::NatMX4 SCC1-PK9::KanMX Δmet15::Smc1L985TEV3-myc9 pBH821 (smc3-E213TAG-HA3 in YEplac181) pBH61 (BPA crosslink, Trp1)</i>
2192	<i>MAT a, ade2-1, trp1-1, can1-100, leu2-3, 112, his3-11, 15, ura3, GAL, psi, Δsmc1::NatMX4 SCC1-PK9::KanMX Δmet15::Smc1L985TEV3-myc9 pBH836 (smc3-S205TAG-HA3 in YEplac181) pBH61 (BPA crosslink, Trp1)</i>
2193	<i>MATa, ade2-1, trp1-1, can1-100, leu2-3, 112, his3-11, 15, ura3, GAL, psi+ SMC1-myc9::NatMX SCC1-PK9::KanMX pBH758 (smc3-K57TAG-HA3 in YEplac181) pBH61 (BPA crosslink, Trp1)</i>
2194	<i>MATa, ade2-1, trp1-1, can1-100, leu2-3, 112, his3-11, 15, ura3, GAL, psi+SCC1-PK9::KanMX SCC3_6His_6FLAG::KANMX pBH758 (smc3-K57TAG-HA3 in YEplac181) pBH61 (BPA crosslink, Trp1)</i>

2195	<p><i>MAT a, ade2-1, trp1-1, can1-100, leu2-3, 112, his3-11, 15, ura3, GAL, psi,</i></p> <p>SCC4_6xHis_FLAG6::KANMX SCC1-PK9::NatMX pBH758 (<i>smc3-K57TAG-HA3 in YEplac181</i>) pBH61 (<i>BPA crosslink, Trp1</i>)</p>
2196	<p><i>MAT a, ade2-1, trp1-1, can1-100, leu2-3, 112, his3-11, 15, ura3, GAL, psi,</i></p> <p>PDS5_6xHis_FLAG6::KANMX SCC1-PK9::NatMX pBH758 (<i>smc3-K57TAG-HA3 in YEplac181</i>) pBH61 (<i>BPA crosslink, Trp1</i>)</p>
2230	<p><i>MAT a, ade2-1, trp1-1, can1-100, leu2-3, 112, his3-11, 15, ura3, GAL, psi+</i></p> <p>Δ<i>smc1</i>::NatMX4 <i>Smc3E202C-HA6</i>::spHis5 SCC1-PK9::KanMX Δ<i>met15</i>::<i>Smc1N1013C-myc9</i></p>
2231	<p><i>MAT a, ade2-1, trp1-1, can1-100, leu2-3, 112, his3-11, 15, ura3, GAL, psi+</i></p> <p>Δ<i>smc1</i>::NatMX4 <i>Smc3E202C-HA6</i>::spHis5 SCC1-PK9::KanMX Δ<i>met15</i>::<i>Smc1R1024C-myc9</i></p>
2232	<p><i>MAT a, ade2-1, trp1-1, can1-100, leu2-3, 112, his3-11, 15, ura3, GAL, psi+</i></p> <p>Δ<i>smc1</i>::NatMX4 <i>Smc3E202C-HA6</i>::spHis5 SCC1-PK9::KanMX Δ<i>met15</i>::<i>Smc1A1028C-myc9</i></p>
2233	<p><i>MAT a, ade2-1, trp1-1, can1-100, leu2-3, 112, his3-11, 15, ura3, GAL, psi+</i></p> <p>Δ<i>smc1</i>::NatMX4 <i>Smc3E202C-HA6</i>::spHis5 SCC1-PK9::KanMX Δ<i>met15</i>::<i>Smc1R1031C-myc9</i></p>
2234	<p><i>MAT a, ade2-1, trp1-1, can1-100, leu2-3, 112, his3-11, 15, ura3, GAL, psi+</i></p> <p>Δ<i>smc1</i>::NatMX4 <i>Smc3E202C-HA6</i>::spHis5 SCC1-PK9::KanMX Δ<i>met15</i>::<i>Smc1I1035C-myc9</i></p>
2286	<p><i>MAT a, ade2-1, trp1-1, can1-100, leu2-3, 112, his3-11, 15, ura3, GAL,</i> <i>psi, Δsmc1::NatMX4</i></p> <p>SCC1-PK9::KanMX Δ<i>met15</i>::<i>Smc1V371TEV3-myc9</i> pBH758 (<i>smc3-K57TAG-HA3 in YEplac181</i>) pBH61 (<i>BPA crosslink, Trp1</i>)</p>
2287	<p><i>MAT a, ade2-1, trp1-1, can1-100, leu2-3, 112, his3-11, 15, ura3, GAL,</i> <i>psi, Δsmc1::NatMX4</i></p> <p>SCC1-PK9::KanMX Δ<i>met15</i>::<i>Smc1P1086TEV3-myc9</i> pBH758 (<i>smc3-K57TAG-HA3 in YEplac181</i>) pBH61 (<i>BPA crosslink, Trp1</i>)</p>
2295	<p><i>MAT a, ade2-1, trp1-1, can1-100, leu2-3, 112, his3-11, 15, ura3, GAL, psi</i></p> <p>SCC1-PK9::KanMX <i>scc2::natMX4</i></p>

	<p><i>lys2:: Scc2P140TEV3_His6_Flag6/HyGMX</i> <i>pBH909 (smc1D588Y_K620TAG-Myc9 in YEplac181)</i> <i>pBH61 (BPA crosslink, Trp1)</i></p>
2296	<p><i>MAT alpha, ade2-1, trp1-1, can1-100, leu2-3, 112, his3-11, 15, ura3, GAL, psi+SCC1-PK9::KanMX</i> <i>scc2TEV215_6xHis_FLAG6::KanMX</i> <i>pBH909 (smc1D588Y_K620TAG-Myc9 in YEplac181)</i> <i>pBH61 (BPA crosslink, Trp1)</i></p>
2298	<p><i>MATa, trp1-1, can1-100, leu2-3, 112, his3-11, 15, ura3, GAL, psi+SCC1-PK9::KanMX</i> <i>scc2::natMX4</i> <i>lys2:: Scc2T150TEV3_His6_Flag6/HyGMX</i> <i>pBH909 (smc1D588Y_K620TAG-Myc9 in YEplac181)</i> <i>pBH61 (BPA crosslink, Trp1)</i></p>
2300	<p><i>MAT a, ade2-1, trp1-1, can1-100, leu2-3, 112, his3-11, 15, ura3, GAL, psi+</i> <i>Δsmc1::NatMX4</i> <i>Smc3E202C-HA6::spHis5</i> <i>SCC1-PK9::KanMX</i> <i>leu2::Smc1S195C-myc9::hphNT1</i></p>
2301	<p><i>MAT alpha, ade2-1, trp1-1, can1-100, leu2-3, 112, his3-11, 15, ura3, GAL, psi+</i> <i>Δsmc1::NatMX4</i> <i>Smc3E202C-HA6::spHis5</i> <i>SCC1-PK9::KanMX</i> <i>leu2::Smc1S195C-myc9::hphNT1</i></p>
2302	<p><i>MAT a, ade2-1, trp1-1, can1-100, leu2-3, 112, his3-11, 15, ura3, GAL, psi+</i> <i>Δsmc1::NatMX4</i> <i>Smc3E202C-HA6::spHis5</i> <i>SCC1-PK9::KanMX</i> <i>leu2::Smc1N202C-myc9::hphNT1</i></p>
2303	<p><i>MAT alpha, ade2-1, trp1-1, can1-100, leu2-3, 112, his3-11, 15, ura3, GAL, psi+</i> <i>Δsmc1::NatMX4</i> <i>Smc3E202C-HA6::spHis5</i> <i>SCC1-PK9::KanMX</i> <i>leu2::Smc1N202C-myc9::hphNT1</i></p>
2304	<p><i>MAT a, ade2-1, trp1-1, can1-100, leu2-3, 112, his3-11, 15, ura3, GAL, psi+</i> <i>Δsmc1::NatMX4</i> <i>Smc3E202C-HA6::spHis5</i> <i>SCC1-PK9::KanMX</i> <i>leu2::Smc1S199C-myc9::hphNT1</i></p>
2305	<p><i>MAT alpha, ade2-1, trp1-1, can1-100, leu2-3, 112, his3-11, 15, ura3, GAL, psi+</i> <i>Δsmc1::NatMX4</i> <i>Smc3E202C-HA6::spHis5</i> <i>SCC1-PK9::KanMX</i> <i>leu2::Smc1S199C-myc9::hphNT1</i></p>
2306	<p><i>MAT a, ade2-1, trp1-1, can1-100, leu2-3, 112, his3-11, 15, ura3, GAL, psi+</i> <i>Δsmc1::NatMX4</i> <i>Smc3E202C-HA6::spHis5</i> <i>SCC1-PK9::KanMX</i> <i>leu2::Smc1K201C-myc9::hphNT1</i></p>
2307	<p><i>MAT alpha, ade2-1, trp1-1, can1-100, leu2-3, 112, his3-11, 15, ura3, GAL, psi+</i> <i>Δsmc1::NatMX4</i> <i>Smc3E202C-HA6::spHis5</i> <i>SCC1-PK9::KanMX</i> <i>leu2::Smc1K201C-myc9::hphNT1</i></p>

2308	<i>MAT a, ade2-1, trp1-1, can1-100, leu2-3, 112, his3-11, 15, ura3, GAL, psi+</i> Δ <i>smc1::NatMX4</i> <i>Smc3E202C-HA6::spHis5</i> <i>SCC1-PK9::KanMX</i> Δ <i>met15::Smc1E1046C-myc9</i>
2309	<i>MAT a, ade2-1, trp1-1, can1-100, leu2-3, 112, his3-11, 15, ura3, GAL, psi+</i> Δ <i>smc1::NatMX4</i> <i>Smc3E202C-HA6::spHis5</i> <i>SCC1-PK9::KanMX</i> Δ <i>met15::Smc1I1049C-myc9</i>
2310	<i>MAT a, ade2-1, trp1-1, can1-100, leu2-3, 112, his3-11, 15, ura3, GAL, psi+</i> Δ <i>smc1::NatMX4</i> <i>Smc3E202C-HA6::spHis5</i> <i>SCC1-PK9::KanMX</i> Δ <i>met15::Smc1Y213C-myc9</i>
2311	<i>MAT a, ade2-1, trp1-1, can1-100, leu2-3, 112, his3-11, 15, ura3, GAL, psi+</i> Δ <i>smc1::NatMX4</i> <i>Smc3E202C-HA6::spHis5</i> <i>SCC1-PK9::KanMX</i> Δ <i>met15::Smc1E209C-myc9</i>
2312	<i>MAT a, ade2-1, trp1-1, can1-100, leu2-3, 112, his3-11, 15, ura3, GAL, psi+</i> Δ <i>smc1::NatMX4</i> <i>Smc3E202C-HA6::spHis5</i> <i>SCC1-PK9::KanMX</i> Δ <i>met15::Smc1R205C-myc9</i>
2313	<i>MAT a, ade2-1, trp1-1, can1-100, leu2-3, 112, his3-11, 15, ura3, GAL, psi+</i> Δ <i>smc1::NatMX4</i> <i>Smc3E202C-HA6::spHis5</i> <i>SCC1-PK9::KanMX</i> Δ <i>met15::Smc1E190C-myc9</i>
2314	<i>MAT a, ade2-1, trp1-1, can1-100, leu2-3, 112, his3-11, 15, ura3, GAL, psi+</i> Δ <i>smc1::NatMX4</i> <i>Smc3E202C-HA6::spHis5</i> <i>SCC1-PK9::KanMX</i> Δ <i>met15::Smc1T1039C-myc9</i>
2315	<i>MAT a, ade2-1, trp1-1, can1-100, leu2-3, 112, his3-11, 15, ura3, GAL, psi+</i> Δ <i>smc1::NatMX4</i> <i>Smc3E202C-HA6::spHis5</i> <i>SCC1-PK9::KanMX</i> Δ <i>met15::Smc1L1042C-myc9</i>
2316	<i>MAT a, ade2-1, trp1-1, can1-100, leu2-3, 112, his3-11, 15, ura3, GAL, psi+</i> Δ <i>smc1::NatMX4</i> <i>Smc3E202C-HA6::spHis5</i> <i>SCC1-PK9::KanMX</i> Δ <i>met15::Smc1S193C-myc9</i>
2363	<i>MAT a, ade2-1, trp1-1, can1-100, leu2-3, 112, his3-11, 15, ura3, GAL, psi+</i> Δ <i>smc1::NatMX4</i>

	<p><i>leu2::Smc1N202C-myc9::hphNT1</i> <i>SCC1-PK9::KanMX</i> <i>Smc3E213C-HA6::His3MX6</i></p>
2367	<p><i>MAT a, ade2-1, trp1-1, can1-100, leu2-3, 112, his3-11, 15, ura3, GAL, psi+</i></p> <p><i>Δsmc1::NatMX4</i> <i>SCC1-PK9::KanMX</i> <i>Δmet15::Smc1R205C-myc9</i> <i>Smc3E213C-HA6::His3MX6</i></p>
2369	<p><i>MAT a, ade2-1, trp1-1, can1-100, leu2-3, 112, his3-11, 15, ura3, GAL, psi+</i></p> <p><i>Δsmc1::NatMX4</i> <i>SCC1-PK9::KanMX</i> <i>Δmet15::Smc1E209C-myc9</i> <i>Smc3E213C-HA6::His3MX6</i></p>
2371	<p><i>MAT a, ade2-1, trp1-1, can1-100, leu2-3, 112, his3-11, 15, ura3, GAL, psi+</i></p> <p><i>Δsmc1::NatMX4</i> <i>SCC1-PK9::KanMX</i> <i>Δmet15::Smc1Y213C-myc9</i> <i>Smc3E213C-HA6::His3MX6</i></p>
2374	<p><i>MAT a, ade2-1, trp1-1, can1-100, leu2-3, 112, his3-11, 15, ura3, GAL, psi+</i></p> <p><i>Δsmc1::NatMX4</i> <i>SCC1-PK9::KanMX</i> <i>Δmet15::Smc1N1013C-myc9</i> <i>Smc3E213C-HA6::His3MX6</i></p>
2376	<p><i>MAT a, ade2-1, trp1-1, can1-100, leu2-3, 112, his3-11, 15, ura3, GAL, psi+</i></p> <p><i>Δsmc1::NatMX4</i> <i>SCC1-PK9::KanMX</i> <i>Δmet15::Smc1R1020C-myc9</i> <i>Smc3E213C-HA6::His3MX6</i></p>
2378	<p><i>MAT a, ade2-1, trp1-1, can1-100, leu2-3, 112, his3-11, 15, ura3, GAL, psi+</i></p> <p><i>Δsmc1::NatMX4</i> <i>SCC1-PK9::KanMX</i> <i>Δmet15::Smc1R1024C-myc9</i> <i>Smc3E213C-HA6::His3MX6</i></p>
2380	<p><i>MAT a, ade2-1, trp1-1, can1-100, leu2-3, 112, his3-11, 15, ura3, GAL, psi+</i></p> <p><i>Δsmc1::NatMX4</i> <i>SCC1-PK9::KanMX</i> <i>Δmet15::Smc1A1028C-myc9</i> <i>Smc3E213C-HA6::His3MX6</i></p>
2386	<p><i>MAT a, ade2-1, trp1-1, can1-100, leu2-3, 112, his3-11, 15, ura3, GAL, psi+</i></p> <p><i>SCC1-PK9::KanMX</i> <i>Δsmc1::NatMX4</i> <i>Δmet15::Smc1R1031C-myc9</i> <i>Smc3E213C-HA6::His3MX6</i></p>
2387	<p><i>MAT a, ade2-1, trp1-1, can1-100, leu2-3, 112, his3-11, 15, ura3, GAL, psi+</i></p> <p><i>Δsmc1::NatMX4</i></p>

	<p>SCC1-PK9::KanMX Δmet15::Smc1I1035C-myc9 Smc3E213C-HA6::His3MX6</p>
2389	<p><i>MAT a, ade2-1, trp1-1, can1-100, leu2-3, 112, his3-11, 15, ura3, GAL, psi+</i></p> <p>Δsmc1::NatMX4 SCC1-PK9::KanMX Δmet15::Smc1T1039C-myc9 Smc3E213C-HA6::His3MX6</p>
2404	<p><i>MAT a, ade2-1, trp1-1, can1-100, leu2-3, 112, his3-11, 15, ura3, GAL, psi+SCC1-PK9::KanMX</i></p> <p>Smc3Q195C-HA6::His3MX6 Δsmc1::NatMX4 Δmet15::Smc1S193C-myc9</p>
2406	<p><i>MAT a, ade2-1, trp1-1, can1-100, leu2-3, 112, his3-11, 15, ura3, GAL, psi+SCC1-PK9::KanMX</i></p> <p>Smc3Q195C-HA6::His3MX6 Δsmc1::NatMX4 Δmet15::Smc1A1028C-myc9</p>
2408	<p><i>MAT a, ade2-1, trp1-1, can1-100, leu2-3, 112, his3-11, 15, ura3, GAL, psi+SCC1-PK9::KanMX</i></p> <p>Smc3Q195C-HA6::His3MX6 Δsmc1::NatMX4 Δmet15::Smc1I1035C-myc9</p>
2410	<p><i>MAT a, ade2-1, trp1-1, can1-100, leu2-3, 112, his3-11, 15, ura3, GAL, psi+SCC1-PK9::KanMX</i></p> <p>Smc3Q195C-HA6::His3MX6 Δsmc1::NatMX4 Δmet15::Smc1T1039C-myc9</p>
2417	<p><i>MAT a, ade2-1, trp1-1, can1-100, leu2-3, 112, his3-11, 15, ura3, GAL, psi+SCC1-PK9::KanMX</i></p> <p>Smc3Q195C-HA6::His3MX6 Δsmc1::NatMX4 Δmet15::Smc1E190C-myc9</p>
2421	<p><i>MAT a, ade2-1, trp1-1, can1-100, leu2-3, 112, his3-11, 15, ura3, GAL, psi+SCC1-PK9::KanMX</i></p> <p>Smc3Q195C-HA6::His3MX6 Δsmc1::NatMX4 leu2::Smc1S199C-myc9::hphNT1</p>
2423	<p><i>MAT a, ade2-1, trp1-1, can1-100, leu2-3, 112, his3-11, 15, ura3, GAL, psi+SCC1-PK9::KanMX</i></p> <p>Smc3Q195C-HA6::His3MX6 Δsmc1::NatMX4 leu2::Smc1S195C-myc9::hphNT1</p>
2425	<p><i>MAT a, ade2-1, trp1-1, can1-100, leu2-3, 112, his3-11, 15, ura3, GAL, psi+SCC1-PK9::KanMX</i></p> <p>Smc3Q195C-HA6::His3MX6 Δsmc1::NatMX4 leu2::Smc1K201C-myc9::hphNT1</p>
2427	<p><i>MAT a, ade2-1, trp1-1, can1-100, leu2-3, 112, his3-11, 15, ura3, GAL, psi+SCC1-PK9::KanMX</i></p> <p>Smc3Q195C-HA6::His3MX6 Δsmc1::NatMX4 leu2::Smc1N202C-myc9::hphNT1</p>
2431	<p><i>MAT a, ade2-1, trp1-1, can1-100, leu2-3, 112, his3-11, 15, ura3, GAL, psi+SCC1-PK9::KanMX</i></p> <p>Smc3Q195C-HA6::His3MX6</p>

	<p><i>Δsmc1::NatMX4</i> <i>Δmet15::Smc1R1031C-myc9</i></p>
2435	<p><i>MAT alpha, ade2-1, trp1-1, can1-100, leu2-3, 112, his3-11, 15, ura3, GAL, psi+ SCC1-PK9::KanMX</i> <i>Smc3Q195C-HA6::His3MX6</i> <i>Δsmc1::NatMX4</i> <i>Δmet15::Smc1L1042C-myc9</i></p>
2612	<p><i>MAT alpha, ade2-1, trp1-1, can1-100, leu2-3, 112, his3-11, 15, ura3, GAL, psi+</i> <i>Δsmc1::NatMX4</i> <i>SCC1-PK9::KanMX</i> <i>Δmet15::Smc1K191CMyC9 integration vector for Cas9-Met15</i> <i>Δsmc3::HIS3</i> <i>ura3::smc3E188C-HA3::URA (integration checked via PCR)</i></p>
2629	<p><i>MAT a, ade2-1, trp1-1, can1-100, leu2-3, 112, his3-11, 15, ura3, GAL, psi,</i> <i>Δsmc3::HIS3</i> <i>ura3::smc3E188C-HA3::URA (integration checked via PCR)</i> <i>Δsmc1::NatMX4</i> <i>SCC1-PK9::KanMX</i> <i>Δmet15::Smc1K180CMyC9 integration vector for Cas9-Met15</i></p>
2631	<p><i>MAT alpha, ade2-1, trp1-1, can1-100, leu2-3, 112, his3-11, 15, ura3, GAL, psi+</i> <i>Δsmc1::NatMX4</i> <i>SCC1-PK9::KanMX</i> <i>Δmet15::Smc1K188CMyC9 integration vector for Cas9-Met15</i> <i>Δsmc3::HIS3</i> <i>ura3::smc3E188C-HA3::URA (integration checked via PCR)</i></p>
2632	<p><i>MAT a, ade2-1, trp1-1, can1-100, leu2-3, 112, his3-11, 15, ura3, GAL, psi+</i> <i>Δsmc1::NatMX4</i> <i>SCC1-PK9::KanMX</i> <i>leu2::Smc1S199C-myc9::hphNT1</i> <i>Δsmc3::HIS3</i> <i>ura3::smc3E188C-HA3::URA (integration checked via PCR)</i></p>
2633	<p><i>MAT alpha, ade2-1, trp1-1, can1-100, leu2-3, 112, his3-11, 15, ura3, GAL, psi+</i> <i>Δsmc1::NatMX4</i> <i>SCC1-PK9::KanMX</i> <i>leu2::Smc1S199C-myc9::hphNT1</i> <i>Δsmc3::HIS3</i> <i>ura3::smc3E188C-HA3::URA (integration checked via PCR)</i></p>
2639	<p><i>MAT a, ade2-1, trp1-1, can1-100, leu2-3, 112, his3-11, 15, ura3, GAL, psi+</i> <i>Δsmc1::NatMX4</i> <i>SCC1-PK9::KanMX</i> <i>leu2::Smc1S195C-myc9::hphNT1</i> <i>Δsmc3::HIS3</i> <i>ura3::smc3E188C-HA3::URA (integration checked via PCR)</i></p>
2640	<p><i>MAT alpha, ade2-1, trp1-1, can1-100, leu2-3, 112, his3-11, 15, ura3, GAL, psi+</i> <i>Δsmc1::NatMX4</i> <i>SCC1-PK9::KanMX</i> <i>leu2::Smc1S195C-myc9::hphNT1</i> <i>Δsmc3::HIS3</i> <i>ura3::smc3E188C-HA3::URA (integration checked via PCR)</i></p>
2642	<p><i>MAT a, ade2-1, trp1-1, can1-100, leu2-3, 112, his3-11, 15, ura3, GAL, psi+</i> <i>Δsmc3::HIS3</i> <i>Δsmc1::NatMX4</i></p>

	<p>SCC1-PK9::KanMX Δmet15::Smc1G152C-Myc9 ura3::smc3V152C-HA3::URA3</p>
2643	<p>MAT alpha, ade2-1, trp1-1, can1-100, leu2-3, 112, his3-11, 15, ura3, GAL, psi, Δsmc3::HIS3 ura3::smc3K160C-HA3 (pBH987)::URA3 Δsmc1::NatMX4 SCC1-PK9::KanMX Δmet15::Smc1S161C-Myc9</p>
2647	<p>MAT alpha, ade2-1, trp1-1, can1-100, leu2-3, 112, his3-11, 15, ura3, GAL, psi+ Δsmc1::NatMX4 SCC1-PK9::KanMX Δmet15::Smc1G152C-Myc9 Δsmc3::HIS3 ura3::smc3G1128C-HA3::URA3 (integration checked via PCR)</p>
2648	<p>MAT a, ade2-1, trp1-1, can1-100, leu2-3, 112, his3-11, 15, ura3, GAL, psi+ Δsmc1::NatMX4 SCC1-PK9::KanMX Δmet15::Smc1K188C-Myc9 integration vector for Cas9-Met15 Δsmc3::HIS3 ura3::smc3K184C-HA3 (pBH986)::URA3</p>
2649	<p>MAT alpha, ade2-1, trp1-1, can1-100, leu2-3, 112, his3-11, 15, ura3, GAL, psi+ Δsmc1::NatMX4 SCC1-PK9::KanMX leu2::Smc1S195C-myc9::hphNT1 Δsmc3::HIS3 ura3::smc3K184C-HA3 (pBH986)::URA3</p>
2650	<p>MAT alpha, ade2-1, trp1-1, can1-100, leu2-3, 112, his3-11, 15, ura3, GAL, psi+ Δsmc1::NatMX4 SCC1-PK9::KanMX Δmet15::Smc1K180C-Myc9 integration vector for Cas9-Met15 Δsmc3::HIS3 ura3::smc3K184C-HA3 (pBH986)::URA3</p>
2654	<p>MAT a, ade2-1, trp1-1, can1-100, leu2-3, 112, his3-11, 15, ura3, GAL, psi+ Δsmc1::NatMX4 SCC1-PK9::KanMX Δmet15::Smc1E184C-Myc9 integration vector for Cas9-Met15 Δsmc3::HIS3 ura3::smc3E188C-HA3::URA (integration checked via PCR)</p>
2655	<p>MAT a, ade2-1, trp1-1, can1-100, leu2-3, 112, his3-11, 15, ura3, GAL, psi+ Δsmc1::NatMX4 SCC1-PK9::KanMX Δmet15::Smc1E184C-Myc9 integration vector for Cas9-Met15 Δsmc3::HIS3 ura3::smc3K184C-HA3 (pBH986)::URA3</p>
2656	<p>MAT a, ade2-1, trp1-1, can1-100, leu2-3, 112, his3-11, 15, ura3, GAL, psi+ Δsmc1::NatMX4 SCC1-PK9::KanMX Δmet15::Smc1K191C-Myc9 integration vector for Cas9-Met15 Δsmc3::HIS3 ura3::smc3K184C-HA3 (pBH986)::URA3</p>
2664	<p>MAT a, ade2-1, trp1-1, can1-100, leu2-3, 112, his3-11, 15, ura3, GAL, psi+</p>

	<p><i>Δsmc1::NatMX4</i> <i>SCC1-PK9::KanMX</i> <i>leu2::Smc1S199C-myc9::hphNT1</i> <i>Δsmc3::HIS3</i> <i>ura3::smc3K184C-HA3 (pBH986)::URA3</i></p>
2665	<p><i>MAT alpha, ade2-1, trp1-1, can1-100, leu2-3, 112, his3-11, 15, ura3, GAL, psi+</i></p> <p><i>Δsmc1::NatMX4</i> <i>SCC1-PK9::KanMX</i> <i>leu2::Smc1S199C-myc9::hphNT1</i> <i>Δsmc3::HIS3</i> <i>ura3::smc3K184C-HA3 (pBH986)::URA3</i></p>
2678	<p><i>MAT a, ade2-1, trp1-1, can1-100, leu2-3, 112, his3-11, 15, ura3, GAL, psi+SCC1-PK9::KanMX</i> <i>pBH623 (smc3Q67TAG_K112Q_K113Q-HA in YEplac181)</i> <i>pBH61 (BPA crosslink, Trp1)</i></p>
2679	<p><i>MAT a, ade2-1, trp1-1, can1-100, leu2-3, 112, his3-11, 15, ura3, GAL, psi+SCC1-PK9::KanMX</i> <i>pBH995 (smc3Q67TAG_K112Q_K113Q_R1008I-HA in YEplac181)</i> <i>pBH61 (BPA crosslink, Trp1)</i></p>
2684	<p><i>MAT a, ade2-1, trp1-1, can1-100, leu2-3, 112, his3-11, 15, ura3, GAL, psi+SCC1-PK9::KanMX</i> <i>Scs2(E822K, L937F):: NatMX</i> <i>pBH623 (smc3Q67TAG_K112Q_K113Q-HA in YEplac181)</i> <i>pBH61 (BPA crosslink, Trp1)</i></p>
2685	<p><i>MAT a, ade2-1, trp1-1, can1-100, leu2-3, 112, his3-11, 15, ura3, GAL, psi+SCC1-PK9::KanMX</i> <i>Scs2(E822K, L937F):: NatMX</i> <i>pBH995 (smc3Q67TAG_K112Q_K113Q_R1008I-HA in YEplac181)</i> <i>pBH61 (BPA crosslink, Trp1)</i></p>
2698	<p><i>MAT a, ade2-1, trp1-1, can1-100, leu2-3, 112, his3-11, 15, ura3, GAL, psi,</i> <i>Δsmc3::HIS3</i> <i>ura3::smc3K184C-HA3 (pBH986)::URA3</i> <i>SCC1-PK9::KanMX</i> <i>Δsmc1::NatMX4</i> <i>Δmet15::Smc1E183CMyc9</i></p>
2699	<p><i>MAT alpha, ade2-1, trp1-1, can1-100, leu2-3, 112, his3-11, 15, ura3, GAL, psi,</i> <i>Δsmc3::HIS3</i> <i>ura3::smc3K184C-HA3 (pBH986)::URA3</i> <i>SCC1-PK9::KanMX</i> <i>Δsmc1::NatMX4</i> <i>Δmet15::Smc1E183CMyc9</i></p>
2700	<p><i>MAT a, ade2-1, trp1-1, can1-100, leu2-3, 112, his3-11, 15, ura3, GAL, psi,</i> <i>Δsmc3::HIS3</i> <i>ura3::smc3K184C-HA3 (pBH986)::URA3</i> <i>SCC1-PK9::KanMX</i> <i>Δsmc1::NatMX4</i> <i>Δmet15::Smc1L185CMyc9</i></p>
2701	<p><i>MAT alpha, ade2-1, trp1-1, can1-100, leu2-3, 112, his3-11, 15, ura3, GAL, psi,</i> <i>Δsmc3::HIS3</i> <i>ura3::smc3K184C-HA3 (pBH986)::URA3</i> <i>SCC1-PK9::KanMX</i> <i>Δsmc1::NatMX4</i> <i>Δmet15::Smc1L185CMyc9</i></p>
2702	<p><i>MAT a, ade2-1, trp1-1, can1-100, leu2-3, 112, his3-11, 15, ura3, GAL, psi,</i> <i>Δsmc3::HIS3</i> <i>ura3::smc3K184C-HA3 (pBH986)::URA3</i> <i>SCC1-PK9::KanMX</i> <i>Δsmc1::NatMX4</i> <i>Δmet15::Smc1K186CMyc9</i></p>
2703	<p><i>MAT alpha, ade2-1, trp1-1, can1-100, leu2-3, 112, his3-11, 15, ura3, GAL, psi,</i> <i>Δsmc3::HIS3</i></p>

	<p><i>ura3::smc3K184C-HA3 (pBH986)::URA3</i> <i>SCC1-PK9::KanMX</i> <i>Δsmc1::NatMX4</i> <i>Δmet15::Smc1K186C-Myc9</i></p>
2728	<p><i>MAT a, ade2-1, trp1-1, can1-100, leu2-3, 112, his3-11, 15, ura3, GAL, psi,</i> <i>Δsmc3::HIS3</i> <i>ura3::smc3K160C-HA6::URA3 (single copy checked via PCR)</i> <i>Δsmc1::NatMX4</i> <i>SCC1-PK9::KanMX</i> <i>Δmet15::Smc1L1120C-Myc9</i></p>
2730	<p><i>MAT alpha, ade2-1, trp1-1, can1-100, leu2-3, 112, his3-11, 15, ura3, GAL, psi+</i> <i>Δsmc1::NatMX4</i> <i>SCC1-PK9::KanMX</i> <i>Δmet15::Smc1S161C-Myc9</i> <i>Δsmc3::HIS3</i> <i>ura3::smc3K160C-HA6::URA3 (single copy checked via PCR)</i></p>
2731	<p><i>MAT a, ade2-1, trp1-1, can1-100, leu2-3, 112, his3-11, 15, ura3, GAL, psi+</i> <i>Δsmc1::NatMX4</i> <i>SCC1-PK9::KanMX</i> <i>Δmet15::Smc1S161C_L1120C-Myc9</i> <i>Δsmc3::HIS3</i> <i>ura3::smc3K160C_N1204C-HA6::URA3 (single copy checked via PCR)</i></p>
2733	<p><i>MAT alpha, ade2-1, trp1-1, can1-100, leu2-3, 112, his3-11, 15, ura3, GAL, psi+</i> <i>Δsmc1::NatMX4</i> <i>SCC1-PK9::KanMX</i> <i>Δmet15::Smc1S161C-Myc9</i> <i>Δsmc3::HIS3</i> <i>ura3::smc3N1204C-HA6::URA3 (single copy checked via PCR)</i></p>
2734	<p><i>MAT a, ade2-1, trp1-1, can1-100, leu2-3, 112, his3-11, 15, ura3, GAL, ::NatMX4</i> <i>SCC1-PK9::KanMX</i> <i>Δmet15::Smc1L1120C-Myc9</i> <i>Δsmc3::HIS3</i> <i>ura3::smc3N1204C-HA6::URA3 (single copy checked via PCR)</i></p>
2777	<p><i>MAT a, ade2-1, trp1-1, can1-100, leu2-3, 112, his3-11, 15, ura3, GAL, psi,</i> <i>Δsmc3::HIS3</i> <i>SCC1-PK9::KanMX</i> <i>ura3::N-FLAG3-Smc3N1204C::ura3 (single copy checked by PCR)</i> <i>leu2::Gal1p-Sic1(9m)/His3p-Gal1/His3p-Gal2/Gal1p-Gal4::Leu2 (single copy)</i> <i>Smc1_S161C::NatMX</i></p>
2779	<p><i>MAT a, ade2-1, trp1-1, can1-100, leu2-3, 112, his3-11, 15, ura3, GAL, psi+SCC1-</i> <i>PK9::KanMX</i> <i>leu2::Gal1p-Sic1(9m)/His3p-Gal1/His3p-Gal2/Gal1p-Gal4::Leu2 (single copy)</i> <i>Smc1_S161C_L1120C::NatMX</i> <i>Δsmc3::HIS3</i> <i>ura3::N-FLAG3-Smc3_K160C_N1204C::ura3 (single copy checked by PCR)</i></p>
2780	<p><i>MAT alpha, ade2-1, trp1-1, can1-100, leu2-3, 112, his3-11, 15, ura3, GAL, psi+SCC1-</i> <i>PK9::KanMX</i> <i>leu2::Gal1p-Sic1(9m)/His3p-Gal1/His3p-Gal2/Gal1p-Gal4::Leu2 (single copy)</i> <i>Smc1_S161C_L1120C::NatMX</i> <i>Δsmc3::HIS3</i> <i>ura3::N-FLAG3-Smc3_K160C_N1204C::ura3 (single copy checked by PCR)</i></p>
2781	<p><i>MAT a, ade2-1, trp1-1, can1-100, leu2-3, 112, his3-11, 15, ura3, GAL, psi+SCC1-</i> <i>PK9::KanMX</i> <i>leu2::Gal1p-Sic1(9m)/His3p-Gal1/His3p-Gal2/Gal1p-Gal4::Leu2 (single copy)</i> <i>Smc1_S161C_L1120C::NatMX</i> <i>ura3::N-FLAG3-Smc3_K160C_N1204C::ura3 (single copy checked by PCR)</i></p>

2783	<p><i>MAT a, ade2-1, trp1-1, can1-100, leu2-3, 112, his3-11, 15, ura3, GAL, psi, Δsmc3::HIS3</i> <i>SCC1-PK9::KanMX</i> <i>ura3::N-FLAG3-Smc3K160C::ura3 (single copy checked by PCR)</i> <i>leu2::Gal1p-Sic1(9m)/His3p-Gal1/His3p-Gal2/Gal1p-Gal4::Leu2 (single copy)</i> <i>Smc1_S161C::NatMX</i></p>
2785	<p><i>MAT a, ade2-1, trp1-1, can1-100, leu2-3, 112, his3-11, 15, ura3, GAL, psi, Δsmc3::HIS3</i> <i>SCC1-PK9::KanMX</i> <i>ura3::N-FLAG3-Smc3K160C::ura3 (single copy checked by PCR)</i> <i>leu2::Gal1p-Sic1(9m)/His3p-Gal1/His3p-Gal2/Gal1p-Gal4::Leu2 (single copy)</i> <i>Smc1_L1120C::NatMX</i></p>
2787	<p><i>MAT alpha, ade2-1, trp1-1, can1-100, leu2-3, 112, his3-11, 15, ura3, GAL, psi+SCC1-PK9::KanMX</i> <i>leu2::Gal1p-Sic1(9m)/His3p-Gal1/His3p-Gal2/Gal1p-Gal4::Leu2 (single copy)</i> <i>Smc1_L1120C::NatMX</i> <i>Δsmc3::HIS3</i> <i>ura3::N-FLAG3-Smc3N1204C::ura3 (single copy checked by PCR)</i></p>
2788	<p><i>MAT a, ade2-1, trp1-1, can1-100, leu2-3, 112, his3-11, 15, ura3, GAL, psi+SCC1-PK9::KanMX</i> <i>leu2::Gal1p-Sic1(9m)/His3p-Gal1/His3p-Gal2/Gal1p-Gal4::Leu2 (single copy)</i> <i>Smc1_S161C_L1120C::NatMX</i> <i>ura3::N-FLAG3-Smc3K112Q_K113Q_K160C_N1204C::URA3 (Checked via PCR)</i></p>
2864	<p><i>MAT a, ade2-1, trp1-1, can1-100, leu2-3, 112, his3-11, 15, ura3, GAL, psi+SCC1-PK9::KanMX</i> <i>leu2::Gal1p-Sic1(9m)/His3p-Gal1/His3p-Gal2/Gal1p-Gal4::Leu2 (single copy)</i> <i>Smc1_K191C::NatMX</i> <i>Δsmc3::HIS3</i> <i>ura3::N-FLAG3-Smc3N1204C::ura3 (single copy checked by PCR)</i></p>
2865	<p><i>MAT a, ade2-1, trp1-1, can1-100, leu2-3, 112, his3-11, 15, ura3, GAL, psi+SCC1-PK9::KanMX</i> <i>leu2::Gal1p-Sic1(9m)/His3p-Gal1/His3p-Gal2/Gal1p-Gal4::Leu2 (single copy)</i> <i>Smc1_L1120C::NatMX</i> <i>Δsmc3::HIS3</i> <i>ura3::N-FLAG3-Smc3K184C::URA3</i></p>
2866	<p><i>MAT a, ade2-1, trp1-1, can1-100, leu2-3, 112, his3-11, 15, ura3, GAL, psi+SCC1-PK9::KanMX</i> <i>leu2::Gal1p-Sic1(9m)/His3p-Gal1/His3p-Gal2/Gal1p-Gal4::Leu2 (single copy)</i> <i>Smc1_K191C::NatMX</i> <i>Δsmc3::HIS3</i> <i>ura3::N-FLAG3-Smc3K184C::URA3</i></p>
2867	<p><i>MAT a, ade2-1, trp1-1, can1-100, leu2-3, 112, his3-11, 15, ura3, GAL, psi+SCC1-PK9::KanMX</i> <i>leu2::Gal1p-Sic1(9m)/His3p-Gal1/His3p-Gal2/Gal1p-Gal4::Leu2 (single copy)</i> <i>Smc1_K191C_L1120C::NatMX</i> <i>Δsmc3::HIS3</i> <i>ura3::N-FLAG3-Smc3K184C_N1204C::URA3</i></p>
2894	<p><i>MAT a, ade2-1, trp1-1, can1-100, leu2-3, 112, his3-11, 15, ura3, GAL, psi+SCC1-PK9::KanMX</i> <i>leu2::Gal1p-Sic1(9m)/His3p-Gal1/His3p-Gal2/Gal1p-Gal4::Leu2 (single copy)</i> <i>Smc1_E209C::NatMX</i> <i>Δsmc3::HIS3</i> <i>ura3::N-FLAG3-Smc3E202C::URA3 (single copy check by PCR) pBH1085</i></p>
2895	<p><i>MAT a, ade2-1, trp1-1, can1-100, leu2-3, 112, his3-11, 15, ura3, GAL, psi+SCC1-PK9::KanMX</i> <i>leu2::Gal1p-Sic1(9m)/His3p-Gal1/His3p-Gal2/Gal1p-Gal4::Leu2 (single copy)</i> <i>Smc1_E209C::NatMX</i> <i>Δsmc3::HIS3</i> <i>ura3::N-FLAG3-Smc3N1204C::URA3 (single copy checked by PCR)</i></p>
2896	<p><i>MAT a, ade2-1, trp1-1, can1-100, leu2-3, 112, his3-11, 15, ura3, GAL, psi+SCC1-PK9::KanMX</i> <i>leu2::Gal1p-Sic1(9m)/His3p-Gal1/His3p-Gal2/Gal1p-Gal4::Leu2 (single copy)</i> <i>Smc1_L1120C::NatMX</i></p>

	<p><i>Δsmc3::HIS3</i> <i>ura::N-FLAG3-Smc3E202C::URA3 (single copy check by PCR) pBH1085</i></p>
2897	<p><i>MATa,ade2-1, trp1-1, can1-100, leu2-3, 112, his3-11, 15, ura3, GAL, psi+SCC1-PK9::KanMX</i> <i>leu2::Gal1p-Sic1(9m)/His3p-Gal1/His3p-Gal2/Gal1p-Gal4::Leu2 (single copy)</i> <i>Smc1_E209C_L1120C::NatMX</i> <i>Δsmc3::HIS3</i> <i>ura::N-FLAG3-Smc3E202C_N1204C::URA3 (single copy check by PCR) pBH1086</i></p>

7.4 Additional figures

7.4.1 Chapter 1 part 1

Table 9: Results of QQ suppressor screen.

Suppressor mutant photos in appendix 7.4.1. A “-” denotes that this combination was not tested in this study.

No.	Smc3 mutation	Rating + <i>R1008I</i>	Rating - <i>R1008I</i>	Rating <i>scc2EKLF</i> + <i>R1008I</i>	Rating <i>scc2EKLF</i> - <i>R1008I</i>	Strain
1	A157V	3	0	-	-	1129, 1346
2	K158E	3	1	-	-	1139, 1336
3	D252N	2	0	-	-	1207 x 700, 1337
4	S260P	3	0	-	-	1209 x 700, 1338
5	N292S	1	0	-	-	1143, 1353
6	Q298R	2	0	-	-	1302, 1347
7	K300R	1	0	-	-	1307, 1339
8	M937T	4	0	-	-	1309, 1365
9	R946G	3	0	-	-	1305, 1366
10	N982D	2	0	-	-	1150, 1367
11	E1124K	3	0	-	-	1153, 1354
12	V1133I	4	0	-	-	1303, 1340
13	Q1143R	3	2	-	-	1308, 1341
14	S1176P	3	0	-	-	1306, 1342
15	R1187G	2	0	-	-	1301, 1343
16	L965F	4	0	-	-	1310, 1368
17	D975E	0	-	-	-	1304
18	N985S	2	0	-	-	1168, 1369
19	E305G	4	0	-	-	1170, 1348
20	D295V	3	0	-	-	1173, 1344
21	L926H	3	0	-	-	1211, 1370
22	C1183S	4	1	-	-	1176, 1355
23	N156D	3	0	-	-	1330, 1349
24	K180R	1	0	-	-	1331, 1345
25	T233A	0	0	-	-	1332, 1350
26	R248G	3	0	-	-	1333, 1351

27	S259P	4	0	-	-	1374, 1371
28	V315G	0	0	-	-	1375, 1372
29	Y359H	3	0	-	-	1334, 1352
30	Control (R1008I)	1	0	4	0	1335, 1356
31	W483R	4	0	-	0	1471, 1694
32	K1201E	4	0	-	-	1378, 1363
33	E1203G	4	0	-	-	1453 x 1454, 1364
34	F41L	3	-	-	-	1379
35	S54F	1	-	-	-	1380
36	L111R	4	-	-	-	1381
37	Q117R	3	-	-	-	1382
38	G110R	2	-	-	-	1383
39	E857G	3	-	-	-	1556
40	Q847R	3	-	-	-	1470
41	D824G	1	-	-	-	1498
42	K689E	4	-	-	-	1500
43	N657S	2	-	-	-	1557
44	S448P	4	-	-	-	1455
45	R381S	4	-	-	-	1559
46	R348G	3	-	-	-	1456
47	Q330R	4	-	-	-	1457
48	S326P	2	-	-	-	1458

7.4.3 Chapter 2 part 4

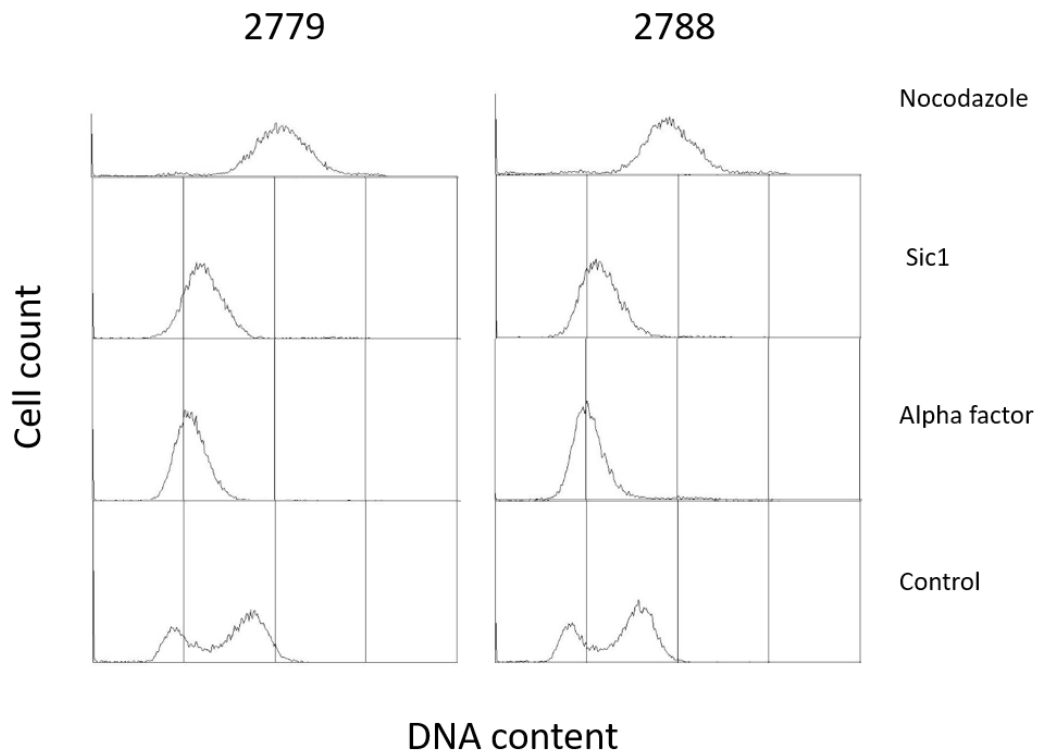


Figure 66: FACS histograms showing DNA content in cultures used during the cell cycle arrest experiments.

The histograms were produced using BD CellQuest Pro software and samples prepared by methods described in 3.2.3.22. The propidium iodide dye used in the methods described stains DNA in dead cells, thus the histograms show relative DNA content. The control histograms show cells of a wide variety of sizes with two peaks representing G1 and G2 cells. The peak positioned closer to the left is composed of cells in the G1 phase of the cell cycle as DNA replication has not occurred at this stage. DNA content is approximately doubled in G2 phase which appears as the peak

on the right. The alpha factor arrest histograms show a single peak at the location of expected G1 cells. This is due to the ability of alpha factor which may arrest “a” mating type yeast cells in G1 phase. The Sic1 arrest histograms show that cells may be maintained in G1 arrest by activating Sic1 promotion. The nocodazole arrest histograms show successful arrest in G2 as the DNA as the peak shows high DNA content.

7.5 Publications

Bürmann, F., Lee, B.G., Than, T., Sinn, L., O’Reilly, F.J., Yatskevich, S., Rappsilber, J., Hu, B., Nasmyth, K., and Löwe, J. (2019). A folded conformation of MukBEF and cohesin. *Nat. Struct. Mol. Biol.* 26, 227–236.